N° d'ordre : **4100**

THÈSE

en vue de l'obtention du : **DOCTORAT**

Centre de Recherche : Centre des Sciences de Matériaux
Structure de Recherche : Laboratoire des Matériaux, Nanotechnologies et Environnement (LMNE)
Discipline : Chimie - Physique
Spécialité : Electrochimie- Corrosion- Matériaux

Présentée et Soutenue le : ***21 / 06 / 2025***

par :

Manal NACIRI

Comparative analysis of the impact of Nitrogen derivatives on the corrosion inhibition of carbon steel in 1M HCl environment

Devant le JURY :

Abdelkbir BELLAOUCHOU	PES	Faculté des Sciences, Université Mohammed V-Rabat	Président
Abdelaziz SABBAR	PES	Faculté des Sciences, Université Mohammed V-Rabat	Rapporteur/Examinateur
Hamid ERRAMLI	MCH	Faculté des Sciences, Université Ibn Tofail-Kénitra	Rapporteur/Examinateur
Abdelaziz AIT ADDI	PES	Faculté des Sciences, Université Ibn Zohr-Agadir	Rapporteur/Examinateur
Mouloud EL MOUDANE	PES	Faculté des Sciences, Université Mohammed V-Rabat	Examinateur
Adil El YADINI	MCH	Faculté des Sciences, Université Mohammed V-Rabat	Examinateur
Yasmina EL AOUFIR	MCH	Ecole Supérieure de l'Education et de la Formation, Université Ibn Tofail-Kénitra	Co-Directrice de thèse
Ahmed GHANIMI	PES	Faculté des Sciences, Université Mohammed V-Rabat	Directeur de thèse

Année Universitaire : 2024 - 2025

Dedication

To my dear parents,

You were my first support, my greatest source of motivation and inspiration. Your unconditional love, sacrifices, and belief in me have enabled me to move forward with determination. This work is the fruit of your kindness and constant encouragement. Thank you from the bottom of my heart.

To my cousins and brother,

You have always been there for me, through the good and the bad times. difficult times. Your presence, your support, and your affection have been a precious strength throughout this journey. Thank you for your presence and your patience.

To my dear family, who have always believed in me and supported me every step of the way. Your love, patience, and encouragement have been my greatest strength.

To my friends, for their invaluable presence, unfailing support, and comforting words in moments of doubt.

To all those who have been there, from near and far, and who have contributed, through a gesture, a word, or a thought, to make this adventure more beautiful and more rewarding.

This work is also yours. Thank you from the bottom of my heart.

Acknowledgements

I would like to express my utmost gratitude to the directors of the Materials, Nanotechnology and Environment Laboratory “LMNE” for having integrated me into its teams. I am truly privileged to have benefited from the human, material, and scientific resources allocated to me. Over the past years, the laboratory leadership under Professor **Abdelkbir BELLAOUCHOU** and previously under Professor **Abdellah GUENBOUR** has cultivated an environment for academic excellence and granted its teams the resources and the necessary support. This enriching working environment has played a crucial role in my research. My heartfelt appreciation and deepest gratitude to all the laboratory members for their benevolence, availability and the enriching exchanges over the years spent at the Laboratory.

I am honored to acknowledge the contributions of Professor **Ahmed GHANIMI** (Faculty of Sciences, Mohammed V University in Rabat), my thesis supervisor. His exceptional work ethic and scientific meticulousness were invaluable to the completion of this work. By striking a perfect balance between guidance and independence, he has allowed me to progress in complete confidence and peace of mind during this period. I would also like to acknowledge the pivotal role played by Professor **Yasmina EL AOUFIR** (Higher School of Education and Training, Ibn Tofail University -Kenitra), my thesis co-supervisor. Her thoroughness, her rigor as well as her close follow-up have immensely contributed to the enrichment of this work. Without her unwavering support throughout the years, this project would not have seen the light of day. To my supervisors, thank you for offering a mentorship that fosters growth and self-reliance.

With profound respect, I convey my sincere gratitude to the President of the jury, Professor **Abdelkbir BELLAOUCHOU** (Faculty of Sciences, Mohammed V University in Rabat), for having agreed to chair this defense. His presence is a considerable honor. As head of the laboratory, his dedication, rigor, sincerity, and his empathy have established a collaborative spirit among all members of the laboratory.

I would like to express my sincere gratitude to Professor **Abdelaziz SABBAR** (Faculty of Sciences, Mohammed V University in Rabat) for the time he has devoted to analyzing and evaluating this research. His judicious and constructive observations were of great value. It is a privilege to once again benefit from his expertise and insights, as I had the honor of being supervised by him during my bachelor’s studies.

I am deeply grateful to the commitment of Professor **Hamid ERRAMLI** (Faculty of Sciences, Ibn Tofail University-Kénitra) for the dedication and time spent in reviewing and evaluating this research. His thoughtful and precise observations have been of immense value and have greatly enriched the quality of this work.

I would like to express my sincere appreciation to the reporting examiner, Professor **Abdelaziz AIT ADDI** (Faculty of Sciences, Ibn Zohr University-Agadir), for his presence and commitment during this examination. His questions and comments were of considerable importance and contributed significantly to the enrichment of this work.

I wish to extend my heartfelt thanks to Professor **Mouloud EL MOUDANE** (Faculty of Sciences, Mohammed V University in Rabat) for his wise advice and support for and for kindly agreeing to be an examiner on this jury. Without forgetting support during the preparation of this thesis.

I would like to express my sincere appreciation for Professor **Adil El YADINI** (Faculty of Sciences, Mohammed V University in Rabat) for the time dedicated to the examination of the thesis, and for his presence and commitment during this examination. I would like to express all my gratitude to him.

Acknowledgement is due to the technical platform of the faculty of sciences of Rabat, in particular to the late Professor **Amine BELFHAILI** (Faculty of Sciences, Mohammed V University in Rabat), for always finding and taking the time to help us obtain SEM images with patience and kindness. We will never forget your kindness. May Allah have mercy on his soul and grant him rest.

My True appreciation to Professor **Aicha SIFOU** (Faculty of Sciences, Mohammed V University in Rabat), for her efficiency, availability, and assistance with the X-ray diffraction analysis.

I wish to offer my sincere thanks to Professor **Hassane LGAZ** (Konkuk University, Seoul, South Korea) for his assistance with the theoretical calculations. His expertise and collaborative spirit have been of great value to the completion of this work.

I would also like to express my gratitude to my family and friends for their unfailing support throughout this adventure. Your encouragement, patience, and confidence in my abilities have given me the motivation I need to complete this project.

Finally, I would like to express my particular gratitude to my friends and colleagues, whose presence and stimulating exchanges not only contributed to the productivity of this period but also enriched its human aspect. I would like to express my gratitude to each and every one of you for the moments of conviviality we've shared, the bursts of laughter, and the mutual support we've shown each other.

Résumé

L'acier au carbone, largement utilisé dans les équipements de raffinage du pétrole, souffre de problèmes de corrosion persistants. Cette recherche explore les propriétés d'inhibition de la corrosion de deux classes d'inhibiteurs organiques à base d'azote : 1,2,4-triazoles et hydrazones, pour atténuer la corrosion de l'acier au carbone dans du HCl 1,0 M. Initialement, un nouveau dérivé du 1,2,4-triazole, le 5-hexylsulfanyl-1,2,4-triazole (HST), a démontré une efficacité d'inhibition remarquable allant jusqu'à 97% à une concentration optimale de 10^{-3} M, avec une efficacité conservée jusqu'à 338 K. Les études électrochimiques ont révélé que le HST agissait comme un inhibiteur mixte, et les isothermes d'adsorption ont indiqué que l'adsorption obéit au modèle de Langmuir. Notre attention s'est ensuite portée sur deux dérivés de l'hydrazone, le N′-[(E)-furan-2-ylméthylidène]-2-(6-méthoxynaphthalen-2-yl)propanehydrazide (NFH) et le 2-(6-méthoxynaphthalen-2-yl)-N′-[(E)-thiophen-2-ylméthylidène]propanehydrazide (NTH). Les deux composés ont montré des performances d'inhibition significatives, le NTH atteignant une efficacité de 93 %, attribuée au groupe thiophène qui améliore l'adsorption. Les études de spectroscopie d'impédance électrochimique (EIS) et de polarisation potentiodynamique (PDP) ont confirmé la nature mixte des deux inhibiteurs. L'adsorption a suivi les isothermes de Langmuir, corroborées par les études de calcul, qui ont également mis en évidence les configurations d'adsorption et les descripteurs de réactivité.

Mots-clefs : Inhibition de la corrosion, triazole, hydrazone, acier au carbone, HCl 1M

Abstract

Carbon steel, widely employed in petroleum refining equipment, suffers from persistent corrosion issues. This research explores the corrosion inhibition properties of two classes of nitrogen-based organic inhibitors: 1,2,4-triazoles and hydrazones, for mitigating carbon steel corrosion in 1.0 M HCl. Initially, a novel 1,2,4-triazole derivative, 5-hexylsulfanyl-1,2,4-triazole (HST), demonstrated a remarkable inhibition efficiency of up to 97% at an optimal concentration of 10^{-3} M, with efficacy retained up to 338 K. Electrochemical studies revealed HST acted as a mixed inhibitor, and Langmuir adsorption isotherms indicated chemisorption as the dominant interaction mode. Subsequently, the focus shifted to two hydrazone derivatives, N′-[(E)-furan-2-ylmethylidene]-2-(6-methoxynaphthalen-2-yl)propanehydrazide (NFH) and 2-(6-methoxynaphthalen-2-yl)-N′-[(E)-thiophen-2-ylmethylidene]propanehydrazide (NTH). Both compounds exhibited significant inhibition performance, with NTH achieving 93% efficiency, attributed to the thiophene group enhancing adsorption. Electrochemical Impedance Spectroscopy (EIS) and Potentiodynamic Polarization (PDP) studies confirmed the mixed inhibitor nature of both compounds. Adsorption followed Langmuir isotherms, corroborated by computational studies, which also highlighted adsorption configurations and reactivity descriptors.

Key-words: corrosion inhibition, triazole, hydrazone, carbon steel, 1M HCl

مُلخَّص

الفولاذ الكربوني، المستخدم على نطاق واسع في معدات تكرير النفط، يعاني من مشاكل تآكل مستمرة .يستكشف هذا البحث خصائص تثبيط التآكل لاثنين من أصناف المثبطات العضوية المحتوية على النتروجين :مشتق التريازول و مشتقين من الهيدرازون، للحد من تآكل الفولاذ الكربوني في محلول حمض الهيدروكلوريك بتركيز1مول/لتر .في البداية أظهر مشتق مشتق جديد من التريازول كفاءة تثبيط ملحوظة تصل إلى 97 %عند التركيز الأمثل مول/لتر ، مع استمرار الفعالية حتى 338 كيلفن .كشفت الدراسات الكهروكيميائية أن مشتق التريازول يعمل كمثبط مختلط، و أشارت منحنيات الامتصاص للانغمير إلى أن التفاعل الكيميائي هو الوضع السائد في التفاعل .بعد ذلك تم التركيز على مشتقين من الهيدرازون و أظهر المركبان أداء تثبيطيا كبيرا، حيث وصلت الكفاءة إلى 93%، و يرجع ذلك إلى تعزيز مجموعة الثيوفين للامتصاص .أكدت دراسات التحليل الطيفي للمقاومة الكهروكيميائية و منحنيات الاستقطاب فعالية المركبين و طبيعتهما المختلطة .تبعت عملية الامتصاص منحنيات الامتصاص للانغمير، و تم تأكيد ذلك من خلال نتائج الحسابات النظرية و التي أوضحت طريقة عمل الجزيئات المثبطة، وكذلك نوع التفاعل بين مواقع الامتزاز النشطة في المثبطات مع سطح الفولاذ.

الكلمات المفتاحية :تثبيط التآكل ، التريازول، الهيدرازون، الفولاذ الكربوني، حمض الهيدروكلوريك

Résumé détaillé

La corrosion est un phénomène naturel qui affecte les métaux lorsqu'ils interagissent avec leur environnement, entraînant leur dégradation progressive. Ce processus, principalement d'origine chimique ou électrochimique, constitue un problème majeur dans de nombreux secteurs industriels et la vie courante. La corrosion se manifeste par la tendance spontanée des métaux à retourner à leurs formes oxydées plus stables, comme les oxydes, les hydroxydes ou les sulfures. Bien que certains produits de corrosion puissent offrir une protection limitée, dans la majorité des cas, ils altèrent fortement les propriétés mécaniques, la fonctionnalité et la durabilité des matériaux métalliques.

La corrosion des métaux représente une menace sérieuse pour l'industrie et l'environnement, en impactant la durabilité des matériaux et des infrastructures, la santé et la sécurité humaine tout en générant des coûts financiers considérables. Son impact économique est colossal, représentant une perte mondiale estimée à plus de 2500 milliards de dollars par an, avec des conséquences dans les domaines du pétrole, du gaz, du transport, de la construction ou encore de l'aéronautique.

Parmi les métaux les plus utilisés dans les installations industrielles, l'acier au carbone est largement privilégié en raison de son faible coût, de ses bonnes propriétés mécaniques et de sa disponibilité. Cependant, sa vulnérabilité à la corrosion, notamment en milieu acide, limite considérablement sa durabilité. L'acide chlorhydrique (HCl), couramment employé dans diverses applications industrielles telles que le décapage, le nettoyage acide et la stimulation des puits pétroliers, est particulièrement agressif vis-à-vis de l'acier. Pour étudier le comportement de la corrosion et évaluer l'efficacité des inhibiteurs dans des conditions bien contrôlées, les chercheurs ont recours à des milieux proches des conditions industrielles dont le HCl 1,0 M est l'un des plus représentatifs.

La connaissance des mécanismes de corrosion et des méthodes de protection contre la corrosion nous permet de préserver de manière significative les matériaux. Plusieurs techniques de qualification et de quantification de la corrosion des métaux et des méthodes de protection contre la corrosion sont utilisées. Des recherches expérimentales sont continuellement menées pour développer de nouvelles méthodes de protection de la corrosion en agissant soit sur le métal lui-même ou sur son environnement.

Face aux enjeux techniques et économiques liés à la corrosion de l'acier au carbone dans les environnements acides, la recherche de solutions de protection efficaces, peu coûteuses et respectueuses de l'environnement est d'une importance cruciale. Parmi les méthodes de protection, l'utilisation d'inhibiteurs de corrosion, en particulier organiques moins toxiques, s'est révélée très prometteuse. Ces composés agissent généralement par adsorption sur la surface métallique, formant une couche protectrice qui bloque ou ralentit les réactions anodiques et cathodiques responsables de la corrosion. Les composés organiques riches en hétéroatomes (azote, soufre, oxygène) sont particulièrement efficaces grâce à leurs interactions spécifiques avec la surface métallique.

Dans ce contexte, le présent travail vise à évaluer l'efficacité de nouveaux composés organiques riches en azote comme inhibiteurs de corrosion de l'acier au carbone en milieu acide chlorhydrique 1 M. Deux familles de molécules ont été étudiées : une molécule dérivée de la triazole (5-hexylsulfanyl-1,2,4-triazole, notée HST) et deux nouvelles molécules dérivées de l'hydrazone, l'une à base de noyau furanne (NFH), l'autre à base de noyau thiophène (NTH). Ces structures ont été sélectionnées pour l'abondance de centres donneurs d'électrons (groupes amine, azométhine, hétérocycles), susceptibles de favoriser une forte adsorption sur la surface de l'acier et une bonne inhibition.

Le mémoire est structuré en quatre chapitres :

- ✓ **Le premier chapitre** propose une synthèse bibliographique sur la corrosion : définitions, mécanismes, formes, cinétique, thermodynamique, corrosion en milieux aqueux et acides, ainsi qu'une revue des méthodes de protection, avec un accent particulier sur les inhibiteurs organiques riches en azote.
- ✓ **Le deuxième chapitre** présente une description des méthodes utilisées, techniques et protocoles expérimentaux : gravimétrie, techniques électrochimiques (polarisation potentiodynamique PDP, spectroscopie d'impédance électrochimique EIS), caractérisations de surface (microscopie électronique à balayage SEM couplée à l'analyse EDX, diffraction des rayons X). Ce chapitre décrit également la technique de simulation numérique et calculs quantiques permettant de modéliser l'évolution du système étudié (théorie de la fonctionnelle de la densité DFT, et simulations de dynamique moléculaire MD).

- ✓ **Les troisième et quatrième chapitre** exposent l'ensemble les résultats obtenus pour l'étude du composé triazolique (HST) puis des hydrazones (NFH et NTH).

Les résultats expérimentaux montrent que les trois composés étudiés possèdent une excellente capacité inhibitrice à une concentration optimale de 10^{-3} M. Le composé HST s'est révélé le plus performant avec une efficacité de 97 %, suivi par NTH (93 %) puis NFH (90 %). Les courbes de polarisation potentiodynamique ont indiqué que tous les inhibiteurs agissent en tant qu'inhibiteurs mixtes, ralentissant à la fois les réactions anodiques, dissolution du métal, et cathodiques, réduction des ions H^+. Les mesures EIS ont montré une augmentation significative de la résistance de transfert de charges (Rtc) en présence des inhibiteurs, traduisant une adsorption efficace et la formation de couches protectrices stables.

Les études de l'effet de température ont révélé une diminution progressive de l'efficacité inhibitrice avec l'augmentation de la température, sur la plage de 298K à 338K. À 338 K, l'efficacité de HST diminue à 89 %, celle de NTH à 77 %, et celle de NFH à 67 %, en raison de la désorption partielle des inhibiteurs à haute température. Cependant, les valeurs négatives de l'énergie libre d'adsorption ΔG_{ads} confirment que l'adsorption reste spontanée, où le chimisorption peut être dominante, bien qu'un certain degré de physisorption soit également impliqué.

Les analyses de surface par SEM-EDX et DRX ont confirmé la présence d'une couche organique protectrice sur les échantillons traités avec les inhibiteurs. La surface de l'acier est nettement moins endommagée en présence des inhibiteurs, et l'analyse élémentaire EDX a révélé la présence d'atomes d'azote, d'oxygène et de soufre, témoignant de l'adsorption des molécules organiques à la surface.

Les calculs théoriques ont conforté les résultats expérimentaux. L'analyse DFT a permis de visualiser les orbitales frontières (HOMO–LUMO), d'évaluer les descripteurs globaux (dureté, électronégativité, potentiel chimique) ainsi que les sites réactifs locaux via les fonctions de Fukui. Ces analyses ont identifié les hétéroatomes (N, S, O) comme principaux centres d'interaction avec le métal. Les simulations de dynamique moléculaire sur la surface Fe(110) ont montré que les trois molécules s'adsorbent préférentiellement selon une configuration parallèle au plan métallique, ce qui maximise l'interaction inhibiteur–surface. Le groupement thiophène dans la molécule NTH favorise des interactions π–d orbitales plus intenses, expliquant sa meilleure performance relative à NFH.

L’étude comparative des deux familles révèle que les hydrazones, en raison de leur taille moléculaire plus importante, peuvent offrir une meilleure couverture de surface. Toutefois, leur efficacité est plus sensible à l’élévation de la température, probablement en raison de la nature peu stable de leur adsorption. Malgré leurs différences structurales, les trois composés partagent des caractéristiques favorables à l’inhibition : structures riches en électrons, présence d’hétéroatomes, planéité partielle permettant une forte interaction avec la surface métallique.

En conclusion, cette étude a permis de démontrer que les dérivés de triazole et d’hydrazone étudiés constituent des inhibiteurs prometteurs pour la protection de l’acier au carbone en milieu acide. Leur efficacité résulte d’un mécanisme d’adsorption mixte, appuyé par des interactions chimiques et physiques avec la surface du métal. L’approche combinée, alliant techniques électrochimiques, analyses de surface et modélisation théorique, a permis de mieux comprendre les relations structure–activité de ces inhibiteurs.

Sur la base de ces résultats expérimentaux et théoriques intégrés, plusieurs perspectives de recherche et de valorisation industrielle sont envisagées. En laboratoire, une piste prometteuse consistera à étudier les effets synergiques potentiels entre les trois inhibiteurs (HST, NFH et NTH) par formulation de mélanges optimisés, capables d’augmenter la protection tout en réduisant la concentration totale nécessaire. Cette optimisation pourrait être conduite via une approche de plans d’expériences systématiques visant à identifier les combinaisons les plus performantes, même dans des conditions plus sévères. Parallèlement, le champ d’application de ces composés peut être élargi à d’autres matériaux métalliques tels que l’aluminium ou des alliages couramment utilisés dans l’industrie, ainsi qu’à d’autres milieux corrosifs comme l’acide sulfurique, l’acide phosphorique ou des environnements alcalins. De telles études permettraient d’évaluer la polyvalence des inhibiteurs et de mieux comprendre leur comportement sous différentes contraintes chimiques.

Du point de vue industriel, une phase de validation à l’échelle pilote mérite d’être envisagée, consistant à faire circuler des solutions d’HCl 1 M inhibées à travers des conduites ou échangeurs thermiques en conditions réelles d’exploitation. La stabilité des formulations inhibitrices serait simultanément testée pour garantir une durée de conservation suffisante, assurant leur praticité en stockage et transport. Une étude économique comparant les coûts de production aux économies opérationnelles (réduction de la maintenance, des arrêts de production et des remplacements de composants dus à la corrosion) permettrait de renforcer la faisabilité industrielle. Enfin, les considérations environnementales et réglementaires seraient prises en compte à travers des évaluations toxicologiques conformes aux standards REACH, une analyse du cycle de vie pour confirmer la biodégradabilité, et l'exploration d'options de production locale afin d'assurer une démarche alignée sur les critères de sécurité, de durabilité et de rentabilité.

Ainsi, cette étude met en évidence l'efficacité des composés HST, NFH et NTH comme inhibiteurs de corrosion de l'acier au carbone dans HCl 1 M, contribuant ainsi au développement de solutions innovantes, performantes et respectueuses de l'environnement pour la protection de l'acier au carbone contre la corrosion acide, et ouvre par ailleurs la voie à de nombreuses possibilités d'optimisation et d'application industrielle, en conciliant performance technique, viabilité économique et responsabilité environnementale.

List of figures

List of tables

List of Acronyms

AC: Alternating Current

AFM: Atomic Force Microscopy

AMPP: Association for Materials Protection and Performance

ASTM : American Society for Testing and Materials

BTBA: Tetrabutylammonium bromide

CAGR: Compound Annual Growth Rate

CE: Counter Electrode

CEFRACOR : Centre Français de l'Anticorrosion

COMPASS: Condensed-phase Optimized Molecular Potentials for Atomistic Simulation Studies

CorrISA: Corrosion Institute of South Africa

COSMO: Conductor-like Screening Model

COSMO-RS: Conductor-like Screening Model for Real Solvents

CPE: Constant Phase Element

CS: carbon steel

CuAAC: copper(I)-catalyzed azide-alkyne cycloaddition

CV : Cyclic Voltammetry

DFT: density functional theory

DNP: Double Numerical plus Polarization

EFSA: European Food Safety Authority

EIS: Electrochemical Impedance Spectroscopy

EN : Electrochemical Noise

EW: Equivalent weight

FMO: Frontier Molecular Orbital

GDP : Gross Domestic Product

GGA: Generalized Gradient Approximation

HOMO-LUMO : Highest Occupied Molecular Orbital–Lowest Unoccupied Molecular Orbital

HST: 5-hexylsulfanyl-1,2,4-triazole

ISO: the International Organization for Standardization

IUPAC: The International Union of Pure and Applied Chemistry

MD: Molecular Dynamics

MS: mild steel

NACE: National Association of Corrosion Engineers

NF: Norme Française

NFH: N´-[(E)-furan-2-ylmethylidene]− 2-(6-methoxynaphthalen-2-yl)propane- hydrazide

NSAIDs: Nonsteroidal anti-inflammatory drugs

NTH: 2-(6-methoxynaphthalen-2-yl)-N´-[(E)-thiophen-2-ylmethylidene]propanehydrazide

NVT/NPT : Numbers of particles, Volume, Temperature, Pressure are constant

OCP: Open-Circuit Potential

ODA: octadecylamine

OM: optical microscopy

PBE: Perdew–Burke–Ernzerhof

PDP: Potentiodynamic Polarization

PZC: Potential of Zero Charge

RE: Reference Electrode

REACH: Registration, Evaluation, Authorization and Restriction of Chemicals

SCE: Saturated Calomel Electrode

SEM/EDX: Scanning Electron Microscopy/ Energy Dispersive X-ray Spectroscopy

TDMs: triazole derivative metabolites

WE: Working Electrode

Wt: Weight

XPS: X-ray Photoelectron Spectroscopy

XRD: X-ray diffraction

Table of contents

General introduction

Corrosion, or the gradual deterioration of metals caused by chemical or electrochemical interactions with their environment, poses a significant threat to the integrity and lifetime of materials in various industrial contexts. It is an unavoidable and spontaneous phenomenon caused by metals' inclination to return to their thermodynamically stable, oxidized forms, such as oxides, hydroxides, carbonates, or sulfides [1]. Although the production of corrosion products such as oxides might provide limited protection in certain cases, corrosion is mainly regarded as a harmful process that jeopardizes both structural and functional integrity [2]. The implications are numerous, ranging from economic losses and environmental degradation to potential hazards to human safety and disruptions to industrial operations.

Globally, the economic cost of corrosion is significant, accounting for around 2.5 trillion USD, or almost 3.4% of global GDP [3]. The problem impacts almost every industry, including oil and gas, construction, maritime, transportation, and aerospace. Corrosion in important applications, such as offshore platforms and pipelines, increases operating hazards and maintenance costs. Offshore steel buildings, for example, have direct corrosion costs estimated at 1.39 to 1.50 trillion USD per year [3]. Furthermore, corrosion in acidic environments, commonly encountered in cleaning, descaling, and well acidizing operations, has emerged as a serious worry due to the strong chemical conditions involved.

Among the metals used in industrial applications, carbon steel is particularly vulnerable to corrosion, yet it remains the most widely employed material due to its favorable balance of mechanical properties, availability, and cost. It is especially prevalent in infrastructure, pipelines, pressure vessels, and equipment used in the petroleum, chemical, and manufacturing sectors [4]. Nevertheless, its sensitivity to deterioration in corrosive media, particularly acidic solutions, requires preventive methods to retain performance and prolong service life.

Hydrochloric acid (HCl) is one of the most commonly used acids in various industrial processes, including acid cleaning, pickling, and oil well stimulation techniques such as matrix acidizing and mud filter cake removal [5,6]. In many of these applications, strong HCl solutions, often ranging from 15 to 20 wt.%, are used, creating very corrosive conditions for steel components [4,7–9]. However, in laboratory investigations, 1 M HCl is often used as a standardized and representative test medium. Its reproducibility, the ability to perform studies under controlled and repeated conditions, makes it excellent for accurately measuring metal corrosion behavior and inhibitor efficacy. As a result, 1 M HCl is used as a starting point in corrosion research, allowing for an initial assessment of inhibitory performance before moving on to experiments under more aggressive, real-world circumstances that simulate industrial concentrations.

To counteract corrosion in such settings, a variety of protective measures have been developed. Among them, the use of organic corrosion inhibitors is renowned for its practicality, cost-effectiveness, and versatility. These compounds generally function by adsorbing onto the metal surface, establishing a barrier that prevents corrosive chemicals from gaining access and interrupting anodic and cathodic processes. Effective inhibitors often include heteroatoms like nitrogen, sulfur, and oxygen, which promote adsorption by electron donation or π-interactions with the metal substrate [6]. As a result, several nitrogen-containing organic compounds, such as imidazolines, Mannich bases, and quaternary ammonium salts, have been researched and used to limit corrosion, notably in the oil and gas industry.

Among these classes of compounds, triazoles and hydrazones have lately received attention for their promising inhibitory performance, structural versatility, and potential for environmental friendliness. Triazoles, specifically derivatives of the 1,2,4-triazole isomer, are known for their high adsorption and film-forming properties, which contribute to their protective effectiveness on steel surfaces [10]. Hydrazones, on the other hand, are Schiff base derivatives distinguished by their C=N-NH- moiety. They include lone pairs on nitrogen atoms, allowing them to function as potent chelating agents and surface-active chemicals in corrosion inhibition [11]. Both triazoles and hydrazones have the ability to tune their inhibitory action by functional group modification, increasing their potential as sustainable alternatives to conventional inhibitors. Furthermore, these compounds are accessible to theoretical modeling and electrochemical characterization, which allows for a better understanding of their inhibitory mechanisms.

Given this framework, the current study seeks to investigate the mitigation of carbon steel corrosion in thev1 M HCl medium with organic nitrogen-containing compounds, specifically triazoles and hydrazones. The work is driven by both practical and scientific reasons, including the ubiquitous use of carbon steel in industry, the importance of acid corrosion conditions, and the promising inhibitory performance of these compounds. This research also continues a line of investigation developed within our laboratory, which has extensively studied corrosion phenomena and the evaluation of organic inhibitors in acidic media.[12–21].

To accomplish this objective, and in addition to the general introduction and the general conclusion, the thesis is structured into four chapters:

- ✓ The first chapter provides a bibliographic overview of corrosion, including its types and forms, mechanisms, and problems in acidic environments. It also gives an overview of current corrosion prevention strategies, focusing on the employment of organic inhibitors, mainly nitrogen-containing compounds.
- ✓ Chapter 2 outlines the experimental approaches used in this study, including solution preparation, surface characterization techniques, electrochemical testing protocols, as well as theoretical methods.
- ✓ Chapters 3 and 4 give the findings and analysis of the corrosion inhibition performance of two families of organic compounds, triazoles and hydrazones, on carbon steel in 1 M HCl. To understand the inhibitory mechanisms, stationary and transient electrochemical methods are employed in conjunction with surface characterization techniques and theoretical computations.

Chapter 1: Bibliographic synthesis and problem positioning

1.1 General points on corrosion

Multiple authoritative definitions of the term corrosion are available. The International Union of Pure and Applied Chemistry (IUPAC) defines corrosion as “an irreversible interfacial reaction between a substance (metal, ceramic, polymer…) and its environment, leading to the degradation of the material”[22]. Corrosion frequently, though not invariably, leads to adverse impacts on the material’s usability. The international standard (ISO 8044: 2024) similarly defines corrosion of metals as “the chemical or electrochemical interaction between a material and its environment, which can lead to deterioration of material properties, the environment, or the function of the system containing the material” [23].

Upon exposure to their natural environment, most metals undergo spontaneous surface oxidation. The corrosion behavior of a metal is intricately associated with the environment in which it is situated. In natural environments, the primary corrosive agents include air, water, and different atmospheric constituents. Corrosion can be categorized into many forms based on its underlying cause, including chemical, electrochemical, bacterial/biological, and erosion-corrosion. The resulting products may manifest in solid, liquid, or gaseous forms.

Each type of corrosion occurs through specific mechanisms and under particular conditions. Nonetheless, apart from their chemical, electrochemical, bacterial, or mechanical nature, these types of corrosion can manifest in various forms of metal deterioration. Among the various forms of corrosion, generalized or uniform corrosion is the most prevalent kind of corrosion. It is characterized by a homogeneous attack on the metal surface, where its dissolution and oxygen reduction are statistically distributed. This leads to an even degradation of the material and a uniform formation of corrosion products, such as red rust on steel. The severity or extent of this corrosion can be assessed through mass loss (mg/dm^2/year) or thickness reduction (mm/year). Conversely, localized corrosion affects only specific areas of the metal exposed to a corrosive environment. It generally results from heterogeneities within the metal, the surrounding medium, or the physico-chemical conditions at the surface. Localized corrosion can be categorized into macroscopic forms, such as galvanic corrosion, crevice corrosion, and pitting corrosion, and microscopic forms, including selective corrosion, stress corrosion, intergranular corrosion, and hydrogen embrittlement.

It should be noted that this thesis focuses primarily on the electrochemical aspect of uniform corrosion of mild steel in 1M HCl acidic medium, as well as the effectiveness of certain compounds in corrosion prevention.

Wet corrosion is an electrochemical process involving the metal and dissolved species in an aqueous solution (the electrolyte). As a redox reaction, corrosion consists of two half-reactions: the anodic oxidation of the metal (Reaction 1) and the cathodic reduction of another species. The primary/predominant cathodic reaction involves oxygen reduction, which takes place at neutral to alkaline pH (Reaction 2.1), and under acidic conditions (Reaction 2.2), as well as the reduction of hydrogen ions in acidic media (Reaction 2.3)[24] :

$$M \rightarrow M^{2+} + 2e^{-} \tag{1}$$

$$O_2 + 2\,H_2O + 4e^{-} \rightarrow 4(OH)^{-} \tag{2.1}$$

$$O_2 + 4\,H^{+} + 4e^{-} \rightarrow 2\,H_2O \tag{2.2}$$

$$2\,H^{+} + 2e^{-} \rightarrow H_2 \tag{2.3}$$

Typically, one or more cathodic processes may transpire depending on the environmental parameters surrounding the metal. The corrosion reaction for an iron substrate process is illustrated in Figure 1.1.

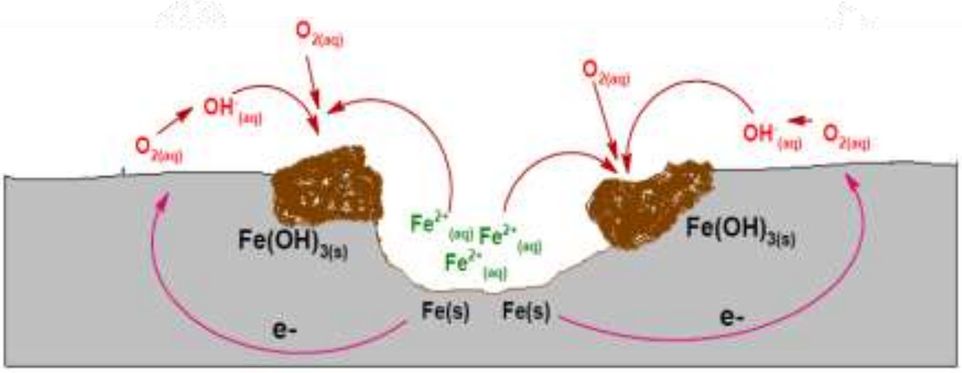

***Figure 1.1**: Electrochemical corrosion of iron in an aqueous environment*

Pourbaix diagrams are utilized to illustrate the thermodynamically favored processes of a particular metal in a defined environment, hence predicting the metal's state under varying pH and potential conditions. However, these diagrams do not convey information regarding the kinetics of the involved processes. The Pourbaix diagram for iron in aqueous solutions at 25°C is represented in Figure 1.2.

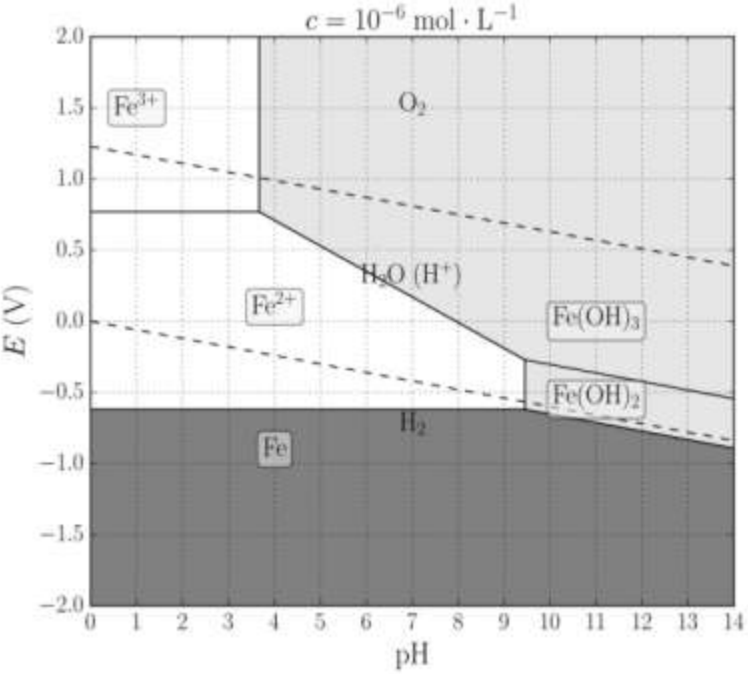

***Figure 1.2**: Simplified E-pH diagram for Fe/H_2O (T=25°C, P=1atm)* [25]

At a concentration of 10^{-6} *M*, the stability domain of water and iron immunity do not overlap, making their coexistence thermodynamically impossible. On the potential-pH diagram, three distinct regions can be identified. The immunity domain, when the metal potential (relative to a reference electrode) falls within the region where it is thermodynamically stable, remains protected from corrosion. This range of potential and pH defines the metal's immunity domain in the solution. The active corrosion domain, if the metal potential lies in a region where its corrosion products are soluble, dissolution continues until equilibrium is reached. Depending on the pH, this corrosion can be either acidic or basic. The passivation domain, when the corrosion products are solid species, such as oxides or hydroxides in various hydrated forms, they can form a protective layer on the metal surface. This layer limits interaction with the solution, thereby reducing corrosion and promoting metal passivation. However, only certain oxides, due to their compact and adherent nature, provide effective protection, whereas hydroxides, generally porous, are often indicative of ongoing corrosion.

The examination of electrochemical kinetics facilitates the assessment of the rate of a redox reaction and the measurement of its kinetic properties [26]. The rate of a chemical reaction is often described as the quantity of moles of atoms reacting per unit time and electrode surface area. Nonetheless, this amount can pose difficulties in direct measurement. Faraday's law estimates the corrosion reaction rate, according to the equation below, which is directly related to the corrosion current density [26].

$$i_{corr} = -n.F.\frac{1}{S}.\frac{dn_{Fe}}{dt} = n.F.v_{corr} \leftrightarrow v_{corr} = \frac{i_{corr}}{n.F} \qquad 3$$

In this context, n denotes the quantity of electrons participating in the redox reaction, while F signifies Faraday's constant (96485 C/mol). The corrosion rate can be regulated through various mechanisms, primarily charge transfer at the metal-solution interface (as observed in acidic corrosion of steel), mass transport of the oxidant or corrosion products (as seen in neutral aerated environments), or a combination of both phenomena [25]. The corrosion rate is affected by several critical factors, including the agitation or stagnation of the medium, where agitation disperses reactive species and inhibits the formation of a protective layer deposit on the metal; the heterogeneity of the metal and environment, where elements such as surface composition, pH, and dissolved oxygen concentration influence corrosion behavior; temperature, as elevated temperatures typically expedite corrosion; and the renewal or stagnation of the medium, as continuous renewal introduces corrosive agents, while stagnation permits their consumption, potentially resulting in equilibrium.

1.2 Steel: definition and classification

The definition and categorization of steel vary depending on the standard used. Two key references in this regard are ISO 4948-1 and NF EN 10020, which provide structured approaches to categorizing steel based on its composition and properties. ISO 4948-1:1982 (currently still under development to become ISO/AWI 4948-1) defines steel as an iron-based alloy with a carbon content not exceeding 2.0%, a standard also recognized in NF EN 10020 [27,28]. Nevertheless, their classification methodologies diverge. ISO 4948-1 categorizes steel largely by its chemical composition, differentiating between unalloyed (non-alloy) steels and alloy steels, without additional subdivisions. Conversely, NF EN 10020 offers a more comprehensive classification by delineating three primary categories: non-alloy steels, stainless steels, and other alloy steels. Moreover, NF EN 10020 categorizes non-alloy steels into quality steels and special steels according to their designated applications and characteristics. Non-alloy quality steels are utilized in broad structural applications and are not bound by rigorous mechanical or chemical property specifications. Examples encompass construction steels and steels utilized in the fabrication of fundamental components. Non-Alloy Special Steels: These steels possess more stringent criteria for purity, mechanical characteristics, or suitability for heat treatment. They are frequently utilized in engineering and automotive applications, where enhanced mechanical properties are required. ISO 4948-1 provides a general classification, but NF EN 10020 gives a more detailed methodology, rendering it especially beneficial for application-specific classification within the European industry.

Building on the general classification of steel, one important category that warrants attention is **carbon steel**. Carbon steel, which contains varying amounts of carbon as its primary alloying element, is further categorized based on the carbon content, affecting its properties and applications. It has a wide application throughout numerous sectors, including construction, electrical systems, transportation, industrial facilities, pipelines for gas and petroleum, thermal systems, hydraulic circuits, and information technology and electronics. Approximately 85% of steel production comprises carbon steel [25], characterized by its affordability, accessibility, high tensile strength, and durability, it is the most prevalent variety utilized in various industries. Carbon steel is commonly utilized in the construction of vessels for aggressive solutions, including acidic and basic solutions, saline solutions, and reagents for reactions, particularly tanks for managing corrosive liquids. Acids such as hydrochloric acid, acetic acid, and sulfuric acid, frequently used in the pickling process, are also vital in petrochemical activities like drilling, fracturing, and acid stimulation in oil exploration [29]. Carbon steels, despite their superior thermal and mechanical qualities, exhibit weak corrosion resistance. This has prompted significant research and development of protective techniques for carbon steel. Notwithstanding the widespread usage of carbon steel and its superior mechanical and thermal qualities, its inadequate corrosion resistance in hostile conditions continues to be a considerable concern, particularly in industrial applications involving acidic solutions. This problem caused reduced lifespans for steel structures, resulting in technical, economic, environmental, and societal issues [30]. The increasing apprehension regarding carbon steel's vulnerability to corrosion is especially pronounced in sectors such as oil extraction and metal pickling, where carbon steel frequently interacts with potent acidic solutions. Consequently, researchers are concentrating on devising corrosion prevention techniques to prolong the lifespan of this extensively utilized material [29,30].

1.3 Steel corrosion

Corrosion is the adverse, localized electrochemical process that occurs when a metal surface interacts with a corrosive environment, such as seawater, acids, etc. In structural steel, mostly composed of iron, this reaction can be regarded as the oxidation of iron and the reduction of other existing species. The oxidation reaction results in the generation of soluble iron cations, hence dissolving the metal. The precipitation of iron salts occurs when the concentration of the iron cation and its corresponding anion surpasses the solubility product of the mineral. An iron hydroxide/oxide layer, generally referred to as rust, typically forms on the surface of steel.

The fundamental electrochemical principles are the anodic reaction: the oxidation of the metal, for instance,

$$Fe \rightarrow Fe^{2+} + 2e^{-} \qquad 4$$

And the cathodic (reduction) reaction: the electrons generated by the anodic reaction are utilized, as previously discussed. The following reactions are reiterated here for clarity,

$$O_2 + 2\,H_2O + 4e^{-} \rightarrow 4(OH)^{-} \qquad 2.1$$

$$O_2 + 4\,H^{+} + 4e^{-} \rightarrow 2\,H_2O \qquad 2.2$$

$$2\,H^{+} + 2e^{-} \rightarrow H_2 \qquad 2.3$$

While Reaction (2.1) illustrates the predominant reaction at neutral pH, Reactions (2.2) and (2.3) are significant for specific industrial processes under acidic circumstances.
Hydrolysis of iron cations Fe^{2+} can transpire in solution, and this process leads to the formation of iron hydroxide $Fe(OH)_2$ and the release of protons H^+ , which create localized acid sites on the metal surface, according to the reaction :

$$Fe^{2+} + 2H_2O \rightarrow Fe(OH)_2 + 2\,H^{+} \qquad 5$$

These sites create an electrochemical cell on the steel surface, featuring localized anodic and cathodic sites, each corresponding to a half-reaction or half-cell. These reactions contribute to the development of small corrosion pits. The positioning of these sites is contingent upon the particular system, and positions may vary over time over a certain surface.

This phenomenon is well depicted in Figure 1.3. It showcases an iron surface in contact with an aqueous electrolyte of neutral or alkaline pH. The processes encompass the dissolution of metal at the anodic site, where metal cations are generated through oxidation and solubilized by the electrolyte medium, alongside the transfer of electrons produced at the anodic site to the cathodic site, where they facilitate the reduction of oxygen and water to yield hydroxide. Dissolved metal ions may react with other species, such as $\mathrm{OH^-}/\mathrm{H_2O}$, to produce $\mathrm{Fe(OH)_2}$ and hydrated ferric oxide, $\mathrm{Fe_2O_3.xH_2O}$ generally referred to as rust, according to [3]:

$$Fe^{2+} + 2OH^- \rightarrow Fe(OH)_2\,(s) \qquad 6$$

$$2Fe(OH)_2\,(s) + (x-1)H_2O \rightarrow Fe_2O_3.xH_2O\,(s) + 2\,H^+ + 2\,e^- \qquad 7$$

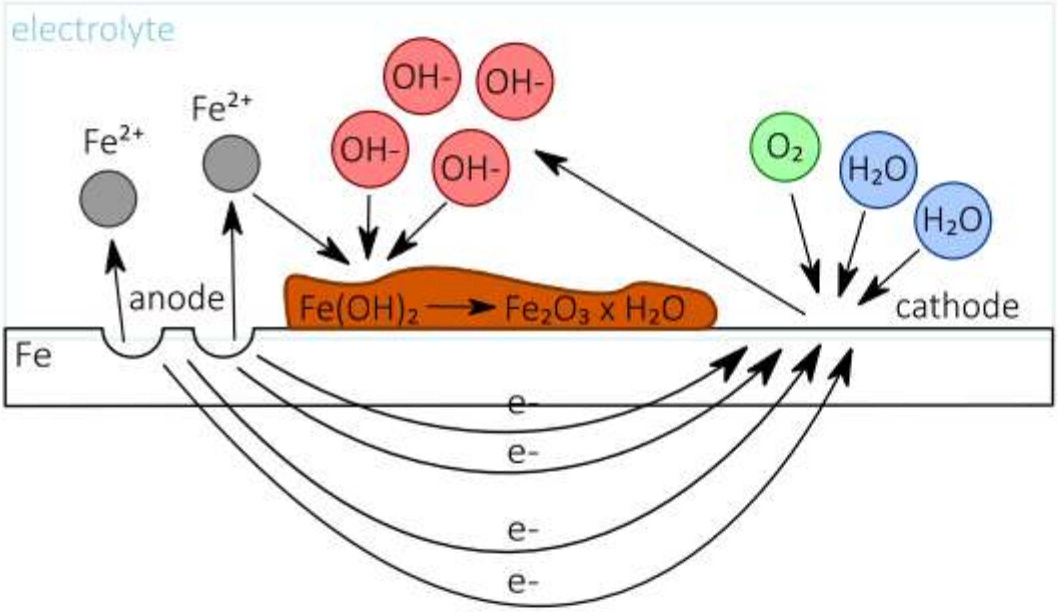

***Figure 1.3** : Schematic representation of an iron surface interacting with a neutral or alkaline electrolyte, illustrating iron dissolution at the anode, the reduction process at the cathode producing OH^-, and the reaction of dissolved Fe^{2+} with H_2O/OH^-, ultimately resulting in rust formation on the surface. [3]*

It is worth mentioning that the precise characteristics of the oxide film developed on iron and steel surfaces are more intricate than previously described and have been thoroughly investigated. It consists of a combination of iron hydroxides and oxides, including different phases of Fe_2O_3 and Fe_3O_4 [3]. Comprehensive studies indicate that iron hydroxide $Fe(OH)_2$ is effortlessly oxidized by dissolved oxygen, resulting in the formation of intermediate

Fe(II)-Fe(III) compounds, including green rust and magnetite. The green rust products are bluish-green Fe(II)-Fe(III) compounds that incorporate anions such as chlorides, carbonates, or sulfate ions. Magnetite, a mixed Fe(II)-Fe(III) iron oxide $(Fe.Fe_2O_3)$, is an ubiquitous corrosion result seen in archeological iron [31] .

Iron (II) hydroxide is susceptible to oxidation, resulting in the formation of iron (III) compounds, including $Fe(OH)_3$or iron oxyhydroxides such as $FeOOH$. Freshly precipitated $Fe(OH)_3$ is amorphous but gradually transforms into a crystalline form, typically one of the irons oxyhydroxides. $\gamma - FeOOH$, known as lepidocrocite, generally forms first but can convert into the more thermodynamically stable goethite, $\alpha - FeOOH$ [31]. In the presence of Cl^-, the iron oxyhydroxide akageneite, $\beta - FeOOH$, may develop [31]. These corrosion products typically manifest as two layers on the iron surface. The innermost layer, adjacent to the metal, contains iron compounds in a reduced oxidation state, such as magnetite Fe_3O_4. The outer layer consists of iron oxyhydroxides in higher oxidation states, including goethite and lepidocrocite. These corrosion product layers may reduce or delay the corrosion rate of iron associated with the initial corrosion process [31].

In the industrial sector, steels endure various pressures associated with using acid solutions like HCl, H_2SO_4, H_3PO_4, HNO3, etc. resulting in corrosion, the mitigation of which poses a significant and intricate issue [25]. The corrosion of mild steel in acidic settings is caused by the simultaneous occurrence of cathodic (reduction) processes and anodic (oxidation) metal dissolution reactions (Figure 1.4). In acidic aqueous conditions, the predominant anodic process is iron dissolution:

$$Fe\ (s) \rightarrow \ Fe^{2+}(aq) + 2e^- \qquad 4$$

where Fe(s) denotes the iron atom relinquishing two electrons to form a 2^+ ion. In acidic conditions, the electrons emitted by Fe are efficiently utilized to decrease the hydrogen ions present in the solution. These hydrogen ions are consumed as:

$$2\,H^+(aq) + \ 2e^- \ \rightarrow \ \ H_2\ (g) \qquad 2.3$$

The areas of the steel surface where these two reactions occur do not necessarily need to coincide spatially, owing to the electrolytic and electrical interaction between them [32]. For each of these half-reactions, based on the Nernst equation, the two formulas for the electrode potential can be established as follows:

$$E_{(Fe/Fe^{2+})} = E_0 - 2.303\,\frac{RT}{2F}\,log\frac{1}{[Fe^{2+}]} \qquad 8$$

$E_{(Fe/Fe^{2+})}$denotes the reaction potential in relation to the standard electrode potential, E_0, as provided in standard reference tables with respect to the standard hydrogen electrode. Likewise, for the reduction of hydrogen ions

$$E_{(H^+/H_2)} = E_0 + 2.303\,\frac{RT}{F}\,log[H^+] \qquad 9$$

Absolute half-cell potentials cannot be directly measured; however, electrode potentials can be ascertained to a reference electrode, such as the standard hydrogen electrode (SHE), which comprises a platinum electrode in an acidic solution subjected to a hydrogen gas stream. Under standard conditions (with hydrogen ion activity at 1 and hydrogen gas pressure at 1 atm), the Standard Hydrogen Electrode (SHE) is assigned a potential of zero volts. The potential of a metal electrode measured against the Standard Hydrogen Electrode (SHE) under standard conditions expresses its standard electrode potential, facilitating the establishment of the electrochemical series. A lower standard electrode potential signifies a greater propensity for the metal to undergo oxidation, rendering it more anodic and reactive, whereas higher values suggest a diminished susceptibility for oxidation, categorizing the metal as noble[3].

For instance, iron possesses a standard electrode potential of $E^0_{(Fe/Fe^{2+})} = -0.44V$, indicating a propensity for corrosion in aqueous conditions where oxidizing agents such as the hydrogen evolution reaction $E^0_{(H^+/H_2)} = 0V$ or the oxygen reduction reaction $E^0_{(O_2/H_2O)} = 1.229V$ in acidic media can facilitate its dissolution.

The propensity of a metal to experience oxidation may be assessed using its standard electrode potential, measured relative to the standard hydrogen electrode under controlled conditions. However, when a material is immersed in a specific environment, it acquires a potential called the corrosion potential E_{corr}, which depends on the interaction between the metal and its surroundings. At this potential, the anodic current associated with the oxidation of the metal i_{anod} is counterbalanced by the cathodic current i_{cath} from the reduction processes in the medium, defining the current of corrosion i_{corr}. $i_{anod} = - i_{cath} = i_{corr}$. In contrast to standard electrode potentials, E_{corr} is not an inherent characteristic of the metal; rather, it fluctuates based on experimental conditions, including reagent concentration and temperature. Observing its progression yields essential insights into corrosion kinetics and morphology, aiding in the evaluation of material degradation in practical conditions [25,33].

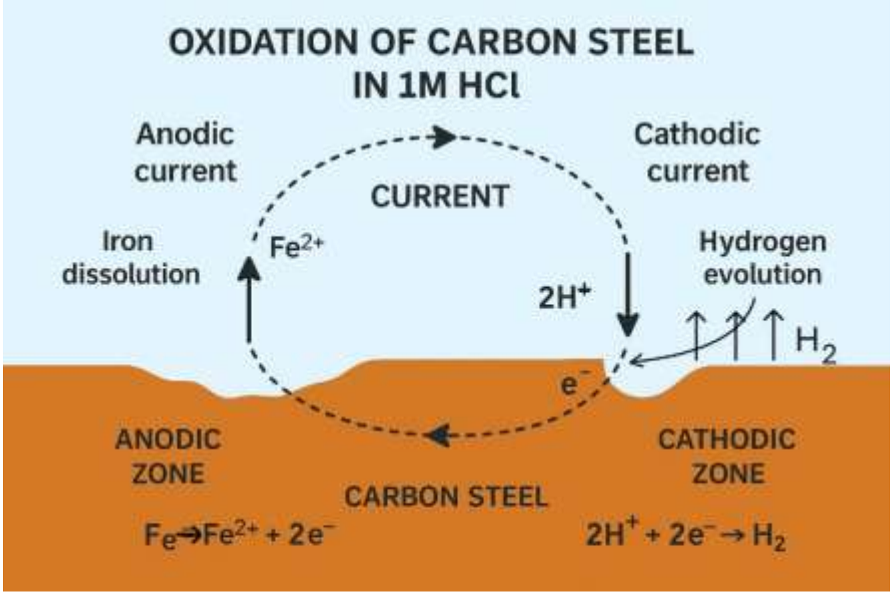

***Figure 1.4**: A Schematic depicting the dissolving mechanism of iron in an acidic medium.*

In acidic conditions such as 1M HCl, Cl^- ions significantly enhance the dissolution of carbon steel by adsorbing onto the surface and weakening the protective oxide layer. The presence of anions such as NO_3^-, Cl^-, and SO_4^{2-} is crucial for interpreting the observed phenomena. The prevailing process for the electro-dissolution of iron, concerning anions adsorbed on the surface, is proposed as follows:

$$Fe + H_2O \leftrightarrow Fe\,(H_2O)_{ads} \qquad 10$$

$$Fe\,(H_2O)_{ads} \leftrightarrow FeOH^-{}_{ads} + H^+ \qquad 11$$

$$FeOH^-{}_{ads} \leftrightarrow Fe(OH)_{ads} + e^- \qquad 12$$

$$Fe(OH)_{ads} \leftrightarrow FeOH^+ + e^- \qquad 13$$

$$FeOH^+ + H^+ \leftrightarrow Fe^{2+} + H_2O \qquad 14$$

Bockris [34], by examining the influence of common anions on the dissolving rate of iron as a function of potential at constant pH and fixed [Fe^{2+}] concentration, successfully categorized these anions based on their adsorption capacity in the following sequence:

$$ClO_4{}^- > SO_4{}^{2-} > Cl^- > CH_3COO^- > NO_3{}^-$$

The findings indicate that the actions of various anions, excluding NO_3^-, align with a paradigm wherein the particular adsorption of the anion alters the accessible surface area for ion/metal exchange. In certain instances, it has been demonstrated that SO_4^{2-} ions enhance the porosity of deposits and facilitate the cycle of sulfate-reducing bacteria, hence promoting bacterial corrosion [34].

Passivation is a chemical or electrochemical process that improves the corrosion resistance of metals and alloys by creating a protective oxide or hydroxide layer on their surfaces. This layer serves as a barrier, diminishing interaction between the metal and its surroundings, thereby retarding corrosion. Numerous metals, including aluminum, stainless steel, and copper, inherently form stable and adhering passive films when exposed to air or water. These films, composed of insoluble or slowly dissolving oxides and hydroxides, are dense, continuous, and protective, substantially restricting the dissolution of metal ions into the surrounding environment [33]. In contrast, carbon steel fails to naturally form a stable passive layer owing to its detrimental interior chemistry. Instead, it experiences fast oxidation and corrosion, rendering conventional passivation techniques ineffective. Alternative methods, like protective coatings, inhibitors, or alloying with elements such as chromium, are frequently essential to enhance corrosion resistance. The efficacy of passivation is dependent upon material characteristics and ambient factors. The chemical composition of the metal or alloy, the presence of supplementary elements, surface structure, and microstructure, as well as the chemical and mechanical state of the surface, are pivotal factors. Environmental factors, such as pH, temperature, oxygen levels, and the presence of corrosive chemicals or microorganisms, affect the stability and protective characteristics of passive films [33]. In contrast to stainless steel, which comprises a minimum of 10.5% chromium and generates a self-repairing chromium oxide Cr_2O_3 layer, or aluminum and copper, which produce robust and adherent aluminum oxide Al_2O_3 and copper oxide Cu_2O layers, carbon steel predominantly forms magnetite Fe_3O_4 and hematite Fe_2O_3 during oxidation. Nonetheless, these iron oxides exhibit porosity, non-uniformity, and susceptibility to cracking, which diminishes their efficacy as protective barriers. Carbon steel is more susceptible to localized corrosion, particularly in harsh conditions with chlorides or acids.

Given its inability to passivate effectively, carbon steel requires alternative corrosion protection strategies. A prevalent method involves the utilization of protective coatings, including paints, polymeric films, or metallic coatings (e.g., galvanization with zinc or aluminization). Inhibitors are extensively utilized, especially in industrial settings where carbon steel is subjected to corrosive substances. These inhibitors may be anodic, cathodic, or mixed-type, functioning by adsorbing onto the metal surface to create a barrier that restricts electrochemical processes. Furthermore, altering the chemical composition of carbon steel by incorporating alloying elements like chromium, nickel, or molybdenum can enhance its corrosion resistance. Additional techniques encompass cathodic protection, utilizing an external sacrificial anode or imposed current to inhibit oxidation, and phosphating or bluing, which entail chemical treatments to improve surface stability. The choice of a suitable protective strategy is contingent upon the particular application, environmental exposure, and financial costs. A thorough discussion of protection methods against corrosion will be provided in the coming sections.

1.4 Cost of corrosion and industrial impact

The study of corrosion and its prevention is paramount due to its devastating impact on infrastructures, the environment, and human safety. Corrosion leads to catastrophic failures in energy, transportation, and manufacturing industries. Defined as the degradation of materials due to environmental interaction, its economic impact is immense, with losses estimated at 3% to 5% of a nation's GDP (gross domestic product), amounting to €1.3-1.4 trillion annually for offshore steel structures alone [3]. The total global cost of corrosion reaches approximately $2.5 trillion, equivalent to 3.4% of global GDP [2,35]. These costs stem from infrastructure maintenance, industrial downtimes, and accidents leading to fatalities and environmental disasters.

Across different regions, corrosion has significant financial consequences. In the United States alone, annual corrosion costs amount to $276 billion (3.1% of GDP), with transportation accounting for $29.7 billion, utilities $47.9 billion, and infrastructure $22.6 billion [2,35]. Similarly, in France, the "centre français de l'anticorrosion" (CEFRACOR) estimates corrosion-related economic losses at €28 billion annually [36]. In Africa, the problem is particularly severe, in South Africa corrosion-related asset failures account for 30% of infrastructure breakdowns, costing ZAR 130 billion ($7.5 billion or 4% of GDP); with indirect costs often three times higher than direct expenses; according to the corrosion institute of southern Africa (CorrISA) [37], an organization registered with the south African government that plays a crucial role in advancing corrosion knowledge and protection techniques within the country. Morocco also struggles with corrosion-related issues, while national assessments are scarce, older studies suggest that costs amount to 5% of GDP [38]. While specific accident reports linked to corrosion failures are limited in Morocco, infrastructure degradation in industrial zones and mining operations, such as the Draa Sfar mine in Marrakech, have raised concerns about structural instability [39]. Beyond economic, corrosion contributes to catastrophic failures that jeopardize human lives and environmental safety. Notable examples include the 1967 Ohio River bridge collapse caused by stress corrosion cracking, which resulted in over 60 fatalities and led to mandatory corrosion testing for civil infrastructure in the United States [35]. Similarly, the Genoa bridge collapse in 2018 killed 43 people when corroded steel cables weakened concrete stays during a storm. Notably, the bridge's designer raised concerns about corrosion risks as early as 1979. Other incidents include the 2021 Surfside condo collapse in Florida, where severe concrete deterioration and rebar corrosion contributed to 98 fatalities, and the 1992 Guadalajara pipeline explosion in Mexico that killed over 200 people and injured 1,500 due to corrosion-induced failures [35]. In December 1999, the oil tanker Erika broke in two off the coast of Brittany, France, spilling approximately 20,000 tons of heavy fuel oil. Investigations confirmed that corrosion had severely weakened the ship's structure, leading to its catastrophic failure. In one of the world's worst industrial accidents, a gas leak at a pesticide plant in Bhopal, India, led to over 15,000 deaths and thousands of long-term health effects. Corrosion of pipelines was identified as one of the contributing factors to this catastrophe.

It is well documented, as just mentioned, that steel corrosion significantly impacts bridges, pipelines, and industrial structures, increasing maintenance costs and failure risks. For concrete structures, the annual global repair and maintenance cost for corrosion-related damages reaches $2.5 trillion [40]. Moreover, the oil and gas sector incur massive losses due to corrosion, with the US petroleum sector spending $3.7 billion annually on maintenance and repairs. In the Niger Delta, corrosion is responsible for over 50% of oil spills, a detailed review on the subject [41] has found that 60-year-old pipelines have led to approximately 7,359 oil spills in 35 years, releasing over 3.1 million barrels of oil valued at $247.6 million. This translates to an average of over 600 spills annually, making Nigeria the global leader in spill accidents. The spills occur across land (6%), swamp (25%), and offshore environments (69%), causing significant damage to ecosystems and endangering wildlife, including 150 fish species. The economic cost of spillage is staggering, with losses exceeding $38 billion in 1978 alone. In comparison, they have found that the cost of corrosion control between 2004-2008 was far less, emphasizing that prevention is more cost-effective than remediation.

The World Steel Association, a prominent international trade body representing steel producers, national and regional steel industry associations, and steel research institutes, plays a pivotal role in the global steel industry by providing authoritative information on steel production, demand, forecasts, and industry trends. It is estimated that 890 metric tons of steel in 2023 were required solely to replace rusted materials [42]. The association highlights the need for sustainable protective methods to reduce this demand. Also, it forecasts that steel demand will grow by 0.4% in 2022 to 1,840.2 Mt, and by 2.2% in 2023 to 1,881.4 Mt. Its studies indicate that 25% of corrosion-related costs could be prevented by applying existing technology. Organizations like NACE (now AMPP) and CorrISA emphasize the importance of adopting Corrosion Management Systems (CMS), which have demonstrated significant efficacy in optimizing lifetime expenses while improving safety and environmental safeguards. For instance, CMS frameworks prioritize the incorporation of corrosion prevention within organizational policies, guarantee the availability of information at all organizational tiers, and engage leadership in decision-making processes. To lessen the cost burden of corrosion, it is crucial to prioritize research on regional impacts and invest in creative solutions.

To sum up, corrosion is still a silent yet devastating problem that needs to be addressed at this point by governments, businesses, and academic institutions. Comprehensive plans that combine cutting-edge technology with strong management systems can greatly lessen its effects while protecting vital resources around the globe.

1.5 Corrosion Protection Methods for Materials

Corrosion mitigation is essential for material protection, seeking to safeguard metallic structures against environmental damage. Diverse ways may be applied, either singularly or in tandem, to inhibit corrosion. These encompass sensible material selection, enhanced component design, use of coatings, electrochemical protection, and the implementation of corrosion inhibitors. The choice of materials is vital for corrosion resistance. Stainless steels are safeguarded by a naturally occurring, chromium-enriched passive oxide layer, typically measuring approximately 2 nm in thickness at ambient temperature. This layer markedly improves their resistance to corrosive conditions, especially in aerated or oxidizing media like nitric acid, organic acids (except formic and oxalic), and diverse aqueous solutions. Stainless steels should be disregarded in settings with hydracids (HCl, HBr, HF), oxidizing chlorides ($FeCl_3$, $CuCl_2$), seawater (particularly warm seawater), thiosulfates, or chlorides with oxygen under stress conditions [1]. Copper demonstrates commendable resistance in both cold and hot freshwater, as well as in deaerated and diluted non-oxidizing acids; however, it is unsuitable for use in oxidizing acids, ammonia and amines, hydrogen sulfide, sulfur, and sulfides, as well as in high-velocity water circulation environments prone to erosion-corrosion[1]. Brasses are

frequently utilized in condenser tubes, whilst cupronickels are used in pumping systems due to their reduced susceptibility to erosion-corrosion.
Optimizing the shape of components is another crucial preventive approach. The geometry of a structure can significantly influences its corrosion resistance. By designing parts to minimize crevices, enhance drainage, and reduce stress concentrations, the risk of localized corrosion can be lowered [3].

The application of coatings offers a robust defense against corrosion. Paint coatings establish a thin protective barrier on metal surfaces, inhibiting contact with corrosive substances and obstructing electrochemical reactions. These coatings typically comprise a binder (such as epoxy, urethane, or acrylic) for film formation, pigments for stabilization and protection (e.g., zinc powder, mica), and a solvent, which may be an organic volatile chemical or water. Multi-layer coatings are frequently employed, with each layer fulfilling a distinct purpose, such as enhancing adhesion or providing corrosion resistance[3]. Nevertheless, organic coatings are not completely impermeable to water, oxygen, and corrosive ions, potentially resulting in corrosion beneath the paint film and subsequent coating failure [3]. The efficacy of coatings is contingent upon surface preparation, especially for ferrous metals, where cleaning and stripping are essential for adequate adherence [43]. Metallic coatings offer enhanced protection via cathodic or anodic mechanisms. Noble metal coatings, like titanium on steel, function as cathodic barriers, whereas less noble coatings, such as zinc on steel (galvanization), offer sacrificial anodic protection. These coatings provide both corrosion protection and ornamental, wear-resistant properties.

Electrochemical protection techniques encompass cathodic and anodic protection. Cathodic protection reduces the electrode potential of the metal, inhibiting oxidation. The notion, initially noted by Sir H. Davy in 1824, was further advanced by H. Becquerel, who proposed employing zinc sheets to safeguard cast iron pipes [44]. This technique is commonly utilized in conjunction with coatings to diminish the current density necessary for protection and to mitigate localized corrosion issues, including stress corrosion cracking and corrosion fatigue. Cathodic protection must be meticulously implemented, since it may induce hydrogen embrittlement in specific alloys[3]. Anodic protection is employed for materials capable of forming a stable passive layer when held at an optimal voltage. This approach is especially appropriate for use in oxygenated acidic environments, including nitric, sulfuric, and phosphoric acids, and is frequently employed in companies managing corrosive chemicals, such as sulfuric acid storage tanks [3,45]. The incorporation of corrosion inhibitors is an effective strategy. These chemical substances, applied in minimal quantities, diminish the corrosion rate by creating a protective coating or modifying the electrochemical processes at the metal surface. Corrosion inhibitors are widely utilized in oil and gas extraction, petroleum refining, chemical production, heavy industry, and water treatment industries [1]. They are especially advantageous in acidic environments, steam systems, and cooling water circuits. The selection of an inhibitor depends upon the corrosive environment and the substrate requiring protection.

Inhibitors are crucial in corrosion control techniques as they offer a flexible and economical method for diminishing material degradation in hostile conditions. Their applications span multiple industries, guaranteeing prolonged service life and improved material performance. The following section will delve deeper into the mechanisms, classifications, and efficiency of corrosion inhibitors in different operational settings.

1.6 Corrosion inhibitors

According to ISO 8044:2024, a corrosion inhibitor is defined as a substance that, when added in small concentrations to a given environment, significantly decreases the corrosion rate of a metal exposed to that environment [23]. Corrosion inhibitors (CIs) are chemical compounds, typically introduced in small quantities to corrosive systems, that mitigate the degradation rate of metals in such environments [33]. The choice of an appropriate inhibitor is contingent on several factors: the metal to be protected, the method of application (e.g., spraying, incorporation in coatings, or solubilization in fluids), the operating conditions (pH, temperature), and whether the protection is intended to be temporary (e.g., during storage or transport) or permanent[32].

1.6.1 Classification by Mode of Action

Corrosion inhibitors can be categorized based on their electrochemical mechanism of action into anodic, cathodic, and mixed inhibitors.

Anodic Inhibitors

Anodic inhibitors function by elevating the corrosion potential and promoting the formation of a passive film on the metal surface. These compounds act at anodic sites where metal dissolution occurs, thereby fostering passivation. However, insufficient concentrations of anodic inhibitors can result in localized corrosion, such as pitting [33]. Examples include chromates, nitrates, molybdates, and tungstates. Chromates and nitrates are oxidizing anions capable of passivating steel in oxygen-deficient environments, while molybdates and tungstates are non-oxidizing and require oxygen for effective passivation [1].

Cathodic Inhibitors

Cathodic inhibitors act by retarding the cathodic reactions involved in corrosion, either by precipitating protective cations onto the metal surface, or by interfering with the reduction reactions of oxygen or hydrogen ions thus providing simpler and less efficient protection compared to anodic inhibitors [33]. The inhibiting action of cathodic inhibitors takes place by three mechanisms: Cathodic poisoning occurs when Inhibitors such as arsenic and antimony compounds impede the recombination and discharge of hydrogen, potentially increasing susceptibility to hydrogen-induced cracking. Cathodic precipitation, Cations like calcium and magnesium form insoluble oxides that deposit on the metal, creating a protective barrier. Furthermore, Oxygen scavenging occurs when Compounds react with dissolved oxygen, reducing its availability for cathodic reactions (e.g., As^{3+} and Sb^{3+} on the dissolution of Fe in acidic media)[1].

Mixed Inhibitors

Mixed-type inhibitors influence both anodic and cathodic reactions. They function primarily by forming a protective film that impedes charge transfer across the metal-solution interface, as indicated by changes in the corrosion potential (E_{corr}) and Tafel slopes [3,32]. Examples include silicates and phosphates, which are commonly employed in water softening to prevent rust formation [1]. Mixed inhibitors are considered safer than purely anodic types, due to their more balanced interaction across electrochemical sites.

1.6.2 Classification by Chemical Nature

In addition to their electrochemical behavior, corrosion inhibitors are classified chemically as either inorganic or organic.

Inorganic Inhibitors

Inorganic inhibitors are extensively used in industrial applications such as water treatment, steel-reinforced concrete protection, and automotive manufacturing [3]. These inhibitors, including chromates (CrO_4^{2-}), dichromates ($Cr_2O_7^{2-}$), and phosphates (PO_4^{3-}), protect metal surfaces by forming either passivating oxide films or precipitated protective layers [46,47].

Chromates, though highly effective, pose significant environmental risks and are being progressively replaced by safer alternatives such as molybdates, tungstates, and phosphates. However, these alternatives generally require the presence of oxidants to achieve similar passivation [46]. Lanthanide salts such as cerium and lanthanum are emerging as environmentally benign options that act via cathodic inhibition by forming insoluble precipitates that hinder oxygen transport [48].

Inorganic inhibitors are typically effective in neutral to alkaline media, as their dissociation products (anions or cations) play a key role in inhibiting corrosion [1]. Common anionic species include XO_4^{n-} types like chromates, molybdates, silicates, and phosphates, while effective cations include Ca^{2+} and Zn^{2+}. Nevertheless, due to their environmental toxicity, particularly the hazards associated with Cr (VI), the use of many inorganic inhibitors is declining [1].

Organic Inhibitors

Organic inhibitors, largely derived from petroleum industry by-products, are widely preferred for their efficiency across broad temperature ranges, compatibility with various metals, water solubility, cost-effectiveness, and lower toxicity [1]. These compounds typically possess benzene rings with functional groups such as –SH, –OH, $-NH_2$, $-NO_2$, and –COOH, which allow them to adsorb strongly onto metal surfaces and form protective layers [6,33]. Their efficiency is often correlated with molecular size, structure, and the nature of functional groups. The general trend in inhibition effectiveness is $O < N < S < P$ [1]. Many organic inhibitors are amphiphilic, comprising a polar head and a non-polar tail, facilitating tight surface adsorption and barrier layer formation. Interestingly, inhibition efficiency does not always correlate with molecular packing density, as less ordered layers can still yield strong protective effects [3]. Organic inhibitors protect metals via mechanisms such as: Adsorption and formation of protective films, Formation of insoluble complexes at anodic sites, and Alteration of electrochemical reactions at both anodic and cathodic sites.

Types of organic inhibitors include azoles, amines, amino acids, sulphonates, and their metal salts. These can be classified based on elemental composition [1]:

- Nitrogen-containing compounds : amines, triazoles, Schiff bases, pyridines, etc.
- Nitrogen and sulfur compounds: thiadiazoles, thiazoles
- Sulfur compounds : thioureas, sulphonates
- Nitrogen and oxygen compounds: oxazoles, phthalimides, plant extracts

Certain halide ions (I^-, Br^-, Cl^-) may enhance inhibitor performance via synergistic effects that alter surface charge and enhance organic molecule adsorption; fluoride, however, is ineffective. Most organic inhibitors function as mixed-type inhibitors, simultaneously influencing anodic and cathodic sites [1,3].

Recent interest has turned toward plant-based or "green" corrosion inhibitors, valued for their sustainability and minimal environmental impact [6]. These compounds, extracted from various plant parts (roots, seeds, bark, leaves, fruits), have demonstrated effectiveness in acidic environments [29]. Their performance is attributed to phytochemicals such as tannins, alkaloids, amino acids, steroids, and flavonoids, which adsorb onto metal surfaces and form protective films [29].

1.6.3 Mechanisms of Corrosion Inhibition

Corrosion inhibitors may operate through several distinct mechanisms:

- Adsorption: Molecules form a barrier layer on the metal surface through physisorption (via Van der Waals forces, hydrogen bonding, or dipole interactions) or chemisorption (through electron sharing with metal atoms, especially via atoms like N, O, S, or P) [32].
- Passivation: Inhibitors anodically polarize the metal to induce passive film formation, shifting the corrosion potential into a passive range [1].
- Precipitation: Inhibitors cause the formation of insoluble surface films by reacting with metal ions or environmental species, thereby physically blocking corrosion sites. This is common with phosphates and silicates, particularly in hard water [1].
- Electrochemical Modification: Some inhibitors increase the surface impedance or reduce the rates of cathodic or anodic reactions, effectively lowering the corrosion current density [32].

An ideal corrosion inhibitor should exhibit high performance at low concentrations and elevated temperatures, remain stable in complex environments, and avoid altering the metal's physical or chemical properties [49]. The choice of an appropriate inhibitor is contingent upon the characteristics of the corrosive agent (e.g., O_2, CO_2, H_2S) and whether the required protection is temporary or long-term (e.g., during machining, cleaning, or storage)[1]. In the present work, we will be focusing on organic inhibitors, specifically nitrogen-containing compounds.

1.7 Nitrogen-containing compounds as corrosion inhibitors

Nitrogen-containing organic compounds are extensively employed as corrosion inhibitors due to their ability to adsorb onto metal surfaces, forming protective barriers that mitigate corrosion processes. The presence of nitrogen atoms, often in conjunction with other heteroatoms like oxygen or sulfur, enhances their electron-donating capabilities, facilitating strong interactions with metal substrates. They promote adsorption onto metal surfaces, resulting in the development of protective coatings that impede corrosion. Adsorption may transpire by physisorption, chemisorption, or a hybrid of both, contingent upon the particular inhibitor and environmental circumstances. The efficacy of these inhibitors is affected by factors like molecule structure, electron density, and the presence of substituent groups. Below is a detailed synthesis of the primary classes of nitrogen-containing compounds, focusing on their properties, synthesis methods, and applications as corrosion inhibitors, particularly for carbon steel.

Amines and Their Derivatives: Amines are among the earliest and most extensively researched organic corrosion inhibitors, due to the existence of a lone electron pair on the nitrogen atom that enhances adsorption onto metallic surfaces. These compounds can establish coordination bonds with unoccupied d-orbitals of metal atoms, leading to the formation of a protective layer that obstructs both anodic and cathodic processes. The inhibitory effect is especially significant in acidic environments, such as 1M HCl, where protonated amine groups demonstrate robust electrostatic interactions with the negatively charged steel surface [50]. Amines are generally produced through the alkylation of ammonia or the reduction of nitriles, nitro compounds, or amides (Figure 1.5). Film-forming amines are among the effective organic inhibitors used for carbon steel in water/steam industrial circuits. Their general formula

R_1-[-NH-R_2-]$_n$-NH_2, with R_1 being an aliphatic hydrocarbon chain containing between 8 and 22 carbon atoms, R_2 being a shorter hydrocarbon chain with 1 to 4 carbon atoms, and n being an integer ranging from 0 to 7. Thanks to their structure, film-forming amines adhere to metal surfaces via their polar amine group, while their nonpolar hydrocarbon chain creates a protective coating, successfully shielding the metal from the corrosive environment. Commercially available film-forming amines comprise N-oleyl-1,3-propanediamine (OLDA) and octadecylamine (ODA) [50].

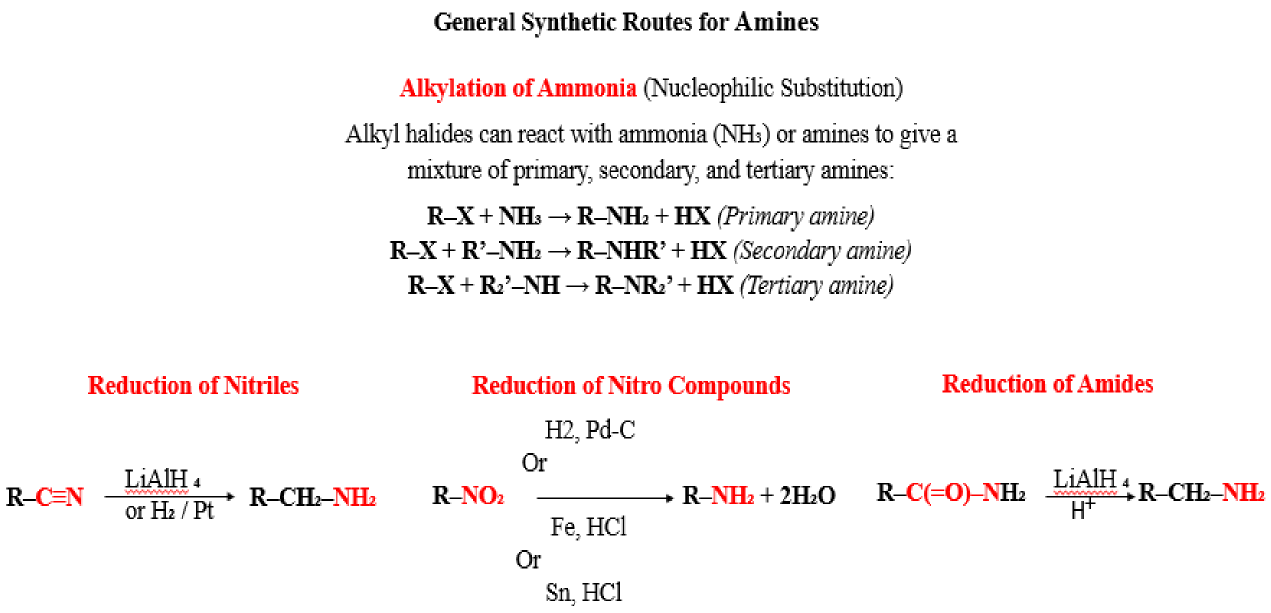

***Figure 1.5**: Schematic summary of the routes of amines synthesis*

Quaternary Ammonium Compounds: Quaternary ammonium salts with the general formula $[R_4N]^+X^-$ are cationic surfactants characterized by a central nitrogen atom linked to four alkyl or aryl groups. Their positive charge promotes adsorption onto negatively charged metal surfaces, creating a persistent, hydrophobic barrier that prevents hostile ions like chloride from reaching the metal substrate. These compounds are particularly advantageous in chloride-rich environments and are produced via the alkylation of tertiary amines with alkyl halides in a nucleophilic substitution reaction (Reaction 15). Research has demonstrated their efficacy in reducing pitting and uniform corrosion in steel, especially in harsh aqueous environments [51]. Highly soluble quaternary ammonium salts are ecologically benign and have good adsorption characteristics owing to their ionic structures. They comprise a cation and an anion, which is anticipated to provide synergistic enhancement in corrosion inhibition. These molecules substantially diminish the extent of corrosion damage at both the cathodic and anodic active corrosion sites. In an overview of modern literature, Abdullayeva [52] has mentioned multiple works that studied the effect of quaternary ammonium salts, among which are the following two. The first study investigated the effect of temperature on the inhibitory properties of seven mono- and dicationic quaternary ammonium bromides on mild steel in 1 M HCl and 1 M H_2SO_4. The methods employed included impedance, polarization resistance, and polarization curves. Two suitable structural models of the interface between metal, 1 M HCl, and the inhibitor were developed to elucidate the processes across varying temperature ranges [53]. In the second study, three gemini-type quaternary ammonium surfactants were synthesized, characterized, and evaluated as corrosion inhibitors for carbon steel in oil well formation water containing sulfide ions. The inhibition efficiency was assessed using electrochemical impedance spectroscopy (EIS) and potentiodynamic polarization techniques. It was found that the inhibitory performance improved with the extension/elongation of the alkyl chain attached to the tertiary nitrogen atom. Furthermore, the adsorption behavior of the inhibitor molecules on the carbon steel surface was found to follow the Langmuir adsorption isotherm [52].

$$R_3N + R'\text{–}X \rightarrow [R_4N]^+X^- \qquad 15$$

N-Heterocyclic Compounds: N-heterocycles are chemicals that incorporate nitrogen atoms in ring structures, frequently aromatic, including triazoles, imidazoles, and pyridines. The nitrogen atoms augment electron density in the system, facilitating effective coordination with metal centers. Their planar configuration facilitates excellent surface coverage and π-electron interactions with metallic d-orbitals, hence augmenting their inhibitory efficacy. Synthesis often entails cyclization reactions utilizing nitrogenous precursors under acidic or basic conditions. These compounds are very effective in acidic corrosion conditions for carbon steel, demonstrating excellent inhibitory efficacy through both physisorption and chemisorption modes [54]. Numerous researchers have concentrated on evaluating one or more N-heterocyclic compounds as corrosion inhibitors. Ettahiri and Al [55], have conducted a comprehensive investigation on pyridazine, quinoxaline, quinoline, indazole, pyridine, benzimidazole, and pyrimidine as corrosion inhibitors. A review conducted by Avdeev et Al. [56] provided a comprehensive overview of the current state of research on the corrosion protection of both ferrous and non-ferrous metals in mineral and organic acid media using nitrogen-containing five-membered heterocyclic compounds (NFHCs). The study examined the effectiveness of these inhibitors in safeguarding a range of metallic substrates, including steels and copper-, zinc-, and aluminum-based alloys, when exposed to acidic environments. Additionally, particular attention was given to elucidating the underlying mechanisms responsible for their protective action. They have concluded that heterocycle derivatives with substantial substituents frequently have the most significant protective effect. They are typically adsorbed onto metal surfaces from mineral acid solutions. Triazoles will be the focus of this thesis, and in the chapters to come, we will examine their protective effect on the corrosion of carbon steel.

Schiff bases are defined by the imine functional group (–C=N–), formed through the condensation of primary amines with aldehydes or ketones. The nitrogen atom's lone pair of electrons in the imine group, in conjunction with neighboring donor atoms, facilitates many coordination sites on the metal surface. This leads to sustained adsorption and effective barrier development. Schiff bases can be customized with diverse substituents to augment solubility, electronic properties, and steric hindrance, hence improving inhibitory efficacy. Their efficacy in preventing the corrosion of carbon steel in acidic settings has been thoroughly documented, particularly when numerous donor atoms (S, O) coexist inside the same molecule [57].

Hydrazones, which are also assessed in detail in the present work, are structurally analogous to Schiff bases and are produced via the condensation of hydrazines with carbonyl compounds (Figure 1.6). The resulting molecule comprises several nitrogen atoms that function as effective electron donors. This structural characteristic facilitates strong adsorption on metallic surfaces and the development of protective layers. Hydrazones frequently exhibit superior inhibitory efficiency relative to basic imines, attributable to the existence of supplementary N–H functionalities that can engage in hydrogen bonding and surface contacts. Recent investigations indicate that hydrazone derivatives can attain over 90% inhibitory efficiency for carbon steel in 1M HCl, contingent upon the chemical design [58].

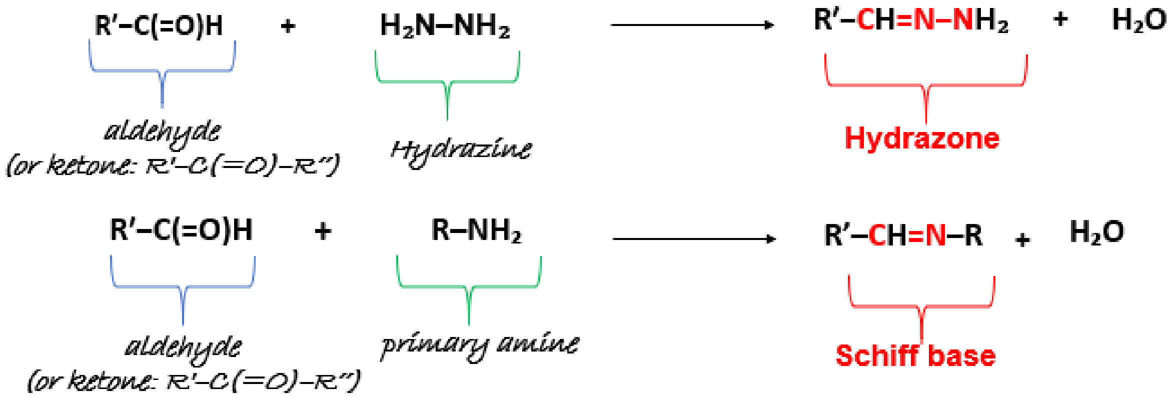

***Figure 1.6** : Synthesis of Schiff bases and Hydrazones*

Amides and Polyamides possess a carbonyl group attached to a nitrogen atom, constituting the functional group –C(=O)–NR2. These compounds can coordinate to metal surfaces through the lone pair on the nitrogen and the carbonyl oxygen. Despite being less reactive than amines or imines, their dual coordination sites can facilitate efficient adsorption and corrosion prevention. Polyamides, comprising repetitive amide units, are very effective in creating consistent protective coatings. Amides are generally produced via condensation reactions between carboxylic acids (or their derivatives) and amines. Their use as corrosion inhibitors for carbon steel is under growing investigation, with reported inhibition efficiency ranging from modest to good [51,59].

Recently, the application of **polymers**, copolymers, grafted polymers, and polymer composites as eco-friendly corrosion inhibitors has garnered significant interest owing to their exceptional film-forming properties and elevated inhibition efficiency. In contrast to small-molecule inhibitors, polymers provide enhanced surface coverage on metal substrates due to their larger molecular size and the inclusion of various anchoring functional groups, which may be nonionic, cationic, anionic, or ampholytic. These groups facilitate robust interactions with the metal surface, promoting the development of stable, protective barriers that efficiently impede corrosive chemicals. The efficacy of polymeric inhibitors is affected by various molecular parameters, including polymer size, molecular weight, chemical composition, and the electronic properties of the anchoring groups, such as electron density, aromaticity, and steric attributes. Functional moieties such as –CHO, –N=N–, –OH, and other donor groups augment performance by promoting adsorption and bonding with the metal contact [60].

Figure 1.7 illustrates an overview of the recurring structural units often present in polymer corrosion inhibitors. A notable subdivision within this category is nitrogen-containing polymers, which integrate nitrogenous functional groups like amines, amides, or imines into their structure. The nitrogen atoms work as effective donor sites, facilitating several interaction points with the metal surface, thus improving the stability and adherence of the protective layer. Their substantial molecular size enhances physical barrier characteristics and facilitates chemisorption via lone pair electron donation. These macromolecules are generally produced through the polymerization of nitrogen-rich monomers or by the post-functionalization of pre-existing polymers. Nitrogen-containing polymers exhibit significant corrosion inhibition for carbon steel, especially in harsh environmental circumstances, and their efficacy can be enhanced by adjusting factors such as molecular weight, functional group density, and chain architecture [61].

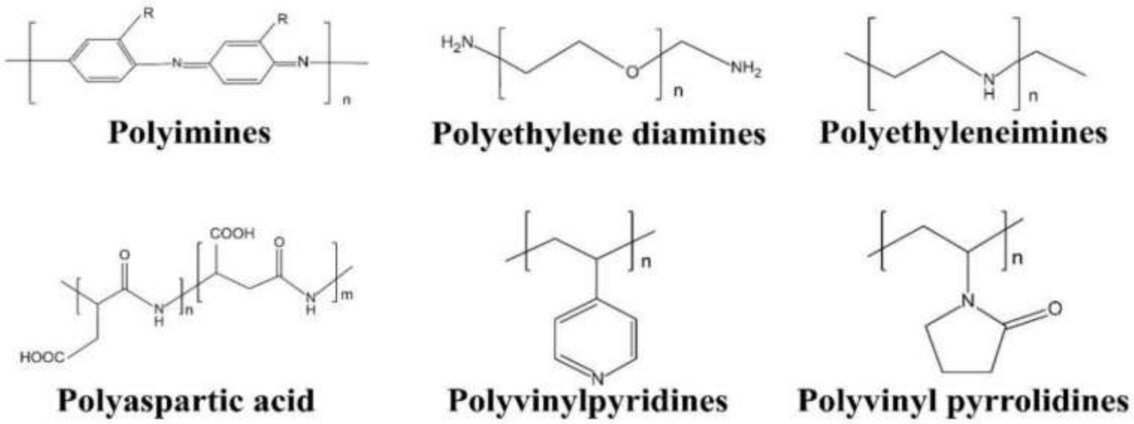

Figure 1.7: *Nitrogen-containing polymers used as corrosion inhibitors*

In conclusion, nitrogen-containing compounds constitute a diverse and effective category of organic corrosion inhibitors for carbon steel. Their effectiveness arises from the lone pair electrons on nitrogen atoms, facilitating robust interactions with metallic surfaces, typically via both physisorption and chemisorption. The structural diversity of these compounds, ranging from tiny molecules to macromolecular polymers, facilitates the adjustment of their physical and chemical properties to enhance performance in particular corrosive conditions.

1.8 Triazoles

As mentioned above, Corrosion is a natural, electrochemical process where metals deteriorate due to reactions with their environment. In industrial settings, mild steel is frequently exposed to acidic environments, such as hydrochloric acid (HCl), during processes like acid pickling, descaling, and oil well acidizing. In these conditions, steel surfaces are prone to aggressive corrosion, leading to material loss and potential structural failures. In order to mitigate corrosion, especially in acidic media, corrosion inhibitors are commonly employed. These substances, when added in small concentrations, significantly reduce the corrosion rate by forming protective films on the metal surface or by altering the electrochemical reactions responsible for corrosion. Triazoles are aromatic nitrogen-heterocyclic compounds consisting of five members, commonly referred to as pyrrodiazoles, with the chemical formula $C_2H_3N_3$ and a molecular weight of 69.07 g/mol. They display two positional isomers (Figure 1.8), and the initial unsubstituted triazole was made by Fischer in 1878 [62].

1,2,3-triazole **1,2,4-triazole**

Figure 1.8*: Isomers of triazole*

The global triazole market is projected to be valued at $741.5 million in 2023, with an anticipated compound yearly growth rate (CAGR) of 4.5% over the forecast period from 2023 to 2033 [63]. In the last five years, the demand for triazole has been rising at an accelerated rate due to its use in diverse sectors, including pharmaceuticals and agriculture.

1.8.1 Industrial Applications and Justification of Triazole Use

Although triazoles, as corrosion inhibitors, represent a minor segment of the global market. it is particularly applicable to maritime copper and steel, which are in significant demand in industries like the oil and gas industry [63]. Triazole derivatives have found wide applications across diverse industrial sectors owing to their structural versatility and desirable physicochemical properties. They are notably used in pharmaceuticals, agrochemicals, dyestuffs, optical brighteners, photoreceptors, and the ink industry, in addition to their role as corrosion inhibitors [2]. In agriculture, triazoles have been used since the 1980s as fungicides for plant protection. They are effective against a variety of plant diseases affecting turf grasses, vegetables, citrus fruits, field crops, and ornamental plants [64]. Triazoles are also extensively utilized in the formulation of biocides available on the global market due to their broad-spectrum antimicrobial activity. These widespread applications are largely attributed to their chemical stability, water solubility, and low sorption tendencies. However, their persistence in the environment and varying degrees of toxicity have raised concerns regarding their ecological footprint[64]. Despite this, triazoles are still favored in many industries due to their functional benefits, particularly their ability to perform at low concentrations without contributing heavy metal residues.

1.8.2 The Eco-Friendly Paradigm: Between Assumption and Evidence

Although triazoles are frequently referred to in the literature as "eco-friendly" and "green" corrosion inhibitors, a closer look shows a more complicated reality. Some studies support this classification by stressing their low toxicity, biodegradability, and environmental friendliness when compared to typical inhibitors such as chromates and nitrites [65,66].

Furthermore, their existence in pharmaceuticals, food-related applications, and biocides appears to indicate a rather safe toxicological profile. Triazole derivatives have been extensively researched for their pharmacological potential, since they demonstrate a wide range of biological activities, including antioxidant, antibacterial, antidepressant, antitubercular, anti-inflammatory, anti-neoplastic, and anticonvulsant effects[66]. This multifunctional bioactivity enables their inclusion in a variety of medication formulations, demonstrating a level of biocompatibility that strengthens their status as low-toxicity chemicals [67].

Triazoles are used as fungicides and insecticides in agriculture, where they protect plants from fungal infections in vegetables, field crops, turf grasses, and citrus fruits. These uses are not only popular but also regulated, and their continuous usage suggests a risk profile that is acceptable under numerous national and international safety norms [64]. Triazoles are also one of the most commonly utilized active ingredients in commercial biocides due to their stability, potency at low doses, and water solubility.

The European Food Safety Authority (EFSA) conducted a comprehensive risk assessment on metconazole, a representative 1,2,4-triazole derivative, and concluded that its toxicological reference values were not exceeded, and its triazole derivative metabolites (TDMs) posed no significant risks [68]. Furthermore, the EFSA evaluation found that metconazole had no endocrine-disrupting capabilities and posed minimal ecotoxicological risk to birds, wild animals, bees, non-target arthropods, earthworms, soil microbes, and aquatic creatures [68].

These findings support the notion that triazole-based chemicals, given their widespread and regulated use in medicine, agriculture, and industry, may be deemed rather safe, especially when compared to more harmful conventional corrosion inhibitors such as chromates and nitrites. However, as stated below, this view must be balanced against growing concerns regarding their environmental permanence and ecotoxicity. Despite common perceptions of triazole derivatives as eco-friendly and green alternatives to conventional corrosion inhibitors, new research has highlighted concerns about their environmental persistence and potential toxicity. Although these compounds are acclaimed for their low effective concentration, low heavy metal content, and non-volatile nature, research has revealed that triazoles are not easily biodegradable and may accumulate in aquatic environments [64]. Their moderate stability in soil and water, as well as their restricted sorption ability, contribute to their persistence, which may result in long-term ecological exposure. Toxicological assessments have indicated varying effects on aquatic creatures. While triazoles are considered practically non-toxic to birds and bees, they have been shown to be harmful to freshwater algae, daphnids, and fish eggs, indicating that their impact varies by species and circumstance[64]. Furthermore, their existence in water systems, often as residues from agricultural runoff or industrial use, raises concerns regarding long-term exposure in non-target organisms. These findings highlight the need for a more nuanced classification of triazoles: while their molecular and operational properties support their classification as green inhibitors, their ecotoxicological footprint suggests caution, especially in large-scale or long-term applications. As a result, while triazoles provide a compelling blend of efficacy, cost-effectiveness, and minimal toxicity in controlled conditions, their environmental fate and impact must be carefully studied. This duality makes them both attractive and contentious options in the ongoing hunt for durable corrosion inhibitors.

1.8.3 Triazoles in Corrosion Inhibition

The corrosion-inhibiting properties of triazoles are directly related to their structural properties. These compounds are aromatic nitrogen-containing heterocycles, with many donor atoms (N, S, O, etc.) and π-electron systems. Such qualities promote adsorption onto metallic surfaces, resulting in the creation of a protective barrier that prevents corrosive substances from entering. It is widely believed that inhibitors act by adsorbing their functional groups onto the metal surface, affecting its electrochemical activity [69]. The efficacy of this adsorption process is determined by physicochemical and electronic parameters, such as electron density at donor atoms, steric factors, and orbital overlap with the metal surface. Triazole-type compounds have outstanding inhibitory activities in a variety of hostile media due to their heterocyclic backbone. They are thermally stable, readily synthesized, and cost-effective, with many performing well at low concentrations [66]. These benefits have inspired much research into the design and optimization of triazole compounds for corrosion inhibition.

Among the numerous triazole-based compounds investigated for corrosion inhibition, 1,2,3-triazole derivatives have received substantial interest due to their structural simplicity, synthetic accessibility, and good corrosion inhibition capabilities. These compounds, notably the 1,4-disubstituted derivatives, are commonly produced using the copper(I)-catalyzed azide-alkyne cycloaddition (CuAAC), a click chemistry process noted for its regioselectivity, mild reaction conditions, and environmental friendliness. 1,2,3-triazoles have shown significant inhibitory efficacy across a wide variety of metals, including mild steel, copper, iron, and aluminum, especially in acidic environments where metal degradation is most pronounced [70]. The anticorrosive activity of two 1,4-disubstituted-1,2,3-triazoles for carbon steel was evaluated using weight loss and electrochemical tests in acidic medium. The results revealed significant inhibitory efficacy (>90%) even at high temperatures (298-343 K). As the concentration of triazoles in this medium grew, so did the inhibitory efficacy. However, the rise in activation energy in the presence of the inhibitors indicated a physisorption process for the inhibitors' contact with the surface of carbon steel [71].

Despite the promising properties of 1,2,3-triazoles, research has recently shifted to 1,2,4-triazole derivatives, which have a wider range of action and better environmental behavior. The structure of 1,2,4-triazoles enables more varied replacements, which improves their adsorption and inhibitory efficacy. A comprehensive review from last year, which gathered recent investigations from 2018-2023, has shown that 1,2,4-triazole derivatives preserve mild steel (MS), carbon steel (CS), and copper in acidic environments [2]. Their inhibitory mechanisms, as measured by potentiodynamic polarization (PDP) and electrochemical impedance spectroscopy (EIS), demonstrate that the molecular geometry and electronic characteristics of 1,2,4-triazoles are ideal for creating strong protective layers on metallic surfaces. Furthermore, the availability of functional groups for derivatization makes 1,2,4-triazoles ideal for specific corrosion applications. Their ease of synthesis, stability under acidic conditions, and consistent inhibitory performance position them as the next generation of organic corrosion inhibitors.

A comprehensive review of 1,2,4-triazole derivatives has demonstrated their remarkable efficiency as corrosion inhibitors for mild steel in 1M HCl, with performance highly dependent on molecular structure, concentration, and electronic properties [72]. Among the studied compounds, 1-amino-1,2,4-triazole-3-thione-based Schiff bases achieved inhibition efficiencies of up to 92.27%, with their behavior modeled by Langmuir adsorption isotherms and confirmed by density functional theory (DFT) calculations. These compounds exhibited mixed-type inhibition, affecting both anodic and cathodic processes[73]. Similarly, 3,5-bis(2-thienyl)-4-amino-1,2,4-triazole (2-TAT) showed high inhibition efficiency (91.3%) at low concentrations (20 mg/L), following Langmuir adsorption and providing effective surface coverage [43]. A focused series of 5-substituted-2-mercapto-1,2,4-triazoles also demonstrated strong efficiencies, with the order of effectiveness governed by the nature and position of heteroatoms, underlining the crucial role of substituents in molecular design [74]. Further, mercapto-1,2,4-triazole Schiff bases containing azomethine linkages exceeded 98% efficiency, operating as mixed-type inhibitors and obeying Temkin isotherm behavior [75]. Substituted pyrazol-1,2,4-triazole conjugates showed inhibition efficiencies ranging from 91.7–94%, with adsorption confirmed to be spontaneous and dominated by chemisorption based on Gibbs free energy (ΔG) calculations [76]. The impact of (1-benzyl-1H-1,2,3-triazol-4-yl) methanol (BTM) and (1-(pyridin-4-ylmethyl)-1H-1,2,3-triazol-4-yl) methanol (PTM) on the corrosion of C38 steel in hydrochloric acid solution at 298 K was assessed using the weight loss technique. At 0.8 mM concentration, the two triazole derivatives demonstrated inhibitory efficiencies greater than 95% and followed the Langmuir adsorption isotherm. An electrochemical impedance spectroscopy investigation found that PTM had a higher corrosion inhibition efficiency than BTM at the same dose, which was consistent with the weight loss data [77].

Across these studies, high inhibition efficiencies are attributed to adsorption facilitated by nitrogen lone pairs and π-electrons, enabling the formation of protective films that mitigate both anodic metal dissolution and cathodic hydrogen evolution. The electron-donating substituents, particularly thione, mercapto, and azomethine groups, were shown to enhance adsorption strength and electron density, thereby boosting corrosion resistance. These findings were corroborated by electrochemical analyses, including potentiodynamic polarization and electrochemical impedance spectroscopy (EIS), both of which consistently demonstrated the mixed-type inhibition behavior of the investigated compounds. Moreover, most derivatives adhered to Langmuir isotherms, indicating monolayer adsorption, while DFT and molecular dynamics simulations provided theoretical validation of experimental observations. Overall, the adaptability, high effectiveness, and tunability of 1,2,4-triazole derivatives highlight their potential as extremely effective corrosion inhibitors in harsh acidic conditions.

Recent studies have verified the excellent corrosion inhibition efficacy of 1,2,4-triazole derivatives, especially when modified with electron-donating substituents. Two newly synthesized compounds, ethyl 2-(4-phenyl-1H-1,2,3-triazol-1-yl) acetate (Tria-CO_2Et) and 2-(4-phenyl-1H-1,2,3-triazol-1-yl) acetohydrazide (Tria-$CONHNH_2$), were tested for their corrosion inhibition performance on mild steel in 1M HCl using potentiodynamic polarization (PDP) and electrochemical impedance spectroscopy (EIS) techniques [78]. Both compounds acted as mixed-type inhibitors, effectively suppressing both the anodic dissolution of the metal and the cathodic hydrogen evolution reaction. At a concentration of 1.0×10^{-3}M, inhibition efficiencies of 95.3% and 95.0%, were achieved for Tria-CO_2Et and Tria-$CONHNH_2$, respectively. Their adsorption on the metal surface followed the Langmuir isotherm, indicating monolayer formation. This was attributed to a combination of physisorption, via electrostatic interaction between protonated triazoles and chloride ions, and chemisorption, which involved lone pair and π-electron donation from nitrogen atoms and substituents to the vacant d-orbitals of iron. DFT simulations showed that Tria-CO_2Et had a lower HOMO-LUMO energy gap, indicating higher reactivity and electron-donating potential. Fukui indices indicated the triazole ring's nitrogen and carbon atoms as the most reactive adsorption centers. These derivatives also retained stability and inhibitory efficacy at high temperatures (up to 328 K), suggesting their resistance to harsh acidic conditions. Comparisons with other known 1,2,4-triazole inhibitors, such as 3,5-bis(disubstituted)-4-amino-1,2,4-triazoles (86% efficiency in 2M H_3PO_4), 5-amino-3-mercapto-1,2,4-triazole (5-AMT) (92% in 1M HCl), and hexyl-substituted triazoles (HST) (97% in 1M HCl), further validate the excellent performance of these newly developed derivatives[79,80]. In addition to these findings, another study assessed a specific 5-mercapto-1,2,4-triazole derivative, which displayed remarkable inhibitory efficiency for mild steel in acidic environments, underlining the importance of structural alterations in enhancing performance[81]. These investigations highlight the importance of molecular design, namely the insertion of heteroatoms, π-systems, and electron-donating groups, in increasing the adsorption strength, reactivity, and inhibitory efficiency of 1,2,4-triazole-based compounds in corrosive environments. Last but not least, El Aoufir and Al [82] conducted a comparative investigation of two 1,2,4-triazole derivatives featuring alkyl chains of varying lengths, specifically 5-octylsulfanyl-1,2,4-triazole (TR8) and 5-decylsulfanyl-1,2,4-triazole (TR10). Their core system is similar to the molecule being investigated in our work. The corrosion inhibition performance of (TR8) and (TR10) was assessed through both experimental approaches and theoretical modeling. The highest inhibition efficiencies, as determined by electrochemical impedance spectroscopy (EIS), reached 92% for TR10 and 88% for TR8.

The adsorption of both inhibitors on the steel surface was found to follow the Langmuir isotherm model. Furthermore, theoretical analyses confirmed that variations in alkyl chain length significantly influence the inhibitory effectiveness, in agreement with the experimental findings.

It is important to note that this review of some 1,2,4-triazole derivatives explored in previous work is not exhaustive (Table 1.1). It is based on bibliographical references consulted.

Table 1.1 *: Listing of some 1,2,4-triazole inhibitors for acid medium*

Type of inhibitor	**Assessed molecule(s)**	**Material, medium, maximum inhibition efficiency η(%)**	**Ref**
1,2,4-triazole derivatives	2[5- 2-pyridyl -1,2,4-triazol-3-yl phenol] (PPT)	Mild steel, 1M HCl, 97.7% at 80 mg/l	[43]
	(Z) -4 - ((2-bromobenzylidene) amino) -5-methyl-2-4-dihydro -3H-1,2,4-triazole-3-thione (2i) **and** (Z) -4 - ((3-bromobenzylidene) amino) -5-methyl-2-4-dihydro-3H-1,2,4 -triazole-3-thione (21)	Mild steel, 1M HCl, At 10^{-3}M : 2i = 89.5% 21=84.5%	[73]
	4-amino-5-mercapto-1,2,4-triazole (AMT) **and** 3- phenyl-4-amino-5-mercapto-1,2,4-triazole (PAMT)	Mild steel, 1M HCl, At 0.4 g/l : AMT = 68.37% PAMT= 88.78%	[74]
	4-amino benzylidene- 3-propyl- 5-mercapto-1 ,2,4- triazole (ABPMT) **and** 4-aminocinnamalidene- 3-propyl- 5-merca pto-1 ,2,4- triazole (ACPMT) **and** 4-aminosalicylidene- 3-propyl- 5-mercapto-1 ,2,4- triazole (ASPMT) **and** 4-aminovanillidene- 3-propyl- 5-merca pto-1 ,2,4- triazole (AVPMT) **and** 4-aminodimethylamino benzylidene- 3-propy 1- 5-mercapto-1,2,4-triazole (ADPMT)	Mild steel, 15% HCl, At 1000ppm: ABPMT= 91.4% ACPMT= 82.8% ASPMT= 97.1% AVPMT=87.1% ADPMT= 85.7%	[75]
	1-(4,5-dihydro-3-phenyl pyridine-1-yl)-2-(1H-1,2,4-triazole-1-yl) ethyl ketones: 4F-DET **and** 4Cl-DET	Mild steel, 1M HCl, At 10^{-3}M : 4Cl-DET=96.86% 4F-DET = 97.24%	[76]
	ethyl 2-(4-phenyl-1H-1,2,3-triazol-1-yl) acetate [Tria-CO2Et] **and** 2-(4-phenyl-1H-1,2,3-triazol-1-yl) acetohydrazide [Tria-CONHNH2]	Mild steel, 1M HCl, At 10^{-3} M: [Tria-CO2Et] =95.3% [Tria-CONHNH2]=95%	[78]
	3,5- bis(4-methoxyphenyl)-4-amino-1,2,4-triazole (T1) **and** 3,5-bis(4-chlorophenyl)-4-amino-1,2,4-triazole (T2)	Mild steel, 2M H3PO4, At 10^{-3} M: T1=86.81%,T2= 86.20%	[79]
	3-(4-ethyl-5-mercapto-1, 2, 4-triazol-3-yl)-1- phenylpropanone (EMTP)	Mild steel, 1M HCl, at 500 ppm : 97%	[81]
	5- octylsulfanyl-1,2,4-triazole (TR8) **and** 5-decylsulfanyl-1,2,4-triazole (TR10)	Mild steel, 1M HCl, At 10^{-3} M: TR10=92% TR8= 88%	[82]

1.9 Hydrazones

Hydrazones are a unique class of nitrogen-containing chemical compounds that are structurally similar to imines and come under the larger group of Schiff bases. The general formula for these compounds is $R_1R_2C=NNH_2$, where R_1 and R_2 are organic substituents. They are distinguished by the presence of a highly reactive azomethine ($C=NNH_2$) group [83]. This azomethine bond, conjugated with a single pair of electrons from the terminal nitrogen atom, has a substantial impact on their physical and chemical properties, mainly through electron delocalization and coordination potential. The nitrogen atoms in the hydrazone moiety serve as nucleophilic sites, whereas the surrounding carbon atom can display both electrophilic and nucleophilic behavior, increasing the molecule's reactivity [83]. Hydrazones are primarily produced by condensation of hydrazines with carbonyl-containing compounds such as aldehydes or ketones in polar solvents, resulting in stable, crystalline products with high yield and purity [30] (Figure 1.9) .

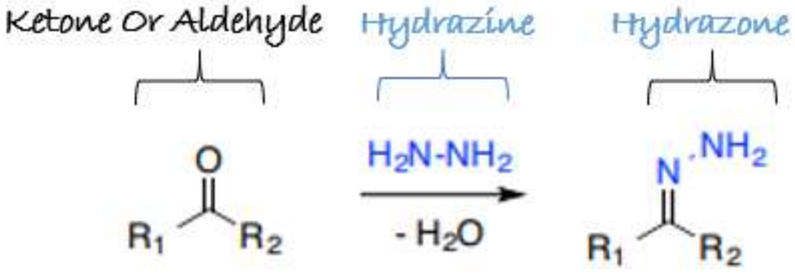

***Figure 1.9** : Synthesis of Hydrazone*

Their synthetic simplicity, combined with structural variety, makes them appealing targets in coordination and medicinal chemistry. The azomethine group in hydrazones (along with the N-N and N-H functionalities) gives them excellent chelating ability, allowing them to form stable complexes with metal ions, which is especially important in their role as ligands in coordination chemistry[83,84]. Their distinct chemical properties, such as excellent thermal stability, crystallinity, and reactivity to both nucleophiles and electrophiles, contribute to their broad range of applications [84,85]. Hydrazones are thus classified as versatile Schiff bases and multidentate ligands. Among azomethine compounds, they are differentiated by the imine's nitrogen atom (C=N) being bound to another nitrogen rather than a carbon, which gives extra chemical and coordination features (Figure 1.10) [86]. These characteristics support their employment not only in medicines and agrochemicals, but also in organocatalysis and corrosion inhibition.

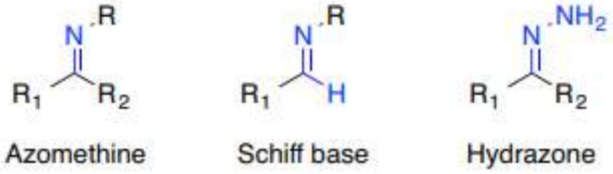

***Figure 1.10**: General structure of Azomethine, Schiff base, and Hydrazones*

1.9.1 Applications of Hydrazones in Pharmaceuticals and Agriculture

Hydrazones, a distinct class of organic molecules of the Schiff base family, have sparked significant interest in pharmaceutical, biomedical, and agricultural research due to their various biological and chemical properties. Their structural characteristics, particularly the azomethine ($C{=}NNH_2$) moiety, enable them to interact with both electrophilic (carbon) and nucleophilic (nitrogen) centers, contributing to a variety of pharmacological actions. These include antibacterial, antifungal, antimalarial, antitubercular, anti-inflammatory, analgesic, anticancer, antitumor, antiplatelet, antihypertensive, anticonvulsant [30,40,83,84].This wide range of activity is attributed to their capacity to influence metabolic processes and bind to a variety of biological targets. Furthermore, their chelating capacity, due to nitrogen donor atoms, enables them to form stable complexes with transition metals, which frequently improves antibacterial activity when compared to uncomplexed ligands [87]. Hydrazones have also been shown to have antioxidant capabilities, especially when functionalized with groups such as hydroxyl, nitro, or methoxy benzene, which affects their ability to neutralize reactive oxygen and nitrogen species [84]. Over the last few decades, substantial scientific research has confirmed their usefulness in chemistry, biology, and medicine [30,84]. Hydrazones are used in agriculture as rodenticides, nematocides, insecticides, pesticides, and plant growth regulators [87]. Their structural versatility and reactivity make them great candidates for multifunctional applications, from drug design to crop protection, underlining their vast societal and scientific importance.

1.9.2 Hydrazones as Corrosion Inhibitors

Hydrazones have emerged as a potent class of organic corrosion inhibitors due to their structural diversity, electronic richness, and chelating activity. The azomethine ($>C{=}NNH_2$) linkage and several heteroatoms (particularly nitrogen and oxygen) operate as active adsorption centers on metal surfaces, contributing to their efficacy [7,88]. These compounds can adsorb onto metals such as copper, nickel, aluminum, and, in particular, carbon steel [30,88], generating protective coatings that prevent anodic metal breakdown and cathodic hydrogen evolution. Adsorption is commonly described using the Langmuir isotherm, which involves a combination of both physisorption and chemisorption [30]. The effectiveness of hydrazones as corrosion inhibitors has been widely proven using chemical, electrochemical, surface analysis, and computational methods such as DFT and molecular dynamics simulations [89]. Several hydrazone derivatives exhibit remarkable inhibition performances: water-soluble hydrazones achieve 95% efficiency against C-steel in HCl , quinolinyl thipropano hydrazones achieve 98%, and dimethoxybenzylidene hydrazones inhibit corrosion by up to 96% [90,91] . Novel compounds such as CBTH and CBFH have efficiencies of 87.1% and 85.3%, respectively, at 2 mM [91], whilst isatin-hydrazones (OIHIHI and OPHIHI) have efficiencies of 96% and 92% in 15 wt.% HCl [8]. The salicylhydrazone derivative HBMH exhibits 90% efficiency at 10^{-3} M in 1 M HCl and largely adsorbs via physisorption [30]. FMAH, a newly synthesized hydrazone, effectively inhibited steel rebar corrosion in ClSCPS solutions, with an efficiency of approximately 81% after 30 days [88]. MeHDZ and HHDZ showed 98% and 94% inhibition on N80 carbon steel in 15 wt.% HCl, respectively, at 5×10^{-3} mol/L[7]. Several investigations found efficient suppression in NaCl/H_2S systems, where hydrazones inhibited corrosion by up to 56%, Chaitra et al. obtained 93% inhibition on mild steel in 0.5 M HCl using freshly synthesized hydrazones [92]. Other intriguing examples are bis-(o-methoxybenzaldehyde)-thiocarbodihydrazone and O-methoxybenzaldehydebenzoyl hydrazone for copper in 3.5%NaCl [93]. Khamaysa et al.[11] demonstrated that HZ-Cl and HZ-OH had efficiencies of 91% and 98%, respectively, in 1 M HCl. En-Nylly et al. [89] demonstrated 94% inhibition at 303 K and 89% at 333 K with another hydrazone drug. These findings, corroborated by SEM, EDX, and theoretical studies, demonstrate the production of protective adsorbed coatings through covalent interactions with the metal surface. Amira et al.[87] developed Schiff base hydrazones (HTZ, HTZS, and HPYS) as corrosion inhibitors for C-steel in 8 M H_3PO_4. HTZS demonstrated up to 83.33% efficiency at 99.00×10^{-3} mol/L and increased surface morphology and iron ion retention, as proven by galvanostatic studies and atomic absorption spectroscopy. This is consistent with previous observations that Schiff bases rich in imine groups and heteroatoms such as N, O, and S have strong corrosion inhibition potential via monolayer adsorption [87]. Collectively, these studies demonstrate the hydrazone family's ability to function as environmentally benign, effective, and adaptable corrosion inhibitors in a variety of acidic conditions.

1.9.3 Naproxen and Naproxen-Based Hydrazones as Corrosion Inhibitors

Hydrazones produced from nonsteroidal anti-inflammatory medications (NSAIDs) have recently received a lot of interest for their dual-function properties, which combine pharmacological efficacy with efficient corrosion inhibition. NSAIDs like naproxen, indomethacin, ibuprofen, and mefenamic acid have a free carboxylic acid group that, when functionalized into a hydrazone moiety, improves both therapeutic performance and industrial applicability by reducing gastrointestinal side effects and allowing metal surface interaction [83,94]. These hydrazones contain electron-donating groups and conjugated systems that improve adsorption onto metal surfaces by coordination bonding of nitrogen and oxygen atoms, resulting in durable protective layers that inhibit both anodic and cathodic corrosion processes[87]. They mostly function as mixed-type inhibitors, and their adsorption typically adheres to the Langmuir isotherm model [95]. Subbiah et al. and Lgaz et al. found that hydrazones generated from NSAIDs, such as mefenamic acid, indomethacin, and ibuprofen, have good inhibitory efficiency in acidic media, particularly against steel corrosion in 1 M HCl [85,96,97]. For example, indomethacin-derived hydrazone HIND inhibited steel rebar by 88.4% at 0.5 mmol/L, with SEM/EDX, AFM, XRD, and XPS demonstrating the creation of a protective barrier that reduced surface roughness from 183.5 nm to 50 nm [85]. Similarly, three mefenamic acid-based inhibitors (HDZ-1, HDZ-2, and HDZ-3) performed admirably, with HDZ-1 achieving 95% inhibition efficiency at 303 K thanks to a dimethylamino substituent that increased electron density and metal interaction [30]. These hydrazones significantly lowered double-layer capacitance while increasing polarization resistance, indicating strong adsorption behavior. Chafiq et al. [98] also showed that PHD-OH and PHD-Cl hydrazones had 96% and 91% inhibitory efficiency, respectively, at 5 mM in 1 M HCl. Naproxen-derived hydrazones have received special attention due to their widespread clinical use and well-defined structure. Naproxen's carboxylic acid group is an important location for hydrazone derivatization, which not only improves anti-inflammatory capabilities but also provides good corrosion inhibition. Chafiq et al.[95] synthesized two naproxen-based hydrazones and tested them on mild steel in 1 M HCl, with inhibitory efficiency of up to 96%. These compounds were found as mixed-type inhibitors that efficiently blocked both anodic and cathodic sites while adhering to the Langmuir isotherm, indicating monolayer surface coverage .A follow-up investigation supported similar findings, stressing the role of molecule structure in adsorption behavior and inhibition strength [95]. Chaouiki et al.[99] investigated naproxen-based hydrazones such as (E)-N′-(2,4-dimethoxybenzylidene)-2-(6-methoxynaphthalen-2-yl) and N′-cyclohexylidene-2-(6-methoxynaphthalen-2-yl)propanehydrazide, which had inhibitory efficiencies of 96% and 84% against mild steel in 1 M HCl at an optimal concentration of 10^{-3} M . These findings support the potential of naproxen-based hydrazones as multifunctional chemicals with both corrosion prevention and medicinal applications. However, despite being labeled "green" in corrosion contexts, some hydrazone derivatives have shown cytotoxic and genotoxic effects in biological systems at higher concentrations, highlighting the need for case-specific environmental and toxicological assessments. Overall, NSAID-derived hydrazones, particularly naproxen-based ones, represent a promising frontier for long-lasting and effective corrosion inhibitors with biological applications (Table 1.2).

***Table 1.2**: Listing of some NSAID-derived inhibitor molecules*

Type of inhibitor	**Assessed molecule(s)**	**Material, medium, maximum inhibition efficiency η(%)**	**Ref**
Hydrazone derivatives	(HIND): (E)-N0-(4-(dimethylamino) benzylidene)-2-(5-methoxy-2-methyl-1H-indol-3-yl)aceto-hydrazide	steel rebar, chloride-contaminated concrete pore solutions at 0.5 mmol/L=88.4%	[85]
	(HDZ1): 2-((2,3-dimethylphenyl)amino)-N′-((1E,2E)-3-phenylallylidene) benzohydrazide a**nd** (HDZ2): (E)-2-((2,3-dimethylphenyl) amino)-N′-(4-hydroxybenzylidene) benzohydrazide a**nd** (HDZ3): (E)-2-((2,3-dimethylphenyl) amino)-N′-(1-phenylethylidene)benzohydrazide a**nd** (HDZ4): N′-cyclohexylidene-2-((2,3-dimethylphenyl)amino)benzohydrazide	Mild steel, 1M HCl, At 5.10^{-3}M: HDZ1=97% HDZ2=94% HDZ3=92% HDZ4=86%	[96]
	(HDZ-S): (E)-2-((2,3-dimethylphenyl) amino)-N'-(thiophen-2-ylmethylene) benzohydrazide a**nd** (HDZ-O): (E)-2-((2,3-dimethylphenyl)amino)-N'-(furan-2-ylmethylene)benzohydrazide	Mild steel, 1M HCl, At 5.10^{-3}M: HDZ-O=88% HDZ-S=92%	[97]
	(PHD-Cl): (E)-N′-(1-(4-chlorophenyl) ethylidene)-2-(6-methoxynaphthalen-2-yl)propanehydrazide a**nd**	Mild steel, 1M HCl, At 5.10^{-3}M: PHD-OH=96% PHD-Cl=91%	[98]

	(PHD-OH): (E)-N′-(1-(4-hydroxyphenyl) ethylidene)-2-(6-methoxynaphthalen-2-yl) propanehydrazide		
	(HYD-1) : (E)-N′-(2,4-dimethoxybenzylidene) -2-(6-methoxynaphthalen-2-yl) propanehydrazide **and** (HYD-2): N′-cyclohexylidene-2-(6-methoxynaphthalen-2-yl) propanehydrazide	Mild steel, 1M HCl, At 5.10^{-3} M: HYD-1=94% HYD-2=84%	[99]
	(CBMP): (E)-N'-(4-chlorobenzylidene)-2-(6-methoxynaphthalen-2-yl) propanehydrazide a**nd** (MMBH): ((E)-2-(6-methoxynaphthalen-2-yl)-N'-(4- methylbenzylidene) propanehydrazide	Mild steel, 1M HCl, At 5.10^{-3}M: MMBH=94% CBMP=90%	[95]

1.10 Conclusion

This chapter has provided a bibliographic foundation directly aligned with the focus of our research. It was essential to highlight the various challenges associated with using aggressive environments, particularly acidic media such as hydrochloric acid. We then reviewed the main strategies used to combat corrosion, with a particular emphasis on the application of organic inhibitors. This literature review serves as a guide to orient the reader to the objectives of this thesis, which is dedicated to investigating the corrosion inhibition of carbon steel in 1 M HCl using novel nitrogen-containing organic inhibitors. The choice of this research topic is justified for several reasons: firstly, it follows within the continuity of the research conducted on this thematic and contributes to the enrichment of ongoing studies within our laboratory; secondly, it addresses critical industrial concerns such as corrosion and scaling, while aiming to identify effective, low-cost, and non-toxic inhibitors or formulations that can provide durable protection against these issues. Lastly, the potential for practical application of the experimental findings in real industrial settings adds further value to this work. To achieve these objectives, we employed both experimental and theoretical approaches, including mass loss measurements, stationary and transient electrochemical techniques, surface characterization methods, density functional theory (DFT), and molecular dynamics simulations.

Chapter 2: Materials, Experimental methods, and Conditions

The intricacy of corrosion phenomena necessitates the application of numerous experimental techniques to ascertain the corrosion rate and the characteristics of the mechanisms that compromise the metal.

This chapter intends to outline the materials utilized, as well as the experimental, electrochemical, and analytical methodologies employed in this work. A detailed account of the materials, electrolyte, and configurations employed facilitates the formulation of an experimental methodology that guarantees reproducible outcomes. Electrochemical techniques are subsequently introduced, emphasizing their significance and pertinence to the investigation of inhibitors. Then, the surface analysis method yields information that frequently enhances the findings derived from electrochemical techniques. Last but not least, theoretical methods come in handy to complement and elucidate the mechanisms of corrosion/inhibition.

2.1 Material, medium, inhibitors

Ferrous metals are extensively used in various industries, including construction and food packaging, among others [31]. The predominant number of frequently machined tools is composed of ferrous metals. In this context, these materials endure many adverse influences, rendering them susceptible to corrosion (elevated temperatures, hydrodynamics, etc.).

This study examines a carbon steel, with its chemical composition detailed in the table below.

***Table 2.1**: Chemical composition of the carbon steel in weight percentage*

Element	**C**	**N**	**Na**	**Mg**	**Cr**	**Mn**	**Fe**
% In weight	1.68	0.65	0.10	0.07	0.39	0.69	Balance

Prior to each immersion in the solutions, the carbon steel samples must be polished using abrasive paper of progressively finer grit (Grades: 180-400-600-1200-1500-2000). Polishing is performed on a rotating disc utilizing a Presi (Minitech 265) polishing machine (Figure 2.1). The samples are subsequently degreased with acetone, rinsed with distilled water, and dried using a stream of air.

Hydrochloric acid is a chemical commonly used in the chemical pickling of steel, acidification of oil wells, ore processing, etc. The concentration of hydrochloric acid is kept at 1mol/l, obtained by diluting concentrated acid of density 1.18 and purity 37% by weight from Sigma-Aldrich.

The working temperature is 298K, whereas for tests targeting the effect of temperature, this is varied from 298K to 338K and kept constant (±2K) during handling at the desired temperature using a circulating thermostat.

Figure 2.1*: Variable speed 20- 700tr/min manual Polishing machine available at LMNE Laboratory*

Our work focuses on investigating the effect of organic inhibitor molecules on the corrosion of carbon steel in 1M HCl. The organic molecules, triazole derivatives and hydrazone derivatives, were synthesized, purified, and characterized in the Medicinal Chemistry Laboratory, Faculty of Medicine and Pharmacy of Rabat, and the Laboratory of Advanced Materials and Process Engineering, Faculty of Sciences of Kenitra, respectively.

2.2 Experimental Techniques and Methods

To examine the corrosion behavior of carbon steel in acidic conditions and evaluate the efficacy of corrosion inhibitors, a combination of experimental methodologies is necessary. These methods provide both qualitative and quantitative insights into corrosion processes and inhibitory mechanisms.

2.2.1 Gravimetric technique

Mass loss measurements serve as an initial technique for investigating the corrosion inhibition of steel in an electrolytic solution, with the benefit of straightforward implementation. Although it is a direct method for determining corrosion rate and inhibitor effectiveness, its use remains limited by the fact that the reproducibility of results is not always evident.

The principle of this method is based on the measurement of the mass loss “Δm” undergone by a sample, of surface area “S”, during a time “t” of immersion in a corrosive solution at constant temperature "T". Mass loss tests were carried out according to the ASTM G31-72 [100] in glass vials. A thermostatically controlled water bath (Figure 2.2) was used to maintain the electrolyte at the desired temperature. Samples are immersed in a 1M hydrochloric acid solution, with and without the addition of different inhibitor concentrations. This method makes it possible to evaluate the corrosion rate.

***Figure 2.2**: Thermostatically controlled water bath used in gravimetric studies at the LMNE Laboratory*

When a plate with surface area "S" and initial mass "m_i" is immersed in a corrosive medium at a given temperature for a given immersion time "t", its final mass decreases as the metal dissolves. The corrosion rate can be calculated using the following equation:

$$C_R = \frac{\Delta m}{S \times t} \qquad 16$$

In the above equation, the corrosion rate is expressed in g.cm^{-2}.h^{-1}. Δm is the mass loss expressed in grams, t represents the immersion time of the specimen in the tested solution, denoted frequently in hours, and S is the exposed area in cm².

The inhibition efficiency can be calculated using the equation:

$$\eta_G(\%) = \frac{C_R - C_{R-inh}}{C_R} \times 100 \qquad 17$$

Where C_R is the corrosion rate in the absence of inhibitor, and C_{R-inh} is the corrosion rate in the presence of inhibitor.

2.2.2 Electrochemical techniques

Electrochemical techniques are essential in examining corrosion mechanisms and their mitigation, especially in corrosive environments like hydrochloric acid. In the context of carbon steel subjected to 1 M HCl, these approaches provide critical insights into the electrochemical behavior at the metal-electrolyte interface and facilitate the quantitative assessment of corrosion rates and inhibition efficiencies.

These methods function via a customized electrochemical cell, in which the metallic specimen is the working electrode (WE). This electrode is submerged in a corrosive electrolyte. It is electrochemically analyzed using a Potentiostat that regulates signals between the working electrode (WE) and auxiliary electrodes, usually a reference electrode (RE) and a counter electrode (CE) or an additional working electrode. Electrochemical signals, including current or potential, can be either applied to the system or evaluated to assess corrosion activity and the efficacy of inhibitors.

Electrochemical procedures can be classified into destructive and non-destructive categories. Destructive techniques, such as linear polarization and cyclic voltammetry (CV), necessitate the application of substantial potentials or currents to induce certain redox processes. Conversely, non-destructive techniques such as electrochemical impedance spectroscopy (EIS) and electrochemical noise (EN) employ minimal signals that prevent significant deviations from equilibrium, therefore maintaining the sample's integrity [101].

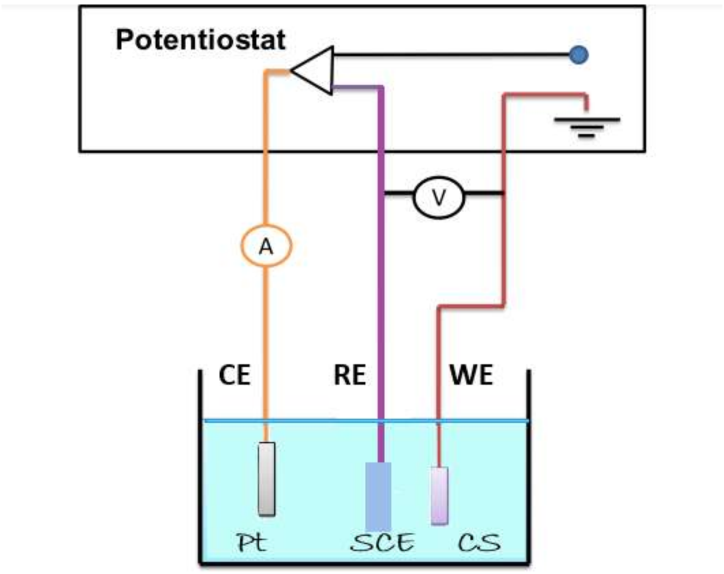

***Figure 2.3**: Schematic of a three-electrode electrochemical cell setup with a potentiostat.*

2.2.2.1 Potentiodynamic polarization

Potentiodynamic polarization is one of the most commonly utilized electrochemical techniques for corrosion studies. It is a steady-state/stationary technique that effectively yields kinetic parameters of the electrochemical reactions involved in corrosion. This technique entails systematically varying the potential of the working electrode, typically carbon steel in this context, while simultaneously measuring the resultant current. The resultant polarization curve yields significant insights into the anodic and cathodic processes occurring at the metal surface. The electrochemical behavior of a corroding metal surface is characterized by the Butler–Volmer equation, which articulates the total current density “i” as the aggregate of anodic and cathodic contributions for a reaction in which the rate is limited by the activation overpotential[26]:

$$i = i_a + i_c = i_{corr}\left\{exp\frac{\alpha nF}{RT}\,\eta - exp\ -\frac{(1-\alpha)nF}{RT}\eta\right\} \qquad 18$$

i represents the net current density (A/cm²) while i_{corr} is the corrosion current density. η represents the overpotential ($E - E_{corr}$). α is a charge transfer coefficient, and n represents the quantity of electrons transported. F denotes the Faraday constant, valued at 96485 C/mol, R is the universal gas constant, valued at 8.314 $J.mol^{-1}.\ K^{-1}$. T represents the temperature measured in Kelvin.

At minimal overpotentials, both anodic and cathodic components substantially influence the current. At elevated overpotentials (either positive or negative), one of the exponential terms prevails, hence simplifying the analysis into the Tafel behavior.

When the overpotential is adequately elevated (about ± 100 mV from the corrosion potential), the Butler–Volmer equation reduces to the Tafel equation, articulated as:

For the anodic component equation:

$$i = i_{corr}\left[exp\frac{\alpha nF}{RT}\,\eta_a\right] \qquad 19$$

By applying the logarithm to both sides of the equation and performing appropriate algebraic rearrangement, the anodic Tafel equation can be derived:

$$\eta_a = \beta_a\, log\, \left(\frac{i}{i_{corr}}\right) \qquad 20$$

Where β_a is the anodic Tafel slope expressed in (mV/decade);

$$\beta_a\ = \frac{2.303\ RT}{\alpha nF} \qquad 21$$

Similarly, for a significant negative overpotential (cathodic polarization), the reaction for the cathodic process:

$$i = -i_{corr}\left[exp\ -\frac{(1-\alpha)nF}{RT}\eta_c\right] \tag{22}$$

The cathodic Tafel equation obtained is:

$$\eta_c = \beta_c\ log\ \left(\frac{i}{i_{corr}}\right) \tag{23}$$

Where β_c is the cathodic Tafel slope expressed in (mV/decade);

$$\beta_c\ = -\frac{2.303\ RT}{(1-\alpha)nF} \tag{24}$$

η_a *and* η_c are the anodic and cathodic overpotentials. βa and βc represent the anodic and cathodic Tafel slopes, respectively, commonly denoted in mV/decade.

The Tafel extrapolation method involves plotting the logarithm of the current density (log i) against potential (E) and extrapolating the linear segments (Tafel regions) to their intersection at the corrosion potential (E_{corr}), as showcased in Figure 2.4. The current at this location is the corrosion current density (i_{corr}). This value is crucial, as it enables the quantitative assessment of the corrosion rate and serves as a fundamental metric for evaluating the efficacy of corrosion inhibitors. The presence of an inhibitor results in a substantial reduction in i_{corr}, signifying efficient corrosion inhibition [3].

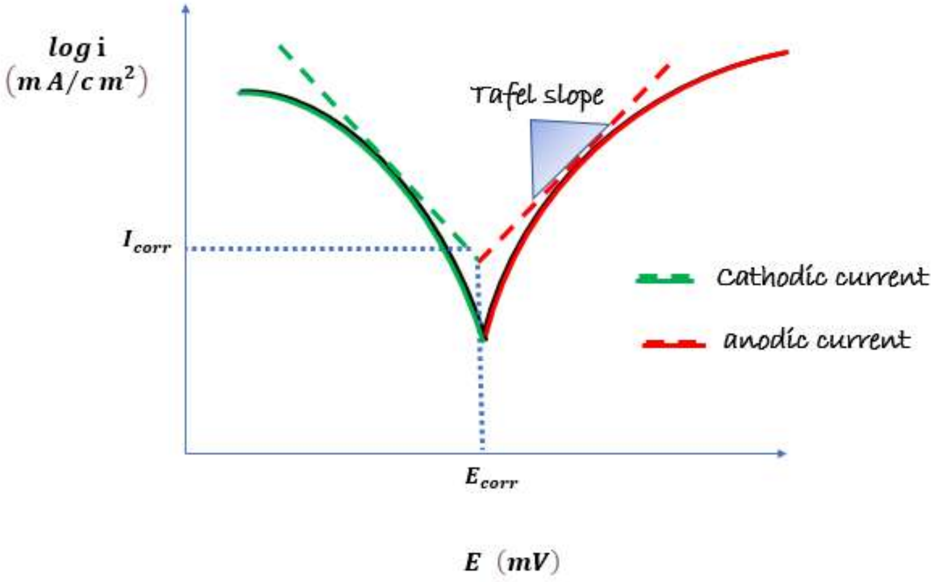

***Figure 2.4**: Schematic illustration of a Tafel slope with anodic and cathodic Tafel slopes observed in a charge transfer-controlled electrochemical system*

In acidic environments, such as 1 M HCl, carbon steel experiences electrochemical corrosion through the subsequent half-cell reactions, the anodic oxidation of iron, and the cathodic reaction of hydrogen ions. At equilibrium, the reaction rates are equivalent, resulting in a net current of zero. Nonetheless, the reactions continue to exhibit dynamic activity. The Tafel approach elucidates the kinetics of redox processes, with variations in E_{corr} or reductions in i_{corr} indicating anodic, cathodic, or mixed-type inhibition [3,101].

Upon obtaining i_{corr}, the corrosion rate (C_R) can be computed using:

$$C_R = C_1 \frac{i_{corr}}{\rho} EW \qquad 25$$

The corrosion rate (C_R) is determined by the metal's density (ρ, in g/cm³), the equivalent weight (EW, dimensionless), and a constant (C_1) that standardizes units. Equivalent weight (EW) denotes the mass of metal that reacts with one Faraday (96489 C) and is calculated by dividing the atomic mass by the oxidation state. For alloys and multivalent components, EW becomes increasingly intricate. For carbon steel, according to the literature[3], the equivalent weight of Fe/Fe^{2+} is 27.92, and the density of structural steel is 7.85 g/cm³. Corrosion current densities (i_{corr}) are often adjusted to μA/cm², and C_1 is 3.27×10^{-3} mm.g.μA^{-1}.cm^{-1}.yr^{-1}.

The inhibition efficiency is calculated using:

$$\eta_{PDP}(\%) = \frac{i_{corr} - i_{corr-inh}}{i_{corr}} \times 100 \qquad 26$$

Where $i_{\text{corr-inh}}$ and i_{corr} denote corrosion current densities with and without the inhibitor, respectively. These calculations are essential for quantifying the protection provided by the tested substances.

The Tafel analysis is an exceptionally effective instrument for characterizing a corroding system. Nonetheless, the considerable applied potentials and the substantial currents indicate that the experimental system may be altered by this measurement. An alternative, less invasive method is now outlined.

2.2.2.2 Electrochemical impedance spectroscopy

Electrochemical Impedance Spectroscopy (EIS) is a versatile and robust technology used in diverse applications such as corrosion monitoring, coating quality assessment, microbiological examination, food product evaluation, and the characterisation of materials for fuel cells and batteries [31].

The theoretical foundations of EIS originate from Oliver Heaviside in the late 19th century, who employed Laplace transforms to streamline frequency-dependent electrical circuits. Despite considerable controversy, these methodologies have become essential to contemporary impedance analysis. EIS experienced substantial popularity in the 1980s, especially within corrosion and coating sciences, increasing from approximately 30 annual publications in 1980 to over 6000 by 2017 [102]. As of now, the number of publications has exceeded 10000. Notwithstanding its extensive application, the analysis of EIS data frequently poses difficulties owing to the intricacy of the systems and the requisite mathematical proficiency.

Fundamentals of EIS

In electrochemical impedance spectroscopy (EIS), an alternating current (AC) potential is applied to an electrochemical cell, usually at the open-circuit potential (OCP) or corrosion potential (E_{corr}). The resultant AC current is quantified, and in an ideal linear system, it will also exhibit a sinusoidal waveform at the same frequency, but with a phase shift to the applied voltage [103].

The impedance Z(ω) is then calculated by dividing the potential by the current using complex arithmetic to maintain the phase information:

$$Z(\omega) = \frac{V(t)}{I(t)} \qquad 27$$

At a time, t, the electrode potential is expressed as a function of its stationary component V_0 and a sinusoidal term:

$$V(t) = V_0 + |\Delta V|\, sin(\omega t) \qquad 28$$

Where ωt describes the pulsation of the signal (related to the frequency by $\omega = 2\pi f$) and ΔV its amplitude.

The sinusoidal perturbation of the potential induces a sinusoidal current, superimposed on the stationary current and shifted in phase by an angle ϕ (Figure 2.5). Its value is therefore given by:

$$I(t) = I_0 + |\Delta I|\, sin(\omega t - \phi) \qquad 29$$

The potential and current signals may be represented as complex numbers in the following manner:

$$V(t) = V_0 e^{j\omega t} \qquad and \qquad I(t) = I_0 e^{j(\omega t - \phi)} \qquad 30$$

Consequently, the impedance Z can be defined as a complex number:

$$Z(\omega) = \frac{V(t)}{I(t)} = \frac{V_0 e^{j\omega t}}{I_0 e^{j(\omega t-\phi)}} = \frac{V_0}{I_0}\frac{e^{j\omega t}}{e^{j\omega t}\, e^{-j\phi}} = Z_0 e^{j\phi} = Z_0\,(\cos\phi + j\,\sin(\phi)) = |Z| exp\,(j\phi) \quad 31$$

By using Euler's Formula:

$$e^{j\phi} = \cos\phi + j\sin\phi \quad 32$$

where, ϕ is a real number, and $j = \sqrt{-1}$, respectively. Consequently, we may express the impedance as a complex number. The real component and the imaginary component are denoted as Z_{Re} and Z_{im} respectively:

$$Z(\omega) = Z_{Re} + j\ Z_{im} \quad 33$$

With $|Z| = \sqrt{{Z_{Re}}^2 + {Z_{im}}^2}$ and $\tan\phi = \frac{Z_{im}}{Z_{Re}}$

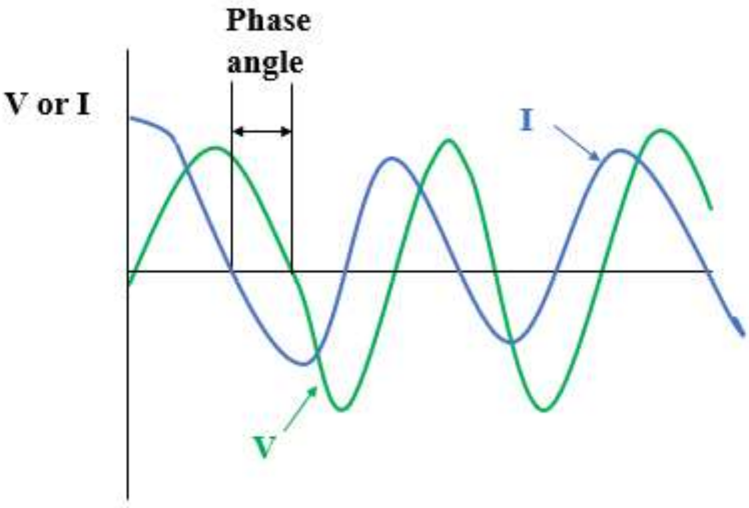

***Figure 2.5**: Sinusoidal potential voltage and current response with a phase angle*

The graphical representation of an impedance in the complex plane for various frequencies is known as the Nyquist diagram. This consists of plotting the imaginary part of the impedance $-Z_{im}$ as a function of its real part Z_{Re}.

In the Nyquist Plot, impedance is represented as a vector (arrow) with a magnitude of |Z|. The angle between this vector and the X-axis (ϕ) is designated as the "phase angle" (Figure 2.6). The graph often includes one or more semicircles. Each semicircle denotes a unique time constant. The appearance of the curve makes it possible to recognize different elementary stages in the corrosion process, and to assess the level of degradation of a metallic material in its environment. Nevertheless, the Nyquist plot possesses a significant drawback in that the frequency cannot be determined merely by examining the plot.

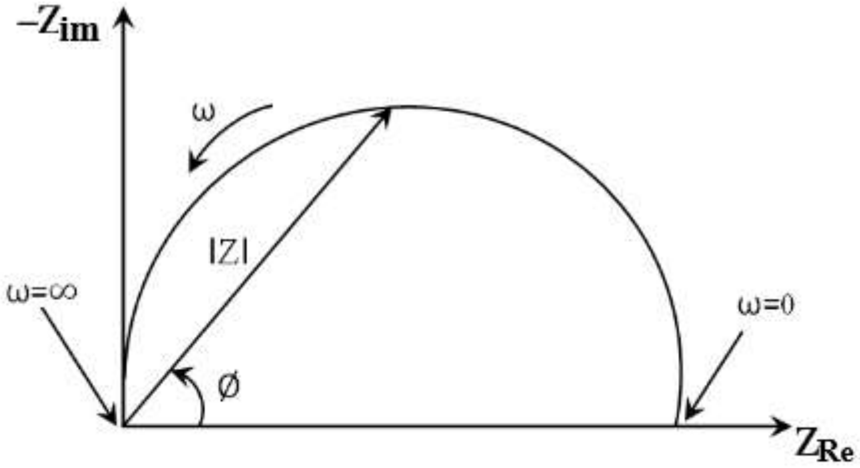

Figure 2.6: *Nyquist plot for a simple electron transfer reaction*

On the other hand, in the Bode diagram, the logarithm of frequency is plotted along the X-axis, and two Y-axes represent the modulus of impedance |Z| and the phase angle φ (Figure 2.7). Analysis of the electrochemical impedance as a function of frequency makes it possible to distinguish the various elementary phenomena as a function of their characteristic frequency.

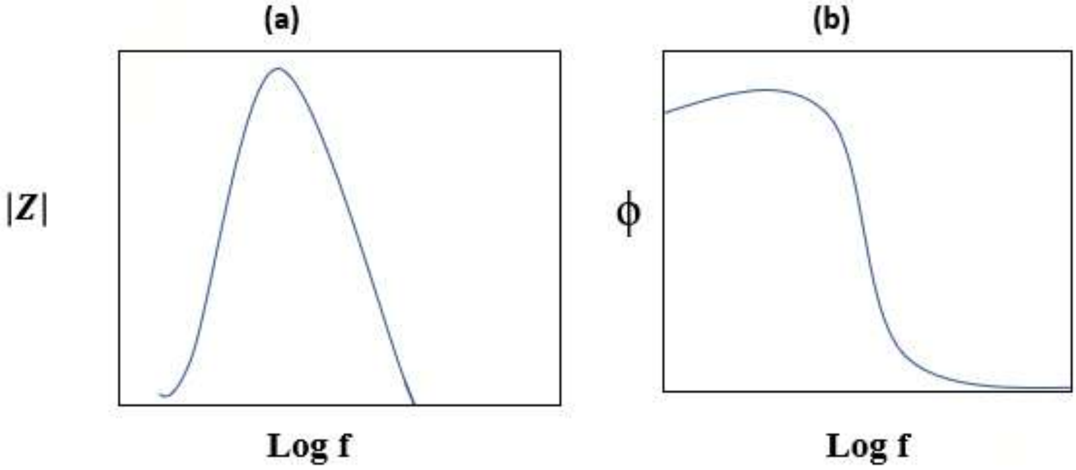

Figure 2.7: *Bode plot for a simple electron transfer reaction*

Because different electrical circuits can often produce similar EIS responses, accurately interpreting an electrochemical system requires a good understanding of its expected behavior. It is important to anticipate the possible electrochemical reactions first to build a meaningful model that reflects the real physical processes. The electrical models used aim to represent key corrosion phenomena at the metal/solution interface, such as charge transfer, diffusion, and adsorption. To make sense of EIS data, researchers typically use Equivalent Electrical Circuits (EECs) made up of idealized components like resistors, capacitors, and inductors. These parts are configured in series or parallel patterns to simulate different processes occurring at the interface. Various types of circuit models have been proposed to match different kinds of EIS plots [104]. The components used in this study are as follows:

Resistor:

The impedance of a resistor is invariant with frequency and comprises solely a real component. Consequently, the impedance of a resistor (Z_R) is equivalent to its resistance (R).

$$Z_R = R \tag{34}$$

The primary types of resistances analyzed in EIS phenomena include ohmic, electrolyte, polarization, and charge transfer resistances [31].

Capacitor:

The impedance of a capacitor is contingent upon frequency and can be determined by:

$$Z_C = \frac{1}{j\omega C} \tag{35}$$

where C is the capacitance. The current phase through the capacitor is shifted by +90°, relative to the voltage phase. The capacitor is used to denote, for instance, the capacitance of the coating and the double-layer capacitance[31].

Inductor:

The impedance of an inductor (Z_L) is frequency dependent and is expressed as:

$$Z_L = j\omega L \tag{36}$$

L denotes the inductance. The current phase through the inductor is changed by -90°, relative to the voltage phase.

Constant phase element

In certain instances, such as surface heterogeneity and the non-ideal capacitive characteristics of a coating, a constant phase element (CPE) is employed instead of a capacitor. Its impedance is expressed as [26]:

$$Z_{CPE} = \frac{1}{Y_0 (j\omega)^n} \tag{37}$$

In this context, Y_0 denotes the constant of the Constant Phase Element (CPE), n signifies the CPE exponent indicative of heterogeneity ($-1 \leq n < 1$); $j = \sqrt{-1}$ is the imaginary unit, and ω is defined as 2πf, where f represents the frequency in Hertz. For n = 0, the Constant Phase Element (CPE) behaves as a resistor; for n = 0.5, it resembles Warburg impedance; for n = 1, it functions as a capacitor; and for n = −1, it acts as an inductor.

The adsorption of an organic inhibitor on the surface of a carbon steel is often described by an equivalent electrical circuit that comprises a CPE:

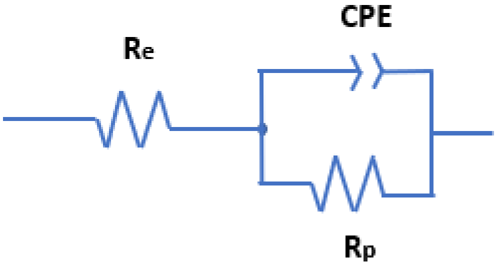

***Figure 2.8**: An Electrical equivalent circuit with CPE*

Where R_e is the resistance of the electrolyte, R_p the polarization resistance. The double layer capacitance value is determined using the following equation :

$$C_{dl} = (QR_P^{1-n})^{\frac{1}{n}} \qquad 38$$

The gradual adsorption of inhibitor molecules onto the substrate is shown on the Nyquist diagram by an expansion of the capacitive loop's diameter, resulting in an increase in R_{ct} and a drop in C_{dl}. The inhibition efficiency from the impedance analysis is calculated based on:

$$\eta_{EIS}(\%) = \frac{R_{p-inh} - R_p}{R_{p-inh}} \times 100 \qquad 39$$

Where R_{p-inh} and R_p are the polarization resistance in the presence and the absence of the inhibitor molecules, respectively.

2.2.2.3 Experimental conditions

The experimental set-up used comprises a three-electrode chemical cell powered by a Potentiostat, linked to a computer for acquiring and processing the results, as showcased in Figure 2.9. The experiments were carried out using two types of potentiostats, Tacussel-Radiometer PGZ 100, accompanied by Volta Master 4.0 Software, and an Origalys potentiostat equipped with Origa Master software. To refine and fit the experimental results, other software was used, such as Ec-Lab and OriginPro 8.5.

The carbon steel specimens were the working electrode (WE), the platinum was the auxiliary electrode/ counter electrode (CE), and a saturated Calomel Electrode ($Hg/Hg_2Cl_2/KCl$) was the reference electrode (RE) (Figure 2.3).

Before each test, the electrode surface must be well polished, washed, and dried. The electrode is held at its corrosion-free potential for 30 minutes, till the system is steady-state and the potential is constant.

EIS tests were performed afterwards at E_{ocp} at a frequency range of 100 kHz to 0.01 Hz with a 10 mV AC signal amplitude.

The current-potential curves are obtained in potentiodynamic mode, with the potential applied to the sample varying continuously at a sweep rate of 0.1 mV/S. This speed enabled us to place ourselves in a quasi-stationary regime. The curves were recorded over a potential range of -600 and -200 mV/SCE.

For all electrochemical measurements, the reproducibility of the results and the reliability of the experimental setup were ensured by performing each test a minimum of three times.

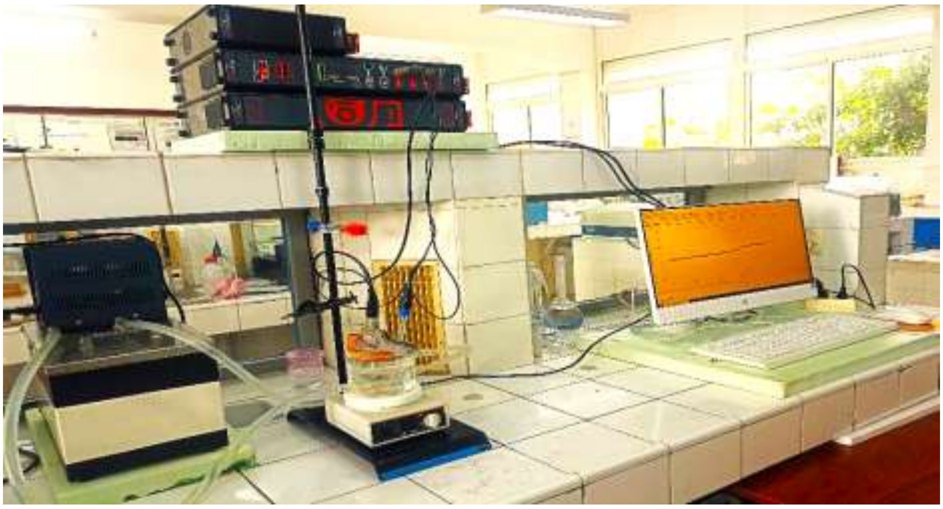

Figure 2.9: *Experimental setup for electrochemical studies at the LMNE laboratory.*

Electrochemical techniques are critical tools in the study of corrosion inhibition, allowing scientists to precisely quantify corrosion rates, identify active electrode reactions, and monitor changes in protection or passivation in real time and under in situ settings. These approaches are particularly useful because they provide macroscopic, surface-averaged insights on corrosion inhibitor performance, environmental aggressiveness, and degradation susceptibility of various materials. However, because the collected data represent overall surface behavior, interpreting results for complex, heterogeneous surfaces like steel, with its various grain patterns and oxide layers, can be difficult. As a result, in order to gain a more complete and accurate knowledge of corrosion mechanisms, electrochemical data are frequently supplemented with surface characterization techniques and theoretical modeling approaches. Together, these approaches provide a more comprehensive and nuanced picture of inhibitor action and corrosion processes.

2.2.3 Surface analysis and characterization techniques

Multiple techniques are used to investigate the crystalline structure and topography of surfaces. Some, such as optical microscopy (OM) and scanning electron microscopy (SEM), give microscopic and morphological information; others, such as X-ray diffraction (XRD), are used to investigate the crystalline structure and phase composition of materials.

2.2.3.1 Scanning electron microscopy

Scanning Electron Microscopy (SEM) is a high-resolution imaging method often used to analyze surface morphology and near-surface features. SEM is useful in corrosion investigations due to its higher resolution than optical microscopy, allowing for accurate detection of surface characteristics and corrosion-induced morphological changes. SEM works by creating a high-energy electron beam from an electron cannon and focusing it using electromagnetic lenses (Figure 2.10). The tiny electron probe interacts with the specimen surface, producing signals such as secondary electrons, backscattered electrons, and distinctive X-rays.

Secondary electrons are released from the surface area, providing high-resolution topographic data. Backscattered electrons caused by elastic interactions with sample atoms provide compositional contrast, with heavier elements appearing brighter than lighter ones. However, since they emanate from deeper locations, their spatial resolution is somewhat lower than secondary electrons. SEM's spatial resolution generally varies between 1 and 20 nm, depending on the acceleration voltage.

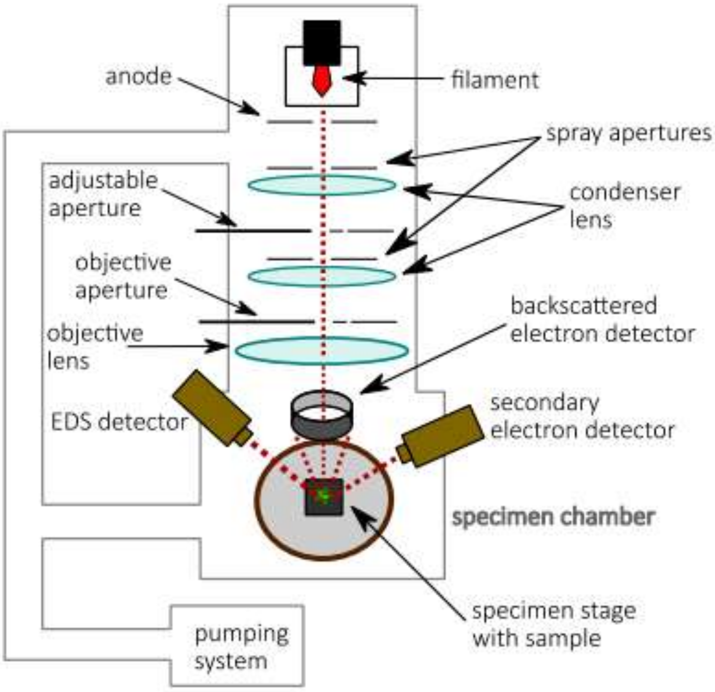

Figure 2.10: *Schematic representation of a scanning electron microscope with secondary electron, backscattered electron, and energy dispersive X-ray detectors.*

Energy Dispersive X-ray Spectroscopy (EDX) with SEM provides qualitative and quantitative elemental analysis. The interaction of the electron beam with the sample atoms ejects inner-shell electrons, which are then relaxed to create X-rays that are distinctive of the elements present. EDX analysis produces spectra with each peak representing a specific element, enabling identification and quantification. EDX's surface sensitivity is restricted since X-rays have a deeper origin than secondary electrons. At 20 kV accelerating voltage, sample depths may reach 1-2 microns. The Energy Dispersive Spectroscopy (EDS) technology detects both big elements (>10 wt%) and small elements (1-10 wt%). However, it is less sensitive to trace elements (below 0.1 wt%), hence oligoelements (<0.01 wt%) often go unnoticed [105]. Furthermore, EDX can generate chemical distribution maps, which provide spatial data on elemental distribution throughout the sample surface. The detection limit varies with surface quality; smoother surfaces have lower detection thresholds[106].

In corrosion research, SEM paired with EDX is critical for morphological characterization, involving recognizing corrosion forms, including pits, fractures, and surface deposits. Moreover, Chemical characterization entails analyzing the composition of corrosion products and identifying contaminants. Researchers use morphological and compositional data to better understand corrosion processes, including degradation routes and inhibitor effects. Thus, the combined SEM/EDX analysis gives complete information by linking surface morphology with chemical composition, which is critical for assessing the protective behavior of corrosion inhibitors.

In this study, SEM imaging was performed on the surface of cleaned and polished carbon steel samples, in both the absence and presence of corrosion inhibitors. The shape of the protective layer generated on the steel surface was investigated after immersion in a 1 M HCl solution for a set number of hours, with and without the optimal inhibitor concentration (equivalent to the highest concentration tested). These investigations were carried out utilizing a JEOL JSM-IT100 scanning electron microscope with an accelerating voltage of 20 kV and an Energy Dispersive X-ray Spectroscopy (EDX) instrument (Figure 2.11).

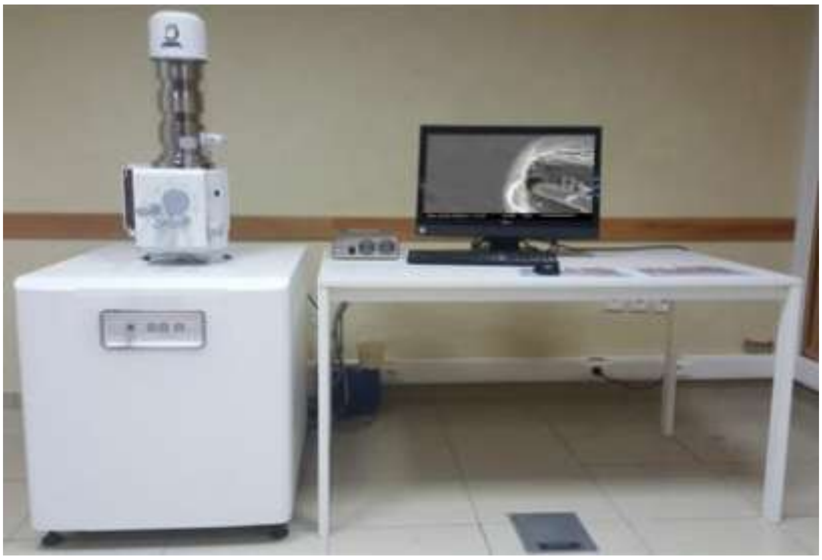

***Figure 2.11**: Scanning Electron Microscope available at the Faculty of Science of Rabat*

2.2.3.2 X-ray diffraction

X-ray diffraction (XRD) is a frequently used analytical method for studying crystalline materials. It identifies metals, alloys, minerals, and corrosion products on suitable thickness surfaces. XRD is important for differentiating between crystalline and amorphous materials because it produces distinct diffraction patterns caused by the interaction of incoming X-rays with the sample's crystal lattice. XRD is based on X-ray scattering by atoms in a crystalline substance. Because X-ray wavelengths are equivalent to inter-atomic distances, diffraction occurs when an incoming X-ray beam interacts with the crystal's regularly spaced atomic planes. W. L. Bragg and his son devised Bragg's law in the early 20th century to explain the phenomenon of diffraction [107]. The equation is:

$$2\, d \sin\theta = n\, \lambda \qquad 40$$

Where the number n represents the order of reflection, λ represents the wavelength of the incident X-rays, d is the distance between atomic planes, and θ represents the angle of incidence (and reflection). When Bragg's condition is met, constructive interference produces severe diffraction peaks at specified angles (Figure 2.12).

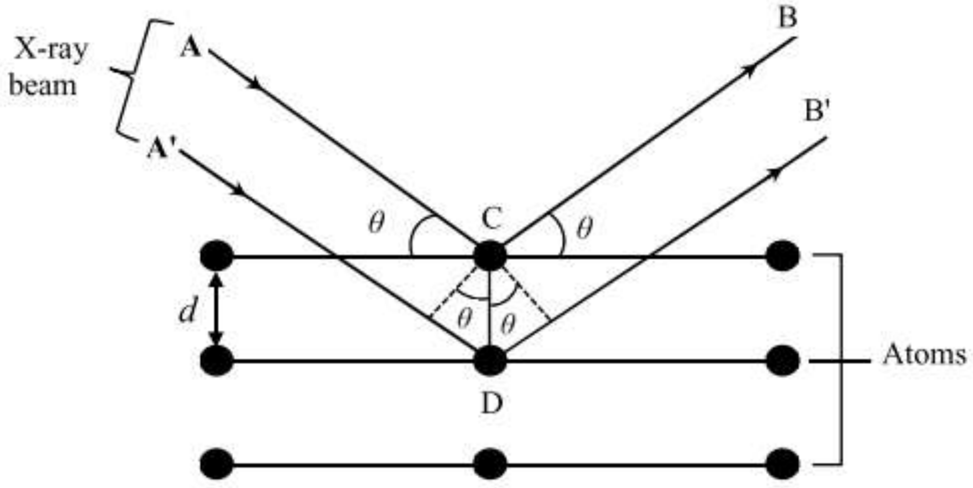

Figure 2.12: *Bragg’s law of diffraction*

X-rays are generated in a cathode ray tube by heating a filament to produce electrons, which are accelerated toward a metal target (commonly copper, molybdenum, iron, or chromium) under a high voltage (typically 40 kV). When high-energy electrons impact a target, they expel inner orbital electrons, creating distinct X-ray spectra. The Kα and K_β lines are often employed. This work used a copper target to create CuKα radiation with a wavelength of 1.5418 Å, resulting in monochromatic X-rays for reliable diffraction observations. The X-rays are then collimated and focused on the sample. As the sample and detector spin, the intensity of diffracted X-rays is recorded as a function of the scattering angle (2θ), yielding a diffraction pattern typical of the crystal structure of the sample. Each crystalline phase generates a separate collection of diffraction peaks, enabling phase identification, determining lattice parameters, and insights into the symmetry and size of the unit cells.

At ambient temperature, a Shimadzu 6100 diffractometer with a copper anode (λCuKα = 1.541838 Å), a THA-1101 thin film fixture, and a CM-4121 monochromator counter were used to conduct XRD studies on the alloy's surface. The samples were scanned at a speed of 2° per minute throughout a 2θ range of 20° to 80°, using a tube voltage of 40 kV and a current of 30mA. Figure 2.13, depicts the Shimadzu 6100 diffractometer setup utilized in these investigations.

While XRD is an effective technique for identifying phases and analyzing crystalline structures, it is only applicable to crystalline materials. Diffraction patterns from amorphous substances or weakly crystalline phases may not be distinguished. Nevertheless, XRD may be used to analyze bulk materials and powders, as long as the sample is homogeneous.

Figure 2.13: *Shimadzu 6100 diffractometer available at the Faculty of Science of Rabat*

2.2.4 Solution analysis techniques: UV-VIS spectroscopy

While SEM and XRD investigations give critical information about the morphology, composition, and crystalline structure of corrosion products formed on the carbon steel surface in the absence and presence of inhibitors, these methods are intrinsically confined to surface characterization. To have a deeper comprehension of the corrosion and inhibition mechanisms, it is vital to look at the behavior of the solution phase. UV-Visible spectroscopy was used in Chapter 4 to evaluate the 1 M HCl solution after immersing the carbon steel samples. UV-Vis spectroscopy detects dissolved metal ions, inhibitor species, and possible reaction products in solution, providing further insights into inhibitor efficacy and corrosion processes.

UV-Visible absorption spectroscopy is based on molecules' capacity to absorb electromagnetic radiation in two primary regions: the ultraviolet (UV) domain, which is between 190 nm and 400 nm, and the visible domain, which is from 400 nm to 800 nm. This radiation is an electromagnetic wave with energy (E) and frequency (ν) connected by the following equation:

$$E = h\,\nu = h\,c\,/\,\lambda \qquad 41$$

Here, h is Planck's constant, c is the speed of light, and λ is the wavelength of the incoming radiation. UV-Visible spectroscopy offers information on the nature of chemical bonds within a sample and is also used to quantitatively assess the quantity of species that absorb in the specified spectral range. This approach is rapid, non-destructive, and often used in chemical and biological examinations, as well as corrosion research [108,109].

When exposed to UV-Visible light, organic compounds may undergo electronic transitions that include σ bonds, π bonds, or non-bonding electron pairs n. The absorption bands seen in the spectra correspond to molecular orbital (MO) transitions involving chromophore groups. Figure 2.14 identifies four major kinds of electronic transitions [110]:

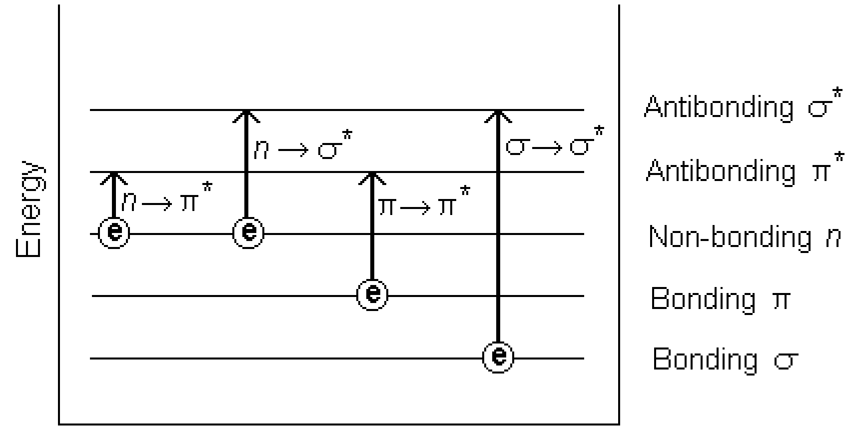

***Figure 2.14**: Presentation of the possible electronic transitions*

- The $\sigma \rightarrow \sigma*$ transition happens in the far UV region (~130 nm) and needs considerable energy to promote an electron from a bonding σ orbital to an antibonding σ orbital.
- The $n \rightarrow \sigma *$ transition occurs when a non-bonding electron (n) is excited to an antibonding $\sigma *$ orbital. It is medium in intensity and occurs between 150 and 250 nm, with alcohols about 180 nm, ethers and halogenated derivatives around 190 nm, and amines around 220 nm.
- The $n \rightarrow \pi *$ transition includes the excitation of a non-bonding electron to an antibondingπ ∗ orbital. It is characteristic of molecules having lone pair electrons on heteroatoms in unsaturated systems and typically emerges beyond 200 nm, for example, between 270 and 295 nm for carbonyl groups (-C=O).
- The π→π ∗ transition occurs in compounds with isolated double bonds and is typically impacted by the presence of heteroatomic substituents. It is usually found at 170 nm in ethylenic compounds.

A UV-Visible spectrophotometer consists of five fundamental components: a radiation source, a wavelength selection device (monochromator), a sample container, a detector, and a data output system [91]. These pieces work together to correctly assess a sample's absorbance in the UV and visible spectral regions. UV-Visible spectroscopy is especially useful since it enables both qualitative and quantitative investigations of organic and inorganic chemical entities that absorb in this range. It is one of the most well-known and used procedures in contemporary analytical chemistry.

In Chapter 4, UV-Visible spectroscopy was used to explore the inhibition of carbon steel corrosion in 1 M HCl. The inhibitory function was investigated by examining the probable complexation of iron ions generated during corrosion with inhibitor molecules[25]. Absorbance spectra were recorded at room temperature using a UV-Visible spectrophotometer (model Jasco V-730) (Figure 2.15) for three types of samples: (i) the 1 M HCl solution containing the inhibitor, (ii) the uninhibited acid solution after immersion of a carbon steel substrate, and (iii) the inhibited acid solution at the optimum inhibitor concentration of 10^{-3} M after 24 hours of substrate immersion. This experimental technique allows for the monitoring of chemical species development in solution, as well as the identification of possible interactions between iron ions and inhibitor compounds.

***Figure 2.15**: UV-Vis spectrophotometer (Jasco model V-730 available at the LMNE Laboratory*

2.3 Theoretical methods for the study of corrosion inhibition

Recent breakthroughs in theoretical and quantum chemistry have made these disciplines essential in materials research. Their value is well proven, whether for predicting the chemical reactivity of organic compounds, linking molecular structure with activity, or proposing and validating methods of interaction between molecules and substrates. Numerous theories have been created to thoroughly examine chemical reactivity. The main strategies include the transition State Theory (TST). This methodology elucidates chemical reaction kinetics by positing a quasi-equilibrium between reactants and an activated complex (transition state). Although very successful at elucidating the mechanics of several events, precisely identifying transition states continues to pose challenges, especially for intricate systems[25]. Likewise, there is the Frontier Molecular Orbital (FMO) Theory, which represents a qualitative framework for elucidating reaction processes, particularly in organic chemistry and the interactions between organic molecules and solid surfaces. It also elucidates spectroscopic and reactivity characteristics using a reduced static methodology [111]. Additionally, the reactivity descriptors are quantities derived from quantum chemical calculations, namely DFT, that characterize molecules in isolation (static) or interaction (dynamic). They aid in identifying active regions within chemical systems and the varieties of molecular interactions [112].

This study focuses on the latter two concepts, FMOs and DFT-based descriptors, to elucidate the interaction processes of organic inhibitors with metallic substrates and to interpret the reported experimental outcomes. Molecular Dynamics Simulations (MDS) were used to investigate the interaction energies between inhibitors and metallic surfaces.

2.3.1 Density Functional Theory (DFT)

While experimental methods provide exceptionally accurate data, comprehending electronic interactions requires theoretical backing. Density Functional Theory is extensively used to forecast electrical characteristics and elucidate experimental findings on corrosion inhibition [113][9][8]. Two fundamental inquiries direct the examination of chemical reactivity: What factors contribute to the varying reactivity of different molecules? What accounts for the increased reactivity of certain locations inside molecules? DFT and FMO theories provide critical insights to overcome these issues.

Density Functional Theory (DFT) is a quantum mechanical approach extensively used to examine the electronic structure of atoms, molecules, and solids. The concept asserts that the ground-state characteristics of a many-electron system may be fully determined from its electron density, as opposed to the many-body wavefunction. Utilizing approximations like the Generalized Gradient Approximation (GGA) or hybrid functionals, DFT allows an accurate and computationally efficient representation of electrical systems. The fundamental mathematical formulations and theoretical derivations that support DFT, together with the relevant equations and approximations, will be elaborated upon in the appendix.

Global and Local Reactivity Descriptors Derived from DFT for corrosion inhibition

The examination of frontier molecular orbitals is a fundamental notion for evaluating molecular reactivity. The energies of the Highest Occupied Molecular Orbital (HOMO) and the Lowest Unoccupied Molecular Orbital (LUMO) dictate the interactions of molecules with other chemical entities or surfaces [112]. The HOMO energy (E_{HOMO}) reflects a molecule's capacity to donate electrons; an elevated E_{HOMO} indicates a stronger propensity to transfer electrons to unoccupied orbitals of acceptor entities, such as the d-orbitals of metal atoms. Conversely, the LUMO energy (E_{LUMO}) indicates the molecule's ability to receive electrons [112]. The energy difference between these two orbitals ($\Delta E = E_{LUMO} - E_{HOMO}$) indicates the molecule's reactivity. A reduced energy gap signifies a more reactive species, promoting electron transfer during adsorption processes [111].

Although HOMO and LUMO energies characterize the overall electrical properties of the molecule, Fukui functions provide a localized viewpoint, pinpointing certain atoms or locations within the molecule that are particularly vulnerable to electrophilic or nucleophilic attack [114]. Fukui indices are determined based on variations in electron density resulting from the addition or removal of one electron.

f^{+} (for nucleophilic attack) :

$$f_K^{+} = q_K(N+1) - q_K(N) \qquad 42$$

f^{-} (for electrophilic attack) :

$$f_K^{-} = q_K(N) - q_K(N-1) \qquad 43$$

Here, q_K denotes the total charge associated with atom *k* within the molecule, representing the electron density at a given spatial position *r* surrounding the molecular structure. N corresponds to the total number of electrons in the neutral molecule, while N+1 refers to the formation of a singly charged anion resulting from the addition of an electron to the lowest unoccupied molecular orbital (LUMO). Conversely, N−1 represents a singly charged cation generated by the removal of an electron from the highest occupied molecular orbital (HOMO) of the neutral species.

These functions assist in forecasting the active sites responsible for interactions with the metal surface, hence enhancing the comprehension of molecular inhibitory processes beyond the capabilities of global descriptors alone.

A significant electronic characteristic affecting adsorption behavior is the dipole moment. The dipole moment (μ) quantifies the distribution of positive and negative charges in a molecule, making it a crucial statistic for evaluating molecular polarity [112]. In the realm of corrosion prevention, chemicals exhibiting elevated dipole moments are often correlated with enhanced contacts with metallic surfaces via physical adsorption processes [115,116]. A high μ value often indicates an increased capacity to orient positively and bond with the charged metal surface, hence improving the inhibitor's efficacy.

Electronegativity (χ) and chemical potential (μ) are two essential notions generated from DFT that characterize a molecule's propensity to attract electrons. The parameters are derived from the ionization potential (I) and electron affinity (A) computed using the HOMO and LUMO energies, respectively, following Koopmans' theory [115].

$$I = -E_{HOMO} \quad , \quad A = -E_{LUMO} \qquad 44$$

resulting in:

$$\chi = -\mu = \frac{I+A}{2} \qquad 45$$

$$\eta = \frac{I-A}{2} \quad (global\ hardness) \qquad 46$$

Electronegativity indicates a molecule's capacity to attract electrons, while chemical potential quantifies the propensity of electrons to escape from the system. The ideas of hardness and softness further elucidate the ease with which a molecule may deform or interact with external entities. By using the values of electronegativity and hardness, one may measure the extent of electron transfer between an inhibitor molecule and a metallic surface, represented by the proportion of electrons transferred, ΔN.

The fraction of electrons transferred (ΔN) assesses the degree of electron donation from an inhibitor molecule to the metal surface. This transfer is essential for stabilizing adsorption and improving corrosion protection [115]. ΔN is determined using the equation :

$$\Delta N = \frac{\Phi_{Fe} - \chi_{inh}}{2\,(\eta_{Fe} + \eta_{inh})} \qquad 47$$

Where Φ and χ_{inh} denote the work function of the iron surface (Fe) and the absolute electronegativity of the inhibitor molecule, respectively, while η_{Fe} and η_{inh} refer to the absolute hardness of iron and that of the inhibitor molecule, respectively. The computation of the ΔN value is more suitably executed using the work function Φ rather than the electronegativity of $\chi._{Fe}$. Consequently, in the computation of ΔN, $\chi._{Fe}$ is substituted with Φ .

DFT simulations provide work function values Φ of 3.91 eV, 4.82 eV, and 3.88 eV for the Fe (100), Fe (110), and Fe (111) surfaces, respectively [117]. The work function value for the Fe (110) surface is 4.82 eV. The global hardness of iron is regarded as zero (η_{Fe} = 0) , based on the premise that, in a metallic mass, the ionization potential (I) is equivalent to the electron affinity (A), as metallic systems exhibit greater softness than neutral metal atoms [118]. Higher ΔN values signify more effective electron transfer, promoting stronger inhibitor adsorption.

Calculation procedure

The geometry of the examined organic molecules was optimized in the ground state in aqueous solvent conditions utilizing "Materials Studio" software (version 7.0, Accelrys Inc.) based on the DMol^3 module. Calculations were performed using Density Functional Theory (DFT), using the Generalized Gradient Approximation (GGA) with the Perdew–Burke–Ernzerhof (PBE) functional and the "Double Numerical plus Polarization" (DNP) basis set, configured to a quality level of 4.4. The solvent's influence was considered by the implicit Conductor-like Screening Model (COSMO) used in the DMol^3 module. The Conductor-like Screening Model for Real Solvents (COSMO-RS) was used to improve the characterization of solvation effects. The "Materials Studio" platform offers very efficient quantum mechanical applications using DFT. These approaches guarantee excellent precision in predicting thermodynamic, kinetic, and structural parameters, hence enhancing the value of the experimental results. This platform provides comprehensive functionality for optimizing molecular and crystalline geometries, investigating reaction routes, and simulating optical, infrared, and Raman spectra.

2.3.2 Molecular Dynamics

Molecular simulation integrates various computational methodologies, particularly Monte Carlo (MC) and Molecular Dynamics (MD), to represent materials as assemblages of discrete particles (atoms, clusters of atoms, molecules, or macromolecules); notably, MD simulations excel in delivering atomistic-level, temporally-resolved insights into corrosion mechanisms, inhibitor adsorption, and metal–electrolyte interfacial phenomena. In molecular dynamics, each atom is subjected to forces determined from an empirical potential energy function. The potential energy is expressed as:

$$V_{total} = V_{bonding} + V_{non-bonding} \qquad 48$$

In this context, binding interactions (bonds, angles, dihedrals) and non-bonded interactions (Van der Waals, electrostatics) are parameterized [111]; the forces correspond to the negative gradient of the total potential energy:

$$F_i = -\nabla_{\mathrm{ri}} V_{total} \qquad 49$$

The forces are included in Newton's equations of motion (37), which are numerically integrated for each i at each timestep to update positions r_i and velocities $\frac{dr_i}{dt}$,to produce the system trajectory.

$$m_i = \frac{d^2 r_i}{dt^2} = F_i \qquad 50$$

m_i is the mass of the particle (atom) and $\frac{d^2 r_i}{dt^2}$ its acceleration. The index i=1, 2…..N runs over all N particles in the simulation box [116].

A standard protocol entails constructing and solvating the system, followed by energy minimization (using steepest descent or conjugate gradient methods) to reduce initial stresses. Subsequently, atom positions and velocities are initialized (rescaled to ensure zero net momentum and achieve the target temperature via $\langle v^2 \rangle = kBT/m$). The system is then equilibrated under NVT/NPT ensembles until bulk properties stabilize, after which production runs are conducted over femtoseconds to nanoseconds timescales to sample pertinent dynamics. From these trajectories, one extracts diffusion coefficients from mean–square displacement, radial distribution functions, coordination numbers, binding energies of inhibitors to metal surfaces, thermodynamic quantities (free-energy profiles, entropy), and dynamical properties (viscosity, dielectric relaxation) [111,116,119,120]. Hence, MD facilitates dynamic sampling of adsorption/desorption events, conformational exploration (augmented by simulated annealing), and quantitative assessments of inhibitor-surface affinities under realistic electrolyte conditions, enabling researchers to clarify at the molecular level how organic inhibitors engage with, and safeguard, metallic surfaces from acid corrosion.

Calculation procedure

All molecular dynamics simulations were conducted in Materials Studio (Forcite module) using the COMPASS III force field inside an NVT ensemble at 303 K. A flawless bcc-Fe crystal was sliced along the (110) plane, selected for its elevated stabilization energy and dense packing, and further optimized before being expanded to a 10 × 10 supercell with a slab thickness of 16 Å to enhance surface area. A neighboring solvent/inhibitor layer (24.82 × 24.82 × 25.14 Å^3) was constructed using the Amorphous Cell tool, including one inhibitor molecule (triazole- or hydrazone-derivative), 491 H_2O molecules, 9 Cl^- ions, and 9 H_3O^+ ions to simulate acidic corrosion conditions. The combined Fe slab and solution block were situated inside a periodic box of 24.82 × 24.82 × 35.69 $Å^3$. Following the preliminary energy reduction (utilizing steepest descent and conjugate gradient methods) to reduce substantial stresses, velocities were assigned and adjusted to ensure zero net momentum and $\langle v^2 \rangle = k_BT/m$. The dynamics were then propagated with a 1 fs timestep for 5,000 ps, using "Fine" Forcite settings. Single-point energies were documented for the whole adsorption system (E_{total}), the metal and solution subsystem ($E_{surface+sol}$), the inhibitor and solution subsystem ($E_{inh+sol}$), and the isolated solution (E_{sol}), facilitating the computation of the adsorption energy:

$$E_{ads} = E_{total} - (E_{surface+sol} + E_{inh+sol} + E_{sol}) \qquad 51$$

2.4 Conclusion

This chapter describes the experimental methodologies used to study the inhibitory efficacy of selected triazole and hydrazone derivatives against steel corrosion in a 1 M HCl solution. A full description of the electrochemical cell configuration and the prepared steel samples was given. The conditions under which electrochemical measurements were performed were also described. To verify the credibility of the data, each electrochemical assay was performed three times. In addition, the experimental conditions for scanning electron microscopy coupled with energy-dispersive X-ray spectroscopy (SEM-EDX), X-ray diffraction, and UV-visible spectroscopy were described, as these techniques were used to supplement and interpret the electrochemical measurements. Finally, theoretical methods were used to supplement the experimental investigation. The goal of this computational research was to link the observed inhibition performance with the chemical and structural properties of each inhibitor under investigation. Wherever feasible, theoretical findings were employed to identify the most probable active sites involved in the adsorption process and to strengthen our knowledge of the molecular inhibitory processes.

Chapter 3: Corrosion inhibition of carbon steel in 1M HCl by a novel triazole derivative: Experimental and theoretical studies

3.1 Introduction

Carbon steel is a widely used material, with various applications in different fields of the industry, thanks to its great mechanical properties, its availability, and its low cost [121]. The one drawback that directly affects this material's endurance is its poor corrosion resistance when in contact with an aggressive medium. Acid solutions are widely used in many industrial processes such as cleaning, etching, descaling and, pickling of metal [122]. In particular, Hydrochloric acid is among the most used mineral acids for acidizing in oil and gas production in order to improve the new wells' productivity, also to restore the aging ones[123]. In the occurrence of these treatments, carbon steel is target to intense corrosion mechanisms, thus, it is of great importance to come up with sensible procedures in order to prevent or at least mitigate the deterioration of these materials. The introduction of corrosion inhibitors into the system is one of the most practical approaches that provide protection to metals against corrosion[124]. There are various inhibitor types and compositions, such as organic compounds, that, compared to inorganic ones, have lower toxicity and better efficiency at small concentrations [125–128]. Since most of the organic molecules studied for anticorrosion applications have reactive sites like Nitrogen, Sulfur, Oxygen, Phosphorus and π-electrons, they could be adsorbed on the metal surface, and hence they can afford adequate protection against corrosion[129]. Among the diverse class of five-membered nitrogen-containing heterocycles, triazoles have attracted considerable attention due to their favorable characteristics, including environmental compatibility, low production cost, and straightforward synthetis routes. A wide range of triazole derivatives have demonstrated significant pharmacological potential, exhibiting activities such as antibacterial, antioxidant, antitubercular, antidepressant, anti-inflammatory, anticonvulsant, and antineoplastic effects [65]. It is in this context that 1,2,4-triazole derivatives seem to be good candidates as organic corrosion inhibitors[130,131]. Many previous works have found that they have a good corrosion inhibition efficiency on carbon steel in acidic medium: HCl [132–134] ,or H_2SO_4 [135,136].

In view of the literature cited above, the purpose of this piece of research is to investigate the inhibition effect of a novel triazole derivative, namely 5-hexylsulfanyl-1,2,4-triazole (HST), an eco-friendly compound, on the carbon steel in 1M HCl. Mass loss measurements were carried out and electrochemical methods were used to study the corrosion/inhibition mechanism. The effect of temperature on the dissolution of iron in the carbon steel both in the presence and in absence of inhibitor molecules has been also studied. The thermodynamic parameters were calculated and discussed. Furthermore, the morphology of the inhibited and uninhibited carbon steel specimens was analyzed by scanning electron microscopy coupled with X-ray detection

(SEM-EDX) also, the crystalline microstructure was evaluated by x-ray diffraction. Furthermore, extensive theoretical analyses were performed at both microscopic and atomic levels utilizing Molecular Dynamics (MD) simulations and Density Functional Theory (DFT) calculations to examine the interfacial adsorption behavior of the triazole derivative on the carbon steel surface and to delineate its chemically reactive regions. These computational methods provide enhanced understanding of the molecule's adsorption characteristics, therefore enabling a more informed discourse on the probable corrosion inhibition mechanism.

3.2 Synthesis of inhibitor

Compound (HST) (referred to as 2a in its synthesis scheme) was synthesized in the Medicinal Chemistry Laboratory, at the Faculty of Medicine and Pharmacy of Rabat, according to the following procedure described in Figure 3.1. We have carried out the condensation of 1,2,4-triazole-5-thione with alkylating agents containing aliphatic chains. The reagents were used in stoichiometric amounts, under the conditions of phase transfer catalysis (liquid-solid) in the presence of potassium carbonate as an inorganic base, in dimethylformamide as solvent and Tetrabutylammonium bromide (BTBA) as a catalyst.

To a solution of 1,2,4-triazole-5-thione (0,01mole) **1** and alkylating agents (0,01mol) in dimethylformamide (50 ml), potassium carbonate (0,016 mol) and (0,0005 mole) of the Tetrabutylammonium bromide (BTBA) as catalyst were added. The mixture was stirred at room temperature for 24hr. The solution was filtered and the filtrate was evaporated. The residue was recrystallized from ethanol to give product **2a** with a yield of 65%.

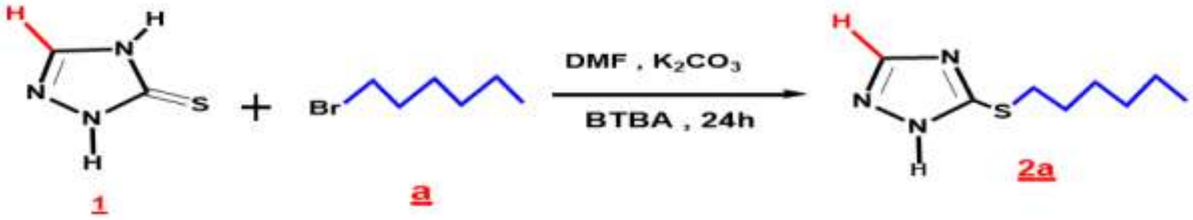

Figure 3.1 : *Mechanistic pathway for synthesis of 5-hexylsulfanyl-1,2,4-triazole*

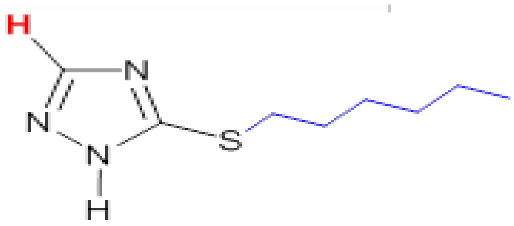

5-hexylsulfanyl-1,2,4-triazole

Chemical formula: $\mathbf{C_8H_{15}N_3S}$

Molecular weight: 185.1 g/mol

3.3 Effect of Concentration

The influence of inhibitor concentration on the corrosion behavior of carbon steel in 1 M HCl was systematically investigated using both gravimetric and electrochemical methods. These techniques provided complementary insights into the efficiency and mechanism of inhibition as a function of inhibitor dosage.

3.3.1 Mass loss measurements

The carbon steel specimens were abraded with different grades of emery papers, washed with distilled water, degreased with acetone, dried, and kept in a desiccator. After being weighed accurately, the specimens were immersed vertically in the corrosive solution in the absence and in the presence of the inhibitor (HST) at different concentrations for 12 hours at a constant temperature of 298 K.

No further increase in inhibition efficiency took place beyond this immersion time. Afterward, they were taken out and rinsed thoroughly with distilled water and acetone, dried, and weighed once again. All measurements were carried out according to ASTM G 31–72[100] standard. The corrosion rate C_R is given by the following Equation:

$$C_R = \frac{K \times W}{A \times t \times \rho} \qquad 52$$

In the above equation, $\rho = 7.86$ g cm^{-3}, W signifies the mass loss expressed in gram, $K = 8.76 \times 10^4$; t represents the immersion time of the specimens inside the tested solution, t is usually denoted in hours, and A is the exposed area in cm^2 [137]

Afterward, they were taken out and rinsed thoroughly with distilled water and acetone, dried and weighed once again.

The inhibition efficiency $\eta_G$can be determined as previously mentioned in equation (17) :

$$\eta_G(\%) = \frac{C_R - C_{R-inh}}{C_R} \times 100$$

Where C_R and $C_{R-inh}$are the corrosion rates in the absence and the presence of the inhibitor compound, respectively.

The values in Table 3.1 show that the increase of the inhibitor's concentration from 10^{-6} to 10^{-3} M causes a decrease in the corrosion rate C_R of the carbon steel from 77 to 34 µg cm² h^{-1}, accompanied by an increase in the inhibition efficiency η_G (%) from 86 % to 93 %. This can be explained by the strong adsorption of inhibitor molecules on the metal surface [138]. Therefore, this result suggests that increasing the inhibitor concentration leads to more adsorbed inhibitor molecules on the carbon steel surface, which block more corrosion active sites, thus preventing mass loss more efficiently.

***Table 3.1:** Parameters obtained from mass loss measurements of the carbon steel after 12 h. immersion in 1.0 M HCl solution with and without the addition of different concentrations of the HST at 298 K.*

[Inhibitor] (M)	C_R **(µg .cm².h^{-1})**	**η_G(%)**
1.0 M HCl	550.6 ± 3.0	-
10^{-6}	77.1 ± 2.0	86
10^{-5}	63.7 ± 2.6	88
10^{-4}	54.6 ± 2.0	90
10^{-3}	34.9 ± 2.5	93

3.3.2 Potentiodynamic polarization

All experiments were performed using Volta lab (Tacussel- Radiometer PGZ 100), driven by a computer equipped with software Voltamaster 4. Measurements are made in a three-electrode, double-walled, thermostatically controlled Pyrex glass cell of 80 mL, with an auxiliary electrode in platinum (Pt) and a reference electrode used in saturated calomel (SCE). The working electrode in CS, in the shape of a rod, has a working surface of 1 cm^2. Before starting a new practice measure, the area of the working electrode is carefully treated, as previously mentioned in Chapter2. The electrode is maintained before each measurement at its corrosion-free potential, which is experimentally established by the location of the MS working electrode in the studied solutions in a time interval of about 30 min, which is proven to be sufficient to attain steady-state open circuit potential (OCP) [139]. Measurements have been achieved in potentiodynamic mode at a scanning rate of 0.1667 mV/s, a potential range between −0.8 VSCE and −0.2 VSCE compared to the corrosion potential, and at a temperature of 298 K. Potentiodynamic polarization curves obtained from carbon steel in 1M HCl with and without the triazole compound (HST) are represented in Figure 3.2. While electrochemical parameters extracted by extrapolation of Tafel lines such as: corrosion potential (E_{corr}), corrosion current density (i_{corr}), anodic and cathodic Tafel slopes (β_a) and (β_c) respectively as well as the inhibition efficiency $\boldsymbol{\eta_{PDP}}$(%) calculated from polarization measurements based on the previously cited equation are gathered in Table 3.2.

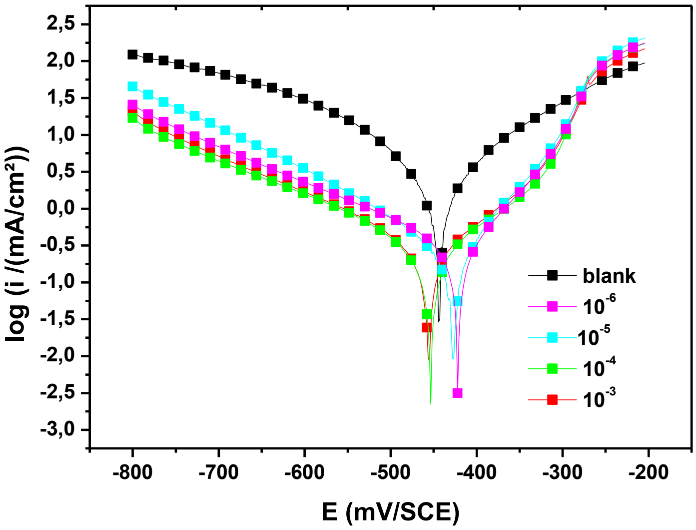

Figure 3.2: *Potentiodynamic polarization curves for carbon steel corrosion in 1M HCl with numerous HST concentrations at 298K.*

In our case, we were working in an acidic solution, so the dissolution of the metal (iron) allows the metal ions to pass from its surface into the solution; this is the anodic reaction. Whereas, the release of hydrogen protons that contribute to the production of H_2 and/or the reduction of oxygen consists the reaction taking place at the cathodic region. The role of an inhibitor is to either trouble the cathodic or the anodic reaction, or both.

Table 3.2: *Electrochemical data from potentiodynamic polarization study for Carbon steel in inhibited and inhibitor-free solution at 298K.*

Medium	**Concentration (M)**	$-E_{corr}$ **(mV/SCE)**	i_{corr} $(\mu A.cm^{-2})$	β_a $(mV.dec^{-1})$	$-\beta_c$ $(mV.dec^{-1})$	$\eta_{PDP}(\%)$
HCl	1	443	2984	149	151	-
HST	10^{-6}	421	265	76	168	91
	10^{-5}	426	187	74	176	93
	10^{-4}	452	132	116	184	95
	10^{-3}	455	58	111	191	98

On the cathodic region, Tafel lines are parallel (Figure 3.2) and cathodic Tafel slopes (β_c) from Table 3.2 remain almost unchanged, suggesting hydrogen protons' reduction on the metal surface is controlled by activation, also, the mechanism of hydrogen evolution is not altered by the addition of the triazole derivative (HST) [140]. This may be a result of the fact that obstruction of the corrosion process is mainly due to the blocking of present active sites over the metal surface [141].

In contrast, on the anodic region, Tafel curves reveal that the inhibition mode of the studied triazole derivative depends on the electrode potential [142]. In fact, for a voltage superior to -250 mV/SCE, we can observe that there is little effect to the presence of the (HST) compound, implying that the steel dissolution is more dominant than the inhibitor molecules' adsorption. When potentials are in the proximity of or below -250 mV, the rise in (HST) concentration generates a decrease in the current densities. In such circumstances, the adsorption rate of (HST) is still higher than its desorption rate. However, when the potentials became more positive than the desorption potential -250 mV, the existence of the triazole compound (even at high concentrations) no longer altered the current-potential characteristics. This can be attributed to an increase in surface area as carbon steel is dissolving and (HST) is being adsorbed to the metal surface simultaneously, so in this case, the desorption rate of the triazole derivative is higher than its adsorption rate. Nevertheless, we can notice that both the anodic and cathodic current densities in the presence of (HST) dropped, hence, the inhibitor hinders the anodic and cathodic reactions.

According to [143,144] an inhibitor molecule can be classified as anodic, cathodic or mixed type based on the displacement of E_{corr} values with and without inhibitor molecules. When the displacement in the absence and presence of the inhibitor is more than 85 mV, the inhibitor molecules are accurately branded as anodic or cathodic type. In our study, we found that displacement of E_{corr} values is less than 85 mV for the studied inhibitor (HST), implying that the synthesized triazole molecule is of mixed type inhibitor.

We can see from the curves, that the addition of increasing concentrations of the inhibitor induced a shift towards the lower region in current densities in comparison to the blank acid medium, accompanied with a significant rise in the inhibition efficiency η_{PDP}. When concentration of inhibitor C_{inh} is maximum i.e 10^{-3} M, i_{corr} decreases from 2984.85 $\mu A.cm^{-2}$ to 58.81 $\mu A.cm^{-2}$ (η_{PDP} of 98%) according to Table 3.2. This outcome confirms that the synthesized triazole molecule can serve as good corrosion inhibitor. The high obtained inhibition efficiency can be related to the molecular structure of the tested compound among other factors. From scheme 3.1, it is observed that inhibitor molecule contains a triazole ring, a long alkyl chain which is an electron donating group, and delocalized π-electrons in its structure. As all such groups actively participate in donor–acceptor (D–A) type of interactions with the empty d orbitals of the carbon steel metallic surface, therefore inhibitor molecules strongly adhere on the carbon steel surface and only small sites are available for the acid attack [141].

The obtained results are in good agreement with the mass loss measurement results: the inhibition efficiency increases with the increase of (HST) concentration, which may suggest that the increase of the inhibitor's concentration prompts the increase of the surface coverage, thus leading to enhanced adsorption on the carbon steel surface and lesser surface area available for corrosion.

3.3.3 Electrochemical impedance spectroscopy

The electrochemical impedance measurement has been conducted in the same environment in which the polarization curves were performed, and at a frequency range of 100 kHz to 10 mHz, with a sinusoidal disturbance potential applying a 0.01 V in amplitude, and with a datum-point density of 10 steps for each decade.

The ability of the triazole derivative (HST) to inhibit the corrosion of carbon steel and retard its rate was investigated by EIS and results are displayed in Figure3.3 and Figure 3.4.

We can see that the impedance response of carbon steel has significantly changed after the addition of the triazole derivative, and this change is manifested in the increase of the diameter of the semi-circles with the increase in the inhibitor's concentration. The Nyquist spectra yields slightly depressed semicircles at high to medium frequencies (at low to medium Z_r) and an inductive (reverse capacitive) feature at lower frequencies (at high Z_r). The capacitive loop can be attributed to the charge transfer resistance that is parallel to the double layer capacitance and this implies that the corrosion of CS is controlled mainly by a charge transfer process [145,146], also, the increase of the diameter is more pronounced as the concentration of the inhibitor increases which can be attributed to the formation of a protective layer at the metal surface that acts as a barrier for the mass and the charge transfer [146]. Whereas, the inductive loop can be attributed to the relaxation process that is obtained by the adsorption of intermediate products such as $(FeCl^-)_{ads}$ in the blank acid solution and $(FeCl^-, inh^+)_{ads}$in the presenec of inhibitor [147–149]. The deviation from the ideal semi-circle shape is mostly due to frequency dispersion known as the depression effect [140,150].

Phase angle and modulus plots are represented in Figure 3.4, Bode plot refers to the existence of a single constant phase that describes the interfacial impedance. Also, it is clear that the increase of absolute impedance at the low frequency values in the Bode plot approves of the higher protection that comes with the increase of the HST's concentration on the carbon steel surface [151]. Based on the appearance of the phase angle plots, we can see that the increase in the inhibitor concentration generates close to 70° absolute value of the phase angle plots, indicating that there is a superior corrosion inhibition behavior attributed to the adsorption of more inhibitor molecules on the metal surface at higher concentrations.

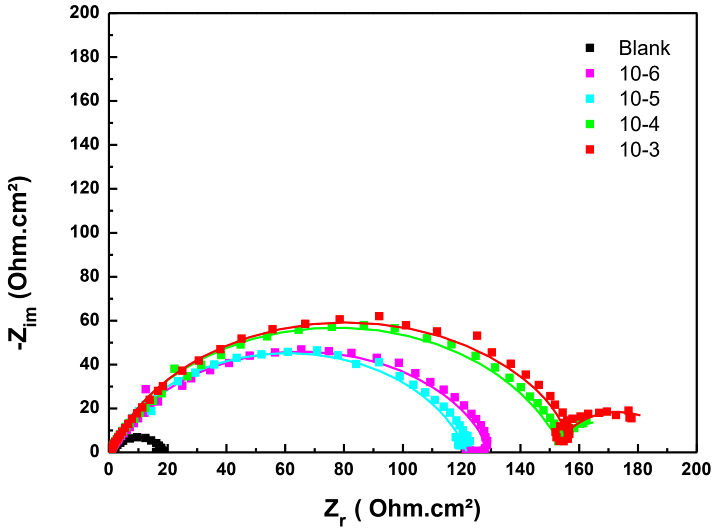

Figure 3.3: *Nyquist plots for the carbon steel in 1M HCl solution containing various concentrations of the triazole derivative at 298K.*

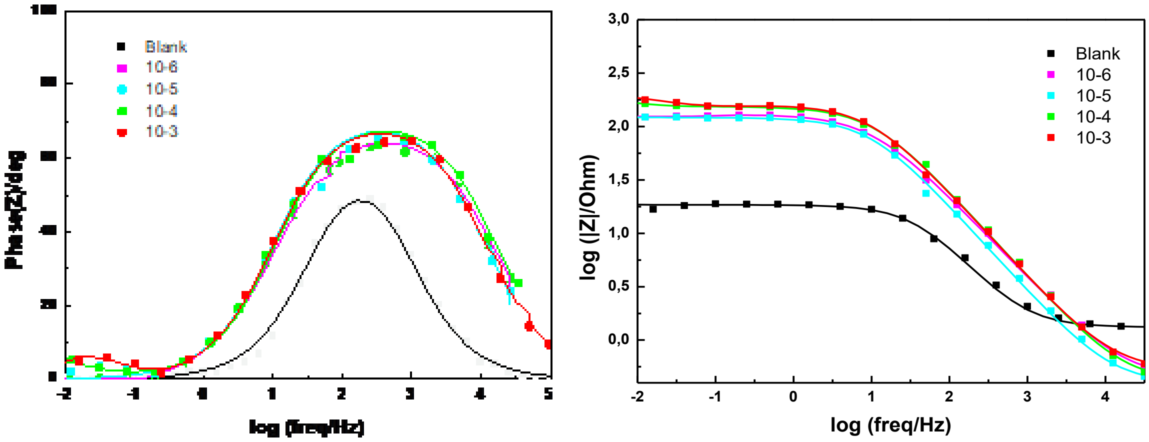

Figure 3.4: *Bode plots for the carbon steel in 1M HCl solution containing various concentrations of the triazole derivative at 298K.*

In order to determine the impedance parameters from the experimental results, the obtained data were fitted to electrical equivalent circuits proper to each case using Ec-Lab software, as shown in *Figure 3.5*a, b and c. The circuits compromise a solution resistance R_s that is referred to as R_1in series with the circuit. R_{ct} is the charge transfer resistance that is referred to as R_2, meanwhile Q_2 or Q_{dl} is the constant phase element (CPE) for the double layer which has been used instead of a pure capacitor in order to compensate the unideal capacitive behavior of the surface due to its inhomogeneity because of its corrosion in the acid medium [114]. The impedance of the CPE (Z_{CPE}) is derived from the following equation[152]:

$$Z_{CPE} = Q^{-1}(j\omega)^{-n} \qquad 53$$

Where the CPE constant Q is in $(\Omega^{-1}.s^{n}.cm^{-2})$, ω is the angular frequency in $(rad.s^{-1})$, j is the imaginary number and n is the phase shift that can be explained as the degree of the surface inhomogeneity[152].

When introducing the concentrations 10^{-6} and 10^{-5}M of the inhibitor respectively, we can notice the appearance of the inductance L and its resistor R_L which are referred to as L_3 and R_3 respectively in the circuit *Figure 3.**5***(b). As the concentration of the triazole compound increases to 10^{-4} and 10^{-3}M, the continuous adsorption of its molecules forms a protective film on the metal surface that has a resistance R_f and a constant phase element Q_f described on the circuit *Figure 3.**5*** (c) as R_4 and Q_4 respectively.

The calculated impedance parameters are given in Table 3.3, including the film capacitance C_f in $(F.cm^{-2})$ and the double layer capacitance C_{dl} in $(\mu F.cm^{-2})$ calculated from Equation 38 according to the Hsu and Mansfeld formula [153] :

$$C_{dl} = (Q\, R_p{}^{1-n})^{\frac{1}{n}}$$

Where R_p is the polarization resistance in $(\Omega.cm^{2})$, that is also used to calculate the inhibition efficiency $\eta_Z(\%)$. In our case, we used the polarization resistance because it generally includes the charge transfer resistance R_{ct}, the diffusion layer resistance R_L, the film resistance R_f in addition to the accumulation of corrosion products at the metal/solution interface resistance R_a. $R_p = R_{ct}+R_L+R_f+R_a$ [147,154]. The contribution of all these resistances must be taken into account.

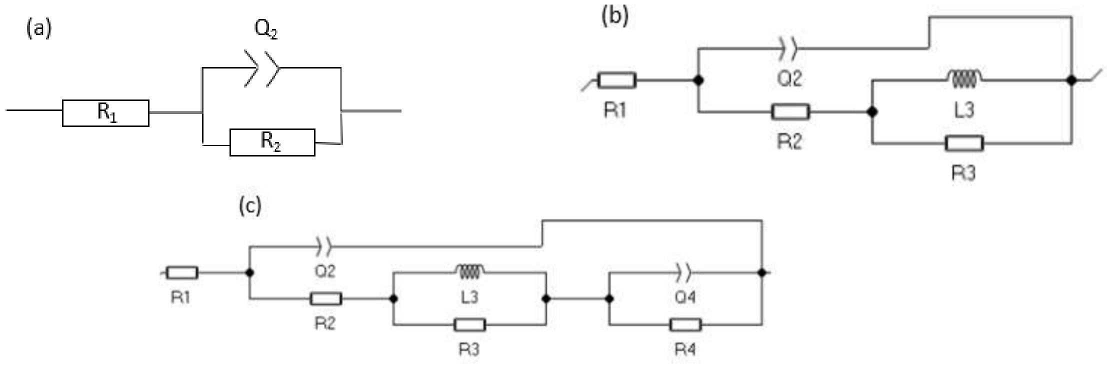

Figure 3.5: *The equivalent circuits models for the corrosion process of CS: (a) in the blank acid medium, (b) in presence of* 10^{-6} *and* 10^{-5} *M of the inhibitor and (c) in presence of* 10^{-4} *and* 10^{-3} *M of the inhibitor.*

***Table 3.3**: The impedance parameters recorded of the carbon steel in 1M HCl medium both in the absence and presence of increasing concentrations of HST compound.*

	Conc (M)	R_s $\Omega.cm^2$	R_{ct} $\Omega.cm^2$	$10^3 Q_{dl}$ $(\Omega^{-1}.cm^{-2}.s^n)$	C_{dl} $\mu F.cm^{-2}$	n_1	R_L $\Omega.cm^2$	L $H.cm^{-2}$	R_f $\Omega.cm^2$	$Q_f(\Omega^{-1}.cm^{-2}.s^n)$	C_f $F.cm^{-2}$	n_2	R_p $\Omega.cm^2$	η_{EIS} (%)
HCl	1	1.345	17.14	0.537	234	0.85	-	-	-	-	-	-	17	-
HST	10^{-6}	0.389	121	0.285	129	0.81	1	0.70	-	-	-	-	122	86
	10^{-5}	0.434	123.5	0.289	114	0.78	7	10	-	-	-	-	130	87
	10^{-4}	0.403	153.9	0.215	100	0.81	1	48×10^{-6}	28	0.65	0.73	0.96	184	90
	10^{-3}	0.518	154.4	0.220	105	0.81	6	3	38	0.19	0.21	0.95	198	91

An attentive examination of the results showcased in Table3.3 shows that the values of R_p increase whereas the values of C_{dl} decrease when we move from the uninhibited solution to the inhibited one, and this behavior is more accentuated when the concentration of the inhibitor increases. This can be due to a decrease in the local dielectric constant and/or an increase in the thickness of the electrical double layer. The drop in the C_{dl} values can also be attributed to the gradual replacement of the water molecules adsorbed on the carbon steel surface by the inhibitor molecules [147,155].This suggests that the triazole derivative is an adsorptive inhibitor meaning that it acts via adsorption leading us to assume that the rise in the polarization resistance is directly related to the adsorption of the inhibitor at the metal/electrolyte interface.

In addition to that, we can see that there is not a very significant shift in the n values after the addition of escalating concentrations of the inhibitor which can help in the prediction of the dissolution mechanism, citing that the charge transfer process controls the dissolution mechanism both in the absence and presence of the triazole derivative [156]. The conclusions taken out from the EIS study concord with both the gravimetric study and the potentiodynamic polarization.

3.4 Adsorption isotherm

To gain deeper insight into the interaction between the inhibitor molecules and the carbon steel surface, adsorption isotherm models were applied to the experimental data obtained from gravimetric and electrochemical studies.

To asses either an inhibitor is efficient or not, we resort to evaluate its ability to be adsorbed on the metal surface and the mechanisms by which this adsorption might occur. Adsorption of organic inhibitor molecules from an aqueous solution is mainly a quasi-substitution action between the organic compounds present in the aqueous phase and the water molecules present at the surface of the electrode, as the metal surface is usually covered with adsorbed water dipoles in aqueous solutions [157].

$$Org_{(sol)} + x\,H_2O_{(ads)} \leftrightarrow Org_{(ads)} + x\,H_2O_{(sol)} \qquad 54$$

Where $Org_{(ads)}$ and $H_2O_{(sol)}$ are the organic species adsorbed on the metallic surface and the water molecule in solution, respectively, x is the size ratio, which is, the number of water molecules replaced by one organic inhibitor.

To gauge the nature and the strength of adsorption of the triazole derivative on the carbon steel surface, the experimental results were fitted to different adsorption isotherm models. The plot of $\frac{C}{\theta}\ vs\ C$ (Equation 55) , where θ are the values of surface coverage obtained from the potentiodynamic polarization measurements corresponding to different inhibitor's concentrations C, can be seen in Figure 3.6, and it exhibits a straight line proving the suitability of the Langmuir isotherm model [158]:

$$\frac{C_{inh}}{\theta} = \frac{1}{K_{ads}} + C_{inh} \qquad 55$$

Where C_{inh} symbolizes the concentration of HST, and K_{ads} signifies the adsorption equilibrium constant. The values of both K_{ads} obtained from the reciprocal of the intercept of the Langmuir isothem and the Gibbs free energy of adsorption $\Delta G°_{ads}$ calculated from the following (Equation 56) [158] are 2×10^{-6} L/mol and −45.9 kJ mol^{-1}, respectively.

$$\Delta G°_{ads} = -RT\ Ln(K_{ads}\ 55.5) \qquad 56$$

Where R is the universal gas constant, T is the absolute temperature of the experiment, and 55.5 is the concentration of water in solution in (mol/l).

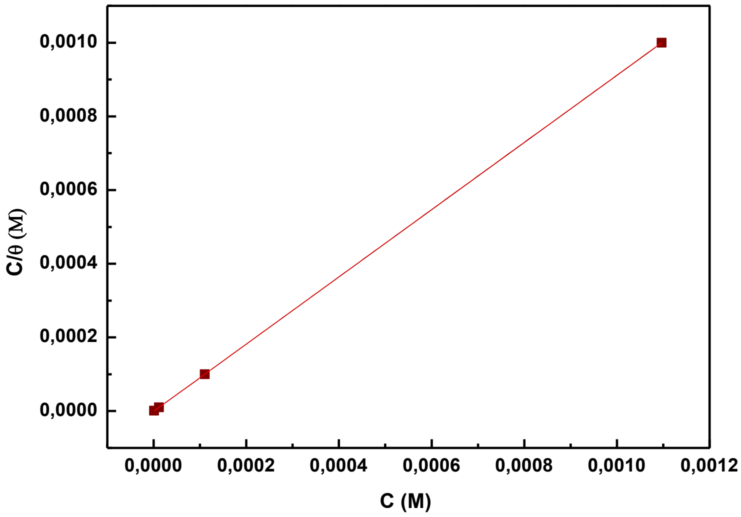

Figure 3.6: *Langmuir adsorption isotherm of (HST) on the carbon steel surface at 298K.*

The high value of K_{ads} implies that the triazole derivative molecules are strongly adsorbed on the carbon steel surface, hence providing better inhibition efficiency [159]. The negative value of $\Delta G°_{ads}$ proves the spontaneity of the adsorption process and the stability of the inhibitor film adsorbed on the metal surface [160].

According to earlier literature [158,161], adsorption free energy $\Delta G°_{ads}$ values around –20 kJ/mol or less negative are typically associated with electrostatic interactions between charged inhibitor molecules and the metal surface, indicating physisorption. In contrast, values near –40 kJ/mol or more negative are often interpreted as evidence of chemisorption, involving the formation of coordinate bonds through electron sharing or transfer between the inhibitor and the metal surface. In the present study, the calculated $\Delta G°_{ads}$ value of –45.9 kJ/mol suggests that the adsorption of the triazole derivative onto carbon steel is primarily chemical in nature. However, this classification has recently been challenged in 2022 [162], as the use of $\Delta G°_{ads}$ alone has proven insufficient to definitively distinguish between physisorption and chemisorption. As such, the adsorption energy values reported here should be viewed as indicative rather than conclusive.

Table 3.4: *Values of K_{ads} and $\Delta G°_{ads}$ for carbon steel in the presence of (HST) in 1M HCl at 298K.*

inhibitor	**R²**	K_{ads} **(L/mol)**	$\Delta G°_{ads}$ **(kJ/mol)**
(HST)	1	$2.\ 10^6$	-45.9

3.5 Effect of temperature

The interaction between the carbon steel electrode and the corrosive acid medium in the absence and presence of the inhibitor molecules can be altered by the temperature of the study [158]. In order to inspect (examine) the effect of the temperature on the inhibition efficiency of the studied triazole derivative, polarization tests were carried out in the temperature range of 298K to 338K in the 1M HCl medium with and without the inhibitor at its optimal concentration, as shown in Figure 3.7. In Table 3.5 are outlined the values of the measured electrochemical parameters such as corrosion potential (E_{corr}) and corrosion current density (i_{corr}), as well as the inhibition efficiency η. From these results, it can be seen that the corrosion current density values slightly increased in the presence of the triazole derivative when increasing temperatures compared to the exempt acid medium, which shows a considerable increase. Also, the inhibition efficiency of the HST compound shifts to a slight extent towards lower values (89% at 333K), which suggests that the inhibitor molecules still get adsorbed on the metal surface, thus it is still efficient at the studied range of temperature.

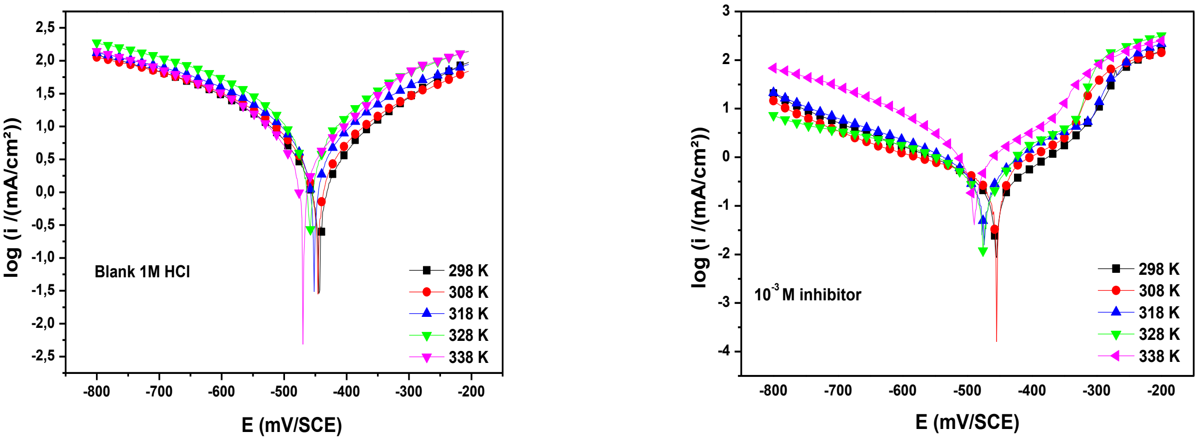

Figure 3.7: *Potentiodynamic polarization curves for corrosion of carbon steel in 1M HCl solution with and without the presence of 10^{-3} M of (HST) at different temperatures.*

***Table 3.5:** Corrosion parameters obtained from weight potentiodynamic polarization of carbon steel in 1 M HCl with and without the addition of various concentrations of (HST) at different temperatures.*

Medium	**Temperature (K)**	i_{corr} ($\mu A.cm^{-2}$)	$-E_{corr}$ (mV/SCE)	**ηPDP(%)**
Blank (1.0 M HCl)	298	2984	443	-
	308	3635	445	-
	318	5114	452	-
	328	7067	458	-
	338	7184	470	-
HST	298	58	455	98
	308	129	453	96.4
	318	310	474	93.9
	328	542	474	92.3
	338	763	489	89.3

The corrosion reaction can be considered as an Arrhenius form process following the equation below [163] :

$$i_{corr} = A.exp\left(-\frac{E_a}{RT}\right) \qquad 57$$

Where (E_a) is the apparent activation energy of the corrosion process, (R) is the universal gas constant, (T) is the absolute temperature, and (A) is the Arrhenius pre-exponential factor.

Figure 3.8 exhibits the Arrhenius plots for corrosion current density of the carbon steel in both the acid medium with and without the inhibitor. While Table 3.6 shows the values of apparent activation energy (E_a) that were determined from the slope of ln (i_{corr}) vs 1/T plots. From these results, it is clear that the value of activation energy in the presence of the (HST) compound (55.20 kJ/mol) is much higher compared to the value obtained in its absence (20.36 kJ/mol), this suggests that the triazole derivative can form an energy barrier to protect the steel surface from corrosion [144,164].

The alternative Arrhenius plots of *Ln* i_{corr} */T vs 1/T* for carbon steel dissolution in the acid media in the presence and absence of the inhibitor shown in Figure3.9, were used to calculate activation parameters such as ΔH_a and ΔS_a based on the following equation [163] :

$$i_{corr} = \frac{RT}{Nh} exp\left(\frac{\Delta S_a}{R}\right) exp\left(-\frac{\Delta H_a}{RT}\right) \qquad 58$$

Where h is Planck's constant, N is the Avogadro number, R is the universal gas constant, ΔH_a is the enthalpy of activation and ΔS_a is the entropy of activation.

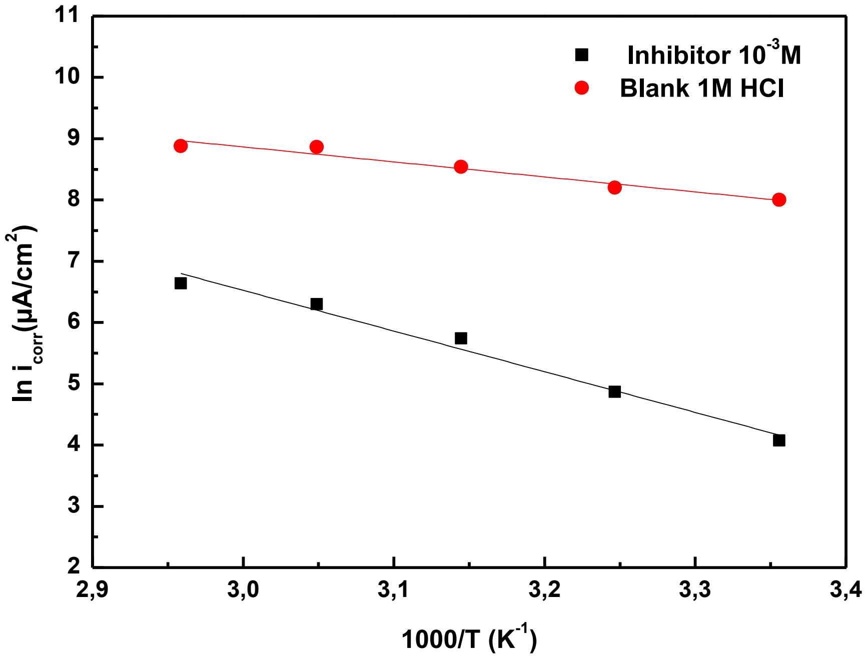

Figure 3.8: *Arrhenius plots of Ln (i_{corr}) vs 1/T for carbon steel in the absence and presence of (HST) compound at its optimal concentration.*

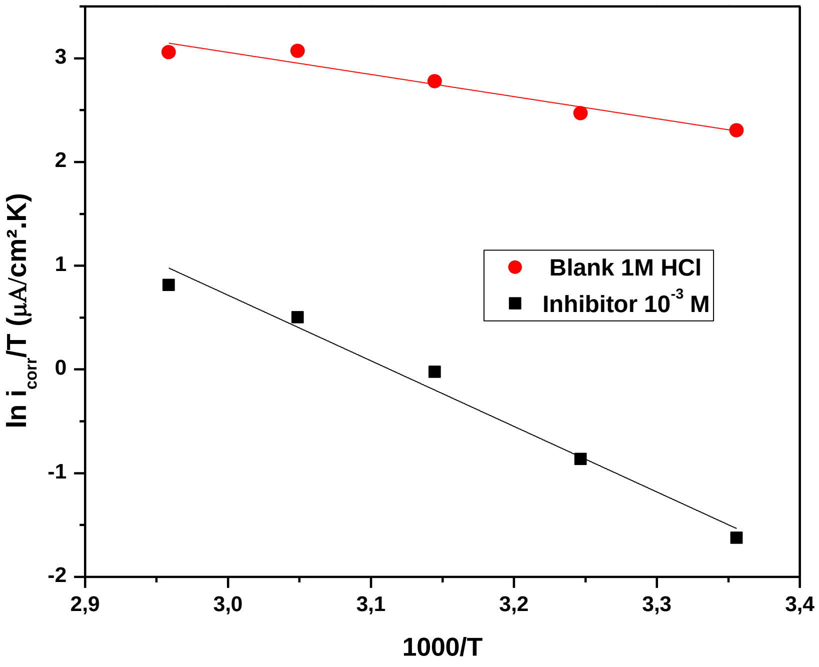

Figure 3.9: *Arrhenius plots of Ln(i_{corr} /T) vs 1/T for carbon steel in the absence and presence of (HST) compound at its optimal concentration*

Table 3.6: *Activation parameters for the steel dissolution in 1M HCl in the absence and the presence of (HST) at optimum concentration.*

Medium	E_a **(kJ/mol)**	ΔH_a**(J/mol)**	ΔS_a **(J/mol. K)**
Blank (1.0 M HCl)	20.36	17.72	-118.82
Inhibitor (10^{-3} HST)	55.20	52.56	-33.79

It is clear from Table 3.6, that on the one hand, the values of enthalpy of activation $\Delta H_a$are positive both in the blank acid solution and in the presence of optimal concentration of inhibitor, this positive shift is manifestation that the adsorption of the (HST) compound on the carbon steel surface is an endothermic process, and that an energy barrier was created in the presence of the triazole derivative. Contrarily, under the same conditions, the values of the entropy of activation are negative; this is due to association of the present inhibitor molecules rather than its dissociation. Furthermore, the ΔS_a value in the presence of (HST) is higher than ΔS_a in the blank uninhibited solution, this suggests that the level of randomness (disorder) increased when going from reactants to the activated complex. This observed rise may be due to the adsorption of the inhibitor molecules from the acid HCl solution which can be considered, as previously mentioned in the adsorption isotherm part, as a quasi-substitution process between the organic (HST) compound molecules present in the aqueous phase and the water molecules already adsorbed at the carbon steel surface [157]. To sum up, when the inhibitor is adsorbed on the metal, the water molecules are desorbed from the surface at the same time, hence increasing the entropy of activation.

3.6 Structural and microscopic characterization

To complement the electrochemical and thermodynamic analyses, structural and surface characterizations were carried out using SEM-EDX and XRD techniques in order to examine the morphology and composition of the carbon steel surface after exposure to the corrosive medium with and without inhibitor.

3.6.1 SEM/EDX study

Scanning electron microscopy was performed using JEOL-Model JSM-IT 100 in conjugation with an energy dispersive spectrometer, with an energy of acceleration of 20 kV, in order to do a morphological examination as well as the composition of the film formed on the carbon-steel specimens' surface after immersion for 12 h in both the blank acid solution 1M HCl and the one containing optimum concentration of the inhibitor. Different locations of the sample were analyzed to ensure the reproducibility of the study.

Figure 3.10 exhibits the SEM micrographs together with the EDS spectra of the polished, uninhibited and inhibited carbon steel, respectively. Figure 3.10 (a&b) shows the SEM micrograph and its corresponding EDS spectra of the carbon steel polished prior to its immersion in the corrosive medium, it shows a smooth surface exempt from any defects, while the spectra represent the characteristic peaks of the elements constituting the studied carbon steel. Figure 3.10 (c&d) represents the SEM image and the corresponding EDS spectra of the carbon steel after its immersion for a period of 12h in the corrosive medium 1M HCl without the studied inhibitor. It can be seen that the metal surface was severely damaged and is heterogenous containing some large and deep holes due to the aggressive attack of the acid, meanwhile the EDS spectra yields additional peaks of chloride and oxygen with an evident decrease in the intensity of iron peaks, proving the important dissolution of the metal in the HCl medium, as well as the disappearance of some elements. In the presence of the triazole derivative at its optimum concentration, it can be observed from Figure 3.10 (e) that the metal surface contained fewer holes and is slightly smoother and more homogenous as a consequence of the reduced attack by the acid solution. The matching EDS spectra in Figure 3.10 (f) shows the disappearance of both the chloride and oxygen peaks accompanied with the appearance of a nitrogen peak which is an element constituting the inhibitor molecule, leading us to confirm that the inhibitor molecules were adsorbed and formed a layer on the carbon steel surface to protect it from corrosion. We can also notice an enhancement in the intensity of the iron peaks, due to the decrease in the metal dissolution.

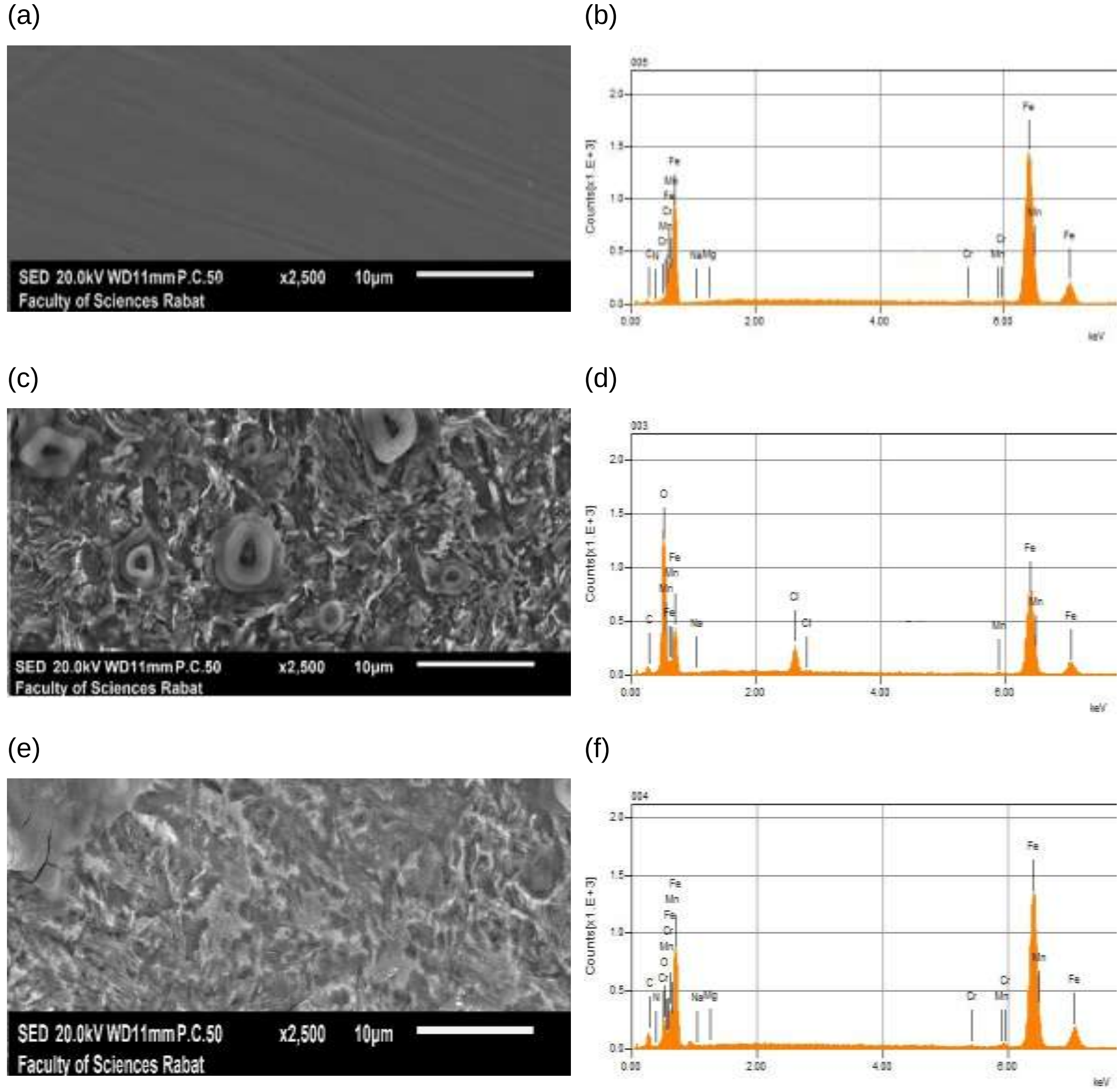

__Figure 3.10:__ SEM images and EDS spectra for carbon steel: polished state (a & b), (c & d) exposed to 1M HCl solution, (e & f) exposed to 1MHCl solution containing 10^{-3} *M of the inhibitor at 298K.*

3.6.2 X-ray diffraction analysis

X-ray diffraction is a technique of great use to identify compounds (elements) when the material has crystallinity or periodicity on the atomic scale. Therefore, it can be used to study the constituent species of corrosion products resulting from the interaction of carbon steel with the corrosive acid media at various conditions. Figure 3.11 shows the X-ray diffraction patterns of the carbon steel surface after immersion for 12 h. in the blank solution (1.0 M HCl) and in the presence of the HST compound. We can see peaks around 2θ = 35° and 36°, which are characteristic of goethite FeOOH; its existence is frequent when working with carbon steel in an environment containing chloride [165]. The intense iron peak appears at around 2θ = 44.65° [166], and it is clear that its intensity almost dropped by half in the presence of the triazole derivative, suggesting its efficiency in blocking the metal dissolution.

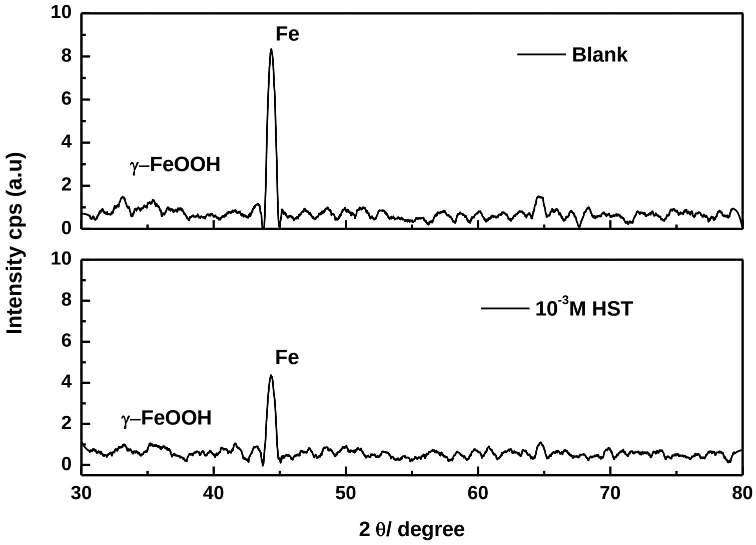

Figure 3.11: *XRD patterns of corrosion products formed on the carbon steel surface after 12h immersion in the blank acid medium and in the optimum concentration of the inhibitor.*

3.7 Computational studies

To complement the experimental findings and gain a deeper understanding of the inhibition mechanism at the molecular level, computational studies were carried out. These theoretical approaches offer valuable insights into the electronic properties, reactive sites, and adsorption behavior of the studied inhibitors. In this context, both quantum chemical calculations based on Density Functional Theory (DFT) and classical Molecular Dynamics (MD) simulations were employed.

3.7.1 DFT calculations

DFT calculations were first conducted to evaluate global and local reactivity descriptors, which help predict the inhibitors' ability to interact with the metal surface.

DFT calculations were performed using the DMol^3 module embedded in the Material Studio (MS, version 7.0) program of Accelrys Inc[167]. Global quantum descriptors and Fukui functions indices were calculated based on generalized gradient approximation (GGA) of Perdew–Burke Ernzerhof (PBE) [168] and "double numeric plus polarization" (DNP, setting to 4.4) basis set. The effect of the solvent was considered in DMol^3 calculations by including COSMO controls [169]. All DFT calculations used DMol^3 default convergence criteria for geometry optimization, and quality is “fine”. For a detailed description of equations used to obtain different theoretical parameters and Fukui functions, please refer to Supplementary Material.

3.7.1.1 Global reactivity descriptors

We have performed first-principles DFT calculations to probe the global and local reactive sites that contribute to the effective adsorption of the triazole derivative on the metal surface. These calculations can also derive information about factors controlling donor-acceptor interactions, and therefore the adsorption capacity and inhibition performance of the tested compound[170,171]. The interfacial binding between the surface of the metal and inhibitor molecules becomes stronger when the interaction between the inhibitor electron-rich atoms and empty d-iron orbitals is essential. This involves charge transfer through electron donation from inhibitor molecules to metal electron-poor sites and in the opposite direction from the iron surface to inhibitor molecules, known as a back donation of electrons. In this regard, frontier orbitals (including HOMO and LUMO) were mainly used to investigate the ability of a molecule to donate (it depends on HOMO) and to accept (it depends on LUMO) electrons [172]. The graphical representation of HOMO and LUMO, as well as the optimized geometries of neutral and protonated molecules of HST are plotted in Figure 3.12. From this figure, we observe that the HOMO/LUMO in neutral and protonated triazole derivative is situated right over the triazole ring and the sulfur atom, implying that this part of the molecule has the significant contribution in donor-acceptor interactions. It should be emphasized here that no differences are observed in the distribution of the orbital when the molecule is protonated. Thus, reactive sites belonging to the triazole ring and sulfur atom of HST are principally responsible for its interactions with iron atoms in both neutral and protonated states. Focusing on the numerical values of the frontier molecular orbitals and other reactivity descriptors allows for a more precise investigation of the inhibitor's ability to interact with iron atoms. However, an accurate evaluation of its quality as an electron donor or acceptor is difficult without comparing its theoretical indices with those of a similar compound. To this end, theoretical parameters of the HST in its neutral and protonated forms are listed in Table 3.7 along with those of a previously published triazole derivative, namely 3-methyl-1,2,4-triazole-5-thione (MTS)[173]. In aqueous acidic solution, the lone pairs of electrons of heteroatoms would facilitate their protonation [174]. It is reported that a higher negative charge of heteroatom results in a high tendency for protonation in the acidic medium[175,176]. Results indicate that Mulliken atomic charges of N1, N2, N4, and S6 are −0.264, −0.081, −0.337, and 0.087, respectively, which means that N4 is the preferred atom for protonation. Results in Table 3.7 show a high electron-donating ability of HST with the Highest Occupied Molecular Orbital (HOMO) energy level at ~ -5.268 eV compared to MST that has a HOMO energy level at ~ -7.507 eV. This result seems to be entirely contrary to Lowest Unoccupied Molecular Orbital (LUMO) energy values, which indicate that MST (LUMO energy level at ~ -3.617) has a robust electron-accepting ability than the HST compound (LUMO energy level at ~ -0.748). However, the experimental inhibition efficiency of HST is higher than that of MST at almost the same operating conditions. This lets us suggest that the corrosion inhibition performance could be increased through the electron donation effect and that this effect has a crucial role in improving the inhibition efficiency of the HST compound. Therefore, we can say that the C6 aliphatic chain better improves the electron donor capacity of 1,2,4-triazole-5-thione than the methyl group. Similarly, the same conclusions can be drawn for the protonated HST compound. It is shown that the electron donation power of organic compounds usually tends to decrease and vice versa for the electron acceptation power when they are in the protonated state. Other quantum chemical parameters, such as energy gap ($\Delta E = E_{LUMO} - E_{HOMO}$) and fracture of electrons transferred (ΔN), could be used as a criterion to evaluate the interaction intensity between the iron surface and the inhibitor's molecule. A decreasing energy gap value indicates strong interactions and the lowest chemical stability of the compound[152]. Whereas, such an increased positive ΔN value will favor electron transfer from the inhibitor's molecule to the iron surface. A closer inspection of the results revealed that MST has the lowest chemical stability as compared to HST, whereas the HST compound has a greater tendency to share its electrons with iron atoms. This tendency tends to decrease in the case of protonated HST compound, while it becomes negative in the case of MST.

It should be noted that a negative ΔN value suggests that the MST molecule can only accept electrons from the iron surface[177]. Again, and bearing in mind experimental outcomes, these results confirm the crucial role of the electron donation in improving the corrosion inhibition performance of the tested triazole derivative, and this conclusion is further confirmed by the positive ΔN value of protonated HST, which means that our compound can share its electrons with iron atoms even in its protonated state. Thus, chemical interactions can be suggested as a significant contributor during the inhibition processes. This is true because of the presence of several heteroatoms and π-electrons along with an aliphatic chain in the molecular structure of the triazole derivative that could increase its interactivity with the iron surface when added to HCl solutions.

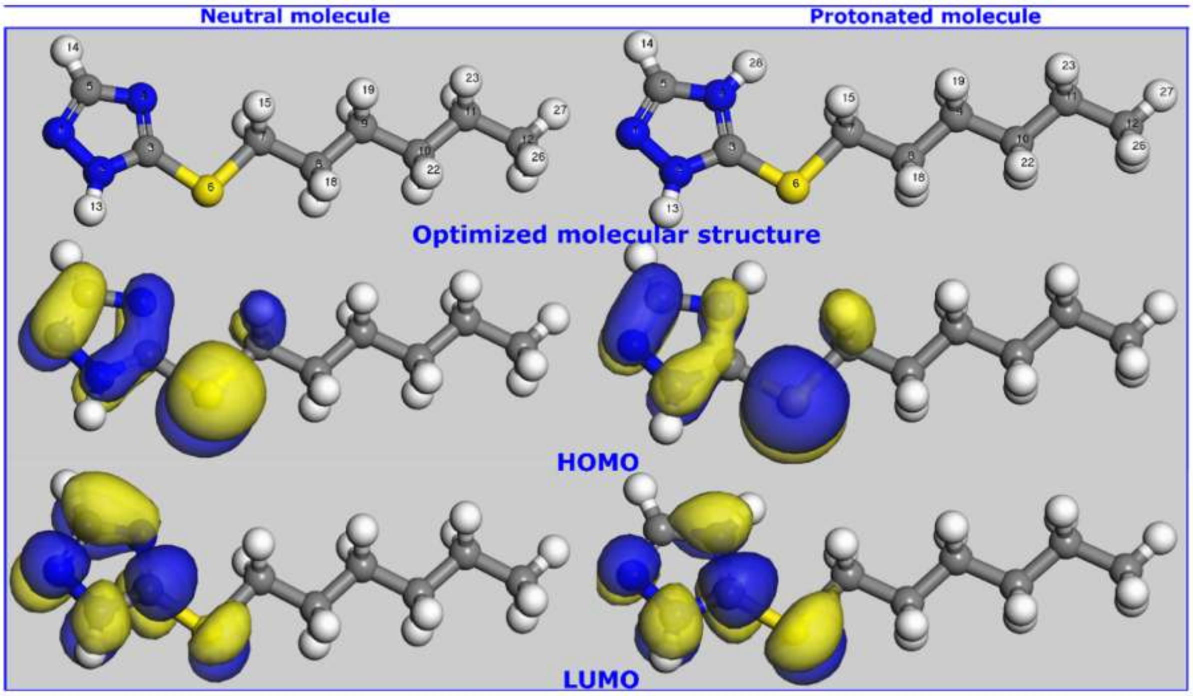

__Figure 3.12__: The optimized geometry, LUMO and HOMO of neutral and protonated inhibitor molecules obtained by DFT.

__Table 3.7:__ Quantum chemical parameters of HST in its neutral and protonated forms along with those of a similar triazole derivative, obtained by DFT.

Parameter	**Value**		
	HST	**HSTH$^+$**	**MTS** [173]
E_{HOMO}, (eV)	−5.268	−6.263	−7.507
E_{LUMO}, (eV)	−0.748	−1.927	−3.617
ΔE, (eV)	4.52	4.336	3.89
η, (eV)	2.26	2.168	1.945
χ, (eV)	3.008	4.095	5.562
ω, (eV)	2.002	3.867	7.952
σ, (eV^{-1})	0.442	0.461	0.514
ε, (eV^{-1})	0.499	0.258	0.125
ΔN	0.401	0.167	−0.190

3.7.1.2 Fukui functions

Moving now to the local reactivity of the investigated triazole derivative. This is usually examined by Fukui function indices that provide vital insights about the electrophilic/nucleophilic properties of a chemical compound [177]. Further, the dual descriptor developed by Morell et al. contributes significantly to a more precise evaluation of the local reactivity of molecules and exhibits good prediction ability in determining the tendency of an atomic site to electrophilic or nucleophilic attacks [178]. Table 3.8 lists the dual descriptor and condensed Fukui functions of nucleophilic attack (indicated by f^+, and $\Delta f > 0$) and electrophilic attack (indicated by f^- , and $\Delta f < 0$) for neutral and protonated HST compounds. Based on the results in Table 3.8, we can observe that, in the case of neutral HST, atoms belonging to 1,2,4-triazole, i.e., N(1), N(2), C(3), N (4), and C(5), exhibit a high positive charge density. Thus, they are the preferred sites for nucleophilic attack. On the other hand, the sulfur atom S(6) is the most prone site to electrophilic attack, followed by C(7). It should be mentioned here that the distribution of Fukui function sites matches well with that of HOMO/LUMO. By looking at the results of the protonated HST molecule, two outcomes are evident. It is observed that the susceptibility of the C(6) to the nucleophilic attack became more apparent, while C(5) became sensitive to the electrophilic attack in the protonated state of the triazole derivative. Overall, the results of neutral and protonated molecules highlight the dependence of the corrosion inhibition effect of the tested triazole on the heteroatoms of the 1,2,4-triazole-5-thione and their contribution in increasing the intensity of donor-acceptor interactions. In the next section, we will detail the interaction between the HST molecule and the iron surface in the presence of corrosive particles using MD simulations.

***Table 3.8:** Fukui functions and dual descriptor of HST molecule in its neutral and protonated forms obtained by DFT.*

	Neutral molecule			**Protonated molecule**		
Atom	f^+	f^-	Δf	f^+	f^-	Δf
N (1)	17.4	12	5.4	11.3	9.8	1.5
N (2)	11.8	6.6	5.2	12.2	7.6	4.6
C (3)	13.4	5.3	8.1	17	4.8	12.2
N (4)	9.2	7.9	1.3	8.2	5	3.2
C (5)	13.1	8.1	5	7.6	8.1	−0.5
S (6)	14	37.6	−23.6	19.6	38.4	−18.8
C (7)	1.8	3.2	−1.4	2	3.6	−1.6
C (8)	0.7	0.8	−0.1	0.8	0.9	−0.1
C (9)	0.4	0.5	−0.1	0.5	0.6	−0.1
C (10)	0.2	0.3	−0.1	0.2	0.3	−0.1
C (11)	0.1	0.1	0	0.1	0.2	−0.1
C (12)	0.1	0.1	0	0.1	0.1	0

3.7.2 Molecular dynamics simulations

For evaluating the performance of the HST molecule effectively and efficiently from a theoretical point of view, it is critical to have an in-depth understanding of its adsorption and its interactions with the iron surface, taking into consideration solvent particles. To this end, MD simulations were performed for neutral and protonated HST molecules in the liquid phase. Figure 3.13 displays the snapshots of top and side views of neutral and protonated triazole molecules obtained when the MD simulations attain the equilibrium state. As seen from the side views, the 1,2,4-triazole-5-thione of both neutral and protonated HST molecules is located near the iron substrate, and it is adsorbed with a planar arrangement. Notably, planar alignment strongly influences the adsorption of inhibitor molecules on the iron surface[113]. In this mode of adsorption, electron donor-acceptor interactions between electron-rich atoms in HST molecules (for instance, N, S, and multiple bonds) and vacant d orbitals of the iron substrate are more likely to occur, which can promote the formation of a coordination bond and therefore reduce the corrosion rate of the iron. The magnitude of energies of interactions of HST molecules with the iron substrate was calculated for a quantitative assessment of the simulation results. Interaction values of neutral and protonated HST molecules are −681.24 kJ mol^{-1} and −679.87 kJ mol^{-1}, respectively. Higher negative interaction energies reveal higher stability of adsorbed molecules and their strong affinity to the iron surface [170]. So, looking at our results, we can say that the interaction energy of both neutral and protonated HST molecules is rather high compared to many published results [179]. As outlined above, this result is due to the high affinity of the HST molecules to the iron surface, which prevents it from corrosion. To examine the effect of temperature on inhibitor-metal interactions, MD simulations were also conducted at 338 K. Inspecting top and side views of the snapshots (Figure3.13), we could see that there are only small differences between results at both temperatures, i.e., 298 K and 338 K. By comparing binding and interaction energies for the two temperatures, we notice that the binding energy is higher at 298 K than at 338 K. It decreases from −681.24 kJmol^{-1} (298 K) to −623.65 kJmol^{-1} (338 K). As already pointed out, by increasing the experimental temperature, the adsorption capacity of the tested compound decreased, and this fact is reflected in the MD results.

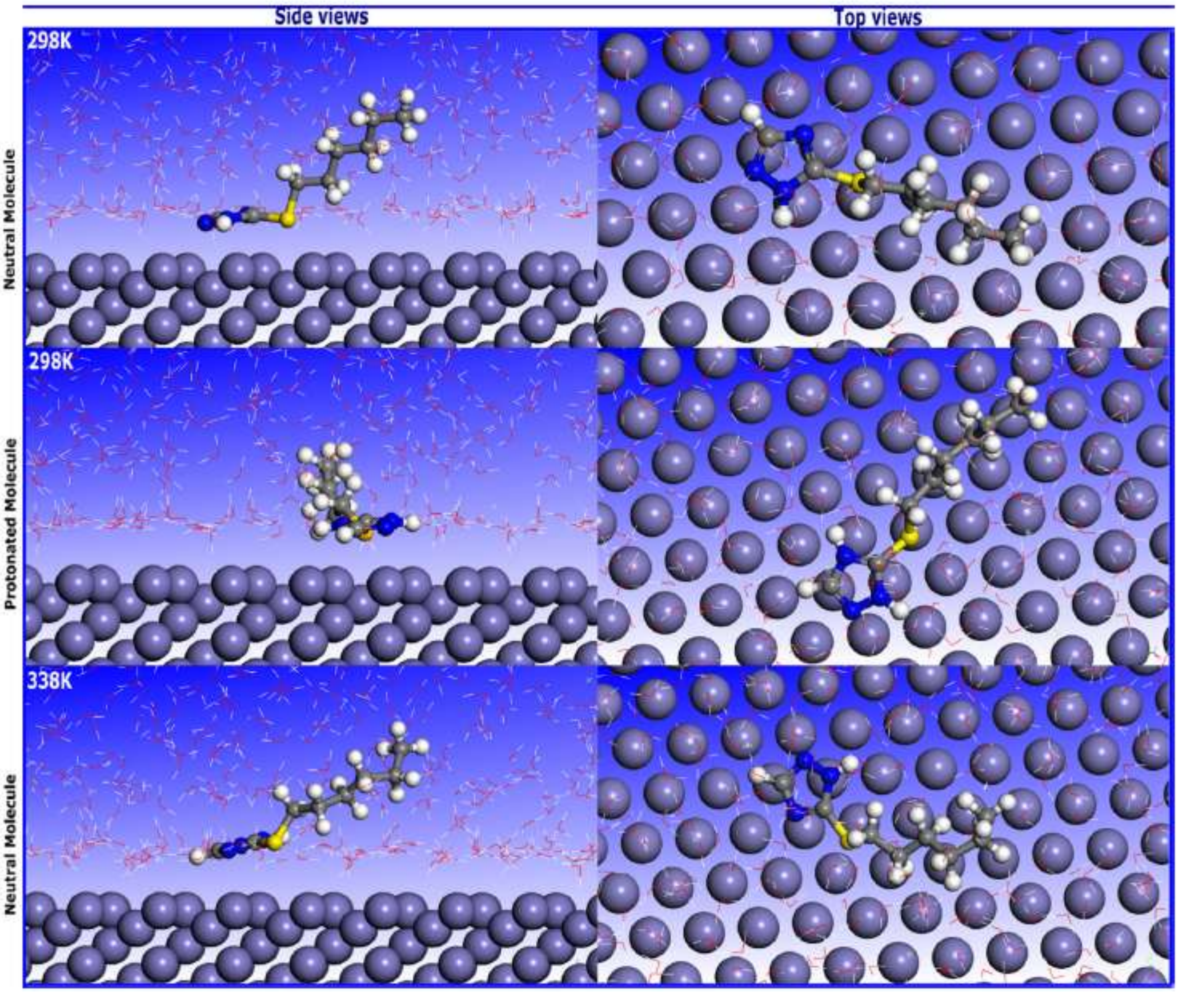

Figure 3.13: *Side and top views of the most appropriate configuration for adsorption of neutral (at 298 and 338 K), and protonated HST molecules on Fe (110) surface obtained by MD simulations in the aqueous solution.*

3.8 Comparison with other 1,2,4-Triazole derivatives

In a survey of available literature, one can find several papers on corrosion inhibition of metals and alloys using triazole derivatives, especially 1,2,3 and 1,2,4-triazole derivatives [65,180,181]. However, unmodified 1,2,4-triazole derivatives are not effective corrosion inhibitors as compared to modified derivatives [182,183]. Thus, the biggest challenge inherent to 1,2,4-triazole derivatives as potential corrosion inhibitors lies in the design of compounds that could have an excellent inhibition efficiency. It is in this context that we embarked on research efforts to develop 1,2,4-triazole derivatives based on the sulfanyl group and carbon chain. Table 3.9 compares the inhibition performance of HST with selected 1,2,4-triazole derivatives used as corrosion inhibitors for steels in acidic medium. It is patently clear that HST exhibits the highest inhibition efficiency with respect to those obtained by the other 1,2,4-triazole derivatives, despite the difference in experimental conditions. Therefore, the potential of the synthesized compound to provide good corrosion inhibition performances can attract sustained scientific attention.

Table 3.9: *Comparison of the inhibition efficiency of HST with the literature data based on other 1,2,4-triazole derivatives as corrosion inhibitors for mild steel in 1.0 M HCl solution evaluated from PDP measurements.*

Inhibitor	**C (M)**	**IE (%)**	**Ref**
4-amino-5-phenyl-4H-1, 2, 4,-triazole-3-thiol (APTT)	1.14×10^{-4}	68.6	[184]
4-amino-5-(2-hydroxy) phenyl-4H-1, 2, 4,-triazole-3-thiol, (AHPTT)	1.14×10^{-4}	70.5	[184]
4-amino-5-styryl-4H-1, 2, 4,-triazole-3-thiol, (ASTT)	1.14×10^{-4}	76.7	[184]
salicylideneamino-3-methyl-1,2,4-triazole-5-thione26 (SAMTT)	1×10^{-4}	59.3	[185]
4-(2,4-dihydroxybenzylideneamino)-3-methyl-1,2,4-triazole-5-thione (DBAMTT)	1×10^{-4}	74.3	[185]
3-amino-1,2,4-triazole (ATR)	2.97×10^{-4}	76.0	[186]
3-bromo-4-fluoro-benzylidene)- [1,2,4]triazol-4-yl-amine (BFBT)	8×10^{-4}	78.1	[128]
(4-trifluoromethyl-benzylidene)- [1,2,4]triazol-4-yl-amine (TMBT)	8×10^{-4}	75.1	[128]
(2-fluoro-4-nitro-benzylidene)- [1,2,4]triazol-4-yl-amine (FNBT)	8×10^{-4}	72.1	[128]
5-hexylsulfanyl-1,2,4-triazole (HST)	1×10^{-4}	95	This work [80]

3.9 Conclusion

The investigation carried out throughout the present study concluded that the inspected triazole derivative is a very good inhibitor for the carbon steel in 1M HCl solution in the temperature range of 298- 333 K. The mass loss measurements confirm this suggestion as well as the electrochemical measurements and the surface analysis techniques. Polarization results show that the HST compound inhibits both the anodic and cathodic reactions, thus, it is a mixed-type inhibitor. The EIS reveals a considerable decrease in the C_{dl} values accompanied by an increase in the polarization resistance, which can be due to the rise in the film thickness formed by the HST molecules adsorbed on the carbon steel surface. It was also found that the adsorption of the inhibitor obeys the Langmuir isotherm model. DFT-based investigations of HST in its neutral and protonated forms showed that its adsorption over the iron surface is mainly based on the electron donation. MD simulations confirmed the high adsorption affinity of HST molecules to the iron surface, and 1,2,4-triazole-5-thione, being electron- rich is primarily responsible for the anticorrosive effect of the HST compound. Besides, results were discussed with reference to previous works in this area. The results indicated that the addition of a sulfanyl group and carbon chain to the 1,2,4-triazole molecule makes it an excellent corrosion inhibitor, thereby providing the highest inhibition efficiency compared to previously studied 1,2,4-triazole derivatives.

Thus, this study could be a target for future research efforts in the corrosion inhibition field.

After demonstrating the efficacy of the triazole derivative (HST) as corrosion inhibitors for mild steel in 1M HCl solution, this research will now shift to hydrazones to further explore the potential of organic inhibitors. Triazoles and hydrazones have significant properties that make them efficient corrosion inhibitors, such as the presence of heteroatoms and conjugated systems, which enable strong adsorption onto the metal surface via donor-acceptor interactions. However, the studied hydrazones are structurally more complicated than triazoles. Hydrazones are bigger molecules that have imine and carbonyl functions in addition to heteroatoms, perhaps enhancing their capacity to create a denser and more protective adsorption layer. This extra complexity allows us researchers, to investigate how molecular size and functional group diversity affect corrosion inhibition efficacy.

Chapter 4: Corrosion inhibition of carbon steel in 1M HCl by novel hydrazone derivatives containing furan and thiophene rings: Experimental and theoretical studies

4.1 Introduction

Hydrazones are a distinct category within the broader family of Schiff bases, known for their crystalline nature which eases purification processes. Their production is typically achieved via one of three methods: condensation reactions between hydrazines and either ketones or aldehydes; the Japp-Klingemann reaction, which involves aryldiazonium salts reacting with beta-keto esters or acids; and the coupling of arylhalides with unsubstituted hydrazones [187].

The penchant for crystallinity, the elevated hydrolytic stability, and the facile preparation are all factors that made these compounds a prominent subject of study throughout the years in organic chemistry [188]. Hydrazones can also be broadly present in nature; biosynthesized by bacteria, fungi, marine orgasms, and plants, also isolated by solvent extraction and fermentation [189]. Their general formula is R1R2-C=N-NH. Hydrazones feature two nitrogen atoms that, despite their shared nucleophilicity, exhibit distinct reactivity profiles. The amino nitrogen displays heightened reactivity, and this is further enhanced due to the conjugation of the carbon-nitrogen double bond with the lone pair of electrons on the terminal nitrogen. Additionally, the carbon within the hydrazone moiety possesses the duality of being both an electrophile and a nucleophile [190]. This dual character provides hydrazones with versatile chemical reactivity, enabling them to engage in a broad range of chemical processes with various nucleophilic and electrophilic species, as well as with different reagents. Moreover, they can be both proton donor and proton acceptor species and display intermolecular and intramolecular hydrogen bonding [191]. The mentioned reactivity characteristics of hydrazone derivatives make them a very significant class of compounds. Indeed, the hydrazone moiety is bioactive with pharmacological and clinical properties. Anti-bacterial properties have been proved in several hydrazone derivatives: Nifuroxazideis an oral antibiotic prescribed in colitis and diarrhea treatment [192]. Furthermore, three compounds within the hydrazone class have demonstrated potent antibacterial properties, effectively inhibiting the growth of bacterial species including Bacillus subtilis, Staphylococcus aureus, Pseudomonas aeruginosa, and Escherichia coli [193]. A series of hydrazone derivatives have been synthesized and evaluated to be inhibitors of Akt (protein kinase B) for lung cancer therapy [194]. Besides, 1 H-pyrazole-5-carbohydrazide hydrazone also showed anti-cancer activity [195]. In the field of corrosion mitigation, the anti-corrosive activity of hydrazones has attracted significant attention. As a matter of fact, these compounds have been used as corrosion inhibitors for copper, nickel, and carbon steel in acidic and basic media [196] . The selection of carbon steel is due to its widespread use in various engineering applications, notably in the gas, oil, and chemical industries [197–200], nevertheless the use of mineral acids; and hydrochloric acid usually; in these industries to improve productivity in pipeline cleaning and oil well acidizing promotes the carbon steel corrosion[113]. The use of hydrazone compounds as corrosion inhibitors for carbon steel in 1.0 mol/L HCl has been reported in a multitude of research papers. Lgaz et al. [94] have carried out an experimental and theoretical study of four hydrazone derivatives (HDZ-1), (HDZ-2), (HDZ-3) and (HDZ-4); they found that all four compounds are mixed-type inhibitors and (HDZ-1) being the most effective with 95% at 5×10^{-3}mol/L. En-nylly et al. [89], studied a hydrazone named HTH; its inhibition efficiency reached 98% at 10^{-3} mol/L and resisted high temperatures by still protecting carbon steel at 89%. Chafiq et al. [201] put a new Schiff base hydrazone to the test (MPAH); it mitigated mild steel corrosion in 1.0 mol/L HCl by 97% at its optimal concentration 5×10^{-3}mol/L. Moreover, Ashassi et al. [202] conducted a synthesis of three series of hydrazone Schiff bases, and all of them were found effective by more than 92% at 10^{-2} mol/L. Khamaysa et al. [58]have also tested three hydrazone derivatives (HZ-OH), (HZ-Me), and, (HZ-Cl), all three acted as mixed-type inhibitors and their inhibition efficacy varied between 91% and 98% at 5×10^{-2}mol/L. In another paper, Khamaysa et al.[203], synthesized HYD(iso), a hydrazone derivative and assessed its efficacy on API 5 L-X60 CS, it showed 96.32% at 5×10^{-3} mol/L and acted as mixed-type inhibitor.

The present work falls within the scope of developing new effective corrosion inhibitors from the class of hydrazone derivatives that are Naproxen-based. Naproxen is a propionic acid derivative utilized as an NSAID in the treatment of joint swelling and symptoms of arthritis. However, its use has been linked to some gastrointestinal side effects, that may be caused by its acidic group. Functionalization of its acid group into hydrazones is a safe and easy way to synthesize new potential corrosion inhibitors [99,204]. Naproxen-based corrosion inhibitors for carbon steel in 1.0 mol/L HCl have been the subject of previous studies: PHD-H and PHD-Br exhibited remarkable corrosion inhibition performance for mild steel reaching 95% at 5×10^{-3} mol/L [205]. Also, PHD-Cl and PHD-OH acted as mixed-type inhibitors of the corrosion of mild steel with PHD-OH exhibiting better efficiency with 96% at 5×10^{-3} mol/L [98]. Furthermore, CBMP and MMBH hindered the corrosion of mild steel by 87% and 93% respectively, at an optimal concentration of 5×10^{-3} mol/L[95], and BPH and MPH also inhibited mild steel corrosion, acting as mixed-type inhibitors, with MPH being more effective at 5×10^{-3} mol/L [83]. Last but not least, HYD-1, HYD-2, HYD-3, and, HYD-4, all four hydrazone derivatives acted as mixed-type inhibitors and displayed highest inhibition efficiencies when used at 5×10^{-3} mol/L [99,206].

As a continuity of the previous works, herein, we investigate the ability of two new hydrazone derivatives, N′-[(E)-furan-2- ylmethylidene]−2-(6-methoxynaphthalen-2-yl)propanehydrazide (NFH) and 2-(6-methoxynaphthalen-2-yl)-N′-[(E)-thiophen-2-ylmethy-lidene]propanehydrazide (NTH) to hinder the corrosion of carbon steel in 1.0 mol/L HCl following a series of tests. Electrochemical measurements of both potentiodynamic polarization (PDP) and electrochemical impedance spectroscopy (EIS) were carried out to apprehend the performance and reaction mechanisms of compounds under study. The potential of both inhibitor compounds to prevent carbon steel corrosion at longer immersion time and high temperatures was also investigated. Furthermore, scanning electron microscopy coupled with X-ray detection (SEM-EDX) was used to examine the morphology of the inhibited and uninhibited carbon steel specimens. Unveiling the mechanism taking place between the metal surface and the inhibitors using solely experimental methods is difficult. That is why, herein, Density Functional Theory (DFT) and molecular dynamics (MD) simulation were conducted to assess the reactivity features of tested compounds and their adsorption configuration on the metal surface, respectively [207–210]. The current research aims to elucidate the mechanisms and efficacy of the compounds under investigation, thereby contributing to ongoing initiatives aimed at ameliorating corrosion-related challenges in industrial settings.

4.2 Synthesis of the inhibitors

The two studied hydrazone derivatives were synthesized in the Laboratory of Advanced Materials and Process Engineering, at the Faculty of Sciences in Kenitra, following the cited steps. Preparation of Methyl 2-(6-methoxynaphthalen-2-yl) Propanoate **(1):** Commencing with Naproxen (11.5 mg, 0.05 mmol), the process involved refluxing the compound with an excess of absolute methanol, facilitated by a catalytic quantity of H_2SO_4 over a period of 8 h. The reaction mixture was then cooled and introduced to crushed ice before being neutralized with $NaHCO_3$. Isolation of the ester was achieved through precipitation, followed by dual water washes to remove any ionic impurities. Recrystallization employing ethanol was conducted, culminating in the acquisition of the ester as white crystalline solids. These crystals displayed a melting point ranging between 89–91 °C. Characterization via infrared spectroscopy yielded absorption bands at 1739 cm^{-1} for the C=O ester, 2975 cm^{-1} for C-H aliphatic stretches, and 3061 cm^{-1} for aromatic C-H stretches in the KBr pellet.

The compound 2-(6-methoxynaphthalen-2-yl) propanehydrazide **(2)** was synthesized by refluxing a mixture containing Naproxen methyl ester (1) (1 mmol) and hydrazine hydrate (5 mmol) for a duration of 20 h. After the reflux, the reaction mixture was allowed to cool, leading to the formation of a solid which was then isolated via filtration. The obtained solid was purified through recrystallization in ethanol, resulting in the hydrazide as a final product with a melting point ranging from 138 to 140 °C. Infrared spectroscopy of the compound, recorded using a KBr pellet, exhibited characteristic peaks at 1635 cm^{-1} attributed to the C=O amide bond, 2931 cm^{-1} corresponding to C-H aliphatic stretches, and 2999 cm^{-1} associated with aromatic C-H stretches. To synthesize hydrazone derivatives **3** and **4**, an equimolar solution of a selected aldehyde (0.01 mmol) and naproxen acid hydrazide (0.01 mol) was prepared in 20 mL of absolute ethanol. To this homogeneous mixture, a catalyst amount of glacial acetic acid was introduced. The resulting solution was subjected to reflux for a period of 6 h. Following this, the mixture was allowed to cool, after which the ethanol was evaporated under vacuum. The solid that precipitated was isolated via filtration and then purified through recrystallization in ethanol, yielding the hydrazone derivative as the final product.

N′-[(E)-furan-2-ylmethylidene]− 2-(6-methoxynaphthalen-2-yl)pro- panehydrazide **(3)** was characterized by the following spectroscopic data: Infrared spectroscopy (IR) analysis, performed with a KBr pellet, revealed absorption peaks at 1656 cm^{-1} corresponding to the C=O amide stretch, 3197 cm^{-1} associated with the N-H stretch, and 1607 cm^{-1} due to the -C=N stretch. Proton nuclear magnetic resonance (^1H NMR) spectra, recorded at 400 MHz in DMSO, displayed chemical shifts (δ) at 1.4 ppm (a doublet for 3 H, methyl group), 3.5 ppm (a quartet for 1 H, aliphatic C-H), 3.8 ppm (a singlet for 3 H, methoxy group), 8.2 ppm (a singlet for 1 H, -CH=N-), 10.4 ppm (a singlet for 1 H, -NH), and a multiplet between 6.6–7.8 ppm for the 9 aromatic protons located in the naphthalene and furan rings. Carbon-13 NMR (^{13}C NMR) spectra displayed signals at 16 ppm for the methyl group (CH_3), 44 ppm for an aliphatic C-H, 55 ppm for the methoxy carbon (OCH_3), a range of 106–149 ppm for the fourteen aromatic carbons in the naphthalene and furan rings, 159 ppm for the C=N carbon, and 173 ppm for the C=O amide carbon.

2-(6-methoxynaphthalen-2-yl)-N′-[(E)-thiophen-2-ylmethylidene] propanehydrazide **(4)** was elucidated using the following spectroscopic data: Infrared (IR) spectroscopy with a KBr pellet revealed the compound’s characteristic vibrational frequencies, including a C=O amide stretch at 1662 cm^{-1}, an N-H stretch at 3190 cm^{-1}, and a -C=N stretch at 1600 cm^{-1}. Proton nuclear magnetic resonance (^1H NMR) spectra obtained at 400 MHz in DMSO exhibited chemical shifts at 1.5 ppm (displaying as a doublet for the 3 H, methyl group), 3.5 ppm (appearing as a quartet for 1 H, aliphatic C-H), 3.8 ppm (a singlet for the 3 H, methoxy group), 8.3 ppm (a singlet for 1 H, -CH=N-), and 10.5 ppm (a singlet for 1 H, -NH). A multiplet spanning 6.6–7.9

ppm was observed for the 9 H, accounting for aromatic protons in the naphthalene and thiophene rings. In the carbon-13 NMR (^{13}C NMR) spectrum, the resonances were recorded at 16 ppm for the methyl group (CH_3), 44 ppm for an aliphatic C-H, 55 ppm for the methoxy carbon (OCH_3), and within the range of 107–146 ppm for the fourteen aromatic carbons present in the naphthalene and thiophene rings. Additionally, signals at 155 ppm for the C=N carbon and 174 ppm for the C=O amide carbon were noted. (Figure4.1).

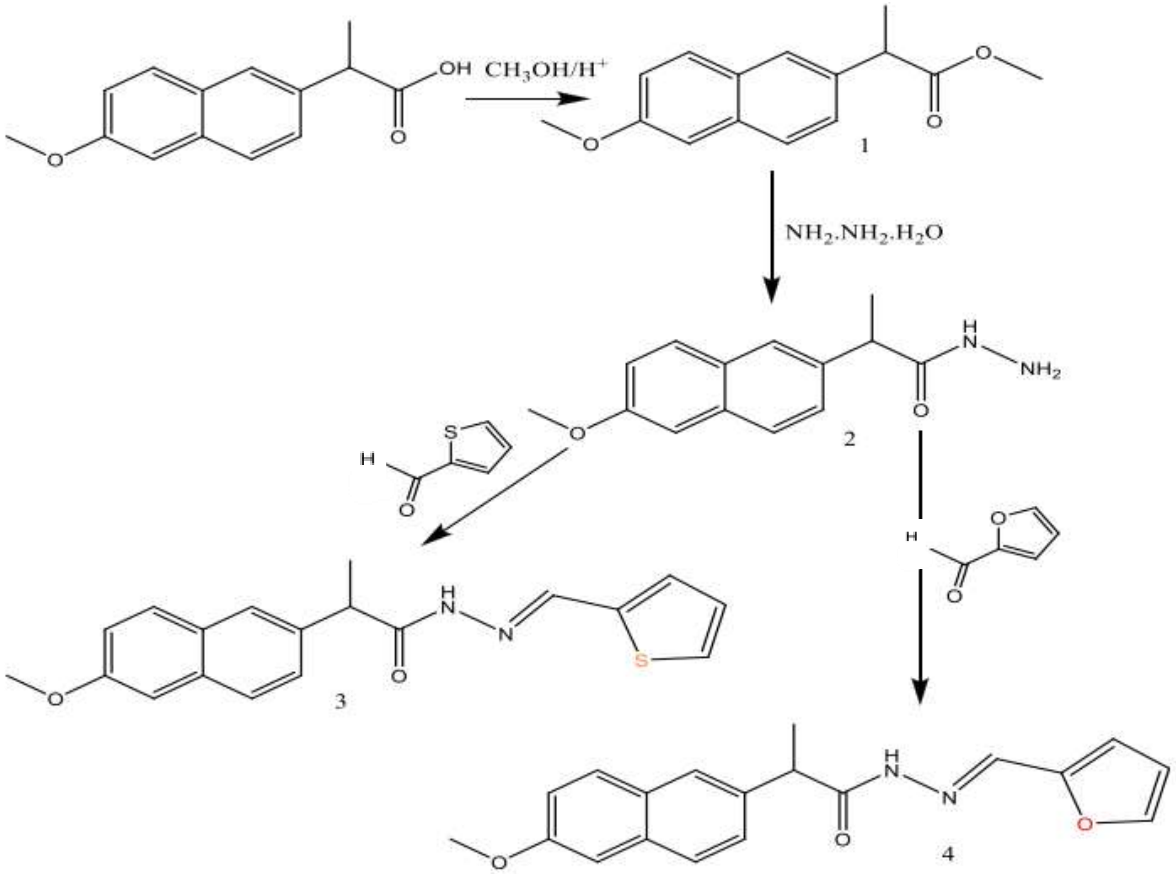

Figure 4.1 : Synthesis procedure of 3 (=NTH), and 4 (=NFH).

4.3 Effect of Concentration

The corrosion inhibition performance of two hydrazone derivatives on carbon steel in 1 M HCl was systematically evaluated using potentiodynamic polarization and electrochemical impedance spectroscopy. These techniques provided complementary insights into the inhibition efficiency and mechanistic behavior as a function of inhibitor concentration.

4.3.1 Potentiodynamics polarization curves

Potentiodynamic polarization study is a staple electrochemical technique in the investigation of the reactions taking place on the surface of carbon steel, through an extensive study of the relationship between the potential and the current density. It allows us to inspect the kinetics of both cathodic and anodic reactions during the corrosion/ inhibition process.

Figure 4.2 displays PDP curves that were recorded following a 30-minute immersion period of the carbon steel specimens in 1.0 mol/L hydrochloric acid solution. These measurements were conducted at varying hydrazone concentrations, spanning from 10^{-6} to 10^{-3} mol/L. The corresponding electrochemical parameters are grouped in Table 4.1.

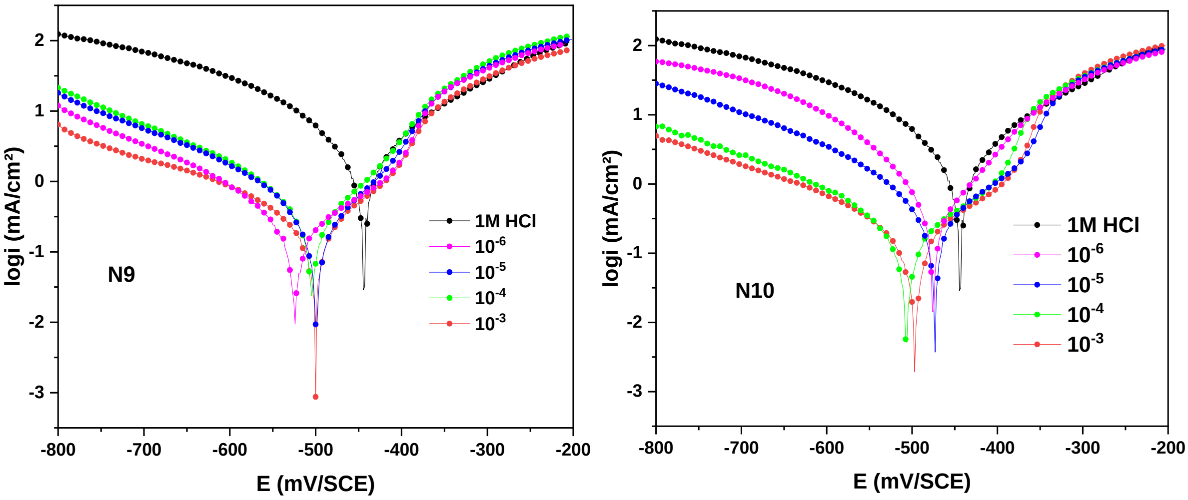

***Figure 4.2** : Potentiodynamic polarization curves of carbon steel in 1 mol/L HCl, with and without inhibitors, measured at 298 K. (a) NFH, and (b) NTH.*

***Table 4.1 :** Comparison of potentiodynamic polarization parameters for carbon steel in the presence and absence of inhibitors at 298 K.*

[Inhibitor] (mol/L)	$-E_{corr}$ (mV/SCE)	i_{corr} $(\mu A\ cm^{-2})$	β_a $(mV\ cm^{-1})$	$-\beta_c$ $(mV\ cm^{-1})$	η_{PDP} (%)
Blank	443	2984	149	151	-
NFH					
10^{-6}	499.3	391.0	87.4	203.0	86.09
10^{-5}	503.9	401.3	86.7	178.4	86.55
10^{-4}	523.2	309.1	127	207.2	89.64
10^{-3}	500.5	207.9	107.8	178.8	93.03
NTH					
10^{-6}	478.9	621.1	70.8	126.7	79.2
10^{-5}	473.0	406.7	114.0	66.5	86.4
10^{-4}	506.1	184.6	118.6	41.4	93.8
10^{-3}	497.2	158.1	107.2	34.8	94.7

From a closer look at the curves, it can be observed that the addition of the hydrazones compounds shifts/displaces them toward the lower current part, in comparison to their absence in the medium. Thus, NFH and NTH inhibit both the dissolution of the metal and the hydrogen ions reduction. Moreover, a decent range of linearity can also be seen indicating that Tafel's law is properly verified. According to the retrieved parameters listed in Table 4.1, a decrease in the corrosion current density to a minimum of 207 µA.cm^{-2} and 158 µA.cm^{-2} is noted for NFH and NTH respectively, once they were added to the acidic media at 10^{-3} mol/L. On the other hand, the displacement in the corrosion potential values between the blank solution and the inhibited one is not very significant. It reaches a maximum of 80 mV and 63 mV for NFH and NTH respectively. Per the literature review [143], an inhibitor can be classified as anodic, cathodic, or mixed-type based on the displacement of E_{corr} of inhibited solutions in comparison to uninhibited values. If the shift is greater than 85 mV, the inhibitor is pointedly cathodic or anodic. However, when the displacement is below 85 mV, the inhibitor is considered a mixed-type. However, this statement does not take into consideration the registered decrease in anodic and/or cathodic branches. A close inspection of PDP curves indicates that both anodic and cathodic branches get inhibited after the addition of both compounds. So, in this scenario, results show a significant displacement in corrosion potential while both anodic and cathodic corrosion reactions are controlled. Thus, it would be more acceptable to classify the investigated inhibitors as mixed-type inhibitors with a more cathodic effect.

Further inspection of the results leads us to conclude that the addition of the hydrazones derivatives to the acid media changes the values of the cathodic Tafel slopes βc, indicating that NFH and NTH affect the kinetics of Hydrogen evolution. When the addition of an inhibitor causes a shift in the Tafel curves without a change in the Tafel slopes, it is most likely because its molecules adsorb to the surface of the metal and block the active sites rather than alter the reaction's mechanism. The difference in the βc values in the presence of the hydrazones, however, implies that the mechanism of the hydrogen reduction reaction is different in the absence of the inhibitors. This might be due to a diffusion effect [13]. The presence of inhibitors prevents the diffusion of corrosive agents to the metal surface. This diffusion barrier helps slow down the corrosion process by reducing the contact between the corrosive acid environment and the carbon steel, thus protecting its degradation. In the same direction, an irregular variation in the anodic Tafel slopes βa can be observed with NFH and NTH compared to the blank solution, suggesting that the hydrazones derivatives impact the iron oxidation. The two hydrazone derivatives possess several heteroatoms with lone pair electrons such as Nitrogen, Oxygen, and Sulfur for NTH which can promote the formation of metal-inhibitors complexes resulting in a change in the carbon steel dissolution.

NFH and NTH both exhibit good inhibition efficiency reaching a maximum of 93% and 94%, respectively at 10^{-3} mol/L. This is a reflection that they effectively reduce the corrosion of carbon steel in 1.0 mol/L HCl. This has been the case for numerous hydrazones derivatives with similar molecular structures previously mentioned in the literature [83,95,99,141]. Nevertheless, a difference in the proportion of efficacy is always recorded; the cause behind it could be the number and/or the nature of the donor groups present in the molecule structure [96]. In the present study, the difference in the molecular structures resides in the presence of a five-membered heterocyclic compound containing oxygen for NFH (furan) and sulfur for NTH (thiophene). The difference in electronegativity, thus their ability to share electrons at the reactive sites on the metal surface might be behind the slight difference noted in efficacy.

4.3.2 electrochemical impedance spectroscopy

As electrochemical impedance spectroscopy is a reliable non-destructive method for examining the mechanisms of electrochemical reactions, this section aims to acquire the electrochemical impedance diagrams for the range of studied inhibitor concentrations. First, in order to confirm the reproducibility of the results previously interpreted, and second, to get new insights regarding the adsorption of hydrazones derivatives on the carbon steel surface. The obtained findings have been extracted and collected to represent the impedance results in their two forms, i.e., Nyquist and Bode. Thorough fitting of the data, polarization resistance R_P, solution resistance R_S and various kinetics parameters governing the corrosion process and reaction mechanism are extracted and listed in Table 4.2.

The EIS diagrams of carbon steel immersed in 1.0 mol/L HCl with and without different concentrations of the hydrazone compounds are shown in Figure 4.3.

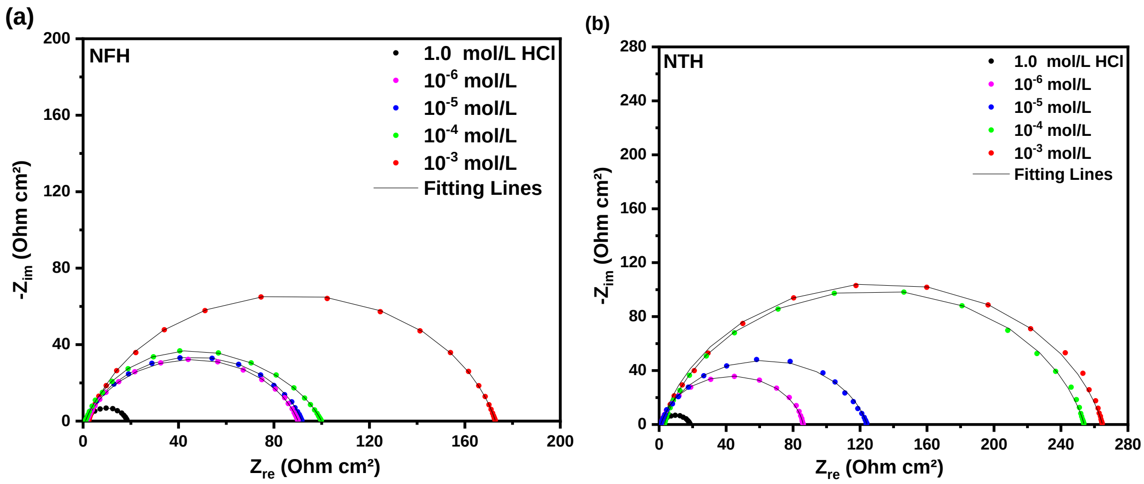

***Figure 4.3** : Nyquist diagrams of Carbon steel with and without different concentrations of NFH (a) and NTH (b) at 298K.*

For both NFH and NTH, the Nyquist diagrams have the same shape, a single depressed semicircle that represents a capacitive loop. This kind of graphic typically indicates that a charge transfer process regulates the corrosion response [201]. Each one of the capacitive loops corresponds to the polarization resistance R_P which is the sum of charge transfer resistance R_{ct}, diffuse layer resistance R_d, the film layer resistance R_f as well as R_a, the resistance attributed to the accumulation of corrosion products formed on the steel surface [80,211]. The fact that whether adding NFH or NTH to the corrosive solution did not alter the pattern of the Nyquist curves can be a sign that the inhibitors did not change the corrosion mechanism of carbon steel.

***Table 4.2** : EIS-derived electrochemical parameters for carbon steel in 1.0 mol/L HCl, featuring both the absence and presence of varying concentrations of NFH and NTH, assessed at 298 K.*

[Inhibitor] mol/L	R_S (Ω cm²)	R_p (Ω cm²)	$10^3 Q$ $(\Omega\ cm^{-2} s^n)$	C_{dl} $(\mu F\ cm^{-2})$	n	η_{EIS} (%)
Blank	1.345	17.14	0.537	234.79	0.85	-
NFH						
10^{-6}	1.87	88.64	0.238	90.90	0.80	80.66
10^{-5}	1.38	90.64	0.171	64.91	0.81	81.1
10^{-4}	1.2	98.96	0.152	63.19	0.83	82.68
10^{-3}	2.26	175.28	0.0998	37.31	0.80	90.22
NTH						
10^{-6}	1.36	84.96	0.097	53.60	0.89	79.82
10^{-5}	1.16	123.28	0.147	66.57	0.84	86.1
10^{-4}	2.45	253.28	0.088	41.44	0.83	93.23
10^{-3}	1.61	264.16	0.071	34.81	0.85	93.51

Moreover, the absence of perfectly shaped semicircles is frequently caused by the steel's surface roughness and inhomogeneities.

From Fig. 4.3 and Table 4.2, it can be observed that the corrosion inhibition ability of the hydrazones derivatives is directly proportional to their concentration. As the concentration of both compounds increases from 10^{-6} to 10^{-3} mol/L, the diameters of the capacitive loops increase, meaning the polarization resistance goes from 88 $\Omega.cm^2$ to 175 $\Omega.cm^2$ for NFH and from 88 $\Omega.cm^2$ to 264 $\Omega.cm^2$ for NTH with an increment in inhibition efficiencies from 80% at 10^{-6} mol/L to 90% and 93% at 10^{-3} mol/L for NFH and NTH, respectively. The rise in R_p values with augmenting inhibitor concentration is attributed to more inhibitor molecules covering the metal surface, resulting in a reduction in metal dissolution. The polarization resistance as a parameter allows us to calculate the double-layer capacitance through the following Equation 38 [152]:

$$C_{dl} = (Q\, {R_p}^{1-n})^{\frac{1}{n}}$$

Where R_p is the polarization resistance and n corresponds to the phase shift, which is related to the inhomogeneities of the double-layer. Q sands the CPE constant. In fitting the impedance data to an equivalent electrical circuit, as depicted in Figure 4.4, we opted for the utilization of a Constant Phase Element (CPE) in lieu of a pure capacitor. This choice was predicated on the presence of surface irregularities on the metal, and the impedance of the CPE is expressed by the subsequent equation 53 [152]:

$$Z_{CPE} = Q^{-1}(j\omega)^{-n}$$

Where the CPE constant Q is in ($\Omega^{-1}.s^{n}\ .cm^{-2}$), ω is the angular frequency in ($rads^{-1}$), j is the imaginary number, and n denotes the deviation index. The values of C_{dl} decreased in presence of both NFH and NTH in comparison to the blank solution, implying the reduction in the local dielectric constant and/or the increase of the double-layer thickness resulted from the formation of a protective layer at the metal/surface interface by displacement of pre-adsorbed water molecules and adsorption of inhibitor molecules [147]. The variation of impedance modulus and phase angle as a function of a large logarithmic frequency range in the absence and presence of hydrazone derivatives is displayed in Figure 4.5.

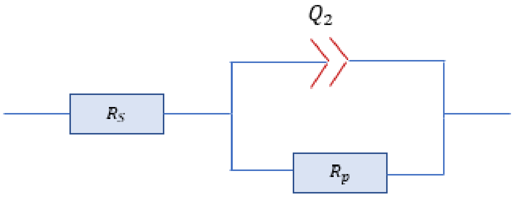

Figure 4.4: *Schematic of the electrical equivalent circuit employed for fitting the electrochemical impedance spectroscopy data.*

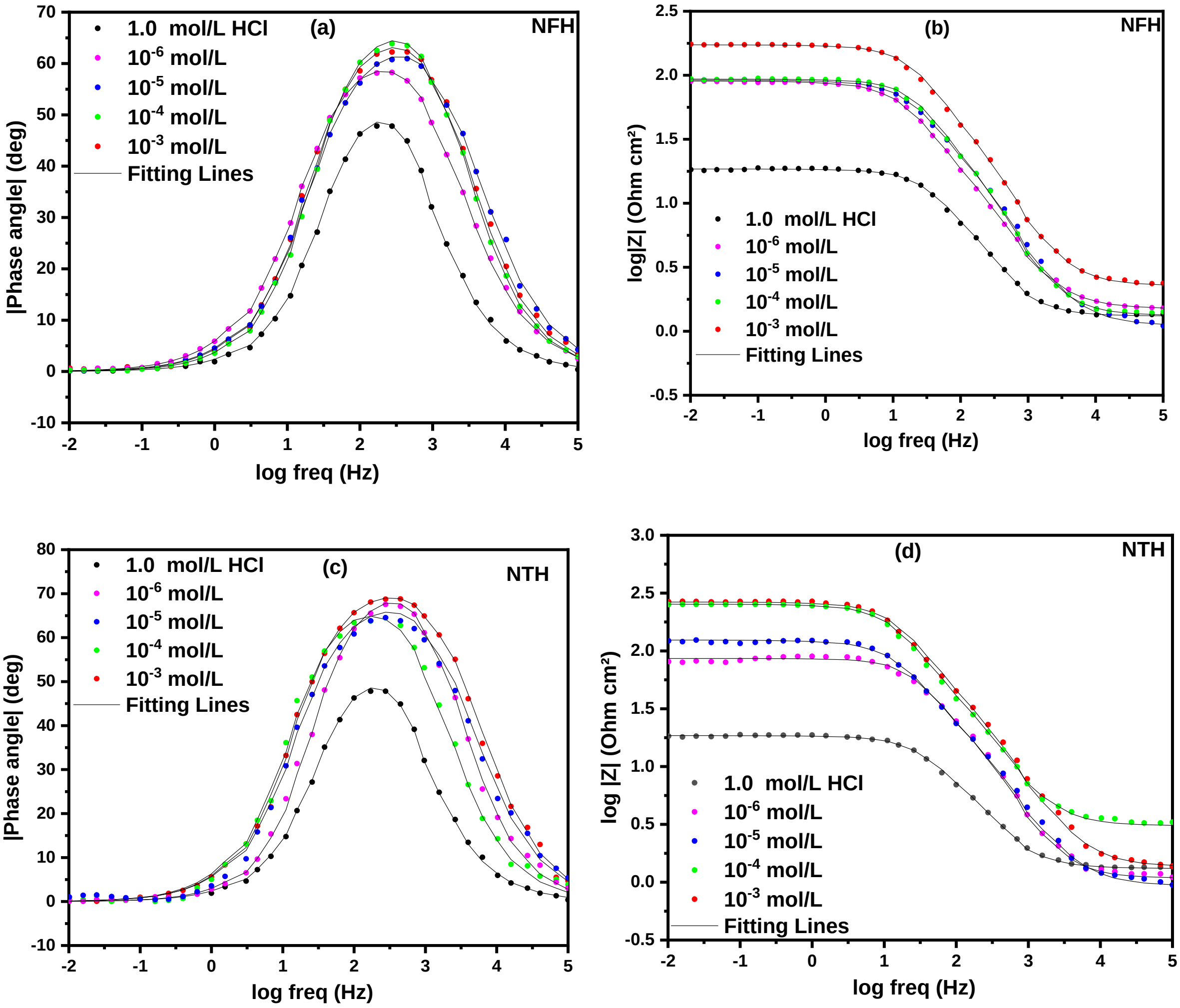

Figure 4.5: *Bode Diagrams for carbon steel with and without NFH and NTH, measured at 298 K. (a), (c) and (b),(d) refer to Bode phase angle and impedance modulus, respectively.*

The Bode phase angle curves present one maximum at intermediate frequencies which increase with the addition of the inhibitors. It reaches a maximum of nearly 65° for NFH and 70° for NTH, which are less than 90° indicating the non-ideal capacitor. The increase in phase angle values is a result of the protective capability of the hydrazones. The presence of only one maximum implies that there is only a one-time constant, thus one relaxation process that occurs at the metal/solution interface by a charge transfer process [212].

The impedance modulus |Z| serves as an index of the extent of corrosion protection afforded to the metal surface. Based on Figure 4.5, at lower frequencies, when the inhibitors NFH and NTH were added to the acid solution, the modulus of impedance increased, reaching its maximum at 10^{-3} mol/L concentration for the two compounds. This observation suggests that the application of hydrazones enhances the corrosion resistance of carbon steel.

The results acquired from the EIS study, are in good agreement with what we obtained from PDP. NFH and NTH hydrazones can truly mitigate the corrosion of carbon steel in 1.0 mol/L HCl, attaining maximum inhibition efficiency at a concentration of 10^{-3} mol/L. The NTH is slightly more effective than NFH by 3%. This difference might be due to the distinct groups attached to the Naproxen base. This same behavior has been reported in previous comparative studies including naproxen-based inhibitors. It has been found that although used in molar hydrochloric acid media at the same concentration of 10^{-3} mol/L, their efficacy varies as shown in Table 4.3. From this table, a discernible trend emerges when observing the impact of specific chemical modifications on the inhibition efficiency. For instance, derivatives featuring bromophenyl, chlorophenyl, and hydroxyphenyl groups, as seen in PHD-Br, PHD-Cl, and PHD-OH, respectively, demonstrate high inhibition efficiencies ranging from 88% to 92%. This suggests that the presence of halogen elements (bromine and chlorine) and the hydroxyl group positively influences the performance, possibly due to enhanced electron density around the aromatic ring, which facilitates stronger interactions with the steel surface. In contrast, the cyclohexylidene derivatives, HYD-4 and HYD-2, exhibit comparatively lower efficiencies of 86% and 79%, respectively. This indicates that the bulky, saturated ring structure of cyclo-hexylidene might hinder optimal interaction with the steel surface, leading to reduced effectiveness. The best performance of (E)-N′-(2,4- dimethoxybenzylidene) − 2-(6-methoxynaphthalen-2-yl) propanehydrazide (HYD-1), with an efficiency of 93%, underscores the beneficial impact of methoxy groups. The methoxy groups, by virtue of their electron-donating nature, likely enhance the electron density of the molecule, thereby improving its adsorption and interaction with the carbon steel surface.

Furthermore, while NTH and NFH, both part of the present work, demonstrate high inhibition efficiencies (90% and 93%, respectively), the slight increase in performance of NTH can be attributed to the presence of a thiophene group as opposed to the furan group in NFH. This suggests that sulfur atoms in the thiophene group may interact more effectively with the steel surface compared to the oxygen atoms in the furan group, possibly due to sulfur's larger atomic size and its ability to form stronger bonds with the metal surface.

This comparative data highlights how subtle structural differences among hydrazone derivatives significantly influence their corrosion inhibition efficiency. The presence and position of specific functional groups, such as halogens, hydroxyl, and methoxy groups, as well as the type of aromatic ring, play a crucial role in determining the extent of interaction and consequent corrosion protection of carbon steel surface in acidic environments.

Table 4.3: *Comparison of the inhibition efficiencies obtained by potentiodynamic polarization of some hydrazone derivatives used as inhibitors for carbon steel in 1.0 mol/L HCl at* 10^{-3} *mol/L of their concentration.*

Hydrazone derivative	**Inhibition efficiency**	**Reference**
(PHD-H):(E)-2-(6-methoxynaphthalen-2-yl)-N'-(1-phenylethylidene)propanehydrazide	87	[205]
(PHD-Br) :(E)-N'-(1-(4-bromophenyl)ethylidene)-2-(6-methoxynaphthalen-2-yl)propanehydrazide	91	[205]
(PHD-Cl):(E)-N′-(1-(4-chlorophenyl)ethylidene)-2-(6-methoxynaphthalen-2-yl)propanehydrazide	88	[98]
(PHD-OH) :(E)-N′-(1-(4-hydroxyphenyl)ethylidene)-2-(6-methoxynaphthalen-2-yl)propanehydrazide	92	[98]
(HYD-3):(E)-N'-(4-methoxybenzylidene)-2-(6-methoxynaphthalen 2-yl)propanehydrazide	89	[206]
(HYD-4):N'-cyclohexylidene-2-(6-methoxynaphthalen-2-yl)propanehydrazide	86	[206]
(HYD-1):(E)-N′-(2,4-dimethoxybenzylidene)-2-(6-methoxynaphthalen-2-yl) propanehydrazide	93	[99]
(HYD-2):N′-cyclohexylidene-2-(6-methoxynaphthalen-2-yl) propanehydrazide	79	[99]
(NFH) : N'-[(E)-furan-2-ylmethylidene]-2-(6-methoxynaphthalen-2-yl)propanehydrazide	90	Present work [213]
(NTH):2-(6-methoxynaphthalen-2-yl)-N'-[(E)-thiophen-2-ylmethylidene]propanehydrazide	93	Present work [213]

4.4 Adsorption isotherm

To get further insight into the interactions between each of the studied hydrazone derivatives and the carbon steel surface, adsorption isotherms were investigated. The inhibition of corrosion within an acidic environment through the addition of an organic inhibitor typically involves its adsorption onto the metal surface. The efficiency of this adsorption process is influenced by several factors, including the type of metal in question, the molecular structure of the inhibiting agent, and the electronic characteristics of the species involved, among other variables [214]. Experimentally derived data were aligned and compared against multiple isothermal models. Determination of the surface coverage has been performed from the impedance measurements following the expression $\theta = \eta_{EIS}/100$ and the correlation factor R^2 was taken into consideration to find the best fit to the experimental information. In the present work, it has been set that the Langmuir isotherm offers better adjustment results since Figure 4.6 reveals a linear correlation between $\frac{C_{inh}}{\theta}$ and C_{inh} at 298 K and the linear regression coefficient is nearly the unit. The Langmuir isotherm model is defined as [215] (same as Equation 55) :

$$\frac{C_{inh}}{\theta} = \frac{1}{K_{ads}} + C_{inh}$$

Where K_{ads} is the adsorption equilibrium constant and C_{inh} is the corresponding concentration of each NFH and NTH, which is related to the free Gibbs energy $\Delta G°_{ads}$ by the following equation[215] (same as 56):

$$\Delta G°_{ads} = -RT\ Ln(K_{ads}\ 55.5)$$

In this context, R represents the universal gas constant, while T denotes the absolute temperature at which the experiment is conducted. The figure 55.5 refers to the molar concentration of water in the solution, expressed in mol/L. The NFH and NTH compounds exhibit monolayer adsorption characteristics and the magnitude of K_{ads} is that NTH (8.41×10^5 L/mol) > NFH (2.07×10^5 L/mol) supporting that NTH provides more adsorption stability, which comes in line with electrochemical findings. The free Gibbs energy is negative for both NFH (−40.3 kJ/mol) and NTH (−43.7 kJ/mol) implying substantial interactions between the organic compounds and the metal surface [141,152].

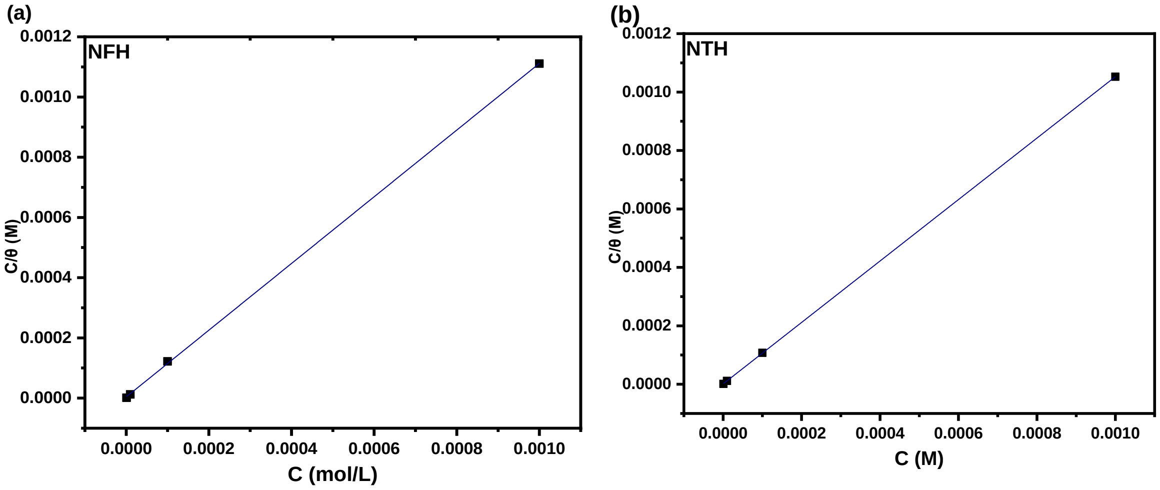

Figure 4.6: Langmuir isotherms for NFH and NTH in 1.0 mol/L HCl at 298 K. (a) and (b) refer to NFH and NTH.

While the order of magnitude of the $\Delta G°_{ads}$values has been utilized to conclude the type of adsorption by which the inhibitors adhere to the metal's surface, this approach has been recently challenged [162], showing that the standard free adsorption energy is not sufficient enough to distinguish between physisorption and chemisorption. Consequently, the data presented herein serve merely as a reference and are not sufficiently conclusive to warrant a definitive interpretation.

4.5 Effect of temperature

Changing the temperatures of the studied system is essential to get insights into the stability of the hydrazones derivatives. In this regard, the three systems, i.e., blank, blank + 10^{-3} mol/L NFH, and blank + 10^{-3} mol/L NTH are put into the test at five temperatures 298 K, 308 K, 318 K, 328 K, and 338 K, using the EIS technique. The Nyquist plots presented in Figure 4.7, display a single imperfect semi-circle in both inhibited and uninhibited systems. The one capacitive loop is confirmed by the one-time constant apparent at all temperatures in the Bode diagrams from Figures 4.7 and 4.8.

The corresponding fitted electrochemical parameters showcased in Table 4.4 are calculated using EC-Lab software based on the equivalent electrical circuit aforementioned in Figure.4.4.

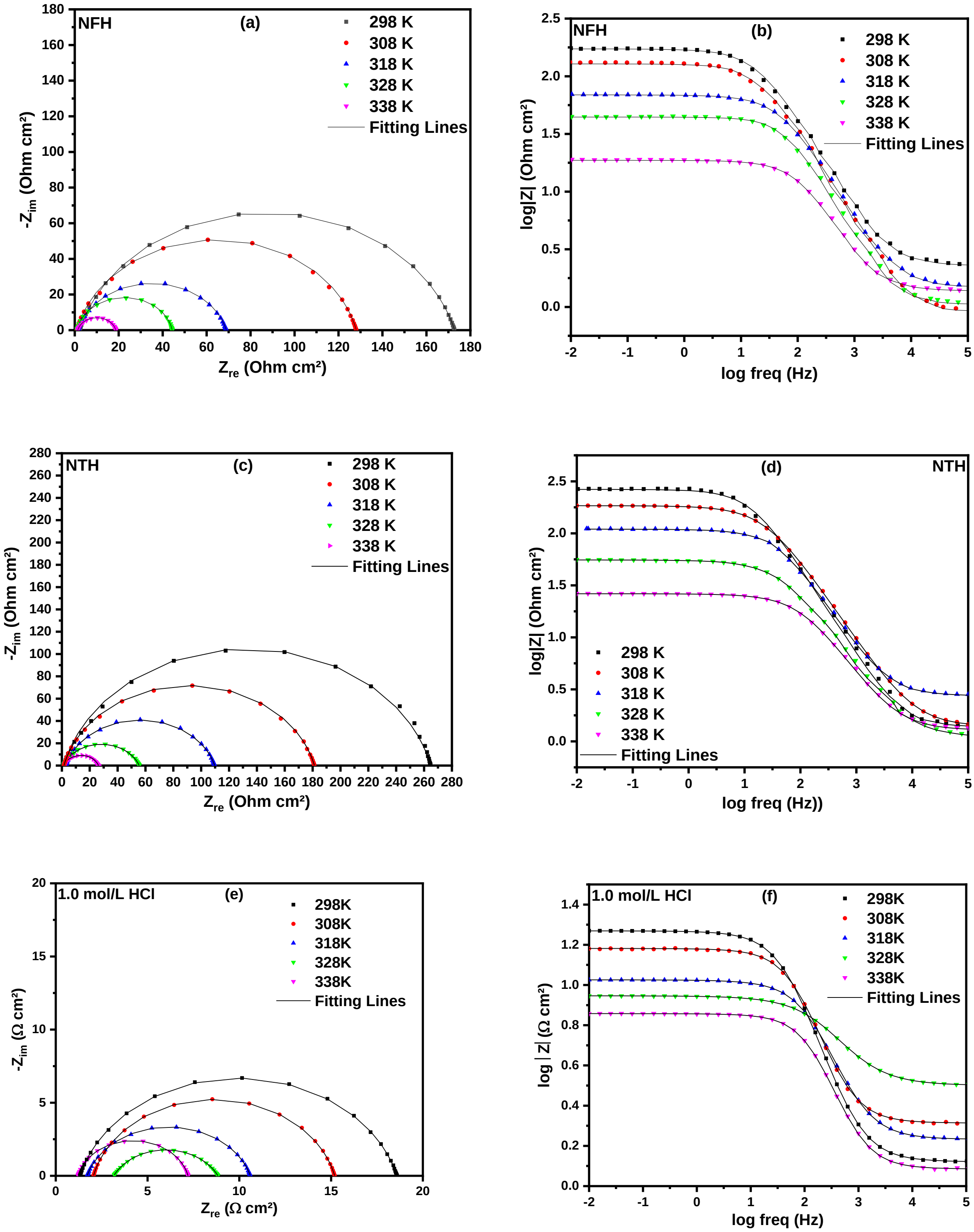

***Figure 4.7**: Nyquist and Bode diagrams at the range of 298K-338K for 1.M HCl exempt and in the presence of NFH and NTH. Subfigures (a & c & e) represent Nyquist diagrams, while (b & d & f) depict impedance modulus diagrams.*

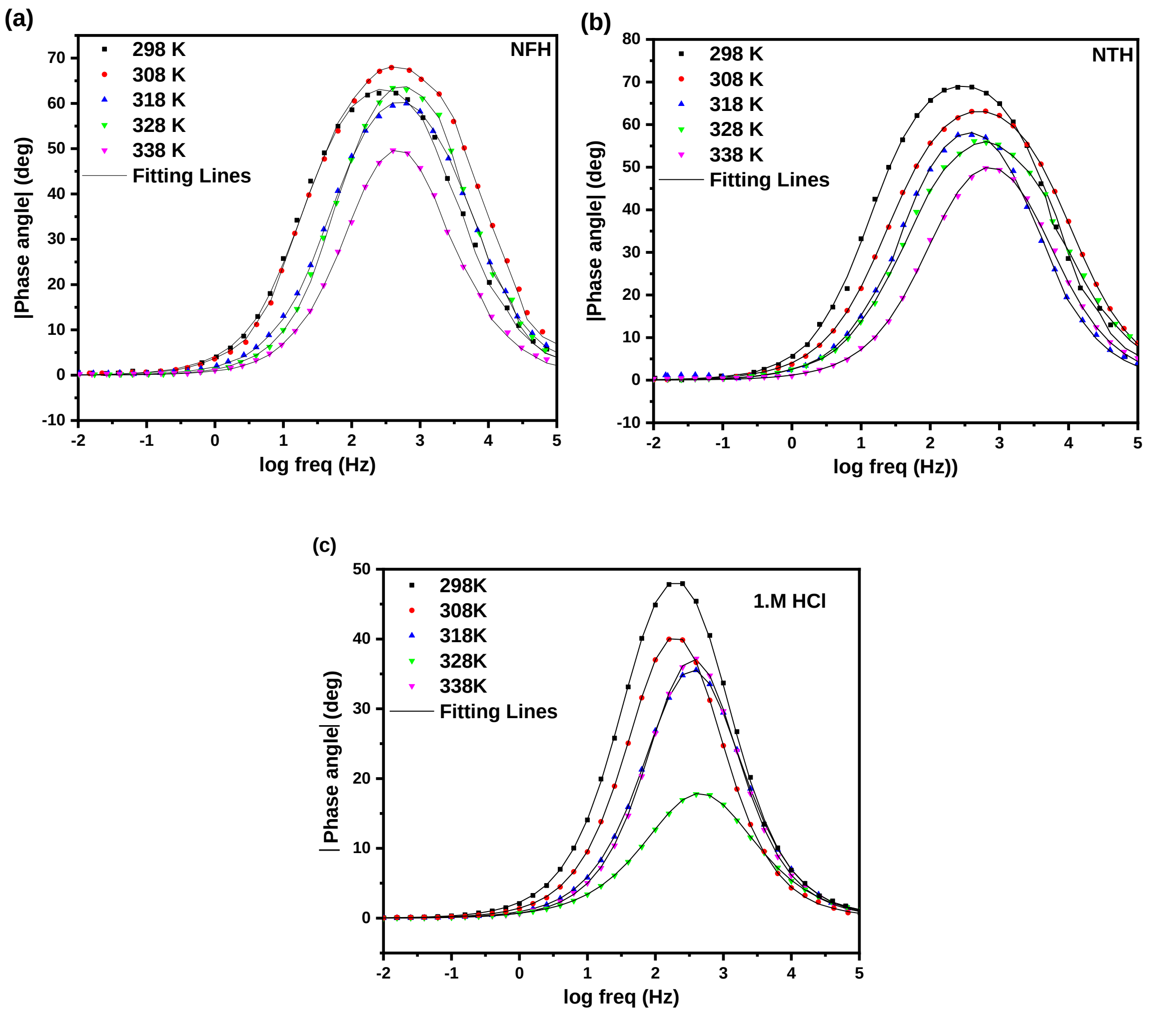

Figure 4.8: *Phase angle variation as a function of logarithmic frequencies in uninhibited and inhibited mediums at 298K-338K. (a & b & c) refer to NFH, NTH, and 1M HCl respectively.*

The rise in temperatures leads to a decrease in polarization resistance values accompanied by a decrease in inhibition efficiencies. This behavior is related to an increase in the carbon steel dissolution, or alternatively, to the desorption of the NFH and NTH molecules from the metal/solution interface inducing a decrement in the degree of surface coverage. This is also noticeable in the impedance modulus values that decrease with increasing temperatures at lower frequencies for the three systems understudy (Figure 4.7). Nevertheless, the values of R_p remain greater on the whole range of temperatures in the presence of the two inhibitors in comparison to the blank medium. The NFH and NTH prevent the corrosion of carbon steel at 338 K by 67% and 77%, respectively. It is probable that the NTH, which contains a thiophene group exhibits greater interaction and affinity towards the surface of carbon steel compared to the NFH, which incorporates a furan group. This distinction can be attributed to the presence of sulfur in the thiophene group of NTH, as opposed to the oxygen found in the furan group of NFH, despite the molecular similarities between NTH and NFH. It is well established that the metal-inhibitor interactions result in a charge transfer between the inhibitor heteroatoms and the vacant d-orbitals of the metal, hence, a heteroatom with lower electronegativity is more prone to form stronger bonds with the metal than a heteroatom with higher electronegativity [216]. The n values fluctuate when increasing temperatures for both hydrazones, still, the surface as a whole behaves with lower heterogeneity. From an energetic view point, it might be due to the inhibitors' adsorption at the most active sites of the metal surface and their isolation or related to the steric hindrance and the different orientations of the molecules [217,218].

***Table 4.4**: Electrochemical parameters in 1.0 mol/L HCl, with and without the presence of NFH and NTH, evaluated across the temperature range of 298K-338K.*

Medium	T (K)	R_S (Ω cm²)	R_p (Ω cm²)	$10^3 Q$ (Ω $cm^{-2} s^n$)	C_{dl} (μF cm^{-2})	n	η_{EIS} (%)
Blank	298	1.345	17.14	0.537	234.7	0.85	-
	308	2.023	13.41	0.386	175.8	0.87	-
	318	1.706	8.89	0.501	152.6	0.82	-
	328	1.221	6.13	0.496	193.1	0.86	-
	338	3.159	5.68	1.023	124.9	0.71	-
Blank + NFH	298	2.258	175.28	0.099	35.9	0.80	90.22
	308	1.122	127.20	0.088	39.8	0.85	89.45
	318	1.842	67.48	0.088	33.1	0.84	86.82
	328	1.312	43.26	0.083	41.3	0.89	85.83
	338	1.720	17.29	0.169	65.3	0.86	67.15
Blank + NTH	298	1.610	264.16	0.071	34.8	0.85	93.51
	308	1.690	184.24	0.792	27.5	0.80	92.72
	318	3.410	106.96	0.074	27.9	0.83	91.69
	328	1.350	54.40	0.167	44.6	0.78	88.73
	338	1.590	25.00	0.167	42.7	0.80	77.28

For more elucidation of the adsorption character of the hydrazone derivatives, the inspection of the thermodynamic parameters is necessary. First of all, the corrosion current density is calculated from the polarization resistance values based on the following equation [219] :

$$i_{cor} = R \times T \times (z \times F \times R_p)^{-1}$$

R is the perfect gas constant and T is the absolute temperature. z and F stand for the valence of iron (z=2) and the Faraday Constant (96485 Coulomb) respectively.

From the above, the inhibitors have been revealed to be temperature dependant, hence the activation parameters can be determined by Arrhenius formulas [220] :

$$i_{corr} = A.\exp\left(-\frac{E_a}{RT}\right)$$

$$i_{corr} = \frac{RT}{Nh} \exp\left(\frac{\Delta S_a}{R}\right) \exp\left(-\frac{\Delta H_a}{RT}\right)$$

In these formulas A is a pre-exponential factor, E_a is the activation energy.

h, N, $\Delta H_a, \Delta S_a$ sand the Plank constant, Avogadro number, Activation enthalpy, and Activation entropy respectively.

As shown in Figure 4.9, the tracking of the logarithm of corrosion current density as a function of 1000/T in 1.M HCl medium without and with the optimal concentrations of the two compounds NFH and NTH, gives straight lines with slopes of $\frac{E_a}{R}$. Estimation of the apparent activation energy is given at Table 17. Set side by side, we can observe that the activation energy for the Blank solution is way lower (27.76 kJ/mol) than the values for NFH (54.85 kJ/mol) and NTH (55.15 kJ/mol). These findings prove that adding NFH and NTH to the acid media mitigates the dissolution of carbon steel, evoking that the adsorption mechanism of the hydrazones molecules on the metal surface involves physisorption. However, according to [221], the increment in activation energy should not be considered decisive given that the removal of the water molecules competitively adsorbed to the metallic surface also requires some activation energy.

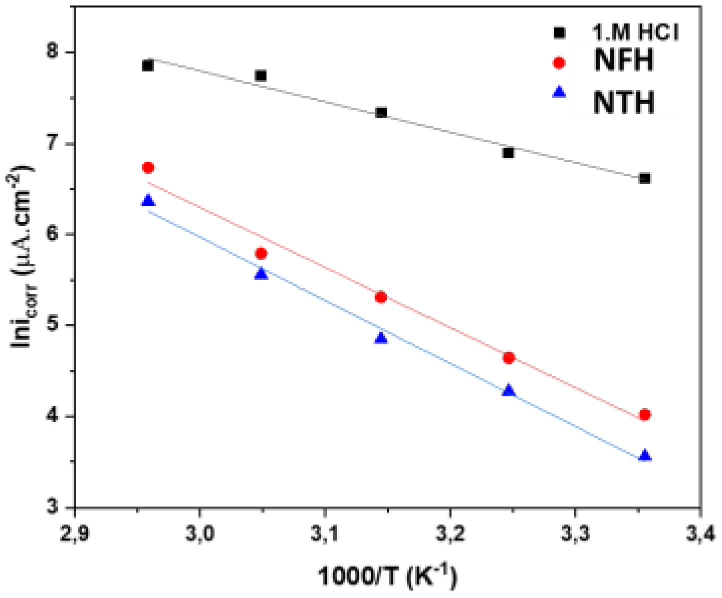

Figure 4.9: *Variation of ln i_{corr} vs 1/T for carbon steel in 1M HCl in the absence and presence of $10^{-3}M$ NFH and NTH*

Figure 4.10 illustrates the variation of ln i_{corr}/T as a function of 1000/T at 1.M HCl, 1.M $HCl + 10^{-3} NFH$, and $1.M\ HCl + 10^{-3} NTH$ respectively. Herein, we found three straight lines with a slope equal to $-\frac{\Delta H_a}{R}$ and an intercept equal to $\frac{R}{Nh} + \frac{\Delta S_a}{R}$. The thermodynamic parameters of activation are gathered in Table 4.

The values retrieved for the enthalpy of activation ΔHa are positive for all three systems under study. The positive sign of the enthalpy is generally assigned to the endothermic nature of the corrosion process. Moreover, adding NFH and NTH to 1M.HCl enhanced the value of ΔHa nearly by double, meaning that the CS dissolution is difficult due to the adsorption of the hydrazones onto the CS/electrolyte interface. Per a review of the literature, an enthalpy value lower than 40 kJ/mol is related to a physisorption process, while a chemisorption process gets close to 100 kJ/mol [222]. In this study, the values of ΔHa are superior to 40 but far from 100 kJ/mol indicating that the adsorption of NFH and NTH on the carbon steel surface is a combination of physisorption and chemisorption. Although the adsorption enthalpy is a more accurate indicator of the strength of the adsorption bond than the adsorption free energy, it should not be solely referred to to determine the type of adsorption, given that chemisorption can result in moderate enthalpy values due to either bond-breaking or large adsorbate distortions [162].

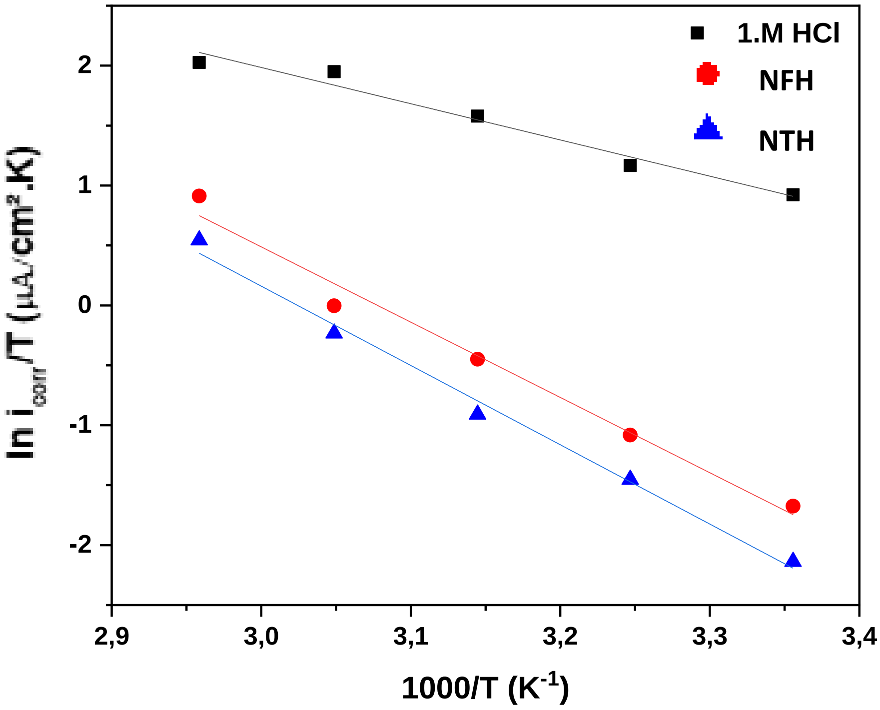

Figure 4.10: *ln i_{corr}/T vs 1/T for carbon steel dissolution with $10^{-3}M$ of NFH and NTH*

Table 4.5: *Thermodynamic activation parameters with and without NFH and NTH*

$IMPEDANCE$	$Ea\ (kJ/mol)$	$\Delta Ha\ (kJ/mol)$	$\Delta Sa\ (J/mol.K)$
HCl	27.76	25.13	-105.7
$HCl + 10^{-3}$ NFH	54.85	52.22	-36.83
$HCl + 10^{-3}$ NTH	55.15	55.01	-31.18

Concerning the entropy of activation, it is a parameter used to depict the phenomenon of order/disorder of the system. The values of ΔSa are negative but they increase with the presence of the inhibitors (Table 4.5). This rise is proof that the disorder increases when the reactants are transformed into activated complexes. It may also be related to the desorption of water molecules from the surface that accompanies the adsorption of organic molecules at the carbon steel surface[157].

4.6 Effect of immersion time

After assessing the effect of concentration and temperature on the performance of tested hydrazones in 1.0 mol/L HCl, we have found that NTH has a higher ability to hinder the corrosion of mild steel thanks in part to the thiophene group attached to the hydrazone. It is now time to assess the impact of immersion time to gain a comprehensive understanding of its inhibition efficacy. To implement that, EIS is a valuable approach for tracking the evolution of the metal-inhibitor system over time since it does not agitate/disturb the double layer at the metal- surface interface, allowing characterization of surface layer alteration, i.e., inhibitor film creation and growth [149]. Carbon steel impedance measurements in 1.0 mol/L HCl in the presence of NTH at optimal concentrations were performed thoroughly for 36 h at 298 K. The obtained Nyquist curves are displayed in Figure 4.11.

Based on Figure 4.11, the diameter of the Nyquist curves decreased as exposure time increased, which may be attributed to greater disintegration of the metal surface during exposure. Moreover, up to 26 h of immersion, the Nyquist diagrams exhibited only one depressed capacitive loop, for which the analogous circuit is the same as the aforementioned in Figure4.4.

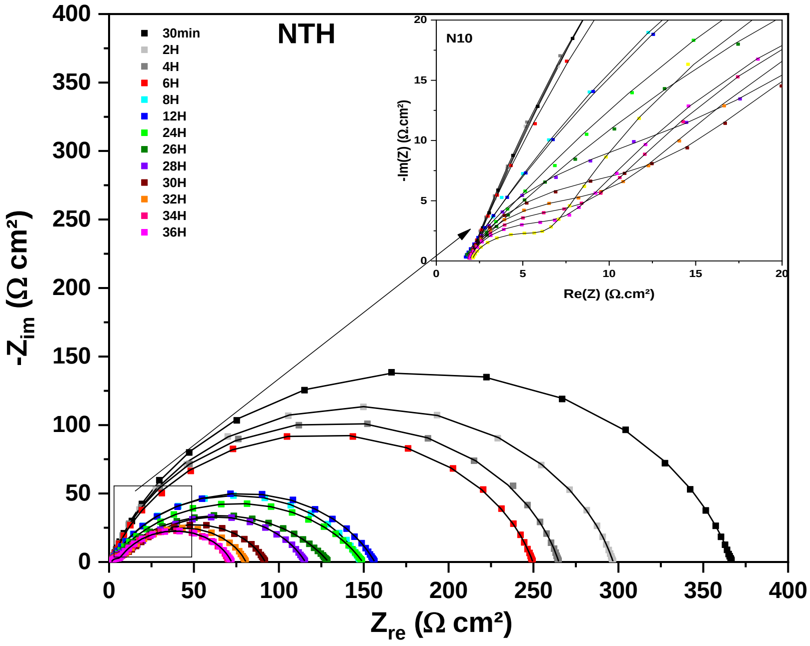

Figure 4.11: *Nyquist diagrams for carbon steel in 1.0 mol/L HCl, featuring a concentration of* 10^{-3} *mol/L of NTH, registered at various immersion durations.*

With immersion times surpassing 28 h, the Nyquist plots began to reveal two distinct capacitive loops with increasing clarity. This phenomenon is recognized as an indication that the carbon steel's corrosion process is active both on the open surface and within its pores. For corrosion to occur under these circumstances, aggressive agents like chloride ions and oxygen must diffuse through the pores to reach and react with the metal substrate. The presence of two capacitive loops in such plots is often interpreted as a sign of under-film corrosion, occurring beneath the protective layer established by the inhibitor, in this case, NTH. This dual-loop behavior is consistent with the electrical equivalent circuit model depicted in Figure 4.12, which can be used to represent the observed electrochemical responses [146].

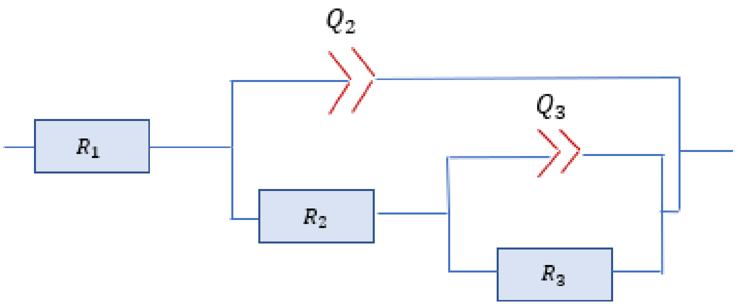

***Figure 4.12:** Equivalent electrical circuit representing corrosion of carbon steel in 1.0 mol/L HCl, featuring an optimal concentration of NTH, applicable at 28 h and subsequent time intervals.*

The polarization resistance is the sum of R_2 and R_3 ($R_p = R_2 + R_3$). R_2 is the film resistance Rf, R_3 is pore resistance which is the sum of charge transfer resistance R_{ct}, diffuse layer resistance R_d and the resistance of the accumulated species R_a. CPE_2 (Q_2) corresponds to film capacitance and CPE_3 (Q_3) to the double layer capacitance. The values of polarization resistance acquired for 36 h from EIS data for NTH are presented in Table 4.6.

***Table 4.6**: Polarization resistance values derived from EIS measurements for carbon steel in 1.0 mol/L HCl, featuring an optimal concentration of NTH, assessed at multiple immersion intervals.*

t (h)	**R_S (Ω cm²)**	**R_{ct} (Ω cm²)**	**$10^3 Q_{dl}$ (Ω $cm^{-2} s^n$)**	**C_{dl} (µF cm^{-2})**	**n_1**	**R_f (Ω cm²)**	**$10^3 Q_f$ ($\Omega cm^{-2} s^n$)**	**C_f (µF cm^{-2}**	**n_2**	**R_P (Ω cm²)**
0.5	1.9	365.3	0.055	24.7	0.82					365.3
2	1.9	295.4	0.058	25.2	0.83					295.4
4	1.8	263.4	0.054	22.7	0.83					263.4
6	1.8	248.1	0.062	25.0	0.82					248.1
8	1.6	147.0	0.130	32.4	0.74					147.0
12	1.5	155.2	0.146	33.5	0.72					155.2
24	1.5	148.1	0.226	39.5	0.66					148.1
26	1.4	128.1	0.391	62.4	0.62					128.1
28	1.8	86.2	0.331	101.4	0.75	18.02	0.046	9.75	0.82	104.2
30	1.8	79.5	0.506	154.5	0.73	11.03	0.031	8.57	0.86	90.5
32	1.9	71.0	0.498	154.3	0.74	8.02	0.023	8.18	0.89	79.0
34	1.9	62.5	0.457	158.1	0.77	6.87	0.031	8.81	0.87	69.4
36	1.9	65.5	0.649	226.7	0.75	5.12	0.023	8.75	0.90	70.6

4.7 Surface and solution characterization

In addition to the electrochemical and thermodynamic investigations, structural and surface characterizations were conducted to gain further insight into the corrosion inhibition process. XRD and UV-Vis analyses were performed for both NFH and NTH inhibitors, while SEM-

EDX analysis was carried out specifically for NTH to examine the effect of immersion time on the steel surface morphology and composition.

4.7.1 UV-Visible spectroscopy

Figures 4.13 and 4.14 exibit the UV-Vis spectra. Before the carbon steel is immersed in the inhibitor molecules, the molecule NFH in a 1M HCl solution at the optimal concentration of 10^{-3} M exhibits two prominent absorption peaks in the UV-Vis spectra at around 260 nm and 270 nm. Similarly, the molecule NTH exhibits a prominent absorption peak in the UV-Vis spectra at around 260 nm. These bands might be ascribed to $\pi \rightarrow \pi^*$ electronic transitions linked to the aromatic systems and the extensive conjugation of the hydrazone structure. The $\pi \rightarrow \pi^*$ transitions denote the excitation of electrons from bonding π orbitals to anti-bonding π^* orbitals, often occurring within this wavelength range for conjugated organic compounds. Furthermore, two less pronounced absorption bands adjacent to each other are seen for NFH and NTH at around 310 nm and 330 nm. These may correspond to $n \rightarrow \pi^*$ transitions, arising from the excitation of non-bonding electrons centered on heteroatoms like nitrogen and oxygen inside the hydrazone functional groups (C=O and C=N). Such transitions often manifest at longer wavelengths and exhibit lesser strength relative to $\pi \rightarrow \pi^*$ transitions.

Following the immersion of carbon steel in the inhibited solution, the UV-Vis spectrum exhibits a hypochromic effect (drop in absorbance), indicating a reduction in the concentration of free inhibitor molecules in the solution as a result of their adsorption onto the steel surface. The locations of the absorption bands remain mostly unaltered post-immersion, indicating that the electronic environment of the molecules in solution has not seen much alteration. For the NFH molecule, the significant reduction in intensity or even the complete disappearance of the peak around 260nm indicates that the species responsible for this transition has been adsorbed onto the metal surface. The behavior of the pronounced peak at 260 nm is notably revealing after immersion of the steel for the NTH as well. A small redshift (toward longer wavelengths) may signify enhanced contact between the inhibitor molecules and the steel surface, modifying the electrical environment without total removal from the solution. Moreover, the appearance of an additional new peak near it at 270nm could be a sign of the formation of metal-inhibitor complexes[109,223,224].

The formation of Fe-inhibitor complexes indicates that the inhibitor molecules are not merely dispersed in solution but actively bind to Fe ions released from the steel surface. This binding process contributes to corrosion protection by blocking active corrosion sites, reducing the availability of free Fe ions for redox reactions, and stabilizing the steel surface. Therefore, the appearance of Fe-inhibitor complexes is a strong indication of the inhibitor's efficiency, demonstrating that the molecules are actively participating in the corrosion inhibition process. Ultimately, for comparative purposes, the UV-Vis examination of the HCl solution devoid of inhibitor after steel immersion reveals a peak around 240 nm, which is ascribed to Fe^{2+} species (e.g., $FeCl_2$ or hydrated Fe^{2+} complexes). This aligns with the first phases of steel dissolving in acidic environments, when Fe^{2+} ions predominate prior to their oxidation to Fe^{3+} [220].

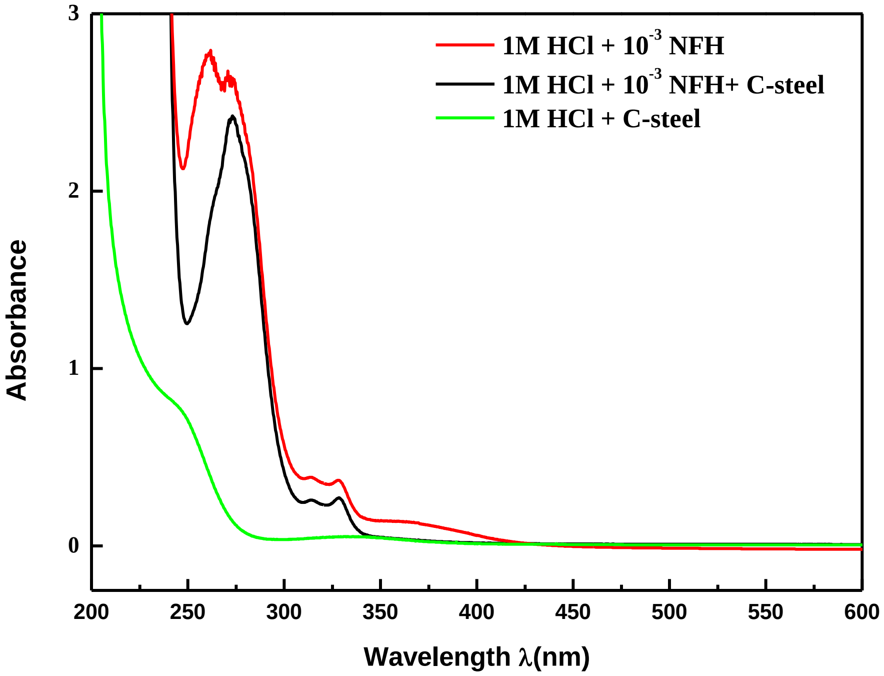

Figure 4.13 *:UV-Vis absorption spectroscopy of the 1 M HCl solution (Blank) and 10^{-3} M of NFH*

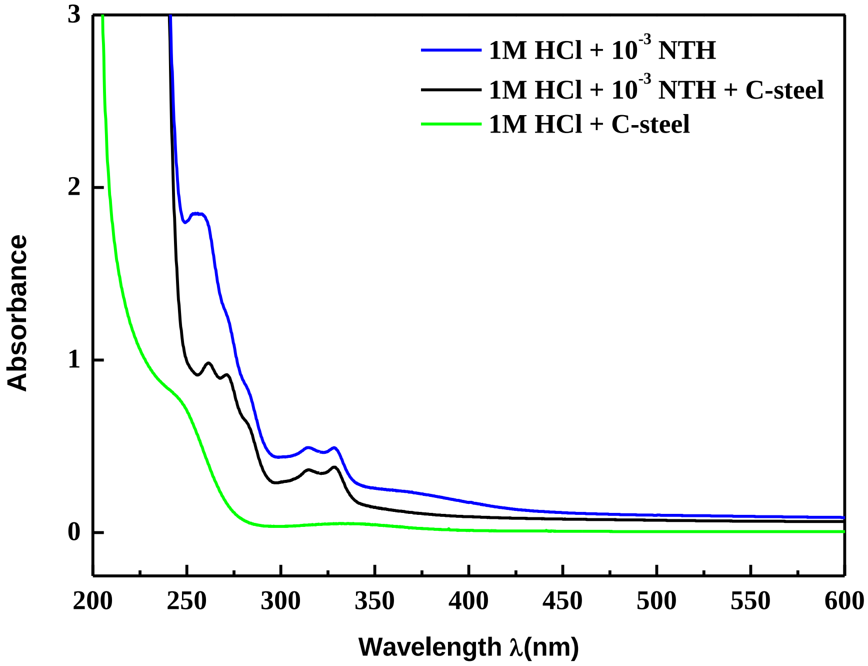

Figure 4.14 *:UV-Vis absorption spectroscopy of the 1 M HCl solution (Blank) and* 10^{-3} *M of NTH*

4.7.2 X-ray diffraction analysis

From the XRD spectra (Figure 4.15), we can observe that both hydrazone inhibitors adsorb onto the steel surface, obstructing active dissolution sites, resulting in a reduction of crystalline iron-oxide peaks at approximately 17°, 25°, 30°, and 65° compared to bare HCl [165,225,226][15]. The sulfur-containing NTH induces the most significant decrease due to stronger S–Fe interactions compared to O–Fe, thereby more effectively inhibiting oxide nucleation.

The α-Fe substrate peaks at approximately 45° and 82° exhibit distinct behaviors: the peak at 45° is most pronounced in plain HCl due to the absence of an overlying film that would attenuate the beam; in HCl + NFH, it declines more steeply than in HCl + NTH because NFH, as a less effective inhibitor, permits the formation of more voluminous oxide corrosion products that scatter X-rays at low angles [227], while NTH effectively inhibits oxide growth, allowing the metal lattice to remain relatively exposed and resulting in only a slight decrease in the 45° reflection. In contrast, the 82° peak decreases with both inhibitors, but to a greater extent for NTH—despite its thinner film—because sulfur's larger atomic number scatters high-angle X-rays more efficiently than oxygen, resulting in a greater attenuation of the 82° reflection by a thin sulfur-rich layer compared to the oxygen-rich NFH film [227]. To definitively verify the effects of surface coverage and heavy-atom scattering, X-ray photoelectron spectroscopy (XPS) must be utilized to quantify the relative concentrations of S and O on the surface and their chemical states, thereby corroborating or disproving the adsorption behavior and film composition deduced from the XRD data.

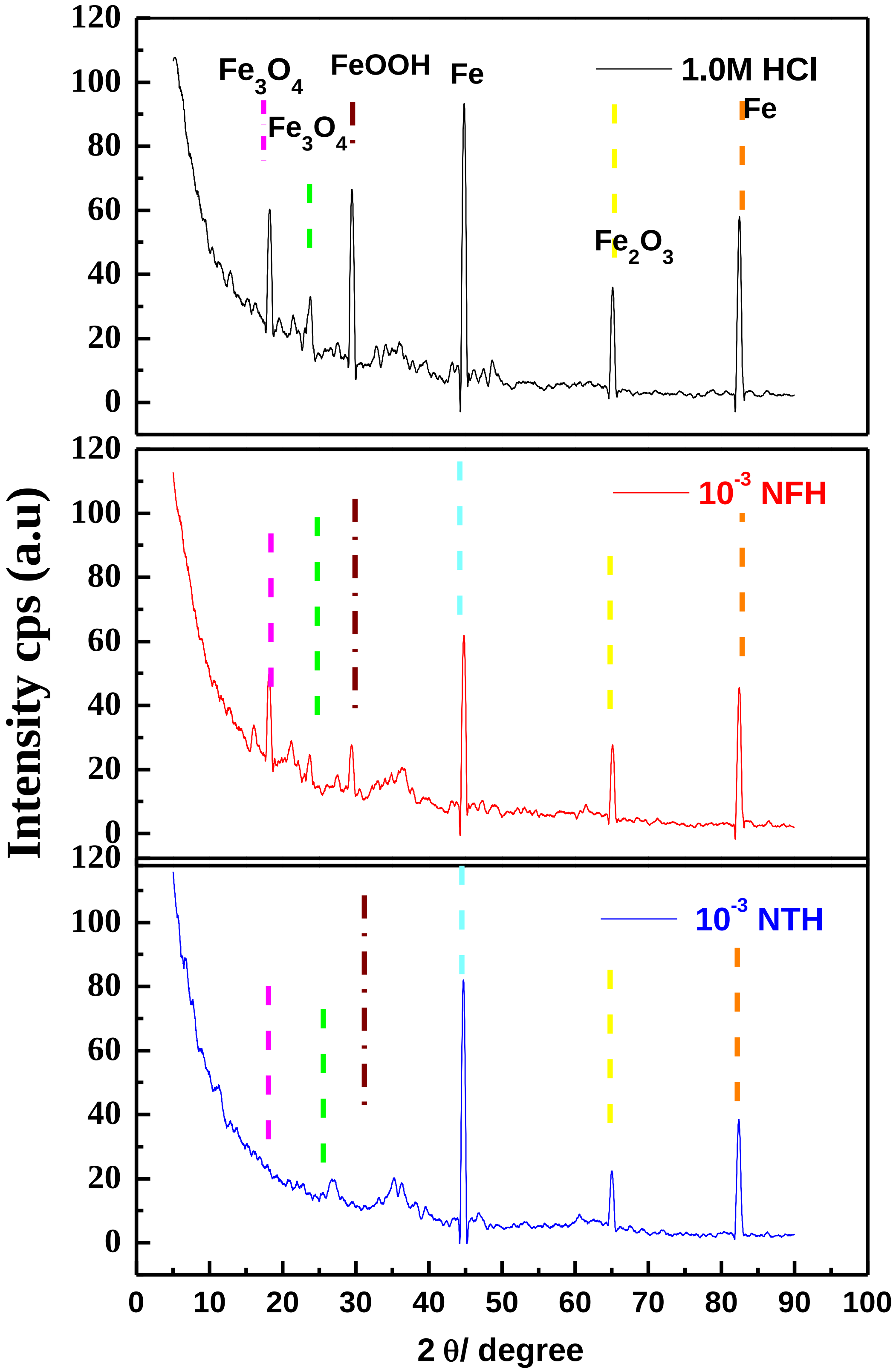

Figure 4.15*: X-ray diffraction pattern of corroded and inhibited CS substrates.*

4.7.3 SEM/EDX analysis

The Scanning electron microscopy method was used to determine and evaluate the form of the surface, to confirm the inhibitors' efficiency, and verify the appearance of a protective layer on the steel's surface after different hours of immersion in 1.0 mol/L HCl. Figure 4.16.(a) shows that after 30 min, the corrosion rate fell significantly due to inhibitor adsorption on the surface of the carbon steel, which formed a protective layer, making the surface smoother and more uniform. As shown in Figure 4.16(b)-(e), the surface became less protective after 30 h immersion in 1.0 mol/L HCl. On the other hand, Figure 4.16(f) shows that the inhibition process decreased after 36 h immersion by observing the damage of the steel surface, which explains the observed decrease of the resistance polarisation from 365.36 $\Omega.cm^2$ to 70.64 $\Omega.cm^2$ for 0.5 h and 36 h, respectively, as revealed from EIS studies.

To detect components on the surface of the carbon steel, an EDX examination was performed. Figure 4.17 shows the EDX spectra with presence of inhibitor NTH at different immersion times. The % mass values of the atoms on the steel surface are included in Table 4.7. The immersion of carbon steel in 1.0 mol/L HCl + 10^{-3} mol/L inhibitor, after 0.5 h, has a low proportion of Fe as shown in Figure 4.17. In addition, the intensity of the C and O peaks is much higher after different immersion times. After 4 h of immersion, we observe the presence of chlorine peaks whose intensity remains approximately stable despite the increase in immersion time. The Table backs up the EDX results, showing that the percentage of oxygen reduced to 29.9% at 0.5 h immersion, compared to 5.3% at 36 h immersion. Furthermore, the percentage mass of iron increased from 45.9% to 73.93% at 0.5 h and 36 h immersion, respectively. The contact of the surface of carbon steel with the inhibitor solution created a protective layer by adsorption of hydrazone molecules. Still, after 36 h immersion, the effectiveness of this layer was reduced by increasing the % mass of the iron and reducing the % mass of the oxygen. These results explain the morphology of the surface shown in SEM and the reduction of the resistance polarization.

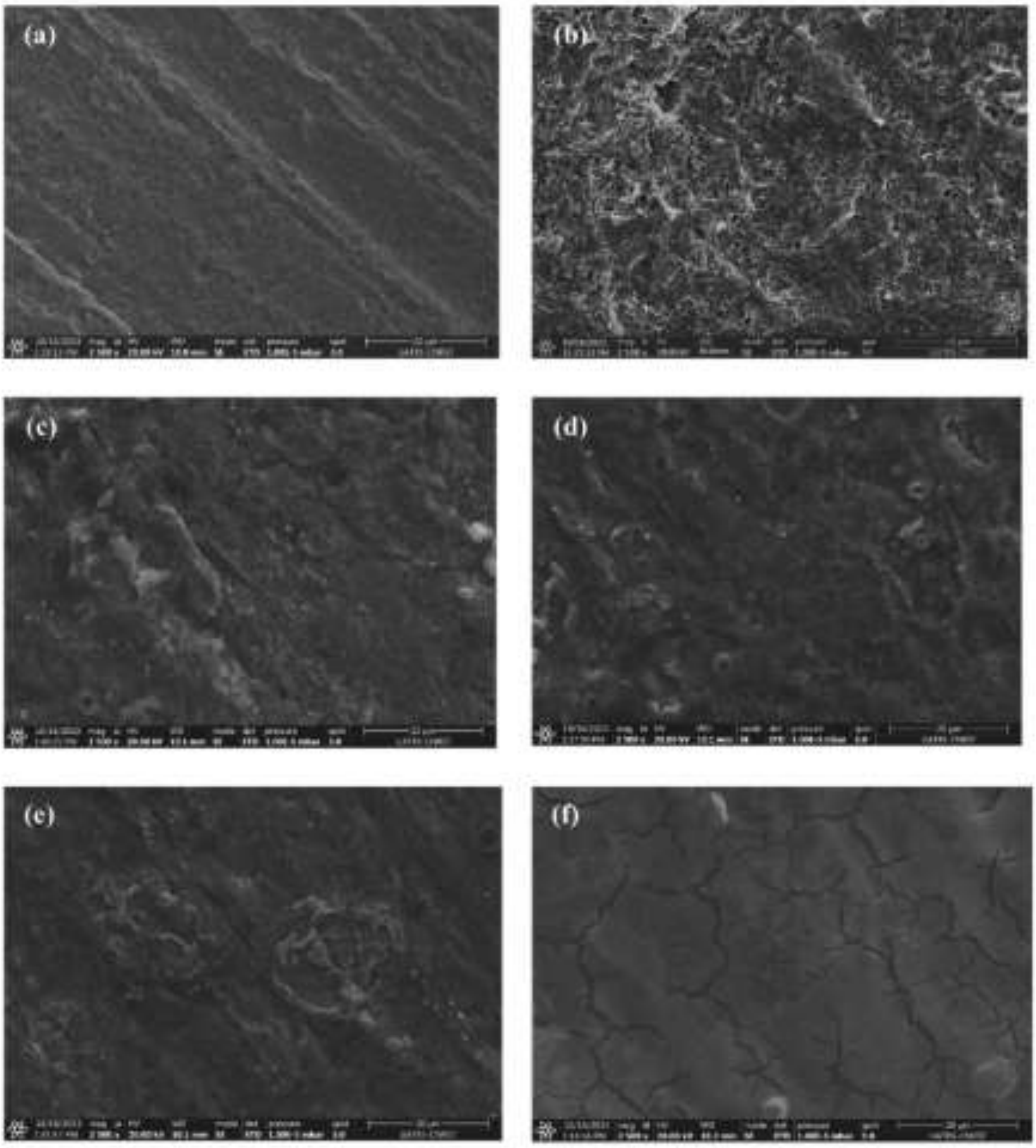

Figure 4.16*: Scanning electron microscopy of the carbon steel surface in 1.0 mol/L HCl solution in the presence of inhibitor NTH with concentration 10^{-3} mol/L after 0.5 h (a), 4 h (b), 8 h (c), 26 h (d), 30 h (e) and 36 h (f). SEM images have been captured at a 20micrometer scale and 2500x magnification.*

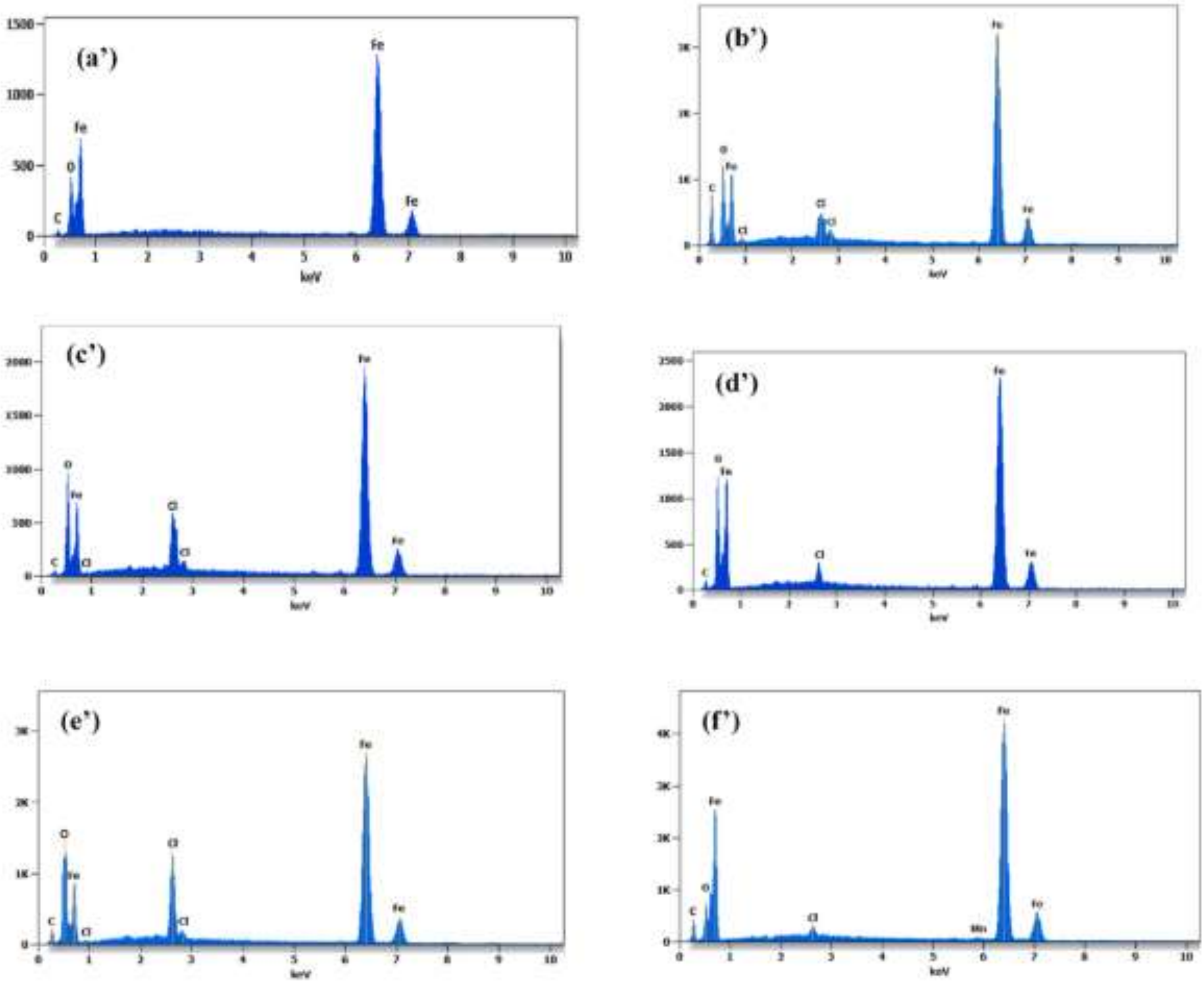

Figure 4.17: *EDX analysis of SEM results for the carbon steel surface in 1.0 mol/L HCl solution in the presence of inhibitor NTH with concentration 10^{-3} mol/L after 0.5 h (a'), 4 h (b'), 8 h (c'), 26 h (d'), 30 h (e') and 36 h (f').*

Table 4.7 *: The percentage of atoms for carbon steel in 1.0 mol/L HCl in the presence of NTH after different immersion times.*

Composition (%mass)	**C**	**O**	**Cl**	**Fe**	**Mn**
0.5h	23.59	29.9	-	45.9	0.61
4h	22.52	22.54	9.3	46.64	-
8h	15.49	23.7	10.33	50.48	-
26h	7.2	26.52	6.2	60.08	-
30h	6.1	15.10	8.1	70.7	-
36h	5.3	9.7	10.27	73.93	0.8

4.8 Potential of Zero Charge (PZC)

Both physical and chemical adsorption are, in most cases, involved in binding the organic compounds to the carbon steel surface in HCl medium. Following protonation of the inhibitor molecules, charge transfer occurs with the unoccupied d-orbitals of the metal. The nature and charge of the metal, the charge or dipole moment of the inhibitors and the adsorption of other competing charged species are all factors that influence the adsorption process [228]. To confirm the nature of the metal surface, its charge can be generated from a subtraction of the potential of zero charge E_{pzc} from the open circuit potential E_{ocp}. It is referenced as Antropov's potential [229]. To collect information on the charge of the carbon steel surface in 1.0 mol/L HCl after the addition of NFH and NTH to the solution at the optimal concentration at 298 K temperature, electrochemical impedance spectroscopy was used. Figure 4.18 depicts the variation of the double-layer capacitance as a function of the voltage applied. The curves give rise to a parabolic shape, attaining a minimum of double-layer capacitance at − 460 (mV/SCE) and − 440 (mV/SCE) for NFH and NTH, respectively. These potential values point to the E_{pzc} of carbon steel in 1.0 mol/L HCl with 10^{-3} mol/L NFH and 10^{-3} mol/L NTH. The values of the open circuit potential are − 428 (mV/SCE) and − 422(mV/SCE) for NFH and NTH, respectively.

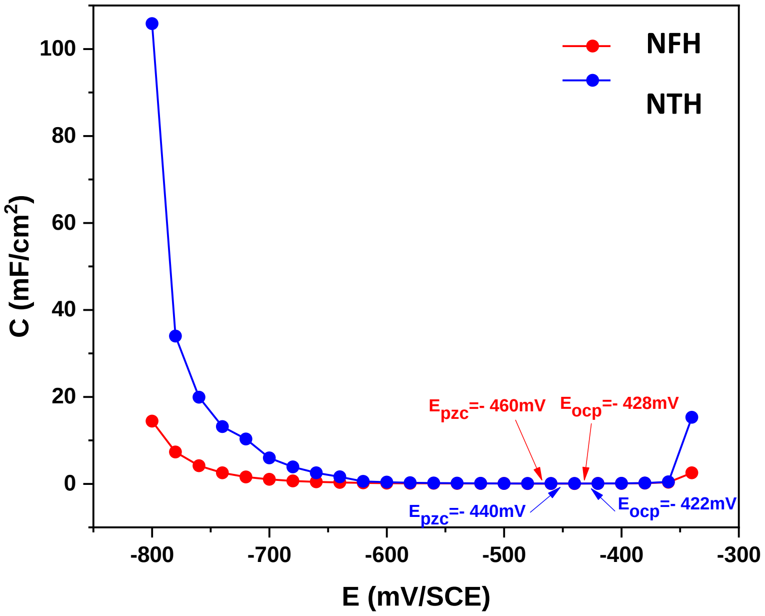

Figure 4.18: *Variation of double-layer capacitance (C_{dl}) as a function of applied voltage for carbon steel in 1.0 mol/L HCl, featuring a concentration of 10^{-3} mol/L for NFH and NTH.*

Antropov's 'rational' potential corrosion, once calculated from the below formula is either positive or negative. $E_r < 0$ implies a negative net charge of the carbon steel surface at open circuit potential while $E_r > 0$ refers to a positive one [230].

$$E_r = E_{ocp} - E_{pzc} \qquad 59$$

Positive E_r values have been found for both NFH (+32 (mV/SCE)) and NTH (+18 (mV/SCE)). This entails that the carbon steel surface bears an excess positive charge under the presence of the hydrazone derivatives in 1.0 mol/L HCl. In this case, we can state that the chloride ions Cl^- negatively charged might initially get adsorbed on the metal surface [231]. The carbon steel then becomes negatively charged as a result of their adsorption. As a consequence, the protonated inhibitor molecules can form an electrostatic bond with the chloride anions already adsorbed on the metal surface [149,232,233]. Moreover, the NFH and NTH molecules may be adsorbed on the carbon steel surface through the unshared pair of electrons present on the heteroatoms, nitrogen, oxygen, and sulfur.

4.9 Computational studies

To further support the experimental observations and elucidate the inhibition mechanism at the molecular scale, theoretical investigations were undertaken. These computational approaches provide important information regarding the electronic structure, molecular reactivity, and adsorption characteristics of the investigated inhibitors (NFH) and (NTH). In this framework, Density Functional Theory (DFT) calculations and Molecular Dynamics (MD) simulations were utilized.

4.9.1 DFT calculations

In order to investigate the electronic structure and assess the reactivity of the hydrazone-based inhibitors, quantum chemical calculations were performed within the Density Functional Theory (DFT) framework. Global and local reactivity descriptors were evaluated to predict the interaction potential between the inhibitor molecules and the metal surface. These computations were carried out using the DMol^3 software, employing the Generalized Gradient Approximation (GGA) functional and the DNP numerical basis set. Solvent effects were incorporated through the Conductor-like Screening Model for Real Solvents (COSMO-RS) to simulate aqueous phase behavior. The calculations were executed under fine integration accuracy, with a self-consistent field (SCF) tolerance set to 1.0×10^{-6} and all-electron core treatment applied. No smearing was applied, and convergence criteria were fixed at 1.0×10^{-5} Ha for energy, 0.002 Ha/Å for maximum force, and 0.005 Å for maximum displacement. All remaining parameters conformed to the fine quality settings of $DMol^3$, enabling precise optimization of molecular geometries and extraction of key quantum descriptors.

4.9.1.1 Global reactivity descriptors

It has been shown from experimental results that the susceptibility of carbon steel to corrosion is ameliorated upon treatment with hydrazone derivatives. Notably, NTH demonstrates superior anti-corrosive efficacy relative to NFH, a difference attributable to the discrete structural and reactive features inherent to these organic molecules, i.e., furan and thiophene moieties. Computational investigations employing DFT with GGA functional were conducted to elucidate these differences. This theoretical approach allows for the extraction of an array of quantum chemical descriptors, including the E_{HOMO}, the E_{LUMO}, the energy gap (ΔE), and various indices representing electrophilic, nucleophilic, and electronic characteristics of molecules under study. These descriptors act as instrumental metrics for assessing molecular reactivity and stability [234]. In the context of molecular reactivity, frontier molecular orbitals, specifically the HOMO and LUMO, serve as established indicators. A less negative E_{HOMO} suggests augmented electron-donating potential, thereby denoting elevated reactivity [234]. Conversely, a more negative E_{LUMO} implies an increased tendency for electron acceptance, also signaling heightened reactivity [234]. Figure 4.19 presents the electron density contours for the HOMO and the LUMO pertaining to the molecules under study. It is observed that the electron density of the HOMO is concentrated largely on the core Naproxen scaffold, while the electron density of the LUMO extends over the substituted groups. This pattern indicates a propensity for the Naproxen moiety to facilitate electron donation to metal surfaces, while the Furan and Thiophene substituents are implicated as primary sites for electron acceptance from iron surfaces.

Table 4.8 lists the quantum chemical parameters of the hydrazones being analyzed. A detailed analysis of the data indicates a disparity in the electronic properties, as manifested by the HOMO and LUMO energy levels of the compounds. The compound NFH is characterized by HOMO and LUMO energies of − 4.836 eV and − 2.324 eV, respectively. In contrast, NTH is associated with HOMO and LUMO energies of − 4.927 eV and − 2.485 eV, respectively.

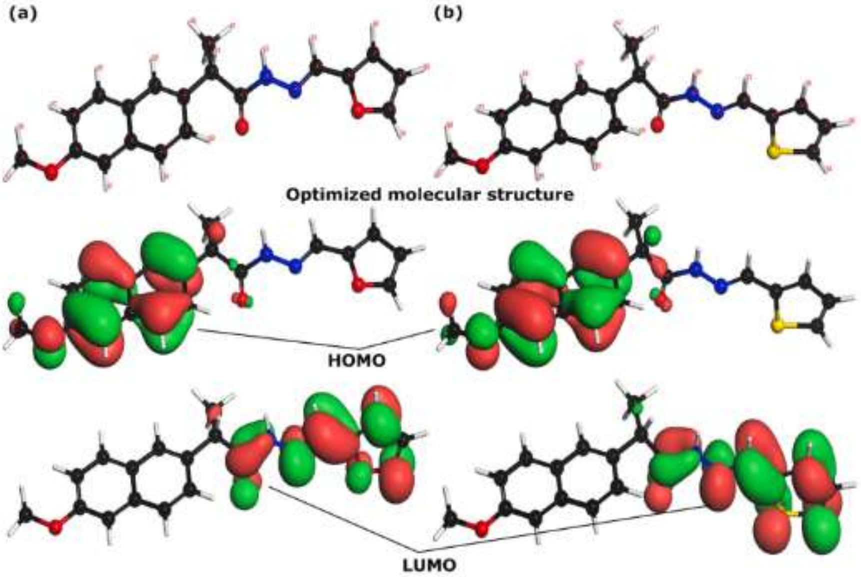

Figure 4.19*: Optimized molecular structures, HOMO and LUMO iso-surfaces of NFH and NTH molecules obtained using DFT/GGA method.*

Table 4.8**:** Quantum chemical parameters of NFH and NTH obtained by DFT/GGA method.

Molecule	E_{HOMO}	E_{LUMO}	ΔE	IE	EA	η	χ	ω	σ	ΔN	ε	ω^{+}	ω^{-}
NFH	-4.836	-2.324	2.51	4.83	2.32	1.25	3.58	5.10	0.79	0.49	0.19	1.07	1.07
NTH	-4.927	-2.485	2.44	4.92	2.48	1.22	3.71	5.62	0.82	0.45	0.17	1.26	4.97

These results suggest a relative superiority of NFH in electron-donating interactions, attributable to a less negative HOMO energy. Conversely, NTH is inferred to have enhanced electron acceptance tendency, which is reflected in a more negative LUMO energy. The energy gap (ΔE) is a pivotal parameter indicative of molecular chemical stability [235]. There exists an inverse relationship between the energy gap and the molecule’s reactivity, with a narrowed energy gap suggesting heightened reactivity [235]. In this study, among the investigated compounds, NTH exhibits a smaller energy gap of 2.44 eV, indicative of a potentially higher reactivity relative to NFH, which displays an energy gap of 2.51 eV. This observation is consistent with the experimentally determined inhibition efficiencies.

Chemical hardness (η) and chemical softness (σ) are conceptual metrics employed to evaluate a molecule’s resistance to electron density redistribution and its predisposition to attract electron, respectively [236]. These characteristics exhibit reciprocal behavior; a molecule with high chemical hardness possesses low chemical softness, and conversely, one with low hardness exhibits increased softness. The magnitude of the energy gap (ΔE) is instrumental in categorizing a molecule as either ’hard’, characterized by a larger ΔE, or ’soft’, associated with a smaller ΔE [237]. Consequently, the hierarchy of chemical hardness and softness can be deduced following the trend observed in the energy gaps of the molecules under examination. The electrophilicity index (ω) quantitatively gauges a molecule's electron-accepting ability[237]. Elevated values of ω are indicative of a molecule's enhanced affinity for electrons. In parallel, a molecule with pronounced nucleophilic characteristics (ε) typically exhibits lower metrics in both chemical potential (μ) and electrophilicity index (ω), with the converse applying to a molecule with prominent electrophilic attributes [238]. Examination of the data in Table4.8 suggests that NTH possesses a higher ω, implying a stronger electron-accepting nature, whereas NFH is comparatively characterized by more pronounced nucleophilic properties.

The parameter ΔN quantifies the potential for electron donation from an inhibitor to a metal substrate. The positive ΔN values for both hydrazones, as delineated in Table 4.8, corroborate the electron donation ability occurring from the inhibitor towards the metallic interface[239]. Experimental observations coupled with quantum chemical analyses reveal that the hydrazone derivative substituted with the thiophene moiety exhibits augmented efficacy as a corrosion inhibitor. This superior inhibitory function correlates with an escalation in reactivity, a characteristic discernible from its quantum chemical descriptors. These findings imply that the inherent reactivity imparted by the thiophene group is integral to the molecule's heightened proficiency in corrosion mitigation, enhancing its interaction with the metallic substrate.

4.9.1.2 Local Reactivity: Fukui Functions

The Fukui function is employed in computational chemistry to ascertain regions within a molecule that are particularly receptive to electrophilic or nucleophilic attack. This descriptor quantitatively expresses the change in electron density at an atomic site due to an infinitesimal increase or decrease in the system's electron number, offering insight into the local reactivity of a molecule. Indices such as f_k^+ and f_k^- are calculated to discern sites within the molecule that are most likely to undergo nucleophilic and electrophilic reactions, respectively[240]. Higher values of these indices signify regions of higher chemical activity. Figure 4.20 details the computed Fukui indices for the hydrazone compounds being studied, indicating the reactive sites that are more able to participate in chemical interactions with the iron surface.

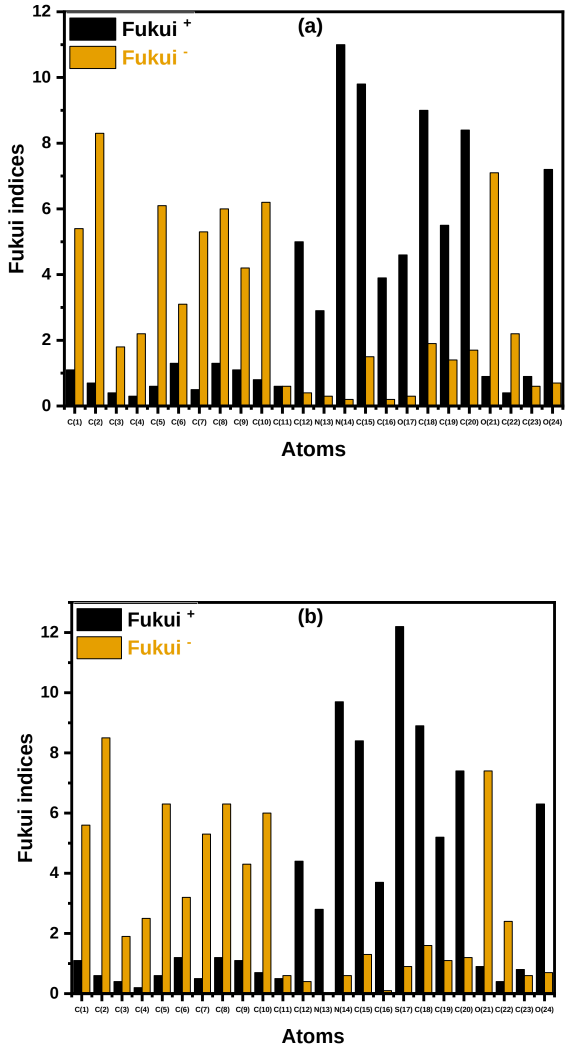

Figure 4.20: *Fukui function indices for (a) NFH and (b) NTH molecules obtained using DFT/GGA method.*

Extending the discussion on Fukui functions, it is important to note that these functions provide nuanced perspectives on the reactivity profile of a molecule, illuminating potential pathways for donor-acceptor interactions. In the present study, the distribution of active sites within both hydrazones mirrors the electron density profiles of their HOMO and LUMO. For NFH, the nitrogen atom N(14) exhibits the most pronounced nucleophilic Fukui index (f_k^+ = 11.0), indicative of its propensity to engage in electron-donating interactions, with the carbon atoms C(15), C(18), C(20), and the oxygen atom O(24) also displaying significant values. In terms of electrophilic reactivity, as delineated by the Fukui index f_k^- , the carbon atoms C(1), C(2), C(5), C(8), and C(10) of NFH are identified as the most reactive. Conversely, for NTH, the sulfur atom S(17) is characterized by the highest nucleophilic Fukui index (f_k^+=12.2), followed by the nitrogen atom N(14), the carbon atoms C(15), C (18), C(20), and the oxygen atom O(24). The highest electrophilic reactivity within NTH is observed at the carbon atoms C(2), C(5), C(8), C (10), and the oxygen atom O(21). These sites are notably prone to engage in donor-acceptor interactions with the iron substrate, suggesting their pivotal role in the formation of a robust inhibitory layer upon contact with iron surfaces. Significantly, the enhanced reactivity of the hydrazone moiety and the heteroatoms within the Furan and Thiophene groups in both molecules underscores their crucial role in the inhibition process.

4.9.2 Molecular dynamics simulation

MD simulations furnish a detailed examination of molecular interactions on an atomistic level, enabling the quantification of interaction energies and providing insight into the qualitative aspects of molecular orientation in simulated corrosive environments[241]. Figure 4.21 represents the most energetically favorable adsorption conformations of the hydrazones under study.

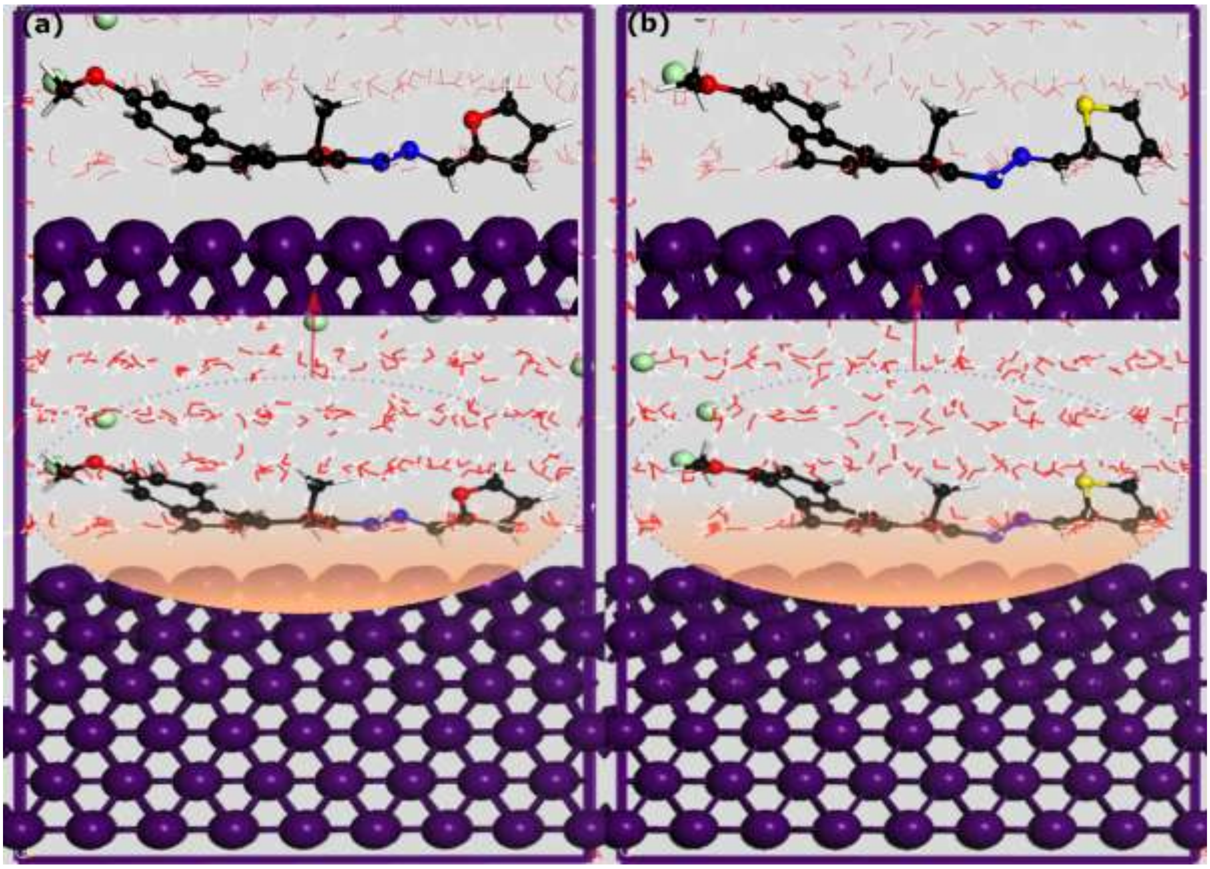

***Figure 4.21**: MD-optimized adsorption configurations of (a) NFH and (b) NTH molecules on Fe (110) surface at 303 K.*

Delving into the adsorption configurations, it is apparent that the NFH and NTH molecules assume an orientation that is predominantly parallel to the Fe(110) surface. Notably, the hydrazone functional groups of both molecules establish close proximity to the iron atoms. This quasi-planar alignment is particularly advantageous, maximizing surface coverage and thereby reinforcing the formation of a protective barrier on the metal substrate. Additionally, it increases the frequency of contact points between the molecules and the iron surface, enhancing the likelihood of interactions with the vacant d-orbitals of iron [235]. The adsorption process is potentially further stabilized by the presence of water molecules, which may energetically favor the parallel orientation, thereby consolidating the stability of the inhibitor layer [235].

It is observed that the moieties of Naproxen, as well as Furan and Thiophene, do not maintain close alignment with the uppermost layer of iron, suggesting a slight deviation from the parallel arrangement. This observation may suggest the presence of multiple potential modes of interaction between the inhibitor molecules and the iron substrate. The interaction energies derived from molecular dynamics simulations for NFH and NTH are computed to be − 131.44 kcal/mol and − 149.52 kcal/mol, respectively. The negative values of these energies indicate energetically favorable interactions with the Fe(110) surface. Conventionally, a more negative interaction energy is indicative of a higher affinity of the molecule for the surface, which in turn suggests more potent corrosion inhibition properties[235]. When these computational findings are juxtaposed with experimental data, the more pronounced interaction energy of NTH with the iron substrate is observed, corroborating its superior efficacy as a corrosion inhibitor.

4.10 Conclusion

This investigation provides an in-depth analysis of the corrosion inhibition capabilities of two hydrazone derivatives, NFH and NTH, on carbon steel in a 1.0 mol/L HCl solution. The study utilized electrochemical approaches, namely potentiodynamic polarization (PDP) and electrochemical impedance spectroscopy (EIS), to ascertain the protective performance of the investigated compounds. Observations indicated a direct relationship between inhibitor concentration and protection efficiency, with maximum inhibition efficiencies observed at 90% for NFH and 93% for NTH. Analysis of PDP measurements classified the hydrazone derivatives as mixed-type inhibitors. Examination of the adsorption behavior of the inhibitors suggested alignment with the Langmuir adsorption isotherm. The effect of raising the temperature to 338 K demonstrated that the hydrazones exhibit enhanced inhibition at elevated temperatures (86% for NFH and 89% for NTH at 328 K), indicating strong adsorptive interactions with the metal substrate. Scanning Electron Microscopy/Energy Dispersive Spectroscopy (SEM/EDS) confirmed the formation of a protective layer on the steel, attenuating corrosion. Investigations into the inhibitory mechanism via Zero Charge Potential (ZCP) elucidated that the hydrazones initially adhere to the positively charged steel surface through electrostatic forces, which are succeeded by robust chemical bonds. Theoretical studies, encompassing quantum chemical computations and molecular dynamics simulations, underscored the superior adsorptive properties of the thiophene-bearing NTH over its Furan-substituted counterpart, NFH.

General Conclusion

This work is part of the ongoing search for innovative new formulations, cost-effective, and relatively non-toxic environmentally benign organic inhibitors of carbon steel corrosion in acidic environments, with a focus on assessing the inhibitory performance of one novel 1,2,4-triazole derivative (5-hexylsulfanyl-1,2,4-triazole, HST) and two hydrazone derivatives (a furan-based NFH and a thiophene-based NTH) in a 1.0 M HCl medium.

To achieve this, we employed stationary and transient electrochemical measurements, namely potentiodynamic polarization alongside electrochemical impedance spectroscopy. Scanning electron microscopy coupled with EDX analysis and X-ray diffraction were used to analyze the surface morphology, thereby highlighting the protective effect of the inhibitor molecules on the steel surface. This experimental study was supplemented by theoretical chemistry methods. These procedures were employed, on the one hand, to confirm the experimental results as thoroughly as possible, and on the other, to establish possible structure–activity correlations for each of the inhibitors studied.

The results obtained from both gravimetric and electrochemical analyses revealed that the maximum inhibition efficiency for all three compounds—HST, NTH, and NFH—was achieved at an optimal concentration of 10^{-3} M, where the triazole derivative HST reached an efficiency of 97%, followed by the hydrazone derivatives NTH at 93% and NFH at 90%. Potentiodynamic polarization (Tafel) measurements showed a notable decrease in corrosion current densities as the inhibitor concentration increased, confirming the inhibitors' mixed-type behavior, capable of affecting both anodic and cathodic reactions. Electrochemical impedance spectroscopy (EIS) further supported these findings by demonstrating a significant increase in charge transfer resistance (R_{ct}) upon addition of the inhibitors to the acidic medium. This increase in R_{ct}, typically represented by a capacitive semicircle in the Nyquist plots, indicates a more resistant interfacial region due to inhibitor adsorption, which becomes more pronounced as the inhibitor concentration rises. The enhanced resistance is attributed to the formation of a protective barrier that hinders charge exchange between the metal surface and the corrosive solution, thereby confirming the inhibitors' effective role in mitigating corrosion of carbon steel in 1M HCl.

Temperature-dependent electrochemical investigations conducted over the 298 K to 338 K range at the optimal inhibitor concentration of 10^{-3} M revealed a decline in inhibition efficiency as the temperature increased, with the most pronounced effect observed for the hydrazone derivative NFH whose efficiency decreased to 67% at 338 K, followed by the hydrazone derivative NTH and the triazole derivative HST, whose efficiency decreased to 77% and 89% at 338 K respectively. This decline is primarily attributed to the thermal destabilization of the inhibitor-metal interface, as elevated temperatures tend to weaken the physical and chemical interactions between the inhibitor molecules and the surface of carbon steel. Both potentiodynamic polarization and electrochemical impedance spectroscopy confirmed this trend, showing a reduction in charge transfer resistance and a relative increase in corrosion current densities at higher temperatures. These findings indicate that the adsorption of inhibitor compounds becomes less stable under thermal agitation, leading to a diminished protective film on the metal surface and, consequently, a lower inhibition performance in more thermally aggressive conditions.

Surface characterization analyses provided clear evidence of the protective effect exerted by the inhibitor molecules on the carbon steel surface in the acidic environment. Scanning electron microscopy (SEM) revealed the formation of a rather uniform and continuous thin film on the inhibited steel surface, indicating a significant reduction in surface degradation and corrosion-related defects compared to untreated samples. This protective film is attributed to the effective adsorption of the organic inhibitor compounds onto the steel substrate. Energy-dispersive X-ray spectroscopy (EDX) further confirmed the presence of heteroatoms such as nitrogen, sulfur, and oxygen within the film, which are characteristic of the functional groups in the triazole and hydrazone derivatives and are likely responsible for strong interactions with the metal surface. Additionally, X-ray diffraction (XRD) analysis demonstrated that the inhibited surfaces exhibited fewer crystallographic alterations typically associated with corrosion processes, reinforcing the conclusion that the adsorbed inhibitor layer acts as a physical and chemical barrier that mitigates the aggressive attack of hydrochloric acid on the carbon steel.

In continuation of the electrochemical investigations and the structural analyses of the inhibited steel surfaces, particular attention was given to the adsorption behavior of the studied compounds in the acidic medium. The adsorption of HST, NTH, and NFH on the carbon steel surface in 1M HCl was found to conform well to the Langmuir isotherm, suggesting monolayer coverage and uniform adsorption sites with minimal intermolecular interaction between adsorbed species. Thermodynamic evaluations, including Gibbs free energy and activation energy measurements, pointed toward a mixed adsorption mechanism involving both physisorption and chemisorption. While the negative values of Gibbs free energy indicate spontaneous adsorption, their magnitudes, along with the observed decrease in inhibition efficiency at elevated temperatures, suggest that chemisorption may be slightly predominant.

However, this cannot be asserted with complete certainty, as the co-existence of physical interactions cannot be ruled out.

To elucidate the molecular origins underlying the observed inhibition efficiencies, Density Functional Theory (DFT) calculations were employed to generate both global and local electronic descriptors for each compound, including HOMO–LUMO energy gaps, electronegativity, and Fukui functions. After optimizing the molecular geometries, analysis of these descriptors allowed for the identification of reactive heteroatomic sites, primarily nitrogen, sulfur, and oxygen atoms, as key contributors to metal surface interactions. The local reactivity analysis provided by the Fukui indices clearly highlighted the atoms most likely to engage in bonding with the steel surface, thereby reinforcing experimental observations. In parallel, Molecular Dynamics (MD) simulations conducted on the Fe(110) surface demonstrated that the most energetically favorable configuration of the inhibitor molecules corresponds to a flat, parallel orientation relative to the metal plane, which maximizes surface coverage and stabilizes the adsorption complex. This optimal alignment was consistently observed for all three inhibitors, confirming their strong surface affinity. Moreover, specific structural features, such as the presence of the thiophene ring in NTH, were shown to enhance π–d orbital interactions with the metal surface, offering a plausible explanation for its slightly superior performance compared to NFH. Altogether, these theoretical insights corroborate the experimental findings and shed light on the structure–activity relationships governing the inhibition mechanisms.

Building on the comprehensive experimental and theoretical insights gained from this study, several avenues for future research and potential industrial application are envisioned. In the laboratory, one promising direction involves investigating the possible synergistic effects between the studied inhibitors; HST, NFH, and NTH by formulating blends that could enhance protection while minimizing the overall concentration required. This could be achieved through a systematic design-of-experiments approach aimed at identifying optimal combinations that retain high inhibition efficiencies, even under harsher conditions. Parallel efforts will focus on expanding the application of these compounds to other metallic materials such as aluminium and commonly used steel-based alloys, as well as evaluating their effectiveness in alternative corrosive media frequently encountered in industry, such as sulfuric acid, phosphoric acid, or alkaline environments. These studies would help broaden the inhibitors’ usability spectrum and offer a more robust understanding of their behavior under varied chemical stresses. Simultaneously, from an industrial perspective, it is proposed to carry out pilot-scale validation in actual processing systems by circulating inhibited 1 M HCl through pipelines or heat exchangers under realistic operating conditions. In tandem, the stability of the inhibitor formulations would be tested to guarantee long enough shelf shelf life, ensuring practicality for storage and transport. An economic evaluation comparing production costs and operational savings through reduced corrosion-related maintenance, downtime, and component replacement would further support industrial integration. Lastly, environmental and regulatory considerations would be addressed through toxicological assessments aligned with REACH standards, life-cycle analysis to confirm biodegradability, and the exploration of local production opportunities, thereby aligning technical efficacy with safety, sustainability, and economic feasibility.

Appendix

Theoretical Foundations of Quantum Chemical Methods in Corrosion Inhibition Studies

1- The Schrödinger Equation and Molecular Properties

In quantum chemistry, the behavior of a molecular system composed of M nuclei and N=2n electrons is governed by the time-independent Schrödinger equation:

$$\boldsymbol{H_{\Psi}(R,r) = E_{\Psi}(R,r)} \qquad \textbf{60}$$

Here, H represents the entire non-relativistic Hamiltonian of the system, E denotes the total energy, Ψ signifies the system's wavefunction, R indicates the coordinates of the nuclei, and r refers to the coordinates of the electrons. Solving this equation, in theory, facilitates the acquisition of several molecular properties: molecule geometry and stability, dipole moments, electronic spectra, and reactivity indicators such as atomic charges and Fukui functions. Nonetheless, obtaining an accurate solution to this equation is only feasible for really basic systems. Approximations must be used for polyatomic molecules.

A closed-shell system with point-like charges (M nuclei and N electrons) may have the total Hamiltonian expressed in atomic units as follows:

$$\mathbf{H}\,(\mathbf{R},\mathbf{r}) = \boldsymbol{T_N(R) + T_e(r) + V_{NN}(R) + V_{Ne}(R,r) + V_{ee}(r)} \qquad \textbf{61}$$

where the terms : $T_N(R) = -\sum_{A=1}^{M} \frac{1}{2M_A} \nabla_A^2$, $T_e(R) = -\sum_{i=1}^{N} \frac{1}{2m_e} \nabla_i^2$, $V_{NN}(R) = \sum_{A=1}^{M} \sum_{B>A}^{M} \frac{Z_A Z_B}{R_{AB}}$, $V_{Ne}(R,r) = -\sum_{A=1}^{M} \sum_{i=1}^{M} \frac{Z_A}{r_{iA}}$, $V_{ee}(r) = \sum_{i=1}^{N} \sum_{j>i}^{M} \frac{1}{r_{ij}}$ represent, respectively: the kinetic energy of nuclei with mass M_A, the kinetic energy of electrons with mass m_e, nucleus–nucleus repulsion with $R_{AB,}$ the distance between nuclei A and B, nucleus–electron attraction with r_{ia}, the distance between nuclei A and electron i, and electron–electron repulsion with r_{ij} the distance between electron i and electron j.

Due to the substantial mass disparity between nuclei and electrons (mass of proton/mass of electron ≈ 1836), Born and Oppenheimer suggested decoupling their movements. This suggests that electrons move inside the domain of fixed nuclei, enabling the molecular wavefunction to be factorized as:

$$\boldsymbol{\psi(R,r) = \psi_R(r)\phi(R)} \qquad \textbf{62}$$

Consequently, the whole Schrödinger equation (1) is condensed to an exclusively electronic issue in a static nuclear configuration (4), with the Hamiltonian simplified to encompass just electronic components (5). The total energy (6) is the aggregate of the electronic energy and the nuclear repulsion component.

$$H_{el}\psi_R^{el}(\vec{r}) = E_R^{el}\psi_R^{el} \qquad 63$$

$$H_{el} = T_e + V_{ee} + V_{eN} \qquad 64$$

$$E_R^{B.O} = E_R^{el} + \sum_{A=1}^{M}\sum_{B>A}^{M}\frac{Z_A Z_B}{R_{AB}} \qquad 65$$

2- Orbital Approximation and Hartree–Fock Theory

The electron wave function Ψ_e is a function that depends on the coordinates of all the electrons in the system. For 2n electrons in the system (2n is chosen for convenience), Ψ_e is a wave function with (2n) x 3 variables, commonly known as Ψ_e (l,2,..... 2n) [25,242,243].

The electron–electron interaction term makes the many-body problem unsolvable in closed form. To address this, Hartree (1928) [25,242,243] proposed the independent particle approximation, where the total wavefunction (7) is a product of single-electron orbitals Φ_i:

$$\psi_e(1,2,\dots,2n) = \prod_{i=1}^{2n}\phi_i(i) \qquad 66$$

However, this version does not adhere to the Pauli exclusion principle. Fock rectified this by formulating the wavefunction, whose abbreviated form for a closed-layer system is written in (8), as a Slater determinant, which ensured antisymmetry in terms of electron exchange [243]. The resultant Hartree-Fock technique introduces the notion of a self-consistent field (SCF), in which each electron flows within an average potential created by the nuclei and other electrons. The Hartree-Fock equations are then solved repeatedly until self-consistency is obtained.

$$\psi_e(1,2,\dots,2n) = \frac{1}{\sqrt{(2n)!}}\begin{pmatrix} \phi_1(1)\alpha(1) & \phi_1(1)\beta(1) & \cdots & \phi_{2n}(1)\alpha(2n) & \phi_{2n}(1)\beta(2n) \\ & \vdots & \ddots & \vdots & \\ \phi_1(2n)\alpha(1) & \phi_1(2n)\beta(1) & \cdots & \phi_{2n}(2n)\alpha(2n) & \phi_{2n}(2n)\beta(2n) \end{pmatrix} \qquad 67$$

3- Linear Combination of Atomic Orbitals (LCAO)

The aim is to provide a simple but accurate approximation of the solutions of the single-electron Schrodinger equation.

$$h\varphi_i = \varepsilon_i \varphi_i \qquad 68$$

To approximate molecular orbitals (MOs), Mulliken (1941) [25,242,243] introduced the LCAO method, which consists of studying a limited collection of m atomic orbitals (AO), which will serve as the foundation for the development of molecular orbitals (these AO being any function without a simple mathematical representation) [25].

And so, the MOs are expressed as linear combinations of a limited number of atomic orbitals (AOs).

$$\varphi_i = \sum_{k=1}^{m} C_{ik}\chi_{ik} \qquad 69$$

This method is crucial in most quantum chemical computations, allowing for accessible approximations to otherwise intractable integrals.

4- Post–Hartree–Fock Methods

Despite the value it holds, Hartree-Fock theory ignores electron correlation. To increase accuracy, post-HF procedures have been developed [242,243]. The Møller-Plesset perturbation theory (MP2, MP3, MP4), which corrects the HF energy with increasing successive orders of perturbation. Also, the Multi-configurational approaches, such as Configuration Interaction (CI) and Multi-Configuration Self-Consistent Field (MCSCF). These methods extend the wavefunction into a linear combination of many Slater determinants, allowing correlation effects to be captured more clearly.

5- Density Functional Theory (DFT)

Density Functional Theory (DFT) provides a more computationally efficient approach than wavefunction-based approaches, especially for larger systems. DFT uses electron density (ρ) (r) as the basic quantity, rather than the many-electron wavefunction.

The fundamentals of DFT have been well discussed in the literature [112,115–117,120]. Its present evolution is the result of advances in the late 1980s, including gradient-corrected and hybrid functionals [115]. The Hohenberg-Kohn theorems [243] provide the mathematical foundation for DFT, stating that the ground-state electron density $\rho(r)$ provides all information about a system's electronic structure. This converts the issue from dealing with a complex wavefunction to dealing with a three-dimensional scalar function, considerably lowering computing complexity.

5-1. First Hohenberg-Kohn theorem

In 1964 [244], Hohenberg and Kohn formulated a foundational result in quantum chemistry that fundamentally redefined how the electronic structure of matter could be described. This result, now known as the First Hohenberg–Kohn Theorem, states:

“The ground-state energy, wavefunction, and all other electronic properties of a many-electron system are uniquely determined by its ground-state electron density ρ(r).”

According to the First Hohenberg–Kohn Theorem**,** the external potential v(r), and thus the Hamiltonian and all electronic properties, are uniquely determined by ρ(r) up to an additive constant. Consequently, ρ(r) also determines the number of electrons.

In other words, for every electronic system regulated by a specific external potential $V_{\text{ext}}(r)$, typically coming from the arrangement of nuclei, the electron density $\rho(r)$ includes all the information needed to define the system's entire quantum mechanical behavior. Importantly, this contains not only the total energy and potential, but also the wavefunction and any observable properties that may be deduced from it.

The theory states that, up to an additive constant, the external potential $V_{\text{ext}}(r)$ is a function of electron density $\rho(r)$. The wavefunction and all measurable observables are functionals of electron density alone, since the Hamiltonian H relies on $V(r)$ and the Schrödinger equation depends on H. This significant reduction shifts quantum physics from relying on the complex many-body wavefunction to using a three-dimensional scalar field: electron density.

Hohenberg and Kohn also demonstrated that energy is a function of electron density, and that the real ground-state density is the one with the lowest energy functional. This provides a variational concept inside the framework of DFT: the proper electron density is the one with the lowest energy functional. As a result, energy becomes a "functional", a function of a function, of electron density, and is written as $E[\rho]$.

The electron density $\rho(r)$ is a positive function defined in three dimensions. It integrates to the total number of electrons (N) and disappears at infinity.

$$\begin{Bmatrix} \boldsymbol{\rho(r) = \int |\Psi(r)|^2 \, dr} \\ \boldsymbol{\rho(r \to \infty) = 1} \\ \boldsymbol{\int \rho(r) dr = N} \end{Bmatrix} \qquad \textbf{70}$$

Knowing the electron density p(r) of a system gives us the number of electrons N, the external potential V(r), and the total energy, which can be written as:

$$\boldsymbol{E_V[\rho(r)] = T_e[\rho(r)] + \int \rho(r)V(r)dr + V_{ee}[\rho(r)] = \int \rho(r)V(r)dr + F_{HK}[\rho(r)]} \qquad \textbf{71}$$

$$\boldsymbol{F_{HK}[\rho(r)] = T_e[\rho(r)] + V_{ee}[\rho(r)]} \qquad \textbf{72}$$

Where,

F_{HK} $[\rho\ (\ r\ )]$ universal functional of Hohenberg Kohn

T_e $[\rho\ (\ r\ )]$ electronic kinetic energy

$V_{ee}[\rho\ (\ r\ )]$ potential energy due to the interaction between electrons (Hartree energy)

5-2. Second Hohenberg-Kohn theorem

The Second Hohenberg–Kohn Theorem: Variational Principle of DFT states: “For a given external potential V(r), the ground-state energy of an electronic system is the minimum value of the energy functional E[ρ(r)], and the electron density ρ(r) that achieves this minimum is the exact ground-state density of the system.”

This theorem expands upon the previous by introducing a variational concept within the context of density functional theory (DFT). It offers a useful method for determining a system's ground-state attributes without having to compute its many-electron wavefunction.

The difficulty of determining the precise ground-state of a quantum system is phrased as a minimization problem. One searches for the electron density $\rho\ (\ r\ )$ that minimizes the total energy functional $E\ [\ \rho\ ]$, given the constraint that the total number of electrons is fixed.

$$\boldsymbol{N = \int \rho(r)dr} \qquad \textbf{73}$$

This leads straight to DFT's basic equation (15), in which the objective is to determine the electron density that produces the lowest energy rather than simply solving the Schrödinger equation [243] :

$$\boldsymbol{\mu = \frac{\delta E[\rho(r)]}{\delta \rho} = v(r) + \frac{\delta F_{HK}[\rho(r)]}{\delta \rho}} \qquad \textbf{74}$$

µ is the chemical potential of the system.

In other words, unlike classical quantum mechanics, DFT applies the variational principle to the energy functional of the electron density rather than the wavefunction itself. This is a significant simplification since electron density is a function of just three spatial factors, regardless of the number of electrons, while the wavefunction is dependent on 3N variables for N electrons.

To recapitulate, all ground-state features of a system defined by a particular external potential V ext (r) V ext(r) may be completely specified by its ground-state electron density ρ (r) ρ(r). When the proper, physical ground-state density is applied, the overall energy of the system is reduced. Thus, the whole DFT technique is predicated on this variational framework, which seeks the lowest energy among all physically allowable densities.

5-3. The Kohn–Sham Method: Orbital-Based Reformulation of DFT

The practical implementation of the Hohenberg–Kohn theorems was made possible by the work of Kohn and Sham (1965) [245]**,** who introduced a computationally feasible method based on the Self-Consistent Field (SCF) approach. This method bridges the gap between wavefunction-based and density-based quantum mechanics. The Kohn-Sham (KS) technique aims to simplify the complicated many-electron system by replacing it with a fictional non-interacting system with the same electron density (ρ) and ρ(r) as the actual one. In this auxiliary system, electrons travel freely in an effective potential $v_{\text{eff}}(r)$ that is carefully built to replicate the exact physical density.

This framework accurately expresses non-interacting electrons' kinetic energy Tas a function of density (ρ). The total energy functional in Kohn-Sham DFT is thus stated as follows:

$$\boldsymbol{E}[\boldsymbol{\rho}(\boldsymbol{r})] = \boldsymbol{T_e}[\boldsymbol{\rho}(\boldsymbol{r})] + \int \boldsymbol{V_{ext}}(\boldsymbol{r})[\boldsymbol{\rho}(\boldsymbol{r})]\boldsymbol{dr} + \boldsymbol{J}[\boldsymbol{\rho}(\boldsymbol{r})] + \boldsymbol{E_{xc}}[\boldsymbol{\rho}(\boldsymbol{r})] \qquad \textbf{75}$$

T_s [ρ] is the non-interacting reference system's kinetic energy,

V_{ext} (r) is the external potential (due to nuclei),

J[ρ] is the classical Coulomb (electron–electron repulsion) term,

E_{xc}[ρ] is the exchange–correlation functional, which incorporates all the unknown quantum mechanical effects, including the difference between real and non-interacting kinetic energies, and the quantum corrections to electron–electron interaction.

The exchange-correlation energy E_{xc} $[\rho]$ is the main issue in Kohn-Sham DFT. Because it cannot be calculated accurately, it must be approximated—typically using techniques such as the Local Density Approximation (LDA), Generalized Gradient Approximation (GGA), or hybrid functionals. The Kohn-Sham equations, developed by applying the variational principle to this energy functional, are similar to Schrödinger equations for fictional electrons [111].

$$\boldsymbol{\theta_i^{KS}\Psi_i(r) = \varepsilon_i\Psi_i^{KS}(r)} \qquad \textbf{76}$$

With

$$\boldsymbol{\theta_i^{KS}} = \left\{-\frac{\bar{\boldsymbol{h}}^2}{\boldsymbol{2m}}\,\boldsymbol{\nabla_i + V_{ee}[\rho(r)] + V_{xc}[\rho(r)] + V_{Ne}[\rho(r)]}\right\} \qquad \textbf{77}$$

θ_i^{KS} Being the operator of electron i and $\Psi_i^{KS}(r)$ the orbital of electron i

Determining the fundamental state of the system depends on the self-consistent resolution of the equations, known as the Kohn-Sham equations (17). These equations are solved self-consistently**:** starting with an initial guess for ρ(r), the orbitals ψ_i(r) are computed, from which a new density is reconstructed [242]:

$$\boldsymbol{\rho(r) = \textstyle\sum_i\ |\Psi i(r)|^2} \qquad \textbf{78}$$

This procedure is carried out until the input and output densities converge, at which point the system's ground-state energy and electron density are determined.
In summary, the Kohn-Sham technique reduces the complicated many-body problem to a manageable set of single-particle equations while preserving key quantum effects via the exchange-correlation functional. This blend of scientific rigor and computing efficiency has made Kohn-Sham DFT the most popular approach in modern electronic structure theory.

5-4. Local Density Approximation (LDA)

One of the first and most extensively used approximations for the exchange-correlation energy functional in Density Functional Theory (DFT) is the Local Density Approximation (LDA). This technique implies that the electron density ρ (r) fluctuates slowly in space.
In this approximation, the exchange-correlation energy per unit volume at a position r relies only on the local electron density ρ (r) , without considering gradients or surrounding density values. In mathematical terms, the total exchange-correlation energy function is given as [246]:

$$\boldsymbol{E_{XC}^{LDA}[\rho(r)] = \int \rho(r)\varepsilon_{XC}[\rho(r)]\, dr} \qquad \textbf{79}$$

$\varepsilon_{XC}$is the exchange-correlation energy per electron in a uniform electron gas with density ρ. LDA's simplicity makes it computationally efficient and unexpectedly successful in a variety of systems, particularly solid-state physics. However, it may be less accurate in systems with quickly fluctuating densities, such as molecular systems, surfaces, or systems with weak interactions, where gradient adjustments (as in the Generalized Gradient Approximation, GGA) often perform better.

5-5. Generalized Gradient Approximation (GGA)

The Generalized Gradient Approximation (GGA) outperforms the Local Density Approximation (LDA) in Density Functional Theory (DFT). LDA implies that the exchange-correlation energy relies simply on the local electron density $\rho(r)$. However, GGA adds sensitivity to the spatial fluctuation of the electron density by including its gradient $\nabla\rho(r)$.

In GGA, the exchange-correlation energy functional is not only a local function of $\rho(r)$, but also relies on the density at each point in space and its rate of change. This enables the approximation to better represent inhomogeneities non the electronic structure, which are frequent in actual molecules and condensed matter systems.

The general form of the GGA exchange-correlation energy functional is as follows [247]:

$$E_{XC}^{GGA}[\rho(r),\nabla\rho(r)] = \int \rho(r)\varepsilon_{XC}[\rho(r),\nabla\rho(r)]\,dr \qquad 80$$

This adjustment makes GGA especially useful in systems where electron density fluctuates quickly, such as molecular bonding areas, surfaces, or transition states. As a consequence, GGA-based functionals usually outperform LDA in molecular chemistry, organometallic complexes, and surface adsorption experiments.

5-6. Hybrid Functionals

Hybrid functionals are a kind of exchange-correlation functional in Density Functional Theory (DFT) that aims to increase the accuracy of traditional approximations by integrating a percentage of the precise exchange energy determined from Hartree-Fock theory. They combine the exchange and correlation components of generalized gradient approximations (GGA) with some nonlocal exact exchange from Hartree-Fock [242,243]. This combination of functional forms produces better results in many systems, notably in quantum chemistry, where electron delocalization and self-interaction errors often restrict the dependability of pure GGA or LDA techniques. Hybrid functionals are normally represented theoretically, but to simplify notation and easy reference, they are often named after the authors who introduced them and the year of publication. For example: Becke invented the exchange functional in 1988, which is denoted as B [248].The correlation functional proposed by Becke in 1995 is B95 [249]. Another well-known correlation function, LYP, is called after Lee, Yang, and Parr[250]. BLYP combines Becke's 1988 exchange with the Lee-Yang-Parr correlation function. B3LYP is a popular hybrid functional that combines Becke's exchange, exact HF exchange, and LYP correlation, with three empirical parameters tuned for thermochemical precision. BPW86 and BPW91 are Becke exchange combinations with the Perdew-Wang correlation functional, established in 1986 and 1991, respectively.

Hybrid functionals achieve an advantageous compromise between computational cost and forecast accuracy, making them indispensable in current computational chemistry, particularly for molecular systems, reaction energetics, and electronic property predictions.

Bibliographic References

[1] X. Wu, PhD diss: Adsorption and thermal stability of 2-mercaptobenzothiazole and 2-mercaptobenzimidazole deposited on Cu(111) surfaces and effects on corrosion inhibition mechanisms, Chimie Paris Tech, Université PSL, 2020.

[2] A. Ashraf, N. Riaz, S. Muzaffar, M. Atif, B. Bashir, Investigating the potential of 1,2,4-triazoles as corrosion inhibitors for copper and steel: A comprehensive review, Next Res. 1 (2024) 100033. https://doi.org/https://doi.org/10.1016/j.nexres.2024.100033.

[3] A. Krautsieder, PhD diss: Innovative Deposition of Corrosion Inhibitors by Abrasive Blasting, Gonville and Caius College, University of Cambridge, 2022.

[4] M. Finšgar, J. Jackson, Application of corrosion inhibitors for steels in acidic media for the oil and gas industry: A review, Corros. Sci. 86 (2014) 17–41. https://doi.org/10.1016/j.corsci.2014.04.044.

[5] N.J.H. Clarence, PhD Diss: New, environmentaly friendly, non-toxic corrosion inhibitors, Texas A&M University, 2021.

[6] B.E.A. Rani, B.B.J. Basu, Green inhibitors for corrosion protection of metals and alloys: An overview, Int. J. Corros. 2012 (2012). https://doi.org/10.1155/2012/380217.

[7] A. El-khlifi, F.Z. Zouhair, M.R. Al-Hadeethi, H. Lgaz, H.S. Lee, R. Salghi, B. Hammouti, H. Erramli, Assessment of Hydrazone Derivatives for Enhanced Steel Corrosion Resistance in 15 wt.% HCl Environments: A Dual Experimental and Theoretical Perspective, Molecules 29 (2024). https://doi.org/10.3390/molecules29050985.

[8] A. Ait, A. Elmoutaouakil, A. Allah, H. Lgaz, Evaluation of N80 Carbon Steel Corrosion in 15 wt .% HCl Using Isatin-hydrazones : A Comprehensive Approach with Chemical , Electrochemical Techniques , and DFTB Calculations, J. Mol. Struct. 1321 (2025) 139910. https://doi.org/10.1016/j.molstruc.2024.139910.

[9] H. Lgaz, H. seung Lee, Facile preparation of new hydrazone compounds and their application for long-term corrosion inhibition of N80 steel in 15% HCl: An experimental study combined with DFTB calculations, J. Mol. Liq. 347 (2022) 117952. https://doi.org/10.1016/j.molliq.2021.117952.

[10] A. zaid, S. Merdas, M. Hayal, Heterocyclic Compounds Containing N atoms as Corrosion Inhibitors: A review, J. Biosci. Appl. Res. 7 (2021) 93–103. https://doi.org/10.21608/jbaar.2021.178505.

[11] O.M.A. Khamaysa, I. Selatnia, H. Lgaz, A. Sid, H.S. Lee, H. Zeghache, M. Benahmed, I.H. Ali, P. Mosset, Hydrazone-based green corrosion inhibitors for API grade carbon steel in HCl: Insights from electrochemical, XPS, and computational studies, Colloids Surfaces A Physicochem. Eng. Asp. 626 (2021) 127047. https://doi.org/10.1016/j.colsurfa.2021.127047.

[12] G. Laadam, F. Benhiba, M. El Faydy, A. Titi, A.S. Al-Gorair, M. Alshareef, H. Hawsawi, R. Touzani, I. Warad, A. Bellaouchou, A. Guenbour, M. Abdallah, A. Zarrouk, Anti-corrosion performance of novel pyrazole derivative for carbon steel corrosion in 1 M HCl: Computational and experimental studies, Inorg. Chem. Commun. 145 (2022) 109963. https://doi.org/10.1016/j.inoche.2022.109963.

[13] G. Laadam, M. El Faydy, F. Benhiba, A. Titi, H. Amegroud, A.S. Al-Gorair, H. Hawsawi, R. Touzani, I. Warad, A. Bellaouchou, A. Guenbour, M. Abdallah, A. Zarrouk, Outstanding anti-corrosion performance of two pyrazole derivatives on carbon steel in acidic medium: Experimental and quantum-chemical examinations, J. Mol. Liq. 375 (2023) 121268. https://doi.org/10.1016/j.molliq.2023.121268.

[14] N. Timoudan, M. El Faydy, A. Titi, I. Warad, F. Benhiba, A. Alsulmi, B. Dikici, A. Touzani, A. Dafali, A. Bellaouchou, F. Bentiss, A. Zarrouk, Enhanced corrosion resistance of carbon steel in an aggressive environment by a recently developed pyrazole derivative: Electrochemical, SEM/XPS/AFM, and theoretical investigation, J. Solid State Electrochem. 28 (2024) 2837–2860. https://doi.org/10.1007/s10008-024-05846-1.

[15] N. Timoudan, A. Titi, M. El Faydy, F. Benhiba, R. Touzani, I. Warad, A. Bellaouchou, A. Alsulmi, B. Dikici, F. Bentiss, A. Zarrouk, Investigation of the mechanisms and adsorption of a new pyrazole derivative against corrosion of carbon steel in hydrochloric acid solution: Experimental methods and theoretical calculations, Colloids Surfaces A Physicochem. Eng. Asp. 682 (2024) 132771. https://doi.org/10.1016/j.colsurfa.2023.132771.

[16] A. Najem, M. Sabiha, M. Laourayed, A. Belfhaili, F. Benhiba, M. Boudalia, I. Warad, A. Bellaouchou, A. Guenbour, A. Zarrouk, New Green Anti-corrosion Inhibitor of Citrus Peels for Mild Steel in 1 M HCl: Experimental and Theoretical Approaches, Chem. Africa 5 (2022) 969–986. https://doi.org/10.1007/s42250-022-00366-9.

[17] F.Z. Eddahhaoui, A. Najem, M. Elhawary, M. Boudalia, O.S. Campos, M. Tabyaoui, A. José Garcia, A. Bellaouchou, H.M.A. Amin, Experimental and computational aspects of green corrosion inhibition for low carbon steel in HCl environment using extract of Chamaerops humilis fruit waste, J. Alloys Compd. 977 (2024). https://doi.org/10.1016/j.jallcom.2023.173307.

[18] A. Najem, O.S. Campos, M. Raji, A. Bellaouchou, H. M.A.Amin, M. Boudalia, Experimental and DFT Atomistic Insights into the Mechanism of Corrosion Protection of Low-Carbon Steel in an Acidic Medium by Polymethoxyflavones from Citrus Peel Waste, Jouranl Electrochem. Soc. 170 (2023).

[19] M. Sabiha, Y. Kerroum, M. El Hawary, M. Boudalia, A. Bellaouchou, O. Hammani, H.M.A. Amin, Investigating the Adsorption and Corrosion Protection Efficacy and Mechanism of Marjoram Extract on Mild Steel in HCl Medium, Molecules 30 (2025) 1–18. https://doi.org/10.3390/molecules30020272.

[20] A. Belafhaili, M. El Hawary, A. Bellaouchou, A. Guenbour, I. Warad, A. Zarrouk, Omeprazole's Inhibitive Activity on the Corrosion of the Al Alloy in 0.5 M H2SO4 Solution, Anal. Bioanal. Electrochem. 15 (2023) 118–136. https://doi.org/10.22034/ABEC.2023.702330.

[21] M. Boudalia, Y. El Bakri, S. Echihi, A. Harmaoui, J. Sebhaoui, A. Bellaouchou, A. Guenbour, M. Tabyaoui, Y. Ramli, E.M. Essassi, Electrochemical methods for monitoring the performance of a novel Triazole derivative as a corrosion inhibitor in the acidic medium, J. Mater. Environ. Sci. 8 (2017) 2094–2104.

[22] I.U. of P. and A.C. (IUPAC) Y.R.- 2025, corrosion, (n.d.). https://doi.org/10.1351/goldbook.C01351 WV - 5.0.0.

[23] International Organization for Standardization, ISO 8044:2024 – Corrosion of metals and alloys — Vocabulary., (2024). https://www.iso.org/obp/ui/fr/#iso:std:iso:8044:ed-6:v1:en.

[24] E. Ferrari, PhD Diss: Understanding the inhibition corrosion mechanisms for copper based alloys by a physico-chemical multi-scale approach, Université Paris-Saclay, 2021.

[25] M. Oubaaqa, Thèse de Doctorat: Etude expérimentale et approche théorique de l'inhibition de la corrosion de l'acier doux en milieu HCl 1M par des composés organiques de type 8-hydroxyquinoléine et des aciers aminés, Univeristé Ibn Tofail, 2022. https://drive.google.com/drive/folders/1TvDoUo8ycT_D6bzDpK7PaQWfihd_XulT.

[26] D. Landolt, Corrosion and surface chemistry of metals, 2007. https://doi.org/10.5860/choice.45-0897.

[27] International Organization for Standardization, ISO 4948-1:1982 Steels — Classification, (n.d.). https://www.iso.org/obp/ui/#iso:std:iso:4948:-1:ed-1:v1:en.

[28] NF EN 10020: Definition and classification of grades of steel, Paris, France: French Standardization Association, 2000., (n.d.).

[29] R.K. Dubey, PhD Diss: Corrosion inhibition with parts of plant products at mild steel surfaces in acidic media, University of Kota, Rajashtan, India, 2020.

[30] A. Fellah, Y. Harek, I. Ichchou, Experimental and DFT studies of a novel salicylhydrazone derivative as a steel corrosion inhibitor, Colloids Surfaces A Physicochem. Eng. Asp. 685 (2024). https://doi.org/10.1016/j.colsurfa.2024.133150.

[31] A. Elbeshary Aldesouki, Doctoral Diss: The use of saturated long carbon chain carboxylic acids and their sodium salts for the corrosion inhibition of lead and iron heritage objects, Faculty of Sciences, GHENT University, Belgium, 2021.

[32] V. Choda, PhD Diss: The electrochemistry of corrosion inhibitors in the oil and gas industry, University of Cambridge, 2020. https://doi.org/10.1002/9783527822140.

[33] S.B. Sharma, PhD diss: Local inhibition by organic molecules of early stage intergranular corrosion of copper and effects on passivation of grain boundaries, Chimie Paris Tech, Université PSL, 2021.

[34] J.O.M. Bockris, D. Drazic, A.R. Despic, The electrode kinetics of the deposition and dissolution of iron, Electrochim. Acta 4 (1961) 325–361. https://doi.org/10.1016/0013-4686(61)80026-1.

[35] J. Dominguez Olivo, PhD Diss: Electrochemical Model of Carbon Dioxide Corrosion in the Presence of Organic Corrosion Inhibitors, Ohio University, 2020.

[36] G.H. Koch, M.P.. Brongers, N.G. Thompson, Y.P. Virmani, J.H. Payer, Corrosion Costs and Preventive Strategies in the United States, Nace Int., 2002. https://rosap.ntl.bts.gov/view/dot/39217.

[37] A. The corrosion institute of Southern Africa, Reducing Corrosion-Related Asset Failure in Africa, n.d. https://www.corrosioninstitute.org.za/.

[38] BENSOUDA Zakariae, Thèse de Doctorat: Extraction, caractérisation et potentiel inhibiteur des huiles essentielles contre la corrosion d'aciers doux dans une solution

chlorhydrique molaire, Université Sidi Mohamed Ben A bdellah, 2018.

[39] K. Clero, S. Ed-Diny, M. Cherkaoui, T. Soror, S. Rziki, M. Achalhi, S. El Fkihi, A. Boanarijesy, A Review of Geotechnical Instabilities Identification and Monitoring At Deep Underground Mines: Case of Draa Sfar Mine in Morocco, Int. J. Civ. Infrastruct. 5 (2022). https://doi.org/10.11159/ijci.2022.008.

[40] K. Subbiah, H.S. Lee, M.R. Al-Hadeethi, T. Park, H. Lgaz, Assessment of the inhibitive performance of a hydrazone derivative for steel in a simulated concrete medium: Establishing the inhibition mechanism at an experimental and theoretical level, Chem. Eng. J. 458 (2023) 141347. https://doi.org/10.1016/j.cej.2023.141347.

[41] A.I. Obike, K.J. Uwakwe, E.K. Abraham, A.I. Ikeuba, W. Emori, Review of the losses and devastation caused by corrosion in the Nigeria oil industry for over 30 years, Int. J. Corros. Scale Inhib. 9 (2020) 74–91. https://doi.org/10.17675/2305-6894-2020-9-1-5.

[42] ., World steel association, world steel in figures, 2022. https://worldsteel.org/data/world-steel-in-figures/world-steel-in-figures-2024/.

[43] F. Bentiss, M. Traisnel, M. Lagrenee, A new triazole derivative as inhibitor of the acid corrosion of mild steel : electrochemical studies , weight loss determination , SEM and XPS, Appl. Surf. Sci. 152 (1999) 237–249.

[44] G.Y. Elewady, Pyrimidine Derivatives as Corrosion Inhibitors for Carbon-Steel in 2M Hydrochloric Acid Solution, Int. J. Electrochem. Sci. 3 (2008) 1149–1161.

[45] Y. El Aoufir, Thèse de Doctorat: Contribution à l'étude de l'inhibition de la corrosion de l'acier au carbone par des composés organiques de type "'benzimidazole'" et " 'benzodiazépine'" en milieu HCl 1M, Université Ibn Tofail, 2017.

[46] A. Kolics, A.S. Besing, P. Baradlai, A. Wieckowski, Cerium Deposition on Aluminum Alloy 2024-T3 in Acidic NaCl Solutions, J. E 11 (2003) 512–516. https://doi.org/10.1149/1.1615995.

[47] M.U. Kendig, S. Jeanjaquet, R. Addison, J. Waldrop, Role of hexavalent chromium in the inhibition of corrosion of aluminum alloys, Surf. Coatings Technol. 140 (2001) 58–66.

[48] S. V Lamaka, M.L. Zheludkevich, K.A. Yasakau, M.F. Montemor, M.G.S. Ferreira, High effective organic corrosion inhibitors for 2024 aluminium alloy, Electrochim. Acta 52 (2024) 7231–7247. https://doi.org/10.1016/j.electacta.2007.05.058.

[49] H. Grafen, E.-M. Horn, H. Schlecker, R. Feser, Corrosion, 3. Corrosion Protection and Testing, ULLMANN'S Encycl. Ind. Chem. (2015).

[50] D. Jero, N. Caussé, N. Pébère, Film-forming amines as corrosion inhibitors: a state-of-the-art review, Npj Mater. Degrad. 8 (2024) 1–12. https://doi.org/10.1038/s41529-024-00523-0.

[51] D.S. Chauhan, M.A. Quraishi, M.A. Jafar Mazumder, S.A. Ali, N.A. Aljeaban, B.G. Alharbi, Design and synthesis of a novel corrosion inhibitor embedded with quaternary ammonium, amide and amine motifs for protection of carbon steel in 1 M HCl, J. Mol. Liq. 317 (2020) 113917. https://doi.org/10.1016/j.molliq.2020.113917.

[52] N. Abdullayeva, NITROGEN-CONTAINING ORGANIC COMPOUNDS AS INHIBITORS OF CORROSION IN AN AQUEOUS MEDIUM, Process.

Petrochemistry Oil Refin. 19 (2018) 282–294. http://dx.doi.org/10.1016/j.gde.2016.09.008%0Ahttp://dx.doi.org/10.1007/s00412-015-0543-8%0Ahttp://dx.doi.org/10.1038/nature08473%0Ahttp://dx.doi.org/10.1016/j.jmb.2009.01.007%0Ahttp://dx.doi.org/10.1016/j.jmb.2012.10.008%0Ahttp://dx.doi.org/10.1038/s4159.

[53] A. Popova, M. Christov, A. Vasilev, Mono- and dicationic benzothiazolic quaternary ammonium bromides as mild steel corrosion inhibitors . Part III : Influence of the temperature on the inhibition process, Corros. Sci. 94 (2015) 70–78. https://doi.org/10.1016/j.corsci.2015.01.039.

[54] J. Wang, L. An, J. Wang, J. Gu, J. Sun, X. Wang, Frontiers and advances in N-heterocycle compounds as corrosion inhibitors in acid medium: Recent advances, Adv. Colloid Interface Sci. 321 (2023). https://doi.org/10.1016/j.cis.2023.103031.

[55] W. Ettahiri, A. Elmoutaouakil, A. Allah, S. Alaoui, S. Lahmidi, D. Zahri, R. Salim, M. Adardour, M. Maatallah, Y. Ramli, A. Baouid, E.M. Essassi, M. Taleb, Recent advances in the development of some N-Heterocyclic compounds as corrosion inhibitors: a review, Jouranl Maroc. Chim. Hétérocyclique 22 (2023) 1–40.

[56] Y.G. Avdeev, Y.I. Kuznetsov, Nitrogen-containing five-membered heterocyclic compounds as corrosion inhibitors for metals in solutions of mineral acids – an overview, Int. J. Corros. Scale Inhib. 10 (2021) 480–540. https://doi.org/10.17675/2305-6894-2020-10-2-2.

[57] D. Jyoti, N. Sandhu, V. Saraswat, Schiff Bases as Corrosion Inhibitors : A Comprehensive Review of Synthesis , Mechanisms , and Applications, Ymer 23 (2024) 722–750.

[58] O.M.A. Khamaysa, I. Selatnia, H. Lgaz, A. Sid, H.S. Lee, H. Zeghache, M. Benahmed, I.H. Ali, P. Mosset, Hydrazone-based green corrosion inhibitors for API grade carbon steel in HCl: Insights from electrochemical, XPS, and computational studies, Colloids Surfaces A Physicochem. Eng. Asp. 626 (2021) 127047. https://doi.org/10.1016/j.colsurfa.2021.127047.

[59] A.S. Fouda, H.S. El-Desoky, M.M. Abdel-Galeil, D. Mansour, Amide Compounds as Corrosion Inhibitors for Carbon Steel in Acidic Environment, Prot. Met. Phys. Chem. Surfaces 58 (2022) 151–167. https://doi.org/10.1134/S2070205122010105.

[60] L. Chen, D. Lu, Y. Zhang, Organic Compounds as Corrosion Inhibitors for Carbon Steel in HCl Solution: A Comprehensive Review, Materials (Basel). 15 (2022) 1–59. https://doi.org/10.3390/ma15062023.

[61] A. David Ebuka, A. Jonathan, P. Ocheje Ameh, A. Crystal, A Review on the Assessment of polymeric materials used as Corrosion Inhibitor of Metals and alloys, Int. J. Ind. Chem. 4 (2013). https://doi.org/10.1007/s40735-018-0207-3.

[62] S. Maddila, R. Pagadala, S.B. Jonnalagadda, 1 ,2,4-Triazoles : A Review of Synthetic Approaches and the Biological Activity, Lett. Org. Chem. 10 (2013) 693–714.

[63] Triazole Market Size, Demand & Growth Forecast Report 2023, 2023. https://www.factmr.com/report/triazole-market.

[64] M.K. Durjava, B. Kolar, L. Arnus, E. Papa, S. Kovarich, U. Sahlin, W. Peijnenburg,

Experimental assessment of the environmental fate and effects of triazoles and benzotriazole, ATLA Altern. to Lab. Anim. 41 (2013) 65–75. https://doi.org/10.1177/026119291304100108.

[65] M. Faisal, A. Saeed, D. Shahzad, N. Abbas, F. Ali Larik, P. Ali Channar, T. Abdul Fattah, D. Muhammad Khan, S. Aaliya Shehzadi, General properties and comparison of the corrosion inhibition efficiencies of the triazole derivatives for mild steel, Corros. Rev. 36 (2018) 507–545. https://doi.org/10.1515/corrrev-2018-0006.

[66] R.T.T. Jalgham, Theoretical, Monte Carlo Simulations and Quantitative Structure Activity Relationship Studies on Some Triazole Derivatives as Corrosion Inhibitors for Mild Steel in 1 M HCl, ES Energy Environ. 13 (2021) 37–49. https://doi.org/10.30919/esee8c476.

[67] K. Belal, A.H. El-Askalany, E.A. Ghaith, A. Fathi Salem Molouk, Novel synthesized triazole derivatives as effective corrosion inhibitors for carbon steel in 1M HCl solution: experimental and computational studies, Sci. Rep. 13 (2023) 1–22. https://doi.org/10.1038/s41598-023-49468-5.

[68] F. Álvarez, M. Arena, D. Auteri, S.B.L.M. Binaglia, Peer review of the pesticide risk assessment of the active substance metconazole, EFSA J. 21 (2023). https://doi.org/10.2903/j.efsa.2023.8141.

[69] W. Li, L. Hu, Z. Tao, H. Tian, B. Hou, Experimental and quantum chemical studies on two triazole derivatives as corrosion inhibitors for mild steel in acid media, Mater. Corros. 62 (2011) 1042–1050. https://doi.org/10.1002/maco.201005965.

[70] M. Hrimla, L. Bahsis, M.R. Laamari, M. Julve, S.E. Stiriba, An overview on the performance of 1,2,3-triazole derivatives as corrosion inhibitors for metal surfaces, Int. J. Mol. Sci. 23 (2022). https://doi.org/10.3390/ijms23010016.

[71] G.O. Resende, S.F. Teixeira, I.F. Figueiredo, A.A. Godoy, D.J.F. Lougon, B.A. Cotrim, F.C. De Souza, Synthesis of 1,2,3-Triazole Derivatives and Its Evaluation as Corrosion Inhibitors for Carbon Steel, Int. J. Electrochem. (2019).

[72] I. Merimi, A. Bitari, Y. Kaddouri, N. Rezki, M. Mohamed, R. Touzani, B. Hammouti, Metal corrosion inhibition by triazoles: A review, Int. J. Corros. Scale Inhib. 11 (2022) 524–540. https://doi.org/10.17675/2305-6894-2022-11-2-4.

[73] I. Merimi, Y.E.L. Ouadi, R. Benkaddour, H. Lgaz, M. Messali, F. Jeffali, B. Hammouti, Improving corrosion inhibition potentials using two triazole derivatives for mild steel in acidic medium : Experimental and theoretical studies, Mater. Today Proc. 13 (2019) 920–930. https://doi.org/10.1016/j.matpr.2019.04.056.

[74] H. Wang, R. Liu, J. Xin, Inhibiting effects of some mercapto-triazole derivatives on the corrosion of mild steel in 1 . 0 M HCl medium, Corros. Sci. 46 (2004) 2455–2466. https://doi.org/10.1016/j.corsci.2004.01.023.

[75] M.A. Quraishi, S. Ahmad, M.Q. Ansari, M.Q. Ansari, Inhibition of steel corrosion by some new triazole derivatives in boiling hydrochloric acid Inhibition of steel corrosion by some new triazole derivatives in boiling hydrochloric acid, Br. Corros. J. 32 (1997) 297–300. https://doi.org/10.1179/000705997798129223.

[76] F. Xu, Triazole derivatives as corrosion inhibitors for mild steel in hydrochloric acid solution, Acta Metall. Sin. 22 (2009) 247–254. https://doi.org/10.1016/S1006-

7191(08)60096-4.

[77] Q. Ma, S. Qi, X. He, Y. Tang, G. Lu, 1,2,3-Triazole derivatives as corrosion inhibitors for mild steel in acidic medium : Experimental and computational chemistry studies, Corros. Sci. 129 (2017) 91–101. https://doi.org/10.1016/j.corsci.2017.09.025.

[78] A. Nahlé, R. Salim, F. El Hajjaji, M.R. Aouad, M. Messali, E. Ech-Chihbi, B. Hammouti, M. Taleb, Novel triazole derivatives as ecological corrosion inhibitors for mild steel in 1.0 M HCl: experimental & theoretical approach, RSC Adv. 11 (2021) 4147–4162. https://doi.org/10.1039/d0ra09679b.

[79] M. Elbelghiti, Y. Karzazi, A. Dafali, B. Hammouti, F. Bentiss, I.B. Obot, I. Bahadur, E.E. Ebenso, Experimental, quantum chemical and Monte Carlo simulation studies of 3,5-disubstituted-4-amino-1,2,4-triazoles as corrosion inhibitors on mild steel in acidic medium, J. Mol. Liq. 218 (2016) 281–293. https://doi.org/10.1016/j.molliq.2016.01.076.

[80] M. Naciri, Y. El Aoufir, H. Lgaz, F. Lazrak, A. Ghanimi, A. Guenbour, ismat H. Ali, M. El Moudane, J. Taoufik, I.M. Chung, Exploring the potential of a new 1,2,4-triazole derivative for corrosion protection of carbon steel in HCl: A computational and experimental evaluation, Colloids Surfaces A Physicochem. Eng. Asp. 597 (2020) 124604. https://doi.org/10.1016/j.colsurfa.2020.124604.

[81] I.A.A. Aziz, I.A. Annon, M.H. Abdulkareem, M.M. Hanoon, M.H. Alkaabi, L.M. Shaker, A.A. Alamiery, W.N.R. Wan Isahak, M.S. Takriff, Insights into corrosion inhibition behavior of a 5-mercapto-1, 2, 4-triazole derivative for mild steel in hydrochloric acid solution: Experimental and dft studies, Lubricants 9 (2021) 1–14. https://doi.org/10.3390/lubricants9120122.

[82] Y. El Aoufir, R. Aslam, F. Lazrak, R. Marzouki, S. Kaya, S. Skal, A. Ghanimi, I.H. Ali, A. Guenbour, H. Lgaz, I.M. Chung, The effect of the alkyl chain length on corrosion inhibition performances of 1,2,4-triazole-based compounds for mild steel in 1.0 M HCl: Insights from experimental and theoretical studies, J. Mol. Liq. 303 (2020). https://doi.org/10.1016/j.molliq.2020.112631.

[83] M. Chafiq, A. Chaouiki, M.R. Al-Hadeethi, I.H. Ali, S.K. Mohamed, K. Toumiat, R. Salghi, Naproxen-based hydrazones as effective corrosion inhibitors for mild steel in 1.0 M HCl, Coatings 10 (2020) 0–17. https://doi.org/10.3390/coatings10070700.

[84] Y. Islam, N. Chafai, O. Moumeni, A. Boublia, M. Mehri, Y. Benguerba, Synthesis , characterization , and comprehensive computational analysis of aromatic hydrazone compounds : Unveiling quantum parameters , evaluating antioxidant activity , and investigating molecular docking interactions, J. Mol. Liq. 403 (2024) 124897. https://doi.org/10.1016/j.molliq.2024.124897.

[85] K. Subbiah, H. Lee, M.R. Al-hadeethi, T. Park, H. Lgaz, Unraveling the anti-corrosion mechanisms of a novel hydrazone derivative on steel in contaminated concrete pore solutions : An integrated study, J. Adv. Res. 58 (2024) 211–228. https://doi.org/10.1016/j.jare.2023.08.016.

[86] D. Specklin, Thèse de Doctorat: Propriétés magnétiques et structurales de complexes moléculaires supportés par des ligands de type acyle-hydrazone, Université de Strasbourg, 2014.

[87] A.S.E.-K. Amira H. E. Moustafa, Hanaa H. Abdel-Rahman, Assem Barakat, Hagar A.

Mohamed, An Exploratory Experimental Analysis Backed by Quantum Mechanical Modeling, Spectroscopic, and Surface Study for C-Steel Surface in the Presence of Hydrazone-Based Schiff Bases to Fix Corrosion Defects in Acidic Media, ACS Omega 9 (2024) 16469–16485. https://doi.org/10.1021/acsomega.4c00199.

[88] K. Subbiah, H. Lee, M.R. Al-hadeethi, T. Park, H. Lgaz, Assessment of the inhibitive performance of a hydrazone derivative for steel rebar in a simulated concrete medium : Establishing the inhibition mechanism at an experimental and theoretical level, Chem. Eng. J. 458 (2023) 141347. https://doi.org/10.1016/j.cej.2023.141347.

[89] M. En-Nylly, S. Skal, Y. El aoufir, H. Lgaz, R.J. Adnin, A.A. Alrashdi, A. Bellaouchou, M.R. Al-Hadeethi, O. Benali, T. Guedira, H.S. Lee, S. Kaya, S.M. Ibrahim, Performance evaluation and assessment of the corrosion inhibition mechanism of carbon steel in HCl medium by a new hydrazone compound: Insights from experimental, DFT and first-principles DFT simulations, Arab. J. Chem. 16 (2023) 104711. https://doi.org/10.1016/j.arabjc.2023.104711.

[90] M.N.H. Moussa, The use of water-soluble hydrazones as inhibitors for the corrosion of C-steel in acidic medium, Mater. Chem. Phys. 105 (2007) 105–113. https://doi.org/10.1016/j.matchemphys.2007.04.007.

[91] T.K. Chaitra, K.N. Mohana, H.C. Tandon, Evaluation of newly synthesized hydrazones as mild steel corrosion inhibitors by adsorption, electrochemical, quantum chemical and morphological studies, Arab J. Basic Appl. Sci. 25 (2018) 45–55. https://doi.org/10.1080/25765299.2018.1449347.

[92] T.K. Chaitra, K.N. Mohana, D.M. Gurudatt, H.C. Tandon, Inhibition activity of new thiazole hydrazones towards mild steel corrosion in acid media by thermodynamic, electrochemical and quantum chemical methods, J. Taiwan Inst. Chem. Eng. 67 (2016) 521–531. https://doi.org/10.1016/j.jtice.2016.08.013.

[93] E.S.M. Sherif, A.H. Ahmed, Synthesizing new hydrazone derivatives and studying their effects on the inhibition of copper corrosion in sodium chloride solutions, Synth. React. Inorganic, Met. Nano-Metal Chem. 40 (2010) 365–372. https://doi.org/10.1080/15533174.2010.492546.

[94] H. Lgaz, I.M. Chung, M.R. Albayati, A. Chaouiki, R. Salghi, S.K. Mohamed, Improved corrosion resistance of mild steel in acidic solution by hydrazone derivatives: An experimental and computational study, Arab. J. Chem. 13 (2020) 2934–2954. https://doi.org/10.1016/j.arabjc.2018.08.004.

[95] M. Chafiq, A. Chaouiki, M.R. Al-Hadeethi, H. Lgaz, R. Salghi, S.K. Abdelraheem, I.H. Ali, S.A.M. Ebraheem, S.K. Mohamed, I.M. Chung, Evaluation of the effect of two naproxen-based hydrazones on the corrosion inhibition of mild steel in 1.0 M HCl, Int. J. Electrochem. Sci. 15 (2020) 9335–9353. https://doi.org/10.20964/2020.09.69.

[96] H. Lgaz, A. Chaouiki, M.R. Albayati, R. Salghi, Y. El Aoufir, I.H. Ali, M.I. Khan, S.K. Mohamed, I.M. Chung, Synthesis and evaluation of some new hydrazones as corrosion inhibitors for mild steel in acidic media, Res. Chem. Intermed. 45 (2019) 2269–2286. https://doi.org/10.1007/s11164-018-03730-y.

[97] H. Lgaz, S. Zehra, M.R. Albayati, K. Toumiat, Y. El Aoufir, A. Chaouiki, R. Salghi, I.H. Ali, M.I. Khan, I.M. Chung, S.K. Mohamed, Corrosion inhibition of mild steel in 1.0 M HCl by two hydrazone derivatives, Int. J. Electrochem. Sci. 14 (2019) 6667–

6681. https://doi.org/10.20964/2019.07.08.

[98] M. Chafiq, A. Chaouiki, M.R. Albayati, H. Lgaz, R. Salghi, S.K. AbdelRaheem, I.H. Ali, S.K. Mohamed, I.M. Chung, Unveiled understanding on corrosion inhibition mechanisms of hydrazone derivatives based on naproxen for mild steel in HCl: A joint experimental/theoretical study, J. Mol. Liq. 320 (2020). https://doi.org/10.1016/j.molliq.2020.114442.

[99] A. Chaouiki, M. Chafiq, H. Lgaz, M.R. Al-Hadeethi, I.H. Ali, S. Masroor, I.M. Chung, Green corrosion inhibition of mild steel by hydrazone derivatives in 1.0 M HCl, Coatings 10 (2020) 0–17. https://doi.org/10.3390/coatings10070640.

[100] ASTM G31-72 (2004) Standard Practice for Laboratory Immersion Corrosion Testing of Metals, (2004).

[101] P. Denissen, Doctoral Diss: In-Situ visual quantification of corrosion and corrosion protection, TU Delft University, the Nederlands, 2020. https://doi.org/10.4233/uuid:64f8f06e-5cc6-40cd-8c8d-722da6304b06.

[102] M.E. Orazem, B. Tribollet, History of impedance spectroscopy, in: Electrochem. Impedance Spectrosc. 2nd Ed., John Wiley & Sons, Inc., 2017.

[103] J.R. Macdonald, E. Barsoukouv, Impedance Spectroscopy Theory, Experiment, and Application, 2nd editio, John Wiley & Sons, Inc., 2005.

[104] M.E. Orazem, B. Tribollet, Electrochemical Impedance Spectroscopy, John Wiley & Sons, Inc., 2008. https://doi.org/10.1002/9780470381588.

[105] S. Nasrazadani, S. Hassani, Modern analytical techniques in failure analysis of aerospace, chemical, and oil and gas industries, in: Handb. Mater. Fail. Anal. with Case Stud. from Oil Gas Ind., Butterwort, 2016. https://doi.org/https://doi.org/10.1016/C2014-0-01712-1.

[106] Y. Kerroum, Thèse de Doctorat: Etude du mécanisme d’action des ions fluorures sur la corrosion et la passivité de la fonte au chrome et de l’alliage 904L en milieux phosphoriques, Faculté des Sciences de Rabat, Université Mohammed V, 2020.

[107] W.H. Bragg, W.L. Bragg, The reflection of X-rays by crystals, Proc. R. Soc. London. Ser. A, Contain. Pap. a Math. Phys. Character 88 (1997) 428–438. https://doi.org/10.1098/rspa.1913.0040.

[108] A.I. Ali, Y.S. Mahrous, Corrosion inhibition of C-steel in acidic media from fruiting bodies of: Melia azedarach L extract and a synergistic Ni2+ additive, RSC Adv. 7 (2017) 23687–23698. https://doi.org/10.1039/c7ra00111h.

[109] M. Oubaaqa, M. Ouakki, M. Rbaa, A.S. Abousalem, M. Maatallah, F. Benhiba, A. Jarid, M. Ebn Touhami, A. Zarrouk, Insight into the corrosion inhibition of new amino-acids as efficient inhibitors for mild steel in HCl solution: Experimental studies and theoretical calculations, J. Mol. Liq. 334 (2021) 116520. https://doi.org/10.1016/j.molliq.2021.116520.

[110] Paul. J. Worsfold, E.A.G. Zagatto, Spectrophotometry | Overview, Encycl. Anal. Sci. (Third Ed. (2019). https://doi.org/https://doi.org/10.1016/B978-0-12-409547-2.14265-9.

[111] H.S. Samuel, U. Nweke-maraizu, G. Johnson, E.E. Etim, A Review of Theoretical

Techniques in Corrosion Inhibition Studies :, Commun. Phys. Sci. 9 (2023) 394–403.

[112] D.K. Verma, Density Functional Theory (DFT) as a Powerful Tool for Designing Corrosion Inhibitors in Aqueous Phase, Adv. Eng. Test. (2018). https://doi.org/10.5772/intechopen.78333.

[113] H. Lgaz, R. Salghi, K. Subrahmanya Bhat, A. Chaouiki, Shubhalaxmi, S. Jodeh, Correlated experimental and theoretical study on inhibition behavior of novel quinoline derivatives for the corrosion of mild steel in hydrochloric acid solution, Elsevier B.V, 2017. https://doi.org/10.1016/j.molliq.2017.08.121.

[114] C. Verma, L.O. Olasunkanmi, E.E. Ebenso, M.A. Quraishi, I.B. Obot, Adsorption Behavior of Glucosamine-Based, Pyrimidine-Fused Heterocycles as Green Corrosion Inhibitors for Mild Steel: Experimental and Theoretical Studies, J. Phys. Chem. C 120 (2016) 11598–11611. https://doi.org/10.1021/acs.jpcc.6b04429.

[115] I.B. Obot, D.D. Macdonald, Z.M. Gasem, Density functional theory (DFT) as a powerful tool for designing new organic corrosion inhibitors: Part 1: An overview, Corros. Sci. 99 (2015) 1–30. https://doi.org/10.1016/j.corsci.2015.01.037.

[116] C. Verma, H. Lgaz, D.K. Verma, E.E. Ebenso, I. Bahadur, M.A. Quraishi, Molecular dynamics and Monte Carlo simulations as powerful tools for study of interfacial adsorption behavior of corrosion inhibitors in aqueous phase : A review, J. Mol. Liq. 260 (2018) 99–120. https://doi.org/10.1016/j.molliq.2018.03.045.

[117] A. Kokalj, On the HSAB based estimate of charge transfer between adsorbates and metal surfaces, Chem. Phys. 393 (2012) 1–12. https://doi.org/10.1016/j.chemphys.2011.10.021.

[118] Z. Cao, Y. Tang, H. Cang, J. Xu, G. Lu, W. Jing, Novel benzimidazole derivatives as corrosion inhibitors of mild steel in the acidic media. Part II: Theoretical studies, Corros. Sci. 83 (2014) 292–298. https://doi.org/10.1016/j.corsci.2014.02.025.

[119] N. Izzah, N. Haris, S. Sobri, Y.A. Yusof, N.K. Kassim, An Overview of Molecular Dynamic Simulation for Corrosion inhibition in ferrous metals, Metals (Basel). (2021) 1–22.

[120] S. Donkor, Z. Song, L. Jiang, H. Chu, An overview of computational and theoretical studies on analyzing adsorption performance of phytochemicals as metal corrosion inhibitors, J. Mol. Liq. 359 (2022) 119260. https://doi.org/10.1016/j.molliq.2022.119260.

[121] D.I. Njoku, Y. Li, H. Lgaz, E.E. Oguzie, Dispersive adsorption of Xylopia aethiopica constituents on carbon steel in acid-chloride medium: A combined experimental and theoretical approach, J. Mol. Liq. 249 (2018) 371–388. https://doi.org/https://doi.org/10.1016/j.molliq.2017.11.051.

[122] E. Gutiérrez, J.A. Rodríguez, J. Cruz-Borbolla, J.G. Alvarado-Rodríguez, P. Thangarasu, Development of a predictive model for corrosion inhibition of carbon steel by imidazole and benzimidazole derivatives, Corros. Sci. 108 (2016) 23–35. https://doi.org/10.1016/j.corsci.2016.02.036.

[123] A. Singh, K.R. Ansari, J. Haque, P. Dohare, H. Lgaz, R. Salghi, M.A. Quraishi, Effect of electron donating functional groups on corrosion inhibition of mild steel in hydrochloric acid: Experimental and quantum chemical study, J. Taiwan Inst. Chem.

Eng. 82 (2018) 233–251. https://doi.org/https://doi.org/10.1016/j.jtice.2017.09.021.

[124] E. Alibakhshi, M. Ramezanzadeh, S.A. Haddadi, G. Bahlakeh, B. Ramezanzadeh, M. Mahdavian, Persian Liquorice extract as a highly efficient sustainable corrosion inhibitor for mild steel in sodium chloride solution, J. Clean. Prod. 210 (2019) 660–672. https://doi.org/https://doi.org/10.1016/j.jclepro.2018.11.053.

[125] M.T. Majd, M. Ramezanzadeh, B. Ramezanzadeh, G. Bahlakeh, Production of an environmentally stable anti-corrosion film based on Esfand seed extract molecules-metal cations: Integrated experimental and computer modeling approaches, J. Hazard. Mater. 382 (2020) 121029. https://doi.org/https://doi.org/10.1016/j.jhazmat.2019.121029.

[126] Y. Qiang, S. Zhang, L. Wang, Understanding the adsorption and anticorrosive mechanism of DNA inhibitor for copper in sulfuric acid, Appl. Surf. Sci. 492 (2019) 228–238. https://doi.org/https://doi.org/10.1016/j.apsusc.2019.06.190.

[127] Y. Qiang, S. Zhang, B. Tan, S. Chen, Evaluation of Ginkgo leaf extract as an eco-friendly corrosion inhibitor of X70 steel in HCl solution, Corros. Sci. 133 (2018) 6–16. https://doi.org/https://doi.org/10.1016/j.corsci.2018.01.008.

[128] T.K. Chaitra, K.N.S. Mohana, H.C. Tandon, Thermodynamic, electrochemical and quantum chemical evaluation of some triazole Schiff bases as mild steel corrosion inhibitors in acid media, J. Mol. Liq. 211 (2015) 1026–1038. https://doi.org/10.1016/j.molliq.2015.08.031.

[129] H.H. Revie, Winston R. Uhlig, Corossion and Corossion Control, 4th ed., John Wiley and Sons Inc., 2008.

[130] E.A. Yaqo, R.A. Anaee, M.H. Abdulmajeed, I.H.R. Tomi, M.M. Kadhim, Aminotriazole Derivative as Anti-Corrosion Material for Iraqi Kerosene Tanks: Electrochemical, Computational and the Surface Study, ChemistrySelect 4 (2019) 9883–9892. https://doi.org/https://doi.org/10.1002/slct.201902398.

[131] D.S. Chauhan, M.A. Quraishi, C. Carrière, A. Seyeux, P. Marcus, A. Singh, Electrochemical, ToF-SIMS and computational studies of 4-amino-5-methyl-4H-1,2,4-triazole-3-thiol as a novel corrosion inhibitor for copper in 3.5% NaCl, J. Mol. Liq. 289 (2019) 111113. https://doi.org/https://doi.org/10.1016/j.molliq.2019.111113.

[132] T. Zhang, S. Cao, H. Quan, Z. Huang, S. Xu, Synthesis and corrosion inhibition performance of alkyl triazole derivatives, Res. Chem. Intermed. 41 (2015) 2709–2724. https://doi.org/10.1007/s11164-013-1381-z.

[133] M.A. Quraishi, D. Jamal, Fatty acid triazoles: Novel corrosion inhibitors for oil well steel (N-80) and mild steel, JAOCS, J. Am. Oil Chem. Soc. 77 (2000) 1107–1111. https://doi.org/10.1007/s11746-000-0174-6.

[134] I. Merimi, R. Benkaddour, H. Lgaz, N. Rezki, M. Messali, F. Jeffali, H. Oudda, B. Hammouti, Insights into corrosion inhibition behavior of a triazole derivative For mild steel in hydrochloric acid solution, Mater. Today Proc. 13 (2019) 1008–1022. https://doi.org/10.1016/j.matpr.2019.04.066.

[135] Z. Tao, W. He, S. Wang, S. Zhang, G. Zhou, Adsorption properties and inhibition of mild steel corrosion in 0.5 M H2SO4 solution by some triazol compound, J. Mater. Eng. Perform. 22 (2013) 774–781. https://doi.org/10.1007/s11665-012-0321-1.

[136] Z. Tao, S. Zhang, W. Li, B. Hou, Adsorption and inhibitory mechanism of 1 H -1,2,4-Triazol-l-yl-methyl-2-(4- chlorophenoxy) acetate on corrosion of mild steel in acidic solution, Ind. Eng. Chem. Res. 50 (2011) 6082–6088. https://doi.org/10.1021/ie101793b.

[137] S.T. Method, iTeh Standards iTeh Standards Document Preview, 08 (2000) 3–4. https://doi.org/10.1520/C1709-18.

[138] I.B. Obot, N.O. Obi-Egbedi, Anti-corrosive properties of xanthone on mild steel corrosion in sulphuric acid: Experimental and theoretical investigations, Curr. Appl. Phys. 11 (2011) 382–392. https://doi.org/10.1016/j.cap.2010.08.007.

[139] E. Kowsari, S.Y. Arman, M.H. Shahini, H. Zandi, A. Ehsani, R. Naderi, A. PourghasemiHanza, M. Mehdipour, In situ synthesis, electrochemical and quantum chemical analysis of an amino acid-derived ionic liquid inhibitor for corrosion protection of mild steel in 1M HCl solution, Corros. Sci. 112 (2016) 73–85. https://doi.org/https://doi.org/10.1016/j.corsci.2016.07.015.

[140] D. Daoud, T. Douadi, S. Issaadi, S. Chafaa, Adsorption and corrosion inhibition of new synthesized thiophene Schiff base on mild steel X52 in HCl and H2SO4 solutions, Corros. Sci. 79 (2014) 50–58. https://doi.org/10.1016/j.corsci.2013.10.025.

[141] H. Lgaz, S.K. Saha, A. Chaouiki, K.S. Bhat, R. Salghi, Shubhalaxmi, P. Banerjee, I.H. Ali, M.I. Khan, I.M. Chung, Exploring the potential role of pyrazoline derivatives in corrosion inhibition of mild steel in hydrochloric acid solution: Insights from experimental and computational studies, Constr. Build. Mater. 233 (2020) 117320. https://doi.org/10.1016/j.conbuildmat.2019.117320.

[142] I. Forsal, L. Lakhrissi, K. Naji, S. Abirou, M. Ebn Touhami, B. Lakhrissi, M. Addou, The efficiency of corrosion inhibitor as given by electrochemical impedance spectroscopy Tafel polarization and weight-loss measurements, Spectrosc. Lett. 43 (2010) 136–143. https://doi.org/10.1080/00387010903261180.

[143] D.K. Singh, S. Kumar, G. Udayabhanu, R.P. John, 4(N,N-dimethylamino) benzaldehyde nicotinic hydrazone as corrosion inhibitor for mild steel in 1 M HCl solution: An experimental and theoretical study, J. Mol. Liq. 216 (2016) 738–746. https://doi.org/10.1016/j.molliq.2016.02.012.

[144] C. Verma, M.A. Quraishi, A. Singh, 2-Amino-5-nitro-4,6-diarylcyclohex-1-ene-1,3,3-tricarbonitriles as new and effective corrosion inhibitors for mild steel in 1 M HCl: Experimental and theoretical studies, J. Mol. Liq. 212 (2015) 804–812. https://doi.org/10.1016/j.molliq.2015.10.026.

[145] F. Bentiss, B. Mernari, M. Traisnel, H. Vezin, M. Lagrenée, On the relationship between corrosion inhibiting effect and molecular structure of 2,5-bis(n-pyridyl)-1,3,4-thiadiazole derivatives in acidic media: Ac impedance and DFT studies, Corros. Sci. 53 (2011) 487–495. https://doi.org/10.1016/j.corsci.2010.09.063.

[146] A.O. Yüce, G. Kardaş, Adsorption and inhibition effect of 2-thiohydantoin on mild steel corrosion in 0.1M HCl, Corros. Sci. 58 (2012) 86–94. https://doi.org/10.1016/j.corsci.2012.01.013.

[147] Z. Salarvand, M. Amirnasr, M. Talebian, K. Raeissi, S. Meghdadi, Enhanced corrosion resistance of mild steel in 1 M HCl solution by trace amount of 2-phenyl-benzothiazole derivatives: Experimental, quantum chemical calculations and molecular dynamics

(MD) simulation studies, Corros. Sci. 114 (2017) 133–145. https://doi.org/10.1016/j.corsci.2016.11.002.

[148] J. Aljourani, K. Raeissi, M.A. Golozar, Benzimidazole and its derivatives as corrosion inhibitors for mild steel in 1M HCl solution, Corros. Sci. 51 (2009) 1836–1843. https://doi.org/10.1016/j.corsci.2009.05.011.

[149] R. Solmaz, G. Kardaş, M. Çulha, B. Yazici, M. Erbil, Investigation of adsorption and inhibitive effect of 2-mercaptothiazoline on corrosion of mild steel in hydrochloric acid media, Electrochim. Acta 53 (2008) 5941–5952. https://doi.org/10.1016/j.electacta.2008.03.055.

[150] D. Daoud, T. Douadi, H. Hamani, S. Chafaa, M. Al-noaimi, Corrosion inhibition of mild steel by new N-heterocyclic compound in 1 M HCl: Experimental and computational study, Corros. Sci. 94 (2015) 21–37. https://doi.org/10.1016/j.corsci.2015.01.025.

[151] M. Mahdavian, S. Ashhari, Corrosion inhibition performance of 2-mercaptobenzimidazole and 2-mercaptobenzoxazole compounds for protection of mild steel in hydrochloric acid solution, Electrochim. Acta 55 (2010) 1720–1724. https://doi.org/10.1016/j.electacta.2009.10.055.

[152] H. Lgaz, I.M. Chung, R. Salghi, I.H. Ali, A. Chaouiki, Y. El Aoufir, M.I. Khan, On the understanding of the adsorption of Fenugreek gum on mild steel in an acidic medium: Insights from experimental and computational studies, Appl. Surf. Sci. 463 (2019) 647–658. https://doi.org/10.1016/j.apsusc.2018.09.001.

[153] S. Martinez, M. Metikoš-Huković, A nonlinear kinetic model introduced for the corrosion inhibitive properties of some organic inhibitors, J. Appl. Electrochem. 33 (2003) 1137–1142. https://doi.org/10.1023/B:JACH.0000003851.82985.5e.

[154] J. Haque, V. Srivastava, C. Verma, M.A. Quraishi, Experimental and quantum chemical analysis of 2-amino-3-((4-((S)-2-amino-2-carboxyethyl)-1H-imidazol-2-yl)thio) propionic acid as new and green corrosion inhibitor for mild steel in 1 M hydrochloric acid solution, J. Mol. Liq. 225 (2017) 848–855. https://doi.org/10.1016/j.molliq.2016.11.011.

[155] C. Verma, M.A. Quraishi, A. Singh, 5-Substituted 1H-tetrazoles as effective corrosion inhibitors for mild steel in 1 M hydrochloric acid, J. Taibah Univ. Sci. 10 (2016) 718–733. https://doi.org/10.1016/j.jtusci.2015.10.005.

[156] M. Özcan, F. Karadağ, I. Dehri, Interfacial Behavior of Cysteine between Mild Steel and Sulfuric Acid as Corrosion Inhibitor, Acta Phys. - Chim. Sin. 24 (2008) 1387–1392. https://doi.org/10.1016/S1872-1508(08)60059-5.

[157] Y. Tang, F. Zhang, S. Hu, Z. Cao, Z. Wu, W. Jing, Novel benzimidazole derivatives as corrosion inhibitors of mild steel in the acidic media. Part I: Gravimetric, electrochemical, SEM and XPS studies, Corros. Sci. 74 (2013) 271–282. https://doi.org/10.1016/j.corsci.2013.04.053.

[158] C. Verma, M.A. Quraishi, E.E. Ebenso, I.B. Obot, A. El Assyry, 3-Amino alkylated indoles as corrosion inhibitors for mild steel in 1M HCl: Experimental and theoretical studies, J. Mol. Liq. 219 (2016) 647–660. https://doi.org/10.1016/j.molliq.2016.04.024.

[159] H. Lgaz, R. Salghi, S. Jodeh, B. Hammouti, Effect of clozapine on inhibition of mild

steel corrosion in 1.0 M HCl medium, Elsevier B.V., 2017. https://doi.org/10.1016/j.molliq.2016.11.039.

[160] A. Anejjar, R. Salghi, A. Zarrouk, H. Zarrok, O. Benali, B. Hammouti, S.S. Al-Deyab, N.E. Benchat, R. Saddik, Investigation of inhibition by 6-bromo-3-nitroso-2-phenylimidazol[1,2-α]pyridine of the corrosion of C38 steel in 1 M HCl, Res. Chem. Intermed. 41 (2015) 913–925. https://doi.org/10.1007/s11164-013-1244-7.

[161] D. Ben Hmamou, R. Salghi, A. Zarrouk, H. Zarrok, R. Touzani, B. Hammouti, A. El Assyry, Investigation of corrosion inhibition of carbon steel in 0.5 M H<inf>2</inf>SO<inf>4</inf> by new bipyrazole derivative using experimental and theoretical approaches, J. Environ. Chem. Eng. 3 (2015) 2031–2041. https://doi.org/10.1016/j.jece.2015.03.018.

[162] A. Kokalj, Corrosion inhibitors: physisorbed or chemisorbed?, Corros. Sci. 196 (2022) 109939. https://doi.org/10.1016/j.corsci.2021.109939.

[163] N.K. Gupta, C. Verma, R. Salghi, H. Lgaz, A.K. Mukherjee, M.A. Quraishi, New phosphonate based corrosion inhibitors for mild steel in hydrochloric acid useful for industrial pickling processes: Experimental and theoretical approach, New J. Chem. 41 (2017) 13114–13129. https://doi.org/10.1039/c7nj01431g.

[164] C.B. Verma, E.E. Ebenso, I. Bahadur, I.B. Obot, M.A. Quraishi, 5-(Phenylthio)-3H-pyrrole-4-carbonitriles as effective corrosion inhibitors for mild steel in 1 M HCl: Experimental and theoretical investigation, J. Mol. Liq. 212 (2015) 209–218. https://doi.org/10.1016/j.molliq.2015.09.009.

[165] A. Hamdy, N.S. El-gendy, Thermodynamic , adsorption and electrochemical studies for corrosion inhibition of carbon steel by henna extract in acid medium, Egypt. J. Pet. 22 (2013) 17–25. https://doi.org/10.1016/j.ejpe.2012.06.002.

[166] R. Karthik, P. Muthukrishnan, S.M. Chen, B. Jeyaprabha, P. Prakash, Anti-corrosion inhibition of mild steel in 1M hydrochloric acid solution by using Tiliacora accuminata leaves extract, Int. J. Electrochem. Sci. 10 (2014) 3707–3725.

[167] B. Delley, From molecules to solids with the DMol3 approach, J. Chem. Phys. 113 (2000) 7756–7764. https://doi.org/10.1063/1.1316015.

[168] J.P. Perdew, K. Burke, M. Ernzerhof, Generalized Gradient Approximation Made Simple, Phys. Rev. Lett. 77 (1996) 3865–3868. https://doi.org/10.1103/PhysRevLett.77.3865.

[169] F. Poshtiban, G. Bahlakeh, B. Ramezanzadeh, A detailed computational exploration and experimental surface/electrochemical analyses of mild steel functionalized by zinc-aminotris methylene phosphonic acid complex film, Appl. Surf. Sci. 495 (2019) 143582. https://doi.org/https://doi.org/10.1016/j.apsusc.2019.143582.

[170] J. Haque, V. Srivastava, D.S. Chauhan, H. Lgaz, M.A. Quraishi, Microwave-Induced Synthesis of Chitosan Schiff Bases and Their Application as Novel and Green Corrosion Inhibitors: Experimental and Theoretical Approach, ACS Omega 3 (2018) 5654–5668. https://doi.org/10.1021/acsomega.8b00455.

[171] A. Singh, K.R. Ansari, M.A. Quraishi, H. Lgaz, Y. Lin, Synthesis and investigation of pyran derivatives as acidizing corrosion inhibitors for N80 steel in hydrochloric acid: Theoretical and experimental approaches, J. Alloys Compd. 762 (2018) 347–362.

https://doi.org/https://doi.org/10.1016/j.jallcom.2018.05.236.

[172] R. Kumar, S. Chahal, S. Kumar, S. Lata, H. Lgaz, R. Salghi, S. Jodeh, Corrosion inhibition performance of chromone-3-acrylic acid derivatives for low alloy steel with theoretical modeling and experimental aspects, J. Mol. Liq. 243 (2017) 439–450. https://doi.org/https://doi.org/10.1016/j.molliq.2017.08.048.

[173] B. AitHaddou, D. Chebabe, A. Dermaj, H. Benassaoui, A. El Assyry, N. Hajjaji, S.I. Ahmed, A. Srhiri, Comparative study of low carbon steel corrosion inhibition in 1M HCl by 1,2,4-triazole-5-thione derivatives, J. Mater. Environ. Sci. 7 (2016) 2191–2200.

[174] M. Ramezanzadeh, G. Bahlakeh, Z. Sanaei, B. Ramezanzadeh, Corrosion inhibition of mild steel in 1 M HCl solution by ethanolic extract of eco-friendly Mangifera indica (mango) leaves: Electrochemical, molecular dynamics, Monte Carlo and ab initio study, Appl. Surf. Sci. 463 (2019) 1058–1077. https://doi.org/https://doi.org/10.1016/j.apsusc.2018.09.029.

[175] I.B. Obot, Z.M. Gasem, Theoretical evaluation of corrosion inhibition performance of some pyrazine derivatives, Corros. Sci. 83 (2014) 359–366. https://doi.org/https://doi.org/10.1016/j.corsci.2014.03.008.

[176] A. Chaouiki, H. Lgaz, R. Salghi, M. Chafiq, H. Oudda, Shubhalaxmi, K.S. Bhat, I. Cretescu, I.H. Ali, R. Marzouki, I.-M. Chung, Assessing the impact of electron-donating-substituted chalcones on inhibition of mild steel corrosion in HCl solution: Experimental results and molecular-level insights, Colloids Surfaces A Physicochem. Eng. Asp. 588 (2020) 124366. https://doi.org/https://doi.org/10.1016/j.colsurfa.2019.124366.

[177] H. Lgaz, K. Subrahmanya Bhat, R. Salghi, Shubhalaxmi, S. Jodeh, M. Algarra, B. Hammouti, I.H. Ali, A. Essamri, Insights into corrosion inhibition behavior of three chalcone derivatives for mild steel in hydrochloric acid solution, J. Mol. Liq. 238 (2017) 71–83. https://doi.org/https://doi.org/10.1016/j.molliq.2017.04.124.

[178] C. Morell, A. Grand, A. Toro-Labbé, New Dual Descriptor for Chemical Reactivity, J. Phys. Chem. A 109 (2005) 205–212. https://doi.org/10.1021/jp046577a.

[179] A.K. Singh, S. Thakur, B. Pani, B. Chugh, H. Lgaz, I.-M. Chung, P. Chaubey, A.K. Pandey, J. Singh, Solvent-free microwave assisted synthesis and corrosion inhibition study of a series of hydrazones derived from thiophene derivatives: Experimental, surface and theoretical study, J. Mol. Liq. 283 (2019) 788–803. https://doi.org/https://doi.org/10.1016/j.molliq.2019.03.126.

[180] H.B. Ouici, O. Benali, Y. Harek, L. Larabi, B. Hammouti, A. Guendouzi, The effect of some triazole derivatives as inhibitors for the corrosion of mild steel in 5 % hydrochloric acid, Res. Chem. Intermed. 39 (2013) 3089–3103. https://doi.org/10.1007/s11164-012-0821-5.

[181] W.H. Li, Q. He, S.T. Zhang, C.L. Pei, B.R. Hou, Some new triazole derivatives as inhibitors for mild steel corrosion in acidic medium, J. Appl. Electrochem. 38 (2008) 289–295. https://doi.org/10.1007/s10800-007-9437-7.

[182] B.D. Mert, M. Erman Mert, G. Kardaş, B. Yazıcı, Experimental and theoretical investigation of 3-amino-1,2,4-triazole-5-thiol as a corrosion inhibitor for carbon steel in HCl medium, Corros. Sci. 53 (2011) 4265–4272. https://doi.org/https://doi.org/10.1016/j.corsci.2011.08.038.

[183] H.H. Hassan, Inhibition of mild steel corrosion in hydrochloric acid solution by triazole derivatives: Part II: Time and temperature effects and thermodynamic treatments, Electrochim. Acta 53 (2007) 1722–1730. https://doi.org/https://doi.org/10.1016/j.electacta.2007.08.021.

[184] M.A. Quraishi, Sudheer, K.R. Ansari, E.E. Ebenso, 3-Aryl Substituted Triazole Derivatives as New and Effective Corrosion Inhibitors for Mild Steel in Hydrochloric Acid Solution, Int. J. Electrochem. Sci. 7 (2012) 7476–7492. https://doi.org/https://doi.org/10.1016/S1452-3981(23)15798-1.

[185] M.S. Kumar, S.L.A. Kumar, A. Sreekanth, Anticorrosion Potential of 4-Amino-3-methyl-1,2,4-triazole-5-thione Derivatives (SAMTT and DBAMTT) on Mild Steel in Hydrochloric Acid Solution, Ind. Eng. Chem. Res. 51 (2012) 5408–5418. https://doi.org/10.1021/ie203022g.

[186] J. Cruz, E. Garcia-Ochoa, M. Castro, Experimental and Theoretical Study of the 3-Amino-1,2,4-triazole and 2-Aminothiazole Corrosion Inhibitors in Carbon Steel, J. Electrochem. Soc. 150 (2003) B26. https://doi.org/10.1149/1.1528197.

[187] K. Mokhnache, H. Khither, S. El-Khamsa, S. Madoui, A. Karbab, N. Charef, L. Arrar, Hydrazones : origin, reactivity and biological activity, Adv. Bioresearch 10 (2019). https://doi.org/10.15515/abr.0976-4585.10.4.19.

[188] H.G. Bonacorso, G.R. Paim, L.M.F. Porte, E.P. Pittaluga, M.A.P. Martins, N. Zanatta, 6-Hydrazinonicotinic acid hydrazide: A useful precursor for chemo- and regioselective synthesis of new heteroaryl-linked pyridinohydrazones, Arkivoc 2012 (2012) 214–225. https://doi.org/10.3998/ark.5550190.0013.819.

[189] J. Patočka, R. Pita, K. Kuča, Gyromitrin, Mushroom Toxin of Gyromitra Spp., Mil. Med. Sci. Lett. 81 (2012) 61–67. https://doi.org/10.31482/mmsl.2012.008.

[190] R. Brehme, D. Enders, R. Fernandez, J.M. Lassaletta, Aldehyde N,N-dialkylhydrazones as neutral acyl anion equivalents: Umpolung of the imine reactivity, European J. Org. Chem. (2007) 5629–5660. https://doi.org/10.1002/ejoc.200700746.

[191] K.P. Balakrishnan, V. Krishnan, STUDIES ON BETA-ARYLHYDRAZONE-IMINE NICKEL(II) COMPLEXES-EXAMPLES OF METAL TEMPLATE SYNTHESES, J. Inorg. Nucl. Chem. 41 (1979) 37–40.

[192] S. Neha, R. Ritu, K. Manju, K. Birendra, A review on biological activities of hydrazone derivatives, Int. J. Pharm. Clin. Res. 8 (2016) 162–166.

[193] M. Malhotra, S. Sharma, A. Deep, Synthesis, characterization and antimicrobial evaluation of novel derivatives of isoniazid, Med. Chem. Res. 21 (2012) 1237–1244. https://doi.org/10.1007/s00044-011-9634-0.

[194] B. Erdönmez, M.D. Altıntop, G. Akalın Çiftçi, A. Özdemir, A. Ece, Design, Synthesis, and Evaluation of a New Series of Hydrazones as Small-Molecule Akt Inhibitors for NSCLC Therapy, ACS Omega 8 (2023) 20056–20065. https://doi.org/10.1021/acsomega.3c02331.

[195] L.W. Zheng, L.L. Wu, B.X. Zhao, W.L. Dong, J.Y. Miao, Synthesis of novel substituted pyrazole-5-carbohydrazide hydrazone derivatives and discovery of a potent apoptosis inducer in A549 lung cancer cells, Bioorganic Med. Chem. 17 (2009) 1957–1962. https://doi.org/10.1016/j.bmc.2009.01.037.

[196] M. Jabeen, A Comprehensive Review on Analytical Applications of Hydrazone Derivatives, J. Turkish Chem. Soc. Sect. A Chem. 9 (2022) 663–698. https://doi.org/10.18596/jotcsa.1020357.

[197] O. Abdellaoui, M.K. Skalli, A. Haoudi, Y.K. Rodi, N. Arrousse, M. Taleb, R. Ghibate, O. Senhaji, Study of the inhibition of corrosion of mild steel in a 1M HCl solution by a new quaternary ammonium surfactant, Moroccan J. Chem. 9 (2021) 044–056. https://doi.org/10.48317/IMIST.PRSM/morjchem-v9i1.21313.

[198] A. Bouchtart, M. Rguiti, K. El Mouaden, A. Albourine, A. Chaouiki, R. Salghi, L. Bazzi, A. Chetouani, Mild steel corrosion inhibition by some heteroatom organic compounds in acetic acid medium, Moroccan J. Chem. 8 (2020) 982–993. https://doi.org/10.48317/IMIST.PRSM/morjchem-v8i4.20562.

[199] A. Hamdouch, A. Anejjar, L. Bijla, S. Gharby, A. Asdadi, B. Chebli, R. Salghi, L.M. Idrissi Hassani, Corrosion inhibition of carbon steel by Vitex agnus castus leaves essential oils from the oasis of Tata, Moroccan J. Chem. 11 (2023) 105–118. https://doi.org/10.48317/IMIST.PRSM/morjchem-v11i1.37301.

[200] O. Id, E.L. Mouden, A. Batah, M. Belkhaouda, R. Salghi, A. Chetouani, Inhibition of Mild Steel Corrosion in 1M Hydrochloric Medium by the cherimoya seeds, Moroccan J. Chem. 3 (2021) 588–601.

[201] M. Chafiq, A. Chaouiki, H. Lgaz, R. Salghi, L. Gaonkar, K.S. Bhat, R. Marzouki, I.H. Ali, I. Khan, H. Shimizu, I. Chung, Synthesis and corrosion inhibition evaluation of a new schiff base hydrazone for mild steel corrosion in HCl medium : electrochemical , DFT , and molecular dynamics simulations studies, J. Adhes. Sci. Technol. 34 (2019) 1283–1314. https://doi.org/10.1080/01694243.2019.1707561.

[202] H. Ashassi-Sorkhabi, A. Kazempour, Z. Frouzat, Superior potentials of hydrazone Schiff bases for efficient corrosion protection of mild steel in 1.0 M HCl, J. Adhes. Sci. Technol. 0 (2020) 1–21. https://doi.org/10.1080/01694243.2020.1794357.

[203] O.M.A. Khamaysa, I. Selatnia, H. Zeghache, H. Lgaz, A. Sid, I.M. Chung, M. Benahmed, N. Gherraf, P. Mosset, Enhanced corrosion inhibition of carbon steel in HCl solution by a newly synthesized hydrazone derivative: Mechanism exploration from electrochemical, XPS, and computational studies, J. Mol. Liq. 315 (2020) 113805. https://doi.org/10.1016/j.molliq.2020.113805.

[204] N. Mamatha, N.S. Babu, K. Mukkanti, S. Pal, 2-(6-Methoxynaphthalen-2-yl)propionic acid (1,3-dimethyl-butylidene)hydrazide, Molbank 2011 (2011) 8–11. https://doi.org/10.3390/M741.

[205] M. Chafiq, A. Chaouiki, M.R. Al-Hadeethi, R. Salghi, A. Ismat H., M. Shaaban K., I.M. Chung, A joint experimental and theoretical investigation of the corrosion inhibition behavior and mechanism of hydrazone derivatives for mild steel in HCl solution, Colloids Surfaces A Physicochem. Eng. Asp. 610 (2021) 125744. https://doi.org/10.1016/j.colsurfa.2020.125744.

[206] A. Chaouiki, M. Chafiq, M.R. Al-Hadeethi, H. Lgaz, R. Salghi, S.K. Abdelraheem, I.H. Ali, S.A.M. Ebraheem, I.M. Chung, S.K. Mohamed, Exploring the corrosion inhibition effect of two hydrazone derivatives for mild steel corrosion in 1.0 M HCl solution via electrochemical and surface characterization studies, Int. J. Electrochem. Sci. 15 (2020) 9354–9377. https://doi.org/10.20964/2020.09.95.

[207] H. Lgaz, H. seung Lee, Interfacial adsorption mechanism of hydroxycinnamic acids on iron surfaces: A computational perspective toward eco-friendly corrosion mitigation strategies, Appl. Surf. Sci. 644 (2024) 158763. https://doi.org/10.1016/j.apsusc.2023.158763.

[208] K. Yang, Z. Cui, E. Li, Y. Shen, L. Zhang, D. Ma, Z. Yuan, Y. Dong, S. Zhang, Modulation of the magnetic, electronic, and optical behaviors of WS2 after metals adsorption: A first-principles study, Chem. Phys. 571 (2023) 111903. https://doi.org/10.1016/j.chemphys.2023.111903.

[209] Z. Cui, H. Wu, Metal atoms adsorbed Ga2O3 monolayer: As a potential application in optoelectronic devices, Micro and Nanostructures 180 (2023) 207613. https://doi.org/10.1016/j.micrna.2023.207613.

[210] H. Lgaz, H.S. Lee, Computational Exploration of Phenolic Compounds in Corrosion Inhibition: A Case Study of Hydroxytyrosol and Tyrosol, Materials (Basel). 16 (2023). https://doi.org/10.3390/ma16186159.

[211] R. Yildiz, An electrochemical and theoretical evaluation of 4 , 6-diamino-2-pyrimidinethiol as a corrosion inhibitor for mild steel in HCl solutions, Corros. Sci. 90 (2015) 544–553. https://doi.org/10.1016/j.corsci.2014.10.047.

[212] M. El Faydy, R. Touir, M. Ebn Touhami, A. Zarrouk, C. Jama, B. Lakhrissi, L.O. Olasunkanmi, E.E. Ebenso, F. Bentiss, Corrosion inhibition performance of newly synthesized 5-alkoxymethyl-8-hydroxyquinoline derivatives for carbon steel in 1 M HCl solution: Experimental, DFT and Monte Carlo simulation studies, Phys. Chem. Chem. Phys. 20 (2018) 20167–20187. https://doi.org/10.1039/c8cp03226b.

[213] M. Naciri, S. Skal, Y. El Aoufir, M.R. Al-hadeethi, H. Lgaz, H. Bidi, M. El Moudane, A. Ghanimi, A. Bellaouchou, Unveiling the influence of furan and thiophene on the corrosion inhibition capabilities of novel hydrazones derivatives in carbon steel/HCl interface: A dual experimental-theoretical study, Colloids Surfaces A Physicochem. Eng. Asp. 686 (2024) 133272. https://doi.org/10.1016/j.colsurfa.2024.133272.

[214] P. Marcus, Corrosion mechanisms in theory and practice: Third edition, Taylor & F, Taylor & Francis Group, 2011.

[215] Y. El aoufir, S. Zehra, H. Lgaz, A. Chaouiki, H. Serrar, S. Kaya, R. Salghi, S.K. AbdelRaheem, S. Boukhris, A. Guenbour, I.M. Chung, Evaluation of inhibitive and adsorption behavior of thiazole-4-carboxylates on mild steel corrosion in HCl, Colloids Surfaces A Physicochem. Eng. Asp. 606 (2020). https://doi.org/10.1016/j.colsurfa.2020.125351.

[216] C. Verma, D.K. Verma, E.E. Ebenso, M.A. Quraishi, Sulfur and phosphorus heteroatom-containing compounds as corrosion inhibitors: An overview, Heteroat. Chem. 29 (2018). https://doi.org/10.1002/hc.21437.

[217] H. Tayebi, H. Bourazmi, B. Himmi, A. El Assyry, Y. Ramli, A. Zarrouk, A. Geunbour, B. Hammouti, Combined electrochemical and quantum chemical study of new quinoxaline derivative as corrosion inhibitor for carbon steel in acidic media, Der Pharma Chem. 6 (2014) 220–234.

[218] M. El Faydy, B. Lakhrissi, A. Guenbour, S. Kaya, F. Bentiss, I. Warad, A. Zarrouk, In situ synthesis, electrochemical, surface morphological, UV–visible, DFT and Monte Carlo simulations of novel 5-substituted-8-hydroxyquinoline for corrosion protection

of carbon steel in a hydrochloric acid solution, J. Mol. Liq. 280 (2019) 341–359. https://doi.org/10.1016/j.molliq.2019.01.105.

[219] M. El Faydy, F. Benhiba, I. Warad, S. Saoiabi, A. Alharbi, A.A. Alluhaybi, B. Lakhrissi, M. Abdallah, A. Zarrouk, Bisquinoline analogs as corrosion inhibitors for carbon steel in acidic electrolyte: Experimental, DFT, and molecular dynamics simulation approaches, J. Mol. Struct. 1265 (2022) 133389. https://doi.org/10.1016/j.molstruc.2022.133389.

[220] M. Afrokh, S. Baroud, Y. Kerroum, A. Hatimi, S. Tahrouch, I. Sadki, I. Warad, A. Guenbour, A. Bellaouchou, M. Tabyaoui, A. Zarrouk, Green approach to corrosion inhibition of carbon steel by fucus spiralis extract in 1M HCl medium, Biointerface Res. Appl. Chem. 12 (2022) 7075–7091. https://doi.org/10.33263/BRIAC125.70757091.

[221] F. Zhang, Y. Tang, Z. Cao, W. Jing, Z. Wu, Y. Chen, Performance and theoretical study on corrosion inhibition of 2-(4-pyridyl)-benzimidazole for mild steel in hydrochloric acid, Corros. Sci. 61 (2012) 1–9. https://doi.org/10.1016/j.corsci.2012.03.045.

[222] P. Mourya, P. Singh, A.K. Tewari, R.B. Rastogi, M.M. Singh, Relationship between structure and inhibition behaviour of quinolinium salts for mild steel corrosion: Experimental and theoretical approach, Corros. Sci. 95 (2015) 71–87. https://doi.org/10.1016/j.corsci.2015.02.034.

[223] M. Ouakki, M. Galai, Z. Benzekri, C. Verma, E. Ech-chihbi, S. Kaya, S. Boukhris, E.E. Ebenso, M.E. Touhami, M. Cherkaoui, Insights into corrosion inhibition mechanism of mild steel in 1 M HCl solution by quinoxaline derivatives: electrochemical, SEM/EDAX, UV-visible, FT-IR and theoretical approaches, Colloids Surfaces A Physicochem. Eng. Asp. 611 (2021). https://doi.org/10.1016/j.colsurfa.2020.125810.

[224] M.A. Ismail, M.M. Shaban, E. Abdel-Latif, F.H. Abdelhamed, M.A. Migahed, M.N. El-Haddad, A.S. Abousalem, Novel cationic aryl bithiophene/ terthiophene derivatives as corrosion inhibitors by chemical, electrochemical and surface investigations, Sci. Rep. (2022). https://doi.org/10.1038/s41598-022-06863-8.

[225] D. Kumar, V. Fahmida, Corrosion inhibition of mild steel in hydrochloric acid using extract of glycine max leaves, Res. Chem. Intermed. 42 (2016) 3489–3506. https://doi.org/10.1007/s11164-015-2227-7.

[226] Y. Abboud, O. Tanane, A. El Bouari, R. Salghi, B. Hammouti, A. Chetouani, S. Jodeh, Corrosion inhibition of carbon steel in hydrochloric acid solution using pomegranate leave extracts, Corros. Eng. Technol. (2015) 1–9. https://doi.org/10.1179/1743278215Y.0000000058.

[227] L. Ma, H. Yong, J.D. Geiser, A. Moreno Carrascosa, N. Goff, P.M. Weber, Ultrafast x-ray and electron scattering of free molecules: A comparative evaluation, Struct. Dyn. 7 (2020) 33–35. https://doi.org/10.1063/4.0000010.

[228] R. Yildiz, An electrochemical and theoretical evaluation of 4,6-diamino-2-pyrimidinethiol as a corrosion inhibitor for mild steel in HCl solutions, Corros. Sci. 90 (2015) 544–553. https://doi.org/10.1016/j.corsci.2014.10.047.

[229] N. Muthukumar, Petroleum Products Transporting Pipeline Corrosion-A Review, in: Role Colloid. Syst. Environ. Prot., Elsevier B.V., 2014: pp. 527–571.

https://doi.org/10.1016/B978-0-444-63283-8.00021-1.

[230] M. Yadav, L. Gope, T.K. Sarkar, Synthesized amino acid compounds as eco-friendly corrosion inhibitors for mild steel in hydrochloric acid solution: Electrochemical and quantum studies, Res. Chem. Intermed. 42 (2016) 2641–2660. https://doi.org/10.1007/s11164-015-2172-5.

[231] R. Solmaz, Investigation of adsorption and corrosion inhibition of mild steel in hydrochloric acid solution by 5-(4-Dimethylaminobenzylidene)rhodanine, Corros. Sci. 79 (2014) 169–176. https://doi.org/10.1016/j.corsci.2013.11.001.

[232] R. Solmaz, Investigation of the inhibition effect of 5-((E)-4-phenylbuta-1,3-dienylideneamino)-1,3,4-thiadiazole-2-thiol Schiff base on mild steel corrosion in hydrochloric acid, Corros. Sci. 52 (2010) 3321–3330. https://doi.org/10.1016/j.corsci.2010.06.001.

[233] R. Solmaz, Investigation of corrosion inhibition mechanism and stability of Vitamin B1 on mild steel in 0.5M HCl solution, Corros. Sci. 81 (2014) 75–84. https://doi.org/10.1016/j.corsci.2013.12.006.

[234] I.B. Obot, D.D. Macdonald, Z.M. Gasem, Density functional theory (DFT) as a powerful tool for designing new organic corrosion inhibitors: Part 1: An overview, Corros. Sci. 99 (2015) 1–30. https://doi.org/10.1016/j.corsci.2015.01.037.

[235] E.E. Ebenso, C. Verma, L.O. Olasunkanmi, E.D. Akpan, D.K. Verma, H. Lgaz, L. Guo, S. Kaya, M.A. Quraishi, Molecular modelling of compounds used for corrosion inhibition studies: a review, Phys. Chem. Chem. Phys. 23 (2021) 19987–20027. https://doi.org/10.1039/D1CP00244A.

[236] L. Guo, Z.S. Safi, S. Kaya, W. Shi, B. Tüzün, N. Altunay, C. Kaya, Anticorrosive effects of some thiophene derivatives against the corrosion of iron: A computational study, Front. Chem. 6 (2018) 1–12. https://doi.org/10.3389/fchem.2018.00155.

[237] N. Islam, S. Kaya, Conceptual Density Functional Theory and Its Application in the Chemical Domain, 1st Editio, 2018. https://doi.org/https://doi.org/10.1201/b22471.

[238] M.R. Albayati, S. Kansız, N. Dege, S. Kaya, R. Marzouki, H. Lgaz, R. Salghi, I.H. Ali, M.M. Alghamdi, I.M. Chung, Synthesis, crystal structure, Hirshfeld surface analysis and DFT calculations of 2-[(2,3-dimethylphenyl)amino]-N’-[(E)-thiophen-2-ylmethylidene]benzohydrazide, J. Mol. Struct. 1205 (2020). https://doi.org/10.1016/j.molstruc.2019.127654.

[239] D.S. Chauhan, K.R. Ansari, A.A. Sorour, M.A. Quraishi, H. Lgaz, R. Salghi, Thiosemicarbazide and thiocarbohydrazide functionalized chitosan as ecofriendly corrosion inhibitors for carbon steel in hydrochloric acid solution, Int. J. Biol. Macromol. 107 (2018) 1747–1757. https://doi.org/10.1016/j.ijbiomac.2017.10.050.

[240] M. Missioui, H. Lgaz, W. Guerrab, H. seung Lee, I. Warad, J.T. Mague, I.H. Ali, E.M. Essassi, Y. Ramli, Synthesis of novel hybrid quinoxaline containing triazole and acetamide moieties by azide-alkyne click chemistry: Experimental and theoretical characterization, J. Mol. Struct. 1253 (2022) 132132. https://doi.org/10.1016/j.molstruc.2021.132132.

[241] H. Lgaz, A. Chaouiki, R. Lamouri, R. Salghi, H.-S. Lee, Computational Methods of Corrosion Inhibition Assessment, in: Sustain. Corros. Inhib. I Fundam. Methodol. Ind.

Appl., American Chemical Society, 2021: pp. 6–87. https://doi.org/doi:10.1021/bk-2021-1403.ch006.

[242] M.F. CHITER, Thèse de Doctorat: Etude théorique d’inhibiteurs verts de corrosion : Adsorption de la 8-Hydroxyquinoléine sur surfaces d’aluminium, Université de Toulouse, INP Toulouse, 2015.

[243] Y. Bulteau, Thèse de Doctorat: Etudes théoriques de dérivés (HqX) de la 8-hydroxyquinoléine: complexes Al(qX)3 et monocouches sur Al(111), Université de Toulouse, 2020.

[244] P. Hohenberg, W. Kohn, Inhomogeneous Electron Gas, Phys. Rev. 136 (1964). https://doi.org/10.1007/BF01198136.

[245] W. Kohn, L.. Sham, Self-Consistent Equations Including Exchange and Correlation Effects, Korean J. Physiol. Pharmacol. 140 (1965).

[246] P. Cornette, Thèse de Doctorat: Approche expérimentale et théorique de l ’ inhibition de corrosion de surfaces métalliques., Université de recherche Paris Sciences et Lettres, Chimie Physique et Chimie Analytique de Paris Centre, 2018.

[247] J.P. Perdew, W. Yue, Accurate and simple density functional for the electronic exchange energy: Generalized gradient approximation, Phys. Rev. B 33 (1986) 8800–8802. https://doi.org/10.1103/PhysRevB.33.8800.

[248] A.D. Becke, Density-fnnctional exchange-energy approximation with correct asymptotic behavior, Phys. Rev. A 38 (1988). https://doi.org/10.1063/1.1749835.

[249] A.D. Becke, Density-functional thermochemistry. IV. A new dynamical correlation functional and implications for exact-exchange mixing, J. Chem. Phys. 104 (1996) 1040–1046. https://doi.org/10.1063/1.470829.

[250] C. Lee, W. Yang, R. G.Parr, Development of the Colic-Salvetti correlation-energy formula into a functional of the electron density, Phys. Rev. B 37 (1988).